Super Immunity: Elucidating the Optimal Strategies for SARS-CoV-2 Immunity

Timothy Andrew Bates

A DISSERTATION

Presented to the Department of Molecular Microbiology and Immunology

Oregon Health and Science University

School of Medicine

In Partial Fulfillment of the Requirements for the Degree of Doctor of Philosophy

March 2023

Dissertation Advisory Committee

Advisor: Fikadu G. Tafesse, Ph.D.

Chair: David Farrens, Ph.D.

Member: David Lewinsohn, M.D., Ph.D.

Member: Jonathan Pruneda, Ph.D.

External Reviewer: Benjamin Burwitz, Ph.D.

I. Table of Contents

SUPER IMMUNITY: ELUCIDATING THE OPTIMAL STRATEGIES FOR SARS-COV-2 IMMUNITY I
I. TABLE OF CONTENTS II
II. COMMON ABBREVIATIONS X
III: ACKNOWLEDGEMENTS XIII
IV: ABSTRACT XV
CHAPTER 1: INTRODUCTION 1
SECTION 1.1: PREFACE 1
Figure 1.1 An abridged timeline of the COVID-19 pandemic 2
SECTION 1.2: SEVERE ACUTE RESPIRATORY SYNDROME ASSOCIATED CORONAVIRUS 3
1.2.1 Phylogeny 3
1.2.2 Virion structure 4
Figure 1.2 Genome composition and virion structure. 5
1.2.3 Replication cycle 6
Figure 1.3 SARS-CoV-2 replication cycle 8
1.2.4 SARS-CoV-2 variants 9
Figure 1.4 SARS-CoV-2 variant naming and prevalence 12
1.2.5 Highly impactful mutations 13
SECTION 1.3: INFECTION & IMMUNITY 14
1.3.1 COVID-19 transmission 14
1.3.2 COVID-19 disease burden 15
1.3.3 Pathogenesis 16
1.3.4 Innate immunity 18
1.3.5 Cellular immunity 18
1.3.6 Humoral immunity 19
1.3.7 Antibody structure and classification 22
Figure 1.5 Antibody composition and classification 23
Figure 1.6 Structure of N-linked and O-linked antibody glycans 29
1.3.7 Generation of antibody diversity 30
1.3.8 B cell expansion and further antibody diversification 32
1.3.9 Secondary infection and memory responses 35
1.3.10 Measurement of antibodies 36
SECTION 1.4: VACCINES 41
1.4.1 A brief history of vaccines 41
1.4.2 COVID-19 vaccines 44
Table 1.1 COVID-19 vaccines with full approval in at least one country 46
1.4.3 A deeper look at mRNA vaccines 46
1.4.4 Immune response to mRNA vaccines 48
CHAPTER 2: CROSS-REACTIVITY OF SARS-COV STRUCTURAL PROTEIN ANTIBODIES AGAINST SARS-COV-2 52
SECTION 2.1: ABSTRACT 53
2.1.1 Graphical Abstract 53
2.1.2 Summary 53
SECTION 2.2: INTRODUCTION 54
SECTION 2.3: RESULTS 57
2.3.1 Sequence similarities of the structural proteins of HCoVs 57
Figure 2.1 Sequence similarity between SARS-CoV and SARS-CoV-2 59
Table 2.1 SARS-CoV antibodies utilized by this study 60

2.3.2 Antibodies of the SARS-CoV structural proteins show cross-reactivities with SARS-CoV-2 by microscopy ... *60*
Figure 2.2 Immunofluorescence of SARS-CoV-2 structural proteins using SARS-CoV antibodies ... 62
2.3.3 Antibodies of the SARS-CoV structural proteins show cross-reactivities with SARS-CoV-2 by immunoblotting ... *63*
Figure 2.3 Biochemical characterization of SARS-CoV antibodies for their cross-reactivity with SARS-CoV-2 proteins ... 64
2.3.4 S antibodies show cross-reactivity in binding ... *65*
Figure 2.4 Binding kinetics and functional testing of Spike-specific antibodies against the RBD of the SARS-CoV-267
2.3.5 S antibodies of SARS-CoV show limited cross-neutralization of SARS-CoV-2 ... *68*
2.3.6 Summary of cross-reactivity of SARS-CoV structural protein-specific antibodies to SARS-CoV-2 structural proteins in various assays ... *69*
Table 2.2 Summary of reagent quality in assays ... 70
SECTION 2.4: DISCUSSION ... 70
SECTION 2.5: METHODS ... 73
Sequence alignment ... *73*
Cell transfection ... *73*
Pseudotyped lentivirus production ... *74*
SARS-CoV-2 virus propagation ... *74*
SARS-CoV-2 infection ... *74*
Immunofluorescence ... *75*
Pseudovirus neutralization assay ... *75*
Focus forming assay (FFA) for live SARS-CoV-2 virus neutralization measurement ... *76*
Enzyme-linked immunosorbent assay (ELISA) ... *77*
RBD protein purification and biotinylation ... *78*
Biolayer interferometry (BLI) ... *78*
RBD Western blot ... *79*
SARS-CoV-2 infected lysate Western blot ... *79*
Quantification and Statistical Analysis ... *80*
SECTION 2.6: SUPPLEMENTAL FIGURES ... 81
Figure S2.1 Alignment of structural proteins for SARS-CoV and SARS-CoV-2 ... 81
Figure S2.2 Immunofluorescence of SARS-CoV-2 structural proteins using SARS-CoV antibodies ... 82
at 63× magnification. ... 82
Figure S2.3 Complete western blot and gel images. ... 83
Figure S2.4 ELISA extended data. ... 85
Figure S2.5 BLI extended data. ... 86
Figure S2.6 SARS-CoV-2 neutralization extended data. ... 87
SECTION 2.7: ACKNOWLEDGMENTS ... 88
2.7.1 Acknowledgments ... *88*
2.7.2 Author contributions ... *88*
CHAPTER 3: NEUTRALIZATION OF SARS-COV-2 VARIANTS BY CONVALESCENT AND BNT162B2 VACCINATED SERUM ... 89
SECTION 3.1: ABSTRACT ... 90
SECTION 3.2: INTRODUCTION ... 90
SECTION 3.3: RESULTS ... 92
3.3.1 Antibody response to BNT162b2 vaccination ... *92*
Figure 3.1 Serum antibody levels of BNT162b2 vaccine recipients and potency of sera to neutralize SARS-CoV-2 variants. ... 94
3.3.2 Antibody response to natural SARS-CoV-2 infection ... *95*

Figure 3.2 Neutralization of SARS-CoV-2 variants by convalescent serum. 97
SECTION 3.4: DISCUSSION 98
SECTION 3.5: METHODS 100
3.5.1 Ethics statement *100*
3.5.2 Serum collection *100*
3.5.3 Cell culture *101*
3.5.4 SARS-CoV-2 growth and titration *101*
3.5.5 SARS-CoV-2 Sequencing *102*
3.5.6 SARS-CoV-2 FRNT *103*
3.5.7 Production of variant RBDs *103*
3.5.8 ELISA *104*
3.5.9 $FRNT_{50}$ and EC_{50} calculation *105*
3.5.10 Statistical analysis *105*
SECTION 3.6: SUPPLEMENTAL TABLES AND FIGURES 106
Table S3.1 List of mutations in B.1.1.7 and B.1.351 SARS-CoV-2 clinical isolates* 106
Table S3.2 List of primers used in this study 107
Figure S3.1 Vaccinee serum $FRNT_{50}$ curves. 108
Figure S3.2 Convalescent serum FRNT50 curves. 109
Figure S3.3 Vaccine response by sex 110
Figure S3.4 Correlates of selected demographic and clinical factors with neutralization in the COVID-19 convalescent cohort. 111
Figure S3.5 Variant focus forming assay phenotypes. 113
SECTION 3.7: ACKNOWLEDGMENTS 114
3.7.1 Acknowledgments *114*
3.7.2 Author Contributions *114*
CHAPTER 4: AGE-DEPENDENT NEUTRALIZATION OF SARS-COV-2 AND P.1 VARIANT BY VACCINE IMMUNE SERUM SAMPLES 115
SECTION 4.1: ABSTRACT 115
SECTION 4.2: INTRODUCTION 116
SECTION 4.3: RESULTS 116
Figure 4.1 SARS-CoV-2–Specific Antibody Levels 116
Figure 4.2 Neutralization of Live SARS-CoV-2 Clinical Isolates 117
SECTION 4.4: DISCUSSION 118
SECTION 4.5: METHODS 119
SECTION 4.6: SUPPLEMENTAL METHODS 119
4.6.1 Serum collection: *119*
4.6.2 SARS-CoV-2 growth and titration: *120*
4.6.3 SARS-CoV-2 FRNT and ELISA *120*
4.6.4 $FRNT_{50}$ and EC_{50} calculation *121*
SECTION 4.7: ACKNOWLEDGMENTS 121
4.7.1 Acknowledgments *121*
4.7.2 Funding *122*
4.7.3 Author contributions *122*
CHAPTER 5: ANTIBODY RESPONSE AND VARIANT CROSS-NEUTRALIZATION AFTER SARS-COV-2 BREAKTHROUGH INFECTION 123
SECTION 5.1: ABSTRACT 123
SECTION 5.2: INTRODUCTION 124
SECTION 5.3: RESULTS 124

Figure 5.1 SARS-CoV-2 Spike Receptor-Binding Domain (RBD)–Specific Antibody Levels After Vaccination and Breakthrough Infection 125
Figure 5.2 Live SARS-CoV-2 Variants Neutralization After Vaccination and Breakthrough Infection..... 126
SECTION 5.4: DISCUSSION 126
SECTION 5.5: METHODS 127
SECTION 5.6: SUPPLEMENTAL METHODS 128
5.6.1 Cohort serum collection: *128*
5.6.2 SARS-CoV-2 variants sequencing: *128*
5.6.3 Enzyme-linked immunosorbent assays (ELISA) and Focus reduction neutralization tests (FRNT): *129*
5.6.4 Statistical analysis *129*
SECTION 5.7 ACKNOWLEDGMENTS 130
5.7.1 Acknowledgments *130*
5.7.2 Funding *130*
5.7.3 Author contributions *130*
CHAPTER 6: VACCINATION BEFORE OR AFTER SARS-COV-2 INFECTION LEADS TO ROBUST HUMORAL RESPONSE AND ANTIBODIES THAT EFFECTIVELY NEUTRALIZE VARIANTS 132
SECTION 6.1: ABSTRACT 133
SECTION 6.2: INTRODUCTION 133
SECTION 6.3: RESULTS 134
6.3.1 Cohort and study design *134*
Table 6.1 Cohort demographics. 135
6.3.2 Antibody levels following breakthrough infection, hybrid immunity, and vaccination alone *135*
Figure 6.1 Antibody levels following breakthrough infection, hybrid immunity, and vaccination alone. 137
6.3.3 Neutralizing antibody titers against SARS-CoV-2 and the variants of concern *138*
Figure 6.2 Antibody levels following breakthrough infection, hybrid immunity, and vaccination alone. 139
6.3.4 Quality of the neutralizing antibody response *140*
Figure 6.3 Neutralizing efficiency and correlation with age. 141
SECTION 6.4: DISCUSSION 142
SECTION 6.5: METHODS 144
6.5.1 Study design *144*
6.5.2 Cohort selection and serum collection *144*
6.5.3 Enzyme-linked immunosorbent assays (ELISA) *145*
6.5.4 Cell culture *146*
6.5.5 SARS-CoV-2 growth and titration *146*
6.5.6 Focus reduction neutralization test (FRNT) *147*
6.5.7 Antibody Dependent Cellular Phagocytosis (ADCP) *148*
6.5.8 Statistical analysis *148*
SECTION 6.6: SUPPLEMENTAL FIGURES 150
Figure S6.1 One versus two vaccine dose hybrid immunity. 150
Figure S6.2 Neutralization by variant. 151
Figure S6.3 Variant neutralization ratios. 152
Figure S6.4 ADCP flow gating scheme. 152
SECTION 6.7: ACKNOWLEDGMENTS 153
6.7.1 Acknowledgments *153*
6.7.2 Funding *153*
6.7.3 Author contributions *153*
CHAPTER 7: OMICRON NEUTRALIZING ANTIBODY RESPONSE FOLLOWING BOOSTER VACCINATION COMPARED WITH BREAKTHROUGH INFECTION 154
SECTION 7.1: ABSTRACT 155

7.1.1 Background *155*
7.1.2 Methods *155*
7.1.3 Findings *155*
7.1.4 Conclusions *156*
SECTION 7.2: INTRODUCTION 156
SECTION 7.3: RESULTS 157
7.3.1 Cohort *157*
Table 7.1 Cohort demographics and clinical data 159
Figure 7.1 Cohort design 160
7.3.2 Approach *160*
7.3.3 Binding antibody responses *161*
Figure 7.2 Antibody response to two-dose vaccination, three-dose vaccination, and breakthrough infection 162
7.3.4 Antibody-dependent cell-mediated phagocytosis *163*
7.3.5 Neutralizing antibody responses *163*
Figure 7.3 Live SARS-CoV-2 neutralization by two-dose vaccination, three-dose vaccination, and breakthrough infection cohorts 164
7.3.6 Antibody response quality *165*
7.3.7 Relative loss of strain-specific neutralizing capacity *166*
Figure 7.4 Quality of the neutralizing antibody response to two-dose vaccination, three-dose vaccination, and breakthrough infection 167
7.3.8 Antibody response versus age and gender *168*
SECTION 7.4: DISCUSSION 168
7.4.1 Discussion *168*
7.4.2 Limitations of the study *170*
SECTION 7.5: METHODS 171
7.5.1 Cohort selection and serum collection *171*
7.5.2 Ethics statement *172*
7.5.3 Enzyme-linked immunosorbent assays (ELISA) *172*
7.5.4 Antibody dependent cellular phagocytosis (ADCP) *172*
7.5.5 SARS-CoV-2 growth and titration *173*
7.5.6 Focus reduction neutralization test (FRNT) *174*
7.5.7 Statistical analysis *174*
SECTION 7.6: SUPPLEMENTAL FIGURES 175
Figure S7.1 Variant neutralization correlation with age 175
Figure S7.2 Relationship between sex and variant neutralization 176
Figure S7.3 Correlation between neutralization and age for individuals <65 years of age 176
SECTION 7.7: ACKNOWLEDGMENTS 177
7.7.1 Acknowledgments *177*
7.7.3 Author contributions *177*
CHAPTER 8: BNT162B2 INDUCED NEUTRALIZING AND NON-NEUTRALIZING ANTIBODY FUNCTIONS AGAINST SARS-COV-2 DIMINISH WITH AGE 178
SECTION 8.1: ABSTRACT 179
SECTION 8.2: INTRODUCTION 179
SECTION 8.3: RESULTS 183
8.3.1 Study Subjects *183*
Table 8.1 Demographics and vaccination status 183
8.3.2 Neutralizing antibody titers of wild type and SARS-CoV-2 variants *183*
Figure 8.1 BNT162b2-induced IgG mediates age-dependent neutralization of WT and SARS-CoV-2 clinical variants 185

8.3.3 Vaccine-specific Fc effector functions *187*
Figure 8.2 Vaccine-specific IgG induction of FcγRIIIa/CD16a effector functions correlate with neutralization of WT and SARS-CoV-2 clinical variants 188
8.3.4 IgG glycosylation *190*
Figure 8.3 Differential fucose and sialic acid on vaccine-specific IgG link to FcγRIIIa/CD16a effector functions 191
8.3.5 Impact of age on antibody Fc effector functions *192*
Figure 8.4 Age influences some, but not all, vaccine-specific antibody FcγR functions 194
8.3.6 Polyclonal functional breadth and magnitude *195*
Figure 8.5 Enhanced BNT162b2 induced polyfunctional antibody breadth and magnitude against SARS-CoV-2 in younger, compared with older, adults 196
SECTION 8.4: DISCUSSION 199
SECTION 8.5: LIMITATIONS OF THE STUDY 203
SECTION 8.6: METHODS 203
8.6.1 Cohort *203*
8.6.2 Cell lines *204*
8.6.3 Primary immune cells *204*
8.6.4 Virus *204*
8.6.5 Enzyme linked immunosorbent assays (ELISA) *205*
8.6.6 Focus reduction neutralization test (FRNT) *205*
8.6.7 Fc receptor binding assays *206*
8.6.8 Non-antigen and RBD-specific IgG glycosylation *207*
8.6.9 Antibody dependent cellular phagocytosis (ADCP) *208*
8.6.10 Antibody dependent neutrophil phagocytosis (ADNP) *209*
8.6.11 Antibody dependent complement deposition (ADCD) *210*
8.6.12 Antibody dependent NK cell activation (ADNKA) *210*
8.6.13 Quantification and statistical analysis *211*
SECTION 8.7: SUPPLEMENTAL FIGURES 213
Figure S8.1 BNT162b2 vaccination induces IgG mediated neutralization of SARS-CoV-2 wildtype (WT) and clinical variants that diminish with age but are not altered by sex 213
Figure S8.2 Vaccine specific IgG induction of FcγRIIIa/CD16 effector functions correlate with neutralization of SARS-CoV-2 variants 215
Figure S8.3 Bulk total non-antigen and vaccine specific IgG glycosylation patterns diverge 217
Figure S8.4 Differential fucose and sialic acid on vaccine specific IgG link FcγRIIIa/CD16a mediated IFNg and TNFa production. 219
Figure S8.5 Minimal relationship between age and vaccine specific antibody dependent complement deposition (ADCD) 220
Figure S8.6 Antibodies function by the combination of Fab and Fc domains 221
SECTION 8.8: ACKNOWLEDGMENTS 222
8.8.1 Acknowledgments *222*
8.8.2 Author Contributions *223*
CHAPTER 9: AN EXTENDED INTERVAL BETWEEN VACCINATION AND INFECTION ENHANCES HYBRID IMMUNITY AGAINST SARS-COV-2 VARIANTS 224
SECTION 9.1: ABSTRACT 224
SECTION 6.2: INTRODUCTION 225
SECTION 9.3: RESULTS 228
9.3.1 A longitudinal cohort of vaccinees with previous COVID-19 displayed improved SARS-CoV-2 neutralization compared to vaccination alone. *228*
9.3.2 A cross-sectional cohort of hybrid immune individuals including both prior infection and vaccine breakthrough *228*
Table 9.1: Demographics 229
Table 9.2: Variants of infections 230

Figure 9.1: Longitudinal cohort of previously infected vaccinees shows improved variant neutralization compared to vaccination alone 230
9.3.3 Elevated antibody levels and neutralizing titers with hybrid immunity. *231*
Figure 9.2: Cross-sectional cohort of individuals with hybrid immunity show improved antibody levels and variant neutralization 232
9.3.4 Improved antibody quality among hybrid immune individuals. *233*
Figure 9.3: Antibody quality and variant cross-neutralization are improved with hybrid immunity 234
9.3.5 The interval between vaccination and natural infection dictates neutralizing titer levels. *235*
Figure 9.4: Exposure interval determines strength of hybrid immunity 236
Variant cross-neutralization improves with greater exposure intervals. *238*
Figure 9.5: Exposure interval increases variant cross-neutralization by hybrid immune sera 239
SECTION 9.4: DISCUSSION 239
SECTION 9.5: METHODS 242
9.5.1 Cohort *242*
9.5.2 Enzyme linked Immunosorbent Assays (ELISA) *243*
9.5.3 Viruses *244*
9.5.4 Focus Reduction Neutralization Test (FRNT) *245*
9.5.5 Statistical Analysis *245*
9.5.6 Study Approval *246*
SECTION 9.6: SUPPLEMENTAL FIGURES 247
Figure S9.1: Variant cross-neutralization by hybrid immune sera is improved compared to vaccination alone 247
Figure S9.2: Infection prior to vaccination group neutralizing responses correlate with exposure interval 248
Figure S9.3: Vaccine breakthrough group neutralizing responses correlate with exposure interval 249
Figure S9.4: Other antibody isotypes correlate less well with exposure interval 250
Figure S9.5: Neutralizing potency index does not correlate with exposure interval 251
SECTION 9.7: ACKNOWLEDGEMENTS 252
9.7.1 Author Contributions *252*
9.7.2 Funding *252*
9.7.3 Acknowledgements *252*
CHAPTER 10: THESIS SUMMARY 253
SECTION 10.1: CHAPTER HIGHLIGHTS 253
10.1.1 Chapter 1 highlights: SARS-CoV-2 ..... *253*
10.1.2 Chapter 2 highlights: Cross-reactivity of SARS-CoV structural protein antibodies against SARS-CoV-2 ..... *253*
10.1.3 Chapter 3 highlights: Neutralization of SARS-CoV-2 variants by convalescent and BNT162b2 vaccinated serum *253*
10.1.4 Chapter 4 highlights: Age-Dependent Neutralization of SARS-CoV-2 and P.1 Variant by Vaccine Immune Serum Samples *253*
10.1.5 Chapter 5 highlights: Antibody Response and Variant Cross-Neutralization After SARS-CoV-2 Breakthrough Infection *253*
10.1.6 Chapter 6 highlights: Vaccination before or after SARS-CoV-2 infection leads to robust humoral response and antibodies that effectively neutralize variants *254*
10.1.7 Chapter 7 highlights: Omicron neutralizing antibody response following booster vaccination compared with breakthrough infection *254*
10.1.8 Chapter 8 highlights: BNT162b2 induced neutralizing and non-neutralizing antibody functions against SARS-CoV-2 diminish with age *254*
10.1.9 Chapter 9 highlights: An extended interval between vaccination and infection enhances hybrid immunity against SARS-CoV-2 variants *254*
SECTION 10.2: VACCINE EFFECTIVENESS 255
SECTION 10.3: HYBRID IMMUNITY 256

SECTION 10.4: THE VARIANTS....257
SECTION 10.5 FUTURE DIRECTIONS....258
SECTION 10.6: FINAL THOUGHTS....259
REFERENCES CITED....261

II. Common Abbreviations

ACE2	Angiotensin converting enzyme 2
ADCC	Antibody-dependent cellular cytotoxicity
ADCD	Antibody-dependent complement deposition
ADCP	Antibody-dependent cellular phagocytosis
ADE	Antibody-dependent enhancement
ADNKA	Antibody-dependent natural killer cell activation
ADNP	Antibody-dependent neutrophil phagocytosis
AID	Activation-induced cytidine deaminase
ARDS	Acute respiratory distress syndrome
BCR	B cell receptor
BEI	Biodefense and Emerging Infections
BLI	Biolayer interferometry
BSA	Bovine serum albumin
BSL-3	Biosafety level 3
CDC	Centers for Disease Control and Prevention
CDR	Complementarity determining region
CH	Constant heavy domain
CL	Constant light domain
CM	Convoluted membrane
CoV	Coronavirus
COVID-19	Coronavirus disease 2019
CPE	Cytopathic effect
CSR	Class-switch recombination
CT	cytoplasmic tail
D	Diversity segment
DC	Dendritic cell
DMEM	Dulbecco's Modified Eagle Medium
DMV	Double membrane vesicle
DSPC	1,2-distearoyl-sn-glycero-3-phosphocholine
E	Envelope protein
EC_{50}	50% effective concentration
ECMO	Extracorporeal membrane oxygenation
ELISA	Enzyme-linked immunosorbent assay
ER	Endoplasmic reticulum
ERGIC	ER-Golgi intermediate compartment
Fab	Fragment antigen-binding
FBS	Fetal bovine serum
Fc	Fragment crystalizable
FcRN	Neonatal fragment crystalizable receptor
FDC	Follicular dendritic cell
FFA	Focus-forming assay
FFU	Focus-forming units

flu	Influenza
FP	Fusion peptide
$FRNT_{50}$	50% focus reduction neutralization titer
GalNAc	N-acetylgalactosamine
GC	Germinal center
GFP	Green fluorescent protein
GISAID	Global Initiative on Sharing Avian Influenza Data
GlcNAc	N-acetylglucosamine
GMT	Geometric mean titer
HCoV	Human coronavirus
HPV	Human papilloma virus
HRP	Horseradish peroxidase
IBV	Infectious bronchitis virus
ICU	Intensive care unit
IF	Immunofluorescence
IFNγ	Interferon gamma
Ig	Immunoglobulin
IgNAR	Immunoglobulin novel antigen receptor
IRB	Institutional review board
J	Joining
LOD	Limit of detection
M	Membrane protein
m1Ψ	N1-methyl-pseudouridine
MBC	Memory B cell
MERS-CoV	Middle east respiratory syndrome coronavirus
MFI	Median fluorescence intensity
MHC	Major histocompatibility complex
N	Nucleocapsid protein
NEAA	Nonessential amino acids
NHEJ	Non-homologous end joining
NK	Natural killer
NPI	Neutralizing potency index
NSP	Non-structural protein
OD	Optical density
OHSU	Oregon Health & Science University
OPD	o-phenylenediamine dihydrochloride
ORF	Open reading frame
Pango	Phylogenetic Assignment of Named Global Outbreak Lineages
PASC	Post-acute sequelae of SARS-CoV-2 infection
PB	Polybasic cleavage site
PBS	Phosphate buffered saline
PBST	Phosphate buffered saline plus tween
PC	Plasma cell
PCR	Polymerase chain reaction

PEG	Polyethylene glycol
PFU	Plaque forming unit
pIgR	Polymeric immunoglobin receptor
$PRNT_{50}$	50% plaque reduction neutralization titer
PS	Penicillin-streptomycin
R_0	Basic reproduction number
RBD	Receptor binding domain
RSV	Respiratory syncytial virus
RT	Reverse transcription
RT	Room temperature
S	Spike glycoprotein
SARS	Severe acute respiratory syndrome
SARS-CoV-2	Severe acute respiratory syndrome associated coronavirus 2
scFv	Single-chain veriable fragment
SHM	Somatic hypermutation
T_{FH}	T follicular helper cell
TM	Transmembrane domain
TMB	3,3',5,5'-tetramethylbenzidine
TNFα	Tumor necrosis factor alpha
UTR	Untranslated region
V	Variable segment
VH	Variable heavy domain
VL	Variable light domain
VLP	Virus-like particle
VNAR	Variable domain of novel antigen receptor
VOC	Variant of concern
VOHC	Variant of high consequence
VOI	Variant of interest
VUM	Variant under monitoring
WA1	Washington isolate of original SARS-CoV-2
WHO	World Health Organization
WT	Wild-type

III: Acknowledgements

Graduate school is a grand adventure, fraught with blind corners and dead ends, but also hidden beauty and exciting mysteries. A dissertation encapsulates the most successful aspects of this journey, but it cannot capture the full experience of perseverance and comradery. While this story is my own, each and every word describes the collective achievement of my colleagues, my friends, and my family.

I want to first thank my mentor, Dr. Fikadu Tafesse, whose enthusiastic optimism kept me motivated, and whose sage advice directly led to the tremendous successes we achieved together. I remain in awe of your ability to multitask, and I will be forever grateful for your commitment to my professional development, and for creating many of my most fruitful opportunities.

I want to thank my dissertation committee. Dr. David Farrens, thank you for taking the time to share your wisdom about the mysterious ways of academic science, and for teaching me how to actively look for and question my assumptions. Dr. David Lewinsohn, thank you for always being a fierce advocate of my career development, and for challenging me to fully consider the many options available and talking through what I really want to do. Dr. Jonathan Pruneda, thank you for helping me work through so many technical problems, and for being so candid about the practical aspects of running a lab. I look up to all of you as role models, not only for how to be a good scientist, but how to be a good human being.

I want to thank the members of my lab. Jules Reyes-Weinstein, Gaelen Guzman, and Scotty Farley, joining the lab together with you and navigating all of the same issues helped make everything feel much more achievable. Hans Leier, Ilaria Merutka, Savannah McBride, and Mila Trank-Greene, thank you for your help in the lab. Your efforts are a large part of making these

projects a success. Thank you to everyone else in the lab for helping foster such a positive environment: Sascha, Aiden, Michael, Michelle, Judah, Teketay, and Sintayehu.

I want to thank my many collaborators. Dr. Bill Messer, thank you for working with me so closely on developing the neutralization assay which has become the cornerstone of my projects, and thank you to the whole Messer lab, particularly Zoe Lyski, Flic Coulter, David Xthona Lee, and Courtney Micheletti, for all your help and engaging discussions. Dr. Marcel Curlin, thank you for helping design such interesting cohorts and collecting samples, and thank you to the Curlin lab, particularly Devin Schoen and Bradie Winders, for helping me organize all of the clinical information. Dr. Lenette Lu, thank you for working with us on such an exciting project. I owe everything I know about antibody glycosylation to you.

I want to thank my fellow graduate students at OHSU for being such a supportive community. It was an honor working with all of you to form the GRU; united we are strong. And thank you to all those who came before my cohort and who imparted valuable lessons and helped preserve our institutional memory.

I want to thank my friends and family, particularly my amazing wife and talented artist, Tephra Bates, who provided endless love and support during my studies, and drew our amazing lab logo (right). Thank you for tolerating my late nights and weekend work, and for supporting me through good times and bad. You are the light of my life, and I cannot imagine having done any of this without you.

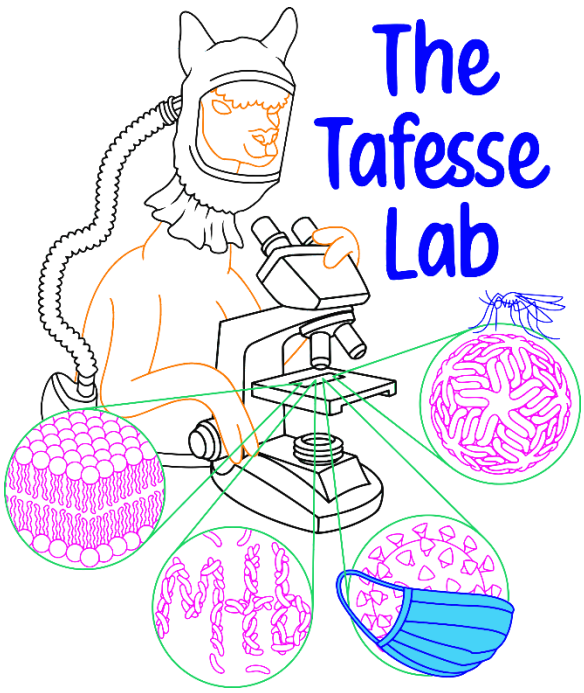

IV: Abstract

The COVID-19 pandemic changed a lot about society in a matter of weeks and reminded us all of our precarious position in the world. However, in the months that followed, we saw tremendous strength and ingenuity in the face of a crisis. The rapid development and delivery of new vaccines saved millions of lives, but because this was the first widely used mRNA vaccine, there is still much to be learned about how they can be further improved. In this dissertation, I will examine the antibodies generated by vaccination and SARS-CoV-2 infection, with a focus on how well they are able to block infection.

My colleagues and I began with the finding that antibodies against the original SARS coronavirus can commonly bind to SARS-CoV-2 proteins, but only rarely block infection. We next compared the antibody response to vaccination versus naturally acquired COVID-19 infection, and we found that vaccination provided much more reliable antibody responses, which better blocked live SARS-CoV-2 (called neutralization). We next looked at the demographic determinants of vaccine response and found that age has a dramatic impact on the level of neutralizing antibodies produced by vaccination.

We next became interested in what happens when someone who was previously infected receives a vaccine, or when someone has a vaccine breakthrough infection. The concept of combined vaccination and infection is called hybrid immunity (or sometimes super immunity), and it is likely to represent the most common form of immunity going forward. We looked at a group of individuals with breakthrough infections that occurred primarily during the Delta wave and found that they had significantly higher neutralizing antibody titers, with a heightened protection against the Delta variant compared to others. Afterwards, we directly compared those individuals with vaccine breakthrough to individuals with infection prior to vaccination and found

that the hybrid immunity resulting from both of these conditions were largely similar. Further, we found that hybrid immunity erases the age dependence of vaccine responses. The booster vaccines first became available during the Omicron era, and we compared the neutralizing antibody response raised by three-dose vaccination compared with breakthrough infection, finding that both were similarly improved over the primary two-dose vaccine course. However, we also observed that Omicron was dramatically more vaccine resistant than the variants that preceded it, and two-dose vaccination was no longer enough to provide robust neutralization.

Interested in the quality of antibodies produced by the vaccines, we revisited our original two-dose vaccinated samples and further investigated the glycosylation (sugar labeling) of their antibodies and how that affected their ability to interact with other parts of the immune system. We found more age-based differences that not only encompassed neutralizing antibody responses, but also antibody effector functions (i.e., their ability to activate other immune responses).

Finally, we looked at the impact of timing on hybrid immunity, focusing on the interval between vaccination and infection. We found a steady improvement with increasing interval lengths up to at least 400 days, showing that regardless of the source of primary exposure, a process of immune improvement occurs in the background for an extended period without any additional antigen exposures. Antibodies do wane over this time, but upon subsequent boosting by either vaccine or breakthrough infection the resulting neutralizing antibody response is higher than with any other combination we have observed so far.

Over the course of this work, we learned a great deal about the antibody response to COVID-19 vaccination both with and without infection. We identified several key factors that affect the development of robust neutralizing immunity and identified potential mechanisms of vaccine-induced non-neutralizing antibody activities.

Chapter 1: Introduction

Section 1.1: Preface

The ongoing coronavirus disease 2019 (COVID-19) pandemic has caused far-reaching effects on our world from strained healthcare systems to stagnating global economies. In this dissertation, I will explore one piece of this vast topic: the development of antibody responses over the course of the COVID-19 pandemic with a focus on vaccine-induced immunity. In contrast to my first two examples of negative effects from COVID-19, the rapid conception and widespread deployment of COVID-19 vaccines will stand as one of humanity's great triumphs in the face of adversity. The lessons learned over the course of this pandemic will improve our preparedness for future disease outbreaks.

As of January 2023, the combined efforts of countless scientists and medical professionals have resulted in nearly 320,000 PubMed-indexed COVID-19-related publications and an abundance of knowledge that has helped shape public policy and direct further research. Our understanding of severe acute respiratory syndrome associated coronavirus 2 (SARS-CoV-2) has evolved tremendously over the course of the pandemic, but so too has the virus itself. The timeline below (Figure 1.1) is included to illustrate the interconnected progression of SARS-CoV-2 research and the pandemic itself[1,2]. The benefits of hindsight can be equally as humbling as they are enlightening, and what seems obvious now is often the result of compounding knowledge and hard fought-empirical data.

There is much yet to be learned about SARS-CoV-2. Even its origin remains a subject of debate[3]. The current leading theory is natural zoonotic transmission and subsequent spread at the Wuhan Seafood Market[4–6], but there is a sizable group that believes SARS-CoV-2 may have originated in a laboratory at the Wuhan Institute of Virology before being inadvertently released[7,8].

Regardless of its true origin, SARS-CoV-2 has led to one of the largest pandemics in recorded history, and we still have much to learn, as a society, about preventing and controlling communicable diseases.

Figure 1.1 An abridged timeline of the COVID-19 pandemic

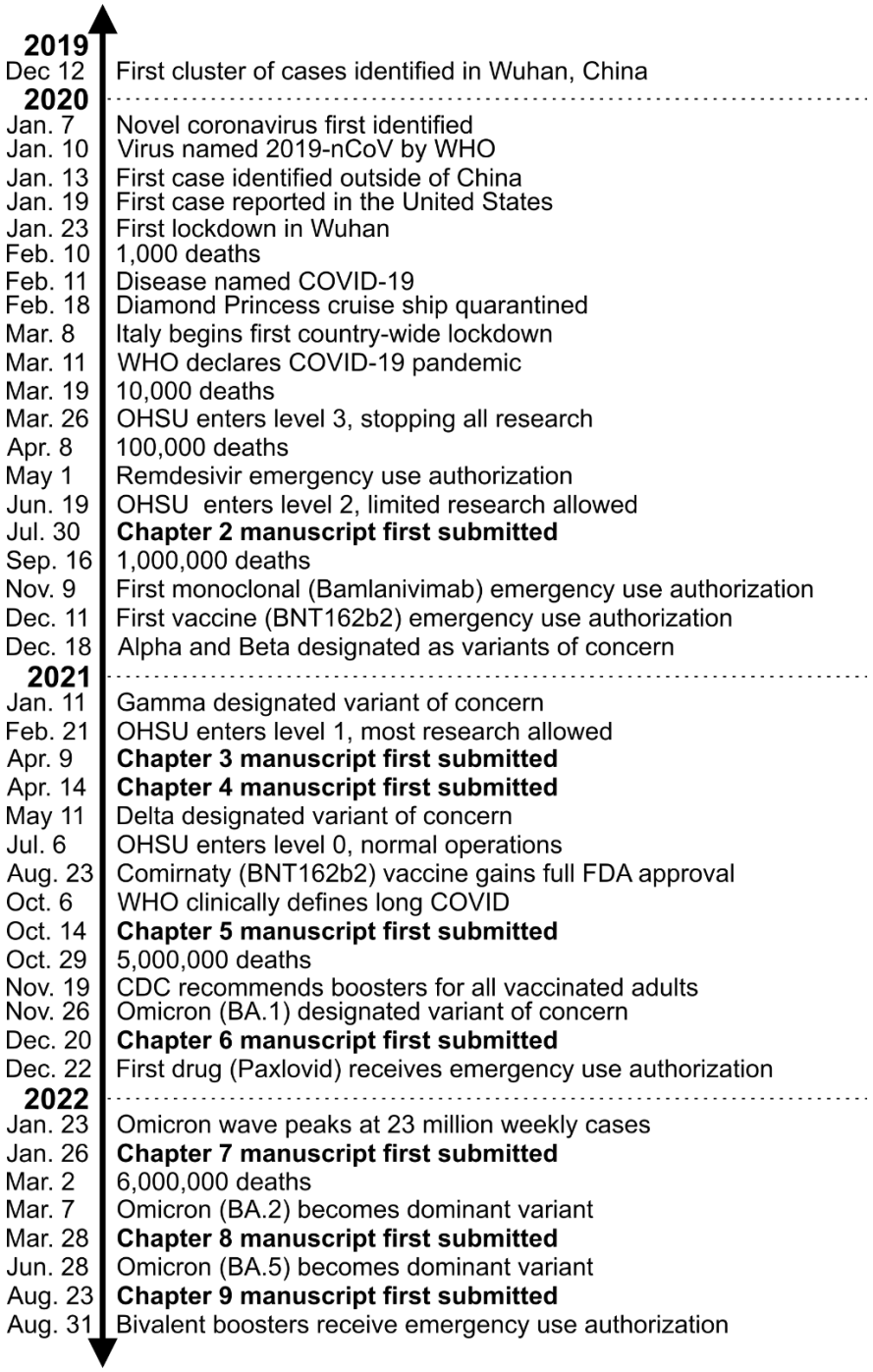

A timeline of the COVID-19 pandemic starting at the first positively identified cases in 2019 in Wuhan, China, through August 2022, when the first variant updated booster became available in the United States. Bold entries show the submission dates of each completed manuscript that make up the chapters of this dissertation.

Section 1.2: Severe Acute Respiratory Syndrome Associated Coronavirus

1.2.1 Phylogeny

Orthocoronavirinae is a subfamily of viruses commonly known as the coronaviruses, which includes SARS-CoV-2[9]. Coronaviruses (CoV) are enveloped, positive-sense RNA viruses with large, non-segmented genomes[10,11]. The name "coronavirus" is derived from their crown-like appearance in electron micrographs, first noted by Dr. David Tyrrell in 1967 after developing improved culture methods for recovering samples from patients with respiratory infections[12,13]. This marked the first identification of coronaviruses in humans, but the first coronavirus to ever be isolated was infectious bronchitis virus (IBV), which was found in chickens in 1931 by Schalk and Hawn and remains a significant agricultural problem to this day[14]. These early investigations into coronaviral diseases were limited by the technology of that time, but were also of limited interest because no coronaviruses were known to cause significant human disease until the first outbreak of severe acute respiratory syndrome (SARS) in 2003[15,16]. Prior to 2003, all known human coronaviruses caused mild disease, colloquially known as the common cold[17].

There are several genera within *Orthocoronavirinae*, of which *Alphacoronavirus* and *Betacoronavirus* contain most coronaviruses that can infect humans. SARS-CoV-2 belongs in genus *Betacoronavirus*, placing it alongside the original SARS-CoV, as well as the Middle East

respiratory syndrome coronavirus (MERS-CoV), and several other common cold viruses, such as HKU1 and OC43[10]. The *Betacoronavirus* genus is further subdivided into several subgenera, including *Sarbecovirus*, which contains SARS-CoV-2, SARS-CoV, as well as other similar SARS-like viruses that infect bats and other mammals[9,18].

1.2.2 Virion structure

Coronaviruses are typified by their distinctive spike (S) glycoproteins, which serve to both bind and enter host cells, but they also produce dozens of other proteins to help with replication. The genome of SARS-CoV-2 contains 15 open reading frames (ORF) that are expressed and cleaved to produce 29 distinct proteins (Figure 1.2A)[18–20], four of which are structural proteins that form the proteinaceous framework of SARS-CoV-2 particles: S, Envelope (E), Membrane (M), and Nucleocapsid (N) (Figure 1.2B). The first two reading frames, ORF1a and ORF1b, produce large polyproteins that are cleaved to form the non-structural proteins responsible for orchestrating numerous critical processes including genome replication, host membrane manipulation, and subversion of host defenses. The other open reading frames, ORF3 through ORF10, also produce proteins with important biological functions, and are often referred to as accessory proteins[21].

Figure 1.2 Genome composition and virion structure.

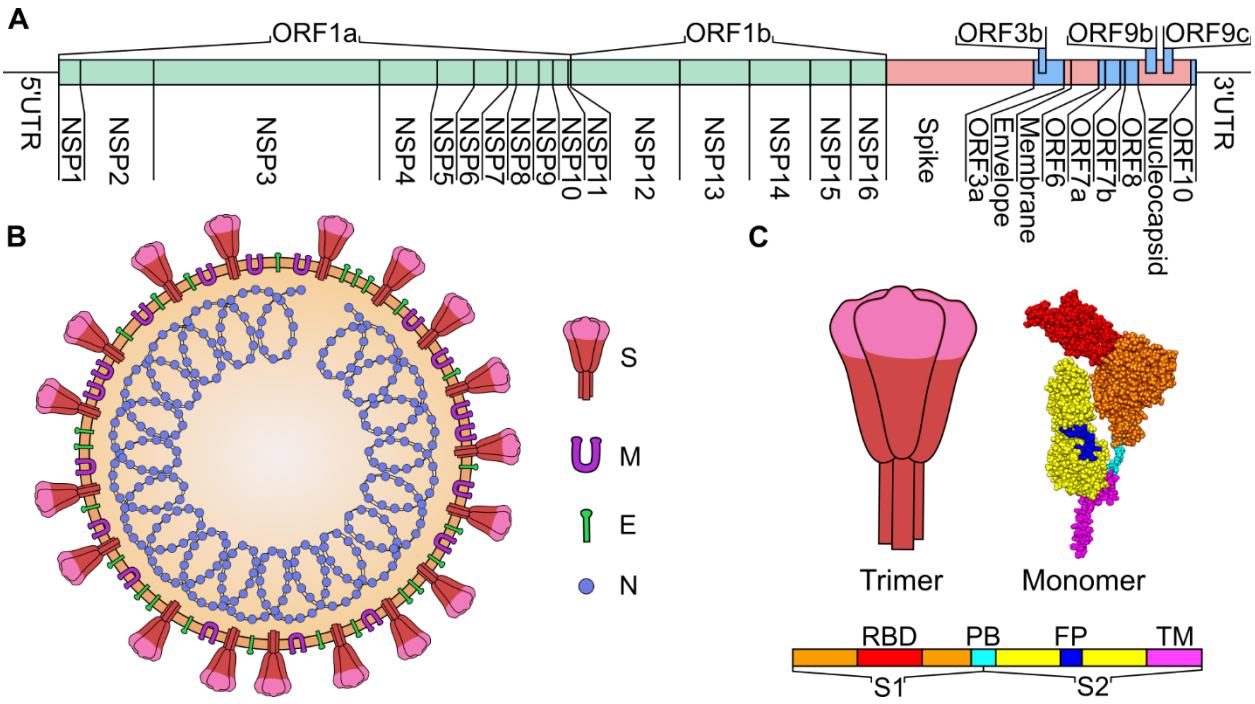

(**A**) The SARS-CoV-2 genome is a single strand of positive-sense RNA which contains open reading frames (ORF) encoding structural (red), non-structural (green), and accessory (blue) proteins. The entire genome is approximately 30 kilobases in length and is bookended by untranslated regions (UTR). (**B**) Virion structure depicting a host-derived lipid envelope studded with Spike, Membrane, and Envelope proteins. The central cavity contains 1 copy of the RNA genome coiled around numerous copies of the Nucleocapsid protein. (**C**) S protein structure. S is always present as a trimer on the viral surface. Each S monomer contains 2 primary domains, S1 and S2. S1 (orange) contains the receptor binding domain (RBD, in red) while S2 (yellow) contains the fusion peptide (FP, in blue) and transmembrane domain (TM, in magenta). The S1/S2 polybasic cleavage site (PB, in cyan) is a short unstructured region between the domains. The TM region shown here is truncated due to difficulties visualizing this region using current

methods. An additional short cytoplasmic tail (CT) is present distal to the TM region but not shown. (PDB: 6XR8).

The surface of SARS-CoV-2 particles are covered with S protein homotrimers (Figure 1.3). The S protein is divided into 2 distinct domains, S1 and S2. S1 is responsible for binding to host cells, which occurs within the receptor binding domain (RBD). Cryo-electron microscopy and fluorescence data have shown that, under physiological conditions, the S protein alternates between RBD up and RBD down conformations, which affects receptor binding and susceptibility to protease cleavage[22]. Only the up state is believed to be capable of binding to the host cell receptor, but it is also more exposed to neutralizing antibodies. Trimers are typically found in mixed states where each spike protein of the trimer independently transitions between the up and down states, and some mutations have been found that can alter the propensity of RBD for the up versus down state[23]. The S2 domain contains the fusion peptide and is responsible for fusing with the host cell membrane. S2 also contains the transmembrane domain and remains attached to the surface of the virus after cleavage, which releases the S1 subunit as a soluble fragment. The other surface-exposed proteins, E and M, help to form the viral envelope[24,25]. E forms a cation channel that impacts viral budding and release via a largely unknown mechanism[26], while M interacts with N to mediate packaging of the RNA genome and facilitate viral assembly[27]. The N protein is the most highly expressed SARS-CoV-2 protein and binds to the RNA genome, facilitating its addition into nascent viral particles[28].

1.2.3 Replication cycle

SARS-CoV-2 infects cells by first binding to angiotensin converting enzyme 2 (ACE2) on the host cell surface (Figure 1.3A)[29–31]. A host cell surface protease, typically TMPRSS2, is needed to activate S to a fusion-capable state by cleaving the polybasic cleavage site within S and releasing

the S1 subunit. This exposes the fusion peptide in the S2 subunit and allows for the necessary conformational changes for fusion of the viral and host membranes (Figure 1.3B). Fusion can occur either directly at the plasma membrane, or viral particles can first be endocytosed and fusion can occur within the endocytic pathway[31,32]. After fusion, the viral genome enters the cytoplasm and is uncoated of N protein. Initial translation produces the first round of ORF1a/b polyproteins which are cleaved into the non-structural proteins (NSP) and other accessory proteins. Together, these proteins remodel the surface of the endoplasmic reticulum (ER) to form double membrane vesicles (DMV) and convoluted membrane (CM) regions[33,34]. The genome is replicated within replication complexes that are also contained within this remodeled space[33]. Single-stranded positive-sense RNA genomes are replicated via a double-stranded RNA intermediate in the DMVs. Following replication, they are brought into the cytoplasm, coated with N protein, and trafficked to the ER-Golgi intermediate compartment (ERGIC), where a single copy of the genome associates with the other structural proteins that are embedded in the ERGIC membrane. Nascent viral particles bud into the ERGIC and are exported via exocytosis.

Figure 1.3 SARS-CoV-2 replication cycle

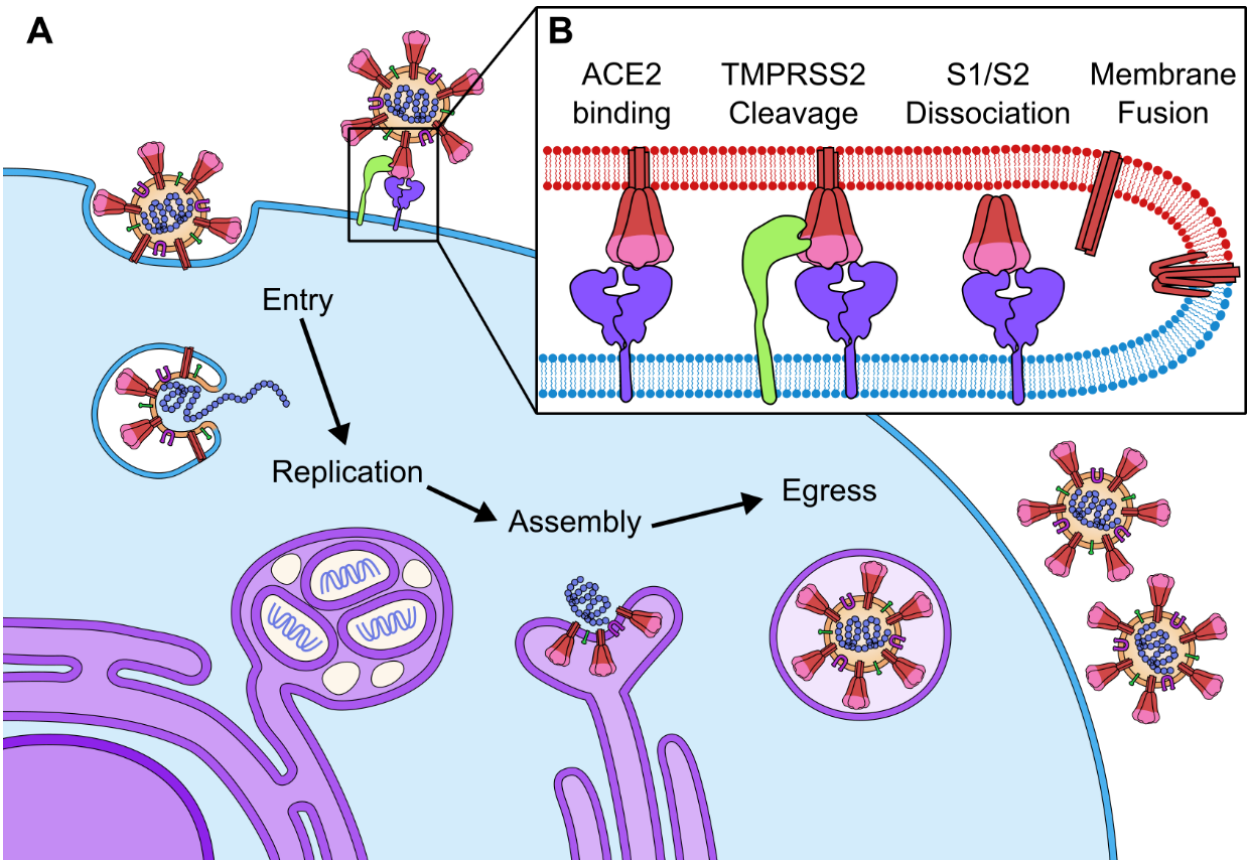

(**A**) Overview of the replication cycle showing entry, genome replication, assembly, and egress of new viral particles. Membrane fusion may occur either directly at the plasma membrane or within the endocytic pathway. The genome is released into the cytoplasm where it is uncoated and primary translation of the ORF1a/b polyproteins begins. Replication complexes form in complex membrane structures which bud from the endoplasmic reticulum (ER). Viral proteins and double stranded RNA are produced in large quantities within these replication complexes. The structural proteins traffic to the ER-Golgi intermediate compartment (ERGIC) where nascent virions bud into the secretory pathway and egress via exocytosis. (**B**) Punchout showing detailed entry process. Intact S in the viral membrane (red) interacts with ACE2 in the host membrane (blue). Host protease (usually TMPRSS2) cleaves S at the polybasic S1/S2 cleavage

site, releasing soluble S1 and membrane-bound S2. The fusion peptide of S2 extends, inserting itself into the host membrane before folding back and pulling the host and viral membranes into close proximity, initiating fusion.

1.2.4 SARS-CoV-2 variants

Mutation is the inevitable process of accumulating genetic changes caused by imperfect replication of the viral genome via the viral RNA-dependent RNA polymerase NSP12. This polymerase prioritizes speed over fidelity in order to replicate its massive genome, but it is followed by a proof-reading exonuclease NSP14[35]. Overall, SARS-CoV-2 generates 10^{-5} to 10^{-3} substitutions per nucleotide site per cell infection, which is substantial given the ~30,000 kb size of the genome[36,37]. This is rate is 10-fold higher than for other RNA viruses (10^{-6} to 10^{-4} substitutions per nucleotide site per cell infection)[38]. Approximately two thirds of mutations do not result in changes to the amino acid sequence of viral proteins; these are called synonymous or silent mutations. The remaining third of mutations do change a protein's amino acid sequence and are called nonsynonymous mutations. Deletion and insertion of nucleotides also occurs, though less frequently because they must occur in groups of three in order to not disrupt the rest of the protein. Generally, whenever the amino acid sequence of a protein is changed, the modified virus is subject to differential selective pressure compared to its parent (i.e., natural selection) leading to a new variant. In principle, a single mutation could be enough to define a new variant, but in practice, individual mutations are far too common to justify naming each one. Different groups have operational terms (e.g., variant, lineage, clade), which are defined pragmatically based on context but generally rely on collections of mutations tracked in isolated samples over time and often focus on functionally differentiable viral isolates. SARS-CoV-2 is tracked by numerous organizations simultaneously, from public health agencies like the Centers for Disease Control and

Prevention (CDC) and the World Health Organization (WHO), and from surveillance/scientific groups such as the Global Initiative on Sharing Avian Influenza Data (GISAID), Phylogenetic Assignment of Named Global Outbreak Lineages (Pango), and NextStrain[39–41].

Due to the number of independent groups working on classification, several naming schemes have found widespread use throughout the pandemic. The first common naming system was based around country of origin, but this was problematic because it incentivized countries to not disclose novel variants to avoid stigma. The WHO devised a naming system based on Greek letters that described epidemiologically-important variants in a tiered structure starting with variants under monitoring (VUM) that posed theoretical risk, variants of interest (VOI) that demonstrated some risk in studies, and variants of concern (VOC) that clearly demonstrated risk in multiple studies[42]. Many public health agencies have similar designation systems, but most are functionally equivalent to the WHO system, which is the primary naming scheme used in the media and in public announcements. The CDC has an additional designation for variants of high consequence (VOHC) that are defined as variants which completely evade current diagnostic tests, vaccines, and treatments, and cause more severe disease. No VOHC has been identified thus far. Scientific groups have developed more nuanced naming schemes which capture greater complexity for use by researchers. Of these, the Pango and NextStrain nomenclatures are used most frequently.

The earliest SARS-CoV-2 samples included two distinct lineages: Pango A and B. It is unclear which came first, so both are interchangeably referred to as the original or ancestral strain. The B lineage later took over, and all of the VOCs are descended from it, which is why nearly all other Pango designations begin with B (Figure 1.4A). The Pango nomenclature attempts to retain phylogenetic information in the naming scheme by including all parental lineages as a prefix to

newly defined lineages such that B.1.1.7 is descended from B.1.1, which is in turn descended from B.1, which is descended from B. One caveat is that longer variant names are often shortened, as in the case of B.1.1.28.1 (Gamma) being shortened to P.1, where the P is equivalent B.1.1.28. Such shorthand has been used extensively for the Omicron (BA) collection of variants. The Nextstrain system prevents this issue by uniquely naming each variant (clade) with the year and a letter based on the date of designation, where 19A was the first clade designated in 2019, and 22C was the third clade designated in 2022. Designation of variants as named clades by Nextstrain is performed manually based on local and global prevalence and prior designation as a VOC[43].

Of the many defined variants, only a handful have ever become a dominant circulating variant (Figure 1.4B). The WHO-defined VOCs are chosen primarily based on prevalence, which is largely a function of transmission advantages. The emergence of each variant has occurred in a different context, in terms of population-level immunity and level of precautions at the time and place where it emerged. This ever-changing context makes it difficult to predict which mutations are likely to be selected for in the future, but certain patterns in SARS-CoV-2 evolution have emerged over time[44–46]. The S protein is a hot spot for amino acid changes. This has been attributed to the protein's importance for viral entry, which is a critical species barrier for coronaviruses[47]. Early distribution of viral lineages across the globe is believed to have been determined primarily by chance[48], but once the majority of the population developed some form of immunity from either infection or vaccination, variants quickly emerged that evaded existing immunity[49–51]. Proposed strategies employed by the variants to gain advantage in the post-vaccine era have included antibody evasion[52,53], improved ACE2 binding[54], increased viral loads[55], and shifted tissue tropism from the lower airways to the nasal epithelium[56].

The number of mutations in each variant has escalated over time. Looking specifically at the S protein, the Alpha variant contains just 9 amino acid changes, while the latest Omicron BQ.1 variant contains 34 changes (Figure 1.4C). It is noteworthy that despite the WHO binning all variants since September 2021 as Omicron, the different Omicron sublineages are quite different from each other in terms of their S protein sequences, as well as their other properties. The BA.1 and BQ.1 variants have 21 differences in the S protein alone.

Figure 1.4 SARS-CoV-2 variant naming and prevalence

A

WHO	Pango	Nextstrain	Date Ideinfied
	B	19A	Dec 2019
Alpha	B.1.1.7	20I	Sep 2020
Beta	B.1.351	20H	Sep 2020
Gamma	P.1[a]	20J	Sep 2020
Delta	B.1.617.2	21A,21I,21J	Mar 2021
Omicron	BA.1[b]	21K	Sep 2021
Omicron	BA.2	21L	Sep 2021
Omicron	BA.4	22A	Jan 2022
Omicron	BA.5	22B	Nov 2021
Omicron	BA.2.12.1	22C	Sep 2021
Omicron	BQ.1[c]	22E	Jan 2022

[a] P = B.1.1.28
[b] BA = B.1.1.529
[c] BQ = B.1.1.529.5.3.1.1.1.1

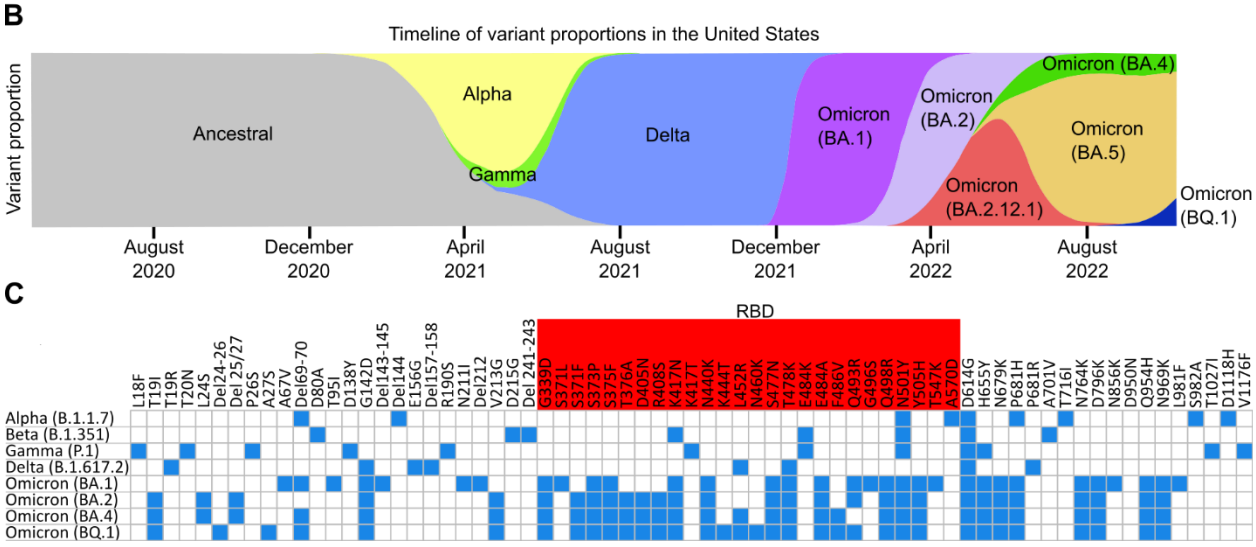

(**A**) Commonly used names for the most consequential SARS-CoV-2 variants. (**B**) Variant proportions in the United States over time. (**C**) Summary of defining spike protein amino acid

changes for the past and present variants of concern. Blue squares indicate the presence of a particular amino acid change in a particular variant. Panel **B** was adapted with permission from covariants.org

1.2.5 Highly impactful mutations

While amino acid changes tend to have an additive effect, there are a number of notorious mutations with well-established impacts on viral fitness or immune evasion. Perhaps the most famous mutation which became fixed early on in the pandemic is D614G. It has been the subject of well over a hundred publications, most of which conclude that it increases SARS-CoV-2 infectivity, in part by increasing the propensity of the RBD for the up position[57,58]. The most studied mutation in the Alpha variant was N501Y, which resides in the RBD, increases ACE2 binding, and evades some antibodies[59,60]. The Beta variant was the first to develop the E484K mutation, which also resides in the RBD and has a substantial impact on neutralizing antibody effectiveness[61,62]. A further RBD mutation that was first noticed in Beta was the K417N mutation, which also contributes to antibody evasion[59,60]. All of these amino acid changes have arisen separately in multiple variants, including contemporary Omicron lineages, suggesting a direct selective pressure in their favor due to their outsized impact on viral fitness via increased antibody evasion and stronger ACE2 binding[63]. There have been several attempts to predict the most likely future mutations that could have a large impact on SARS-CoV-2 vaccine resistance, many of which have been borne out in real-world variants[59,64,65]. While there are countless other mutations, the S mutations described here have continued to provide a strong selective advantage for the virus and thus have repeatedly appeared in novel variants.

Section 1.3: Infection & Immunity

1.3.1 COVID-19 transmission

The primary route of entry for SARS-CoV-2 is now known to be via airborne droplets that are either inhaled or get into the eyes[66–69]; however early in the pandemic there was considerable debate about the most important transmission routes[70,71]. Initial confusion around the precise definition of aerosols led to authorities declaring that SARS-CoV-2 did not exhibit airborne transmission[72], but instead was spread primarily through fomites (i.e., contaminated surfaces)[73]. Regardless of route, the greatest predictor of transmission is time spent in close proximity to infected persons, and both N95 masks and eye protection are recommended to prevent infection in high risk environments[74,75].

The overall transmissibility of SARS-CoV-2 is quite high compared to other pathogens. This can be estimated by the basic reproduction number (R_0), which gives a statistical measure of contagiousness by estimating the number of secondary infections an individual will cause in a fully susceptible population[76,77]. R_0 was estimated to be around 2.5 during the early pandemic, but has increased over time as more transmissible variants emerge, with estimates of up to 8.2 as of May 2022. To put this number in context, measles is often regarded as the most transmissible disease and is frequently cited as having an R_0 of between 12 and 18[78], whereas MERS-CoV has so far been unable to cause widespread outbreaks due to its low estimated R_0 of about 0.5[79]. While R_0 can be useful for making general statements about a pathogen's infectiousness, the actual ability to spread within a population is highly dependent on other factors such as population density, vaccination, existing immunity from previous outbreaks, control measures, and more[76,78]. Perhaps more telling of SARS-CoV-2 infectiousness is its pattern of repeated global outbreaks, often called waves, driven by regular emergence of novel variants.

1.3.2 COVID-19 disease burden

Given the global spread and high transmission rate of SARS-CoV-2, the number of COVID-19 cases has grown to quite a large number. Officially confirmed case counts exceed 636 million as of November 2022[80], and there is good evidence that this is a substantial undercount of true cases, which could be up to 30 times greater than reported cases in the United States and even more elsewhere around the world[81–84]. The prevalence of at-home testing, while helpful to individuals, has only exacerbated the underreporting of COVID-19 cases as self-tested positive individuals are less likely to engage in official testing from medical providers unless their symptoms become more serious. Another factor at play is the rate of asymptomatic infection. The best evidence for the asymptomatic rate arose from cruise ships like the Diamond Princess, where 46.5% were asymptomatic at the time of testing, and 19.2% are believed to have been infected but never developed symptoms[85]. The median age of Diamond Princess passengers was 69 years old, while the crew (a quarter of the total occupants) had a median age of 36. The death rate on the Diamond Princess was 1.3%, which is similar to the overall average death rate of the entire pandemic of 1.03% as of November 2022[80,85]. However, even deaths have been difficult to track properly, and while official counts as of January 2023 put global cumulative deaths at around 6.6 million[80], the true number of excess deaths caused by COVID-19 may be 18 million or more[86–88]. Further, exposure does not always lead to infection. In a challenge study of healthy young volunteers inoculated with 10 infectious particles each, only 53% became infected, as measured by subsequent daily PCR testing[89]. Another study of household contacts during the Delta variant wave found that household contacts of COVID-19 patients had a 25% chance of infection if vaccinated, and 38% if not[90]. Instead, many now support the idea that SARS-CoV-2 is spread primarily via "superspreaders," with several studies showing that approximately 80% of infections

may be transmitted by <20% of people[91,92]. The reason for this phenomenon is largely driven by substantial heterogeneity in viral shedding, the underlying cause of which remains unknown[93]. Given the scale of infections and the length of the pandemic, it seems likely that most people in the world have been infected with SARS-CoV-2 at some point during the pandemic.

1.3.3 Pathogenesis

Due to its reliance on ACE2 and surface protease, SARS-CoV-2 preferentially infects specific cell types during early infection including multiciliated cells in the upper airway, sustentacular cells in the nasal passages, and Type II pneumocytes in the lungs[31,94,95]. The physiological function of ACE2 is to prevent pathogenic overactivation of the Renin/Angiotensin/Aldosterone system. Numerous other tissues in the body also express ACE2 and can thus be infected, such as goblet cells in the gut, the collecting ducts of the kidneys, and endothelial cells in the heart and brain[96–98]. While diarrhea is a common symptom of COVID-19 due to high expression of ACE2 in the gut, and viral RNA is often shed in the feces, pulmonary involvement is more often associated with serious disease[98,99]. The most severe form of COVID-19 is called acute respiratory distress syndrome (ARDS) and is characterized by fluid in the lungs caused by rampant inflammation, leading to poor gas exchange and eventually hypoxemia[95,100]. At this stage, lung damage is significant, and many patients require mechanical ventilation or extracorporeal membrane oxygenation (ECMO). Unfortunately, these treatments cannot address the underlying cause of the ARDS and are simply a means of buying time while the body attempts to fight off the infection and heal enough of the lung damage to breathe unassisted[101,102]. Thankfully, most COVID-19 cases do not result in critical illness. Looking at the Diamond Princess data, approximately 10% of symptomatic infections required intensive care during the early pandemic[85]. However, many factors contribute to the likelihood of hospitalization and

survival, including age, comorbidities, and vaccination status[103–105]. Even the particular variant that causes an infection has been suggested to play a role in relative risk of that infection. Realistically, this is nearly impossible to measure given the many confounding variables including the vastly different levels of population level immunity over time from both vaccination and previous infection, and the difficulty of accurately determining infection history[106–108].

Prompt induction of type I and III interferon responses is critical to controlling SARS-CoV-2, and their absence promotes severe disease[95,109]. Impaired control of viral replication in the lungs leads to productive infection within the lungs, peaking at around 3-5 days post infection and escalating damage to the alveoli[100]. This epithelial damage combined with the ongoing viral infection causes imbalance in the clotting response, leading to excessive fibrin buildup in the alveoli[95,110]. There are several biomarkers of severe disease including the proinflammatory cytokine IL-6, clot breakdown product D-dimer, and growth factor TGF-β[95,100]. Treatment with anti-inflammatory drugs like corticosteroids, IL-6 blocking antibodies, or JAK1/2 inhibitors have been shown to increase survival of severe COVID-19 patients, indicating that severe pathology is driven in large part by uncontrolled inflammation[95,100,109]. Further, COVID-19 can lead to long-lasting symptoms, a disease known as post-acute sequelae of SARS-CoV-2 infection (PASC), long-haul COVID, long COVID syndrome, post-COVID-19 condition, or simply long COVID. Much less is known about PASC than COVID-19 itself, but it often presents with a combination of symptoms including neurological issues like “brain fog” and anosmia, general fatigue, clotting disorders, and immune dysregulation[111]. A large fraction of COVID-19 cases result in PASC, with estimates up to 12% of patients having symptoms that last longer than 12 weeks; most people who develop PASC continue to experience at least one symptom for at least 6 months[109,111].

1.3.4 Innate immunity

The immune response to SARS-CoV-2 depends on the severity of disease as well as numerous other factors including sex, age, and comorbidities. As with most infectious diseases, the innate immune response is first to respond, often acting before the virus can take hold. The innate immune system is responsible for the 47% of individuals who did not become infected in the challenge study[112]. Interferon levels show similar kinetics to viral titers, and impaired interferon responses are highly predictive of severe disease development[100,113]. While this early innate response sets the pace for the rest of the infection, the adaptive response is critical to clear the virus and prevent repeat infections.

1.3.5 Cellular immunity

Despite the topic of this dissertation, it would be remiss not to highlight the importance of cellular immunity in COVID-19. The first cytotoxic $CD8^+$ T cells are observed around 7 days post infection, while viremia is still high[113]. However, for reasons that currently remain poorly understood, severe COVID-19 is often accompanied by a profound drop in the population of T cells[100,113]. In mild disease, robust $CD8^+$ killer T cell and Th1 $CD4^+$ helper T cell responses correlate with viral clearance[113,114]. There is also evidence from a study of B cell-deficient cancer patients that shows $CD8^+$ responses alone provide some protection against severe disease[115,116]. T cells are known to target peptides from nearly all SARS-CoV-2 proteins, and even target some out-of-frame peptide sequences which are incidentally produced during infection[117]. Because of the breadth of peptides that can be targeted by T cells, it is more difficult for SARS-CoV-2 to evade cellular immunity than antibodies through mutation, though cytotoxic T cells cannot interact with viruses until they are already actively infecting cells. Another avenue by which T cells

participate in viral immunity is through $CD4^+$ helper T cells, including T follicular helper (T_{FH}) cells, which are critical for potentiating antibody responses[118] but are not strictly required[119].

1.3.6 Humoral immunity

SARS-CoV-2-specific antibodies first appear an average of 11 days after infection, and once an individual has detectable levels of antigen-specific antibodies they are referred to as seroconverted[120,121]. Antibodies are immunoglobulins (Ig) produced by B cells, which develop through a multi-step process that requires coordination of several different organ systems, typically starting in the bone marrow. The bone marrow contains a type of common blood cell progenitor called hematopoietic stem cells, which continuously generate a multitude of immune and non-immune cell types including lymphocytes, so-called because of their prevalence in the lymphatic system (e.g., lymph nodes). Lymphocytes include B cells, T cells, natural killer (NK) cells, and a handful of other immune cell types[122]. B cells differentiate from a common lymphoid progenitor cell while still in the bone marrow through a series of genetic rearrangements to construct a unique antibody gene. This genetic rearrangement is the primary step for generating the immense diversity of antibodies found within individuals.

To better understand antibodies, it is important to recognize their role in preventing illness. In a general sense, antibodies develop with the purpose of recognizing non-self-substances within the body and interfering with their ability to cause harm. There are many ways for an individual antibody to accomplish this task, but the simplest is just blocking activity through physical binding. When the antigen is on the surface of a virus, this process is called neutralization. When enough of the entry proteins (S in the case of SARS-CoV-2) are blocked by antibodies, a virus will be unable to enter cells and be rendered harmless. Neutralization is thought to be one of the primary mechanisms of protection from SARS-CoV-2[123–125], and robust neutralizing antibody responses

are a correlate of protection for viral infections in general[126–131]. For SARS-CoV-2 specifically, the most common mechanism of neutralization is direct competition with ACE2 or steric hinderance of its interaction with the S glycoprotein. However, some antibodies have demonstrated the ability to disrupt S function by locking it in an inactive formation or perturbing the S1/S2 interaction[132–134]. An additional mechanism that does not fall under the category of traditional neutralization but is nonetheless very common is mucosal trapping of pathogens before they are able to reach epithelial barriers[135].

Beyond COVID-19, many neutralizing antibodies are known which block the effects of microbial toxins, while others can have direct antimicrobial effects through simply binding to their target in sufficient numbers[136–138]. The key to neutralization is twofold: having high enough affinity for an antibody to meaningfully interact with its antigen, and maintaining a sufficient concentration in the affected tissue to overwhelm invading forces. Thus, the challenge of neutralization as a mechanism of protection is this maintenance of functional concentrations of high-quality antibodies, which is further complicated by the fact that a proper neutralizing response should ideally prevent the repeated colonization and signal that an immune response is still necessary. How can the immune system remain ever vigilant for deadly pathogens without incidentally developing a life-long immune response against beneficial microbes? While the scope of this question is vast, an important part of the answer lies in the more nuanced effector functions of antibodies.

Antibodies act as signals to many innate and adaptive immune cells (and some non-immune cells), causing them to behave in specific ways. A simple form of this is opsonization, which is essentially an “eat me” signal from antibodies to phagocytic cells such as macrophages or granulocytes, driving them to take up the opsonized material in a process called antibody-

dependent cellular phagocytosis (ADCP)[139,140]. Opsonization can also refer to the labeling of a pathogen with complement, which is an innate immune pathway that utilizes serum complement proteins to rapidly inactivate pathogens and signal for their removal via phagocytosis. When antibodies are the precipitating factor, this process is called antibody-dependent complement deposition (ADCD)[135,139,141]. Antibodies can also signal for the destruction of infected cells by cytotoxic cells (e.g., NK cells) in a process called antibody-dependent cellular cytotoxicity (ADCC)[135,136,139,142]. There are numerous other roles for antibodies such as marking proteins for antigen presenting cells (e.g., dendritic cells [DC] and follicular dendritic cells [FDC]) or triggering the release of cytokines and chemoattractants. Antibody signaling can be either inflammatory (such as an allergic response) or inhibitory (such as activation of peripheral tolerance). A wholly detrimental process that must also be mentioned is antibody-dependent enhancement of infection (ADE), a process by which sub-neutralizing levels of antibody facilitate infection of primarily phagocytic cells. This process has not been convincingly observed in COVID-19 but is known to occur in other instances as in the unfortunate case of Dengvaxia, a dengue virus vaccine. Dengvaxia caused some recipients to experience more severe disease if vaccinated before natural infection[143]. The many different effector functions and emergent behaviors of antibodies are continuously tuned by the immune system, immunomodulatory drugs, or immune evasive pathogens to achieve what is, depending on the frame of reference, a more favorable outcome. One of the mechanisms of tuning antibody behavior is through the expression of different varieties of antibodies, called classes or isotypes, each of which is optimized for distinct signaling roles and cellular interactions.

1.3.7 Antibody structure and classification

Regardless of class, all antibodies contain the same basic functional components: two binding fragments often referred to as the fragment antigen-binding (Fab), and one signaling fragment often referred to as the fragment crystallizable (Fc), which are all linked together with a flexible hinge region (Figure 1.5A). Every antibody is composed of four separate proteins that are connected via disulfide bonds. This includes two copies each of the heavy-chain and light-chain proteins (Figure 1.5B). Both the heavy and light chains are composed of multiple domains, where the N-terminal domain is a variable domain that determines antigen specificity and is attached to constant domains that are determined by the antibody's class.

Figure 1.5 Antibody composition and classification

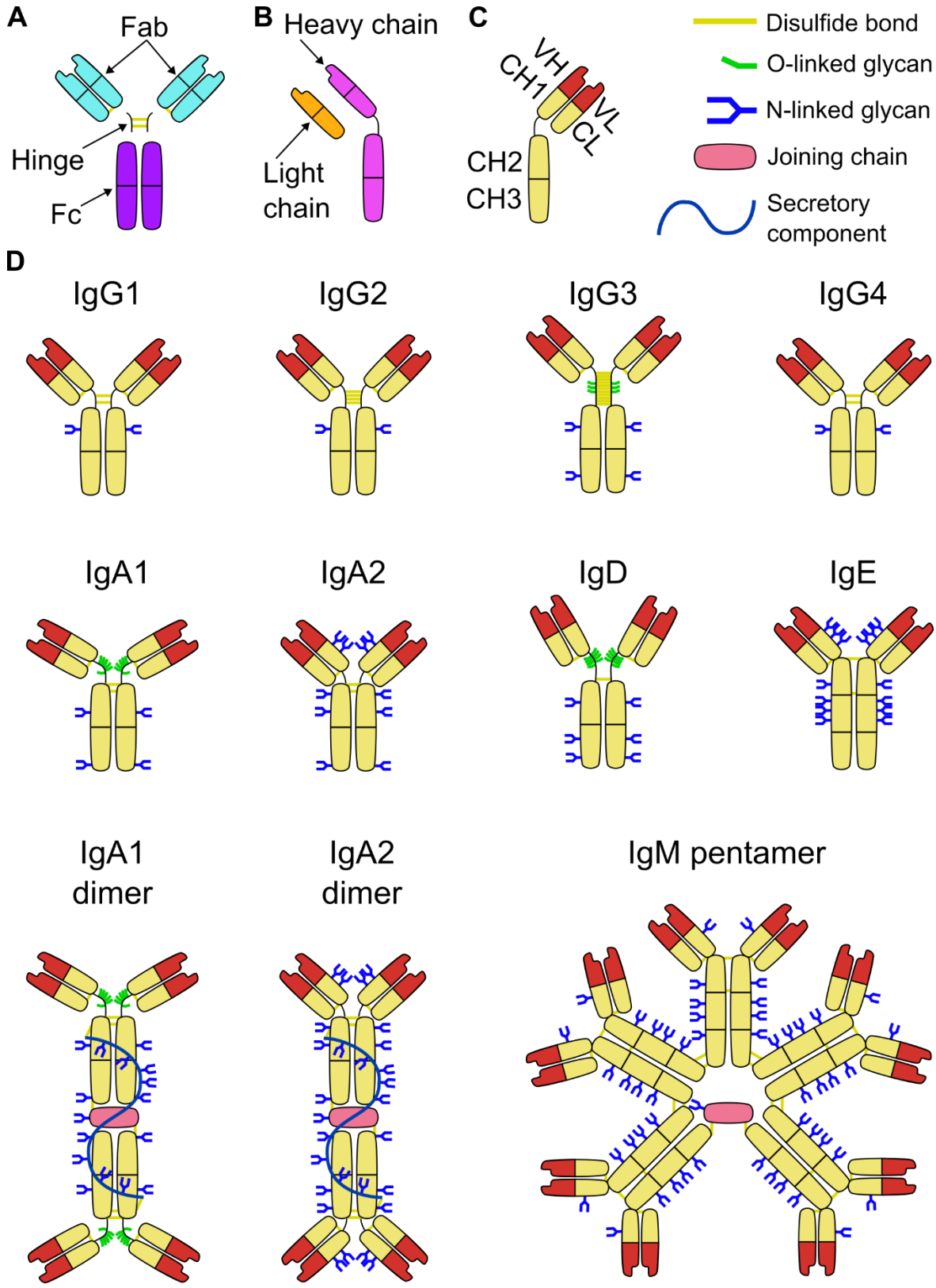

(**A**) Functional antibody fragments include the fragment antigen-binding (Fab), hinge, and fragment crystallizable (Fc). (**B**) The different peptides contained within an antibody include the heavy and light chains that are connected with disulfide bonds. (**C**) The domain structure of the heavy and light chains including the variable light (VL) domain, the constant light (CL) domain, the variable heavy (VH) domain and the constant heavy (CH) domains, of which three are depicted (CH1, CH2, and CH3), although some antibody classes (IgE and IgM) have an additional CH4 domain (not shown). (**D**) The primary antibody classes and subclasses and their respective glycosylation patterns. The IgG class contains 4 subclasses in humans (IgG1, IgG2, IgG3, and IgG4) that differ primarily in the hinge region and in glycosylation pattern. The IgA class contains 2 subclasses in humans (IgA1, and IgA2) that differ substantially in glycosylation pattern and hinge flexibility. Both IgA subclasses are frequently also expressed as a secretory dimer that includes one copy each of two additional proteins: the joining (J) chain and the secretory component. The IgD, IgE and IgM classes do not contain any subclasses, but soluble IgM is almost exclusively expressed as a pentamer (or hexamer without the J chain) connected with disulfide bonds in the CH4 domain and a single J chain.

Each light chain contains a single constant domain, while heavy chains contain between three and four constant domains (Figure 1.5C). The variable domain of each antibody is unique to each B cell clone but shares a common overall structure called the immunoglobulin fold. The specificity of each variable domain is dictated by its three complementarity-determining region (CDR) loops that each protrude from the globular core of the variable domain. One variable light (VL) and one variable heavy (VH) domain interact to form the final paratope, which is the precise arrangement of amino acid residues that bind to an antigen. The part of the antigen that is bound by the paratope is known as its epitope.

The constant domains are determined by the class of the antibody, which a B cell commits to during the late stages of its development. Humans produce five main classes (isotypes) of antibodies with distinct functional roles: IgA, IgD, IgE, IgG, and IgM (Figure 1.5D). The IgA and IgG classes are further split into two (IgA1 and IgA2) and four (IgG1, IgG2, IgG3, and IgG4) subclasses, respectively.

IgG antibodies are the most abundant class found in blood and are the most likely to be neutralizing, making them highly relevant to SARS-CoV-2 immunity[144,145]. IgG1 is the most abundant subclass in human blood. It is also the most commonly used antibody subclass for engineering, and herculean efforts have been made to fully define its clinical impacts. Due to its ability to bind to both inhibitory and activating receptors, IgG1 is able to perform most core antibody functions without substantial modification[139,145–149]. IgG2 is the second most abundant subclass in human serum and is noteworthy for its unique Fc receptor specificity and its resistance to proteolytic cleavage[144,145]. IgG3 is a rare subclass, making up only 4% of IgG in human serum, and has an extended hinge region with additional glycosylation sites that make it bind even more strongly than IgG1 to the activating receptors on phagocytes and NK cells[144,150]. However, IgG3 is also removed from circulation faster than any other IgG subclass for two reasons: its extended hinges are more prone to proteolytic cleavage, and it interacts more weakly with the neonatal Fc receptor (FcRN) that is responsible for recycling antibodies back into circulation after being taken up by cells[139]. IgG4 is another rare subclass that looks similar to IgG1, but has generally reduced effector functionality, and tends to be favored for antigens with repeated exposure such as allergens[144,150].

IgA antibodies are typically discussed for their role as secreted antibodies on mucus membranes and are actually produced in larger quantities than IgG, though most of it is secreted

and quickly shed[151,152]. There is increasing evidence that IgA levels in the nasopharyngeal mucosa are important for SARS-CoV-2 immunity, particularly at early stages which are predominated by infection of mucosal surfaces[152,153]. IgA is present in both peripheral blood and at mucosal surfaces, but in order to be secreted into mucosal tissues, it must be dimerized, which involves expression of two antibodies linked with a joining (J) chain protein. The J chain is recognized by the polymeric immunoglobin receptor (pIgR) on the apical surface of the mucosal epithelium and transported to the luminal side, where it is released by cleaving off the end of the receptor, leaving it attached to a heavily glycosylated protein fragment called the secretory component[154]. The most abundant subclass in both peripheral blood and mucosal surfaces is IgA1, which contains a longer and more flexible hinge region with additional O-linked glycosylation sites[151,152]. IgA2 is less prevalent in most tissues (except for the colon) and more frequently binds to polysaccharides[154]. There are some differences in effector function between the subclasses that have been attributed mostly to differences in glycosylation[151].

IgM antibodies are unique for several reasons. Because of germline gene arrangement, they are the class produced during B cell development and are expressed on the surface of immature B cells[155]. Soluble IgM is also the first antibody class produced by newly activated B cells and is primarily expressed in pentameric form with five antibodies linked together with a single J chain, and less frequently as a hexamer with no J chain[145,156]. Because of its multimerization, IgM can take maximal advantage of avidity, which is the increased binding strength due to the summation of multiple lower affinity interactions. This makes IgM class antibodies with low affinity Fabs more functional than other classes would be with the same Fab sequence. IgM is also a potent activator of complement, allowing for targeted removal of pathogens without an excessive inflammatory response[157,158]. Another interesting subset of antibodies are the natural IgMs, which

are unmodified germline antibodies created by a subset of B cells that are produced from birth and throughout life in the liver[155,158]. These antibodies are relatively low affinity but polyreactive against many common pathogens and they require no antigen recognition to be produced in significant amounts[158].

IgD and IgE antibodies are less well studied than IgG, IgA,and IgM. IgD is an important class for antibody development and is produced as a surface-expressed molecule on immature B cells after leaving the bone marrow[155], while IgE is involved in allergic responses and binds particularly strongly to surface receptors on mast cells, thus triggering degranulation upon recognition of antigen[139].

Each of these antibody classes and subclasses has distinct immunological roles and drives different responses based on their interactions with specific receptors. A common feature across all antibody classes is the presence of glycosylation sites on the heavy chain that can further tune specific responses and, in some cases, can entirely change an antibody from pro-inflammatory to anti-inflammatory or vice versa. There are two types of glycosylation sites: N-linked, which can only be attached to asparagine residues, and O-linked, which can be attached to either serine or threonine. N-linked glycans are more well studied and are built around a core glycan composed of two N-acetylglucosamine (GlcNAc) sugars attached to three mannose sugars that form two branches that are each capped with an additional GlcNAc (Figure 1.6A). There are a set of possible modifications that can be added to this structure, including a fucose on the lowermost GlcNAc (core fucosylation), an additional GlcNAc branch between the existing mannose branches (bisecting GlcNAc), and the terminal GlcNAc units can each be labeled with one unit of galactose that can then be further labeled with one sialic acid. In total, there are 36 possible glycans that can be built with this set of modifications, most of which have been observed *in vivo*[144]. Different

glycans can be attached to each site on an antibody, and the mirrored sites on either heavy chain need not match. Each modification can have profound effects on receptor binding, and the precise impact of each modification on each subclass is an area of ongoing study where much has been uncovered already. For example, the lack of core fucosylation or addition of bisecting GlcNAc of IgG are associated with enhanced ADCC[159–161], sialylation has been shown to cause anti-inflammatory effects[162,163], and the lack of galactose is thought to be pro-inflammatory[164,165]. However, many modifications affect each other: sialylation requires prior galactosylation, and bisecting GlcNAc blocks the enzyme needed for core fucosylation[144,166].

O-linked glycans are much less well studied and more varied in their presentation. There are several different types of o-glycans, but those identified so far on antibodies have been core 1 mucin type glycans (Figure 1.6B)[167]. Antibody o-linked glycosylation occurs specifically in the hinge regions and then only on IgG3, IgA1, and IgD. Galactose-deficient o-linked glycosylation of IgA1 may contribute to kidney damage through increased aggregation[168], but no study thus far has shown specific effects on receptor binding or on effector function from different o-glycans[169]. N-linked glycans, however, are altered by genetics, age, disease, and vaccines, all of which impact immunity[139,144]. At a basic level, glycosylation is regulated by altering expression and activity levels of glycosyltransferase enzymes in the ER, but details about this regulatory pathway are poorly understood[170].

Figure 1.6 Structure of N-linked and O-linked antibody glycans

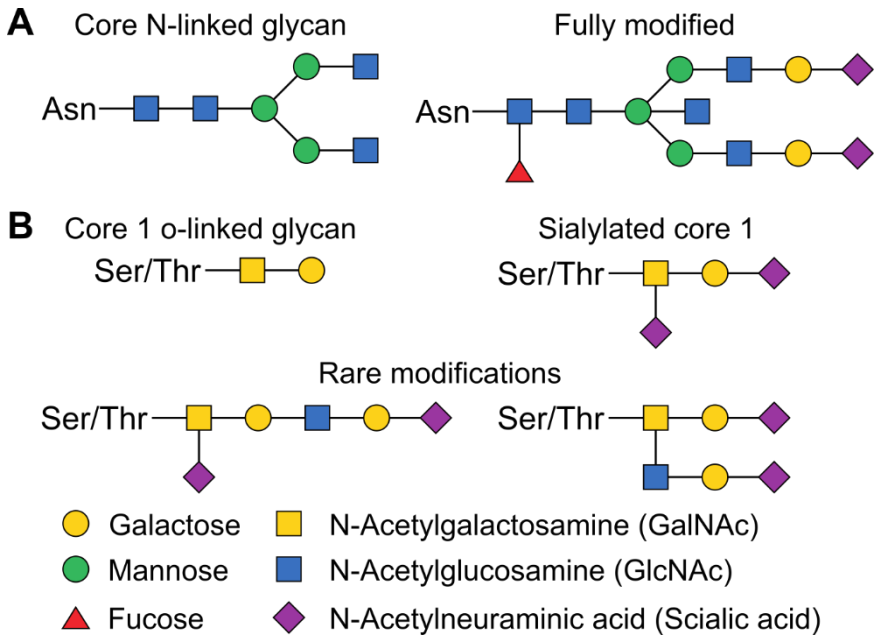

(**A**) N-linked glycans found on antibodies always attach to asparagine and must contain at least the core glycan (left), which can have any possible combination of additional modifications displayed (right). (**B**) O-linked glycans found on IgA1, IgD, and IgG3 antibodies attach to either serine or threonine and typically contain a core 1 glycan (left) that is commonly sialylated (left). Additional modification is possible but rarely observed. Two rare modifications that have been observed on naturally-produced IgA1 antibodies are shown (bottom).

Many seminal works that have helped elucidate antibody form and function have been performed in animal models, so it is worth noting that while all vertebrates produce antibodies, many have evolved distinct classes and subclasses which differ substantially from those found in humans[171]. For example, mice contain the same five basic classes of antibody, but do not have any IgA subclasses, and have five IgG subclasses (IgG1, IgG2a, IgG2b, IgG2c, and IgG3) instead of four. This is important because much of the current knowledge we have about antibody development is performed in mouse models. Other mammals such as rats, rabbits, goats, and

horses are also commonly used to produce antibodies for research purposes, and each has a slightly different number of IgA and IgG subclasses. Camelid species (camels, llamas, alpacas, etc.) produce special IgG2 and IgG3 subclass antibodies that lack the ability to interact with a light chain and are thus referred to as heavy-chain-only antibodies, which are used to generate single domain antibodies, or nanobodies. Leaving the world of mammals, things begin to change more dramatically. Chickens produce only three classes of antibody: IgM, IgA, and IgY. In fact, antibodies were first discovered in chickens. The "B" in B cell stands for bursa of Fabricius, which is an organ in chickens responsible for hematopoiesis and B cell development[172]. Other "lower vertebrates" (e.g., reptiles and amphibians) also produce these three types of antibodies except many produce an IgX in place of IgA, and new isotypes such as amphibian IgF have been recently discovered[173]. Perhaps the earliest lineage of animals to have humoral immunity are the cartilaginous fish (sharks, skates, rays, chimaeras, and ratfish), which diverged about 450 million years ago, produce IgM, IgW (similar to IgD), and immunoglobulin novel antigen receptor (IgNAR; similar to heavy-chain-only antibodies)[174]. IgNAR antibodies are currently being used to generate shark-based single domain antibodies, also called variable domain of novel antigen receptor (VNAR), which are loosely similar to camelid-based nanobodies[175].

1.3.7 Generation of antibody diversity

During early B cell development, the first irreversible step is the generation of the heavy chain gene. The locus responsible for the VH domain contains multiple copies of three distinct gene fragments: the variable (V), diversity (D), and joining (J) segments. The RAG1/2 recombinases are responsible for initiating the VDJ recombination process, which randomly selects and combines one segment of each type[176,177]. The number of possible sequences is tremendous because there are approximately 57 V regions, 23 D regions, and six J regions that are

imperfectly combined by a non-homologous end joining (NHEJ) mechanism, and there is ongoing debate about how many of the numerous additional pseudogenes may be functional in some capacity[178]. The construction of a functional heavy chain gene is a critical checkpoint in B cell development, which is temporarily expressed on the cell surface in conjunction with a surrogate light chain to verify productive recombination and in so doing becomes a pre-B cell[179].

After the successful generation of a functional heavy chain gene, the pre-B cell then generates a light chain from one of two distinct VL loci that are found on completely different chromosomes: kappa (κ) with 41 V and five J regions, and lambda (λ) with 34 V and five J regions[178]. One of these light chain loci is selected randomly by each pro-B cell and VJ recombination occurs, so named because the light chains lack D regions. The matching of this light chain with the heavy chain generated previously creates approximately 3 million possible gene segment combinations, though biased selection leads to some combinations arising more often than expected. This is further compounded by the error-prone NHEJ process which is theorized to increase the total pre-immune antibody diversity to approximately 10^{12} possible sequences; however, this number has yet to be empirically substantiated[180,181]. Furthermore, there are several hundred known alleles for these gene segments that one may inherit, leading to even greater diversity at the population level[178].

The newly constructed antibody gene is initially expressed in a surface-bound form called the B cell receptor (BCR), which can sense antigen binding. Before leaving the bone marrow, the immature B cells are first tested for autoreactivity to self-proteins, which results in apoptosis, further recombination of the light chain, or permanent quiescence (anergy)[182]. At this stage, antibodies are referred to as mature naïve B cells, because they express a randomly generated BCR that is fully formed and non-self-reactive but has not yet encountered an antigen to which it can

bind. The naïve B cells then leave the bone marrow and traffic to the spleen where they must wait until they encounter an antigen that they can engage with or else they will eventually die. Successful antigen binding signals the utility of a particular B cell clone, which then rapidly expands into several distinct populations that execute specific tasks, such as producing large quantities of soluble antibodies, further improvement of antibody binding through somatic hypermutation, and generation of a long-lived memory response.

1.3.8 B cell expansion and further antibody diversification

In the case of a SARS-CoV-2 infection, it is important to start producing useful antibodies as fast as possible. We know from numerous studies that it takes between one and two weeks to develop detectable antibody levels after first encountering a new antigen[183–188]. Much of this delay is due to the time it takes for naïve B cells to activate before they can start producing antibodies, because there are a multitude of naïve mature B cells available at any given time, at least a few of which are usually capable of binding to a newly encountered antigen. Specific VDJ combinations and light/heavy chain combinations are known to perform better against specific antigens, which should ideally be represented in the mature B cell repertoire at the time of infection[189]. The number 10 billion is often used by news and educational websites for the total number of B cells in an adult human, and while I found no peer-reviewed research to confirm this, it is probably a reasonable guess. For example, a study of human B cell counts in peripheral blood found total $CD19^+$ cell counts of 200 per microliter in adults, which would be 1 billion cells assuming five liters of blood volume, thus arriving at the correct order of magnitude after considering the even larger number of B cells in the spleen, bone marrow, and other tissues which are not circulating in the blood[190]. Some antigens, usually polysaccharides with repetitive epitopes, are able to activate immature B

cells directly in the periphery; these are called T cell-independent antigens because they can activate B cells without the assistance of a $CD4^+$ helper T cell[191].

Much more relevant to SARS-CoV-2, however, are the T cell-dependent antigens that comprise most proteins. Due to immune cell developmental pathways that prevent autoimmunity, only mature B cells are capable of T cell-dependent activation, which takes place in secondary lymphoid organs such as the spleen and lymph nodes[192]. Activation is initiated when a naïve mature B cell encounters its cognate antigen presented by an FDC. The B cell will internalize the antigen that bound to its BCR, display peptide fragments on major histocompatibility complex (MHC) II receptors, and wait for a cognate T_{FH} cell to both recognize one of these peptides and provide stimulatory signals to activate the B cell, allowing it to proliferate. Some of the new cells will move to the extrafollicular space and immediately become short-lived plasma cells (PC) that produce IgM[193], while others will traffic to follicles and establish a germinal center (GC) in which they will undergo an affinity maturation process that will improve the quality of their antibodies[194]. This step involves a process known as somatic hypermutation (SHM) that utilizes a particular enzyme. This particular enzyme, called activation-induced cytidine deaminase (AID), induces DNA damage semi-specifically within the Ig gene, the imperfect repair of which generates new diversity in the previously clonal population inside the GC[195]. This process is tightly controlled, and B cells that either become autoreactive or fail to improve sufficiently undergo apoptosis. In each round of SHM, only the top 10% or so of B cells survive, and in order to do so a B cell must obtain antigen from an FDC by physically ripping it from the FDC cellular membrane, internalizing it, and presenting the fragments to a T_{FH}[195,196]. There are many GCs throughout the body, and at any given time, each one can hold approximately 100 unique clones comprised of newly entering founder cells and cells that have already undergone one or more rounds of SHM[195].

Class-switch recombination (CSR) is another process that occurs simultaneously within GCs whereby the antibody genes recombine to replace the original IgM gene with that of a different class[197]. Cytokine signals can drive B cells towards specific antibody classes, which allows the immune system to preferentially generate antibodies that will be useful against a specific pathogen[197].

Clones that leave the GC then proliferate and differentiate into long-lived PCs and memory B cells (MBC), creating a second wave of antibody production that follows very shortly behind the first wave of IgM from the short-lived extrafollicular PCs[195]. Current evidence also suggests that young GCs tend to produce more memory B cells with relatively few mutations, while mature GCs produce more PCs with more mutations[196]; more mutations generally equate to greater affinity, but also greater specificity (i.e., less breadth). This mechanism is thought to balance rapid production of high affinity antibodies with the creation of memory B cells that are not overly specialized based on a single encounter with antigen. However, different antigens and pathogens may also promote different response kinetics.

SARS-CoV-2 results in particularly poor initial IgM production (possibly due to pre-existing coronavirus immunity[198]), so IgG and IgA, which come from this second wave antibody production, are often the first to reach detectable levels in the serum around day 11 post-infection[121]. Antibody levels following primary infection with SARS-CoV-2 peak 4-5 weeks post infection and then decline over the following months with a half-life of roughly 26 days[199–201]. This decline is nonlinear and combines the rapid loss of short-lived PCs with the slower waning of long-lived PCs that are derived from GC optimized B cells. However, some of the long-lived PCs can migrate to the bone marrow, where they can live almost indefinitely and continue to

produce antibodies. SARS-CoV-2 infection successfully induces long-lived bone marrow PCs and MBCs[202,203].

1.3.9 Secondary infection and memory responses

Once the primary immune response has set up the first round of memory cells, most of which are class switched, then additional exposure to antigen will result in a much more rapid response with much higher antibody levels[155]. Furthermore, continued GC activity may persist for an indeterminate amount of time after recovery from infection, depending on poorly understood factors including the long-term availability of antigen[204,205]. Reactivation of MBCs can occur with or without T cell help, depending on the form of the antigen; soluble antigens are less effective at reactivating MBCs and thus require T cell assistance, whereas membrane-bound antigens appear to be more potently activating and less T cell-dependent[196,206]. Additionally, class switched MBCs tend to reactivate more easily than IgM memory B cells, and IgG MBCs in particular reactivate the most readily[207]. Reactivation can mean a memory B cell returns to a secondary lymphoid organ to go through more rounds of GC-mediated SHM, or it can differentiate into a PC and start producing antibodies. The current hypothesis for this is that IgG and other class switched memory cells tend to have greater levels of SHM and are more useful against highly related antigens but are susceptible to escape by variants, while IgM memory cells tend to have fewer mutations and form a backup population of memory cells that initially bind relatively poorly but retain the plasticity of naïve B cells and can be tuned by SHM to target new pathogen variants[196]. This further suggests that the immune system has evolved to deal with the threat of pathogen antigenic drift, which escapes existing humoral memory.

1.3.10 Measurement of antibodies

Knowledge is power in the fight against infectious disease, and we must understand as much as possible about how the immune system responds to threats in order to create better medicines. This knowledge comes in the form of data and in the form of theoretical frameworks that are used to interpret that data. Technological advancements have led to continuous progress in the battery of tests and assays available to us today, but it is important to remember that much of the groundwork laid by early pioneers in immunology was performed using simple techniques and elegant experiments that often involved injecting the bodily fluids from diseased animals into other healthy animals or vice versa. These practices have largely fallen out of favor due to cost and ethical concerns, replaced by modern assays that typically use highly optimized reagents to provide DNA sequences, glycan profiles, and antibody functional measurements. This was very apparent in the early stages of the SARS-CoV-2 pandemic when it took less than a month to isolate, culture, image, and sequence this virus that was previously unknown to science[208].

Nearly everyone will be familiar with some of the specific tests for SARS-CoV-2, such as the lateral-flow rapid antigen test (which uses N-specific antibodies), and the PCR test for measuring viral genome concentration in a sample[209]. Direct measurement of antibody levels is less common for the general public, but routinely performed in the laboratory environment. Enzyme-linked immunosorbent assays (ELISA) are the workhorses of many serology labs because they quickly and accurately determine the concentration of nearly any biomolecule, provided that reagents exist that specifically bind to it. Reagents for measuring human antibodies in serum are extremely common and validated off-the-shelf, high-throughput assays already exist for measuring levels of specific antibody classes[210].

The largest studies in the SARS-CoV-2 immunity field tend to rely on extremely simple metrics in order to simplify workflow and increase cohort size (and therefore power). Relative infection risk is seen commonly because it requires no laboratory tests beyond what is already performed as part of medical care for individuals[211–214]. More sophisticated studies will also look at total spike or nucleocapsid antibody levels measured by ELISA[215,216]. This helps correlate infection risk data with an objective serological measurement, but not all antibodies are created equal, and total anti-S antibody levels often fail to pick up nuances in antibody quality that can dramatically affect infection risk. Nonetheless, data from ELISA experiments are incredibly useful and are usually tested by performing the assay on a serial dilution of a blood sample. Data from these experiments are fit to a dose-response curve, and an EC_{50} value can be calculated, quantifying the amount of blood necessary to give 50% signal in the assay. However, what exactly this value means depends on many factors including the quality of the reagents, the precise quantities used, and even the incubation time at each step. Because of this, it is best not to compare ELISA results between different laboratories, but instead compare them within the studies from a single laboratory. The inability to compare ELISA results between labs can be alleviated by using a validated commercial ELISA kit and careful controls, but caution should be exercised regardless.

When simple antibody concentration is insufficient, many labs will also attempt to measure the ability of patient samples to neutralize virus[217–219]. The ideal method for characterizing this ability involves combining live SARS-CoV-2 with patient samples and measuring how much a blood sample is needed to block the virus from infecting cells. Plaque assays (invented in 1952 by Renato Dulbecco of DMEM fame) are traditionally used for this measurement[220]. In a plaque assay, a monolayer of cells is infected with a small number of infectious viral particles in a viscous media that prevents the virus from rapidly spreading throughout the entire plate. Being restricted

to a localized area, the virus spreads from cell to cell, killing a small circle (i.e., forming a plaque) as it goes. The number of plaques, also referred to as the plaque forming units (PFU), quantifies the amount of infectious virus that was added to the well. Performing this assay with serially diluted blood samples can provide the amount of blood necessary to block infection. The PFU data at different sample concentrations can then be fit to a dose response curve, which gives the quantity that blocks 50% of infection, i.e., the 50% plaque reduction neutralizing titer ($PRNT_{50}$). This assay is the gold standard when it comes to measuring viral infectivity[221–223], but it works best for highly cytolytic viruses, which rapidly kill cells and form clear plaques. SARS-CoV-2 prefers to keep its host cells alive because its mechanism of viral egress does not require rupturing the cell. As a result, alternative methods are needed for measuring SARS-CoV-2 infectivity.

The focus forming assay is an ideal option to circumvent this issue[222]. Foci are regions of infected cells in a monolayer with viscous media, similar to a plaque except they cannot be read by eye and must be developed with a reagent. Most common for this purpose is a SARS-CoV-2-specific antibody linked to an enzyme, like horseradish peroxidase (HRP), which can convert a soluble precursor into a solid dye within infected cells, creating colored spots (foci) that can be counted. When measured in this way, the quantity measured is called the 50% focus reduction neutralization titer ($FRNT_{50}$). Plaque and focus assays produce incredibly reliable results, but require a significant amount of time and resources, particularly for pathogens with biosafety concerns like SARS-CoV-2, which is classified as a biosafety level 3 (BSL-3) pathogen in the United States, requiring dramatically more training and safety equipment than BSL-2.

For this reason, assays to estimate neutralizing titer without using live virus are used by many labs. An easy but less accurate version utilizes a competition ELISA, which tests the ability of antibodies to block the S-ACE2 interaction[224,225]. More common and more accurate are

pseudoviral assays, which use live BSL2 viruses (such as a lentivirus) that have been engineered to express the S glycoprotein instead of their natural receptor[226–229]. Pseudoviral assays are more accurate because they involve antibodies blocking (or failing to block) S-bearing viral particles from binding and fusing with ACE2-displaying cells. In order to make quantification easier, the pseudovirus can also be engineered to express a reporter such as green fluorescent protein (GFP) or luciferin[226]. Newer systems have also been created that attempt to better recreate the SARS-CoV-2 virus, such as virus-like particles (VLP) that contain the primary structural proteins and a reporter gene in a replication-deficient particle[230]. Both pseudovirus and VLPs allow for rapid generation of S variant particles and do a remarkable job of recapitulating the entry stages of SARS-CoV-2 infection. They have been extremely useful in assays for testing monoclonal antibodies and patient samples against new and theoretical S protein variants; however, these assays ultimately need to be compared to real plaque/focus assays with genuine SARS-CoV-2 in order to validate their accuracy and check for unanticipated effects such as altered spike protein glycosylation on pseudoviral particles[231,232].

For antibody assays, most studies use patient serum samples. Serum is a blood product that results from collecting whole blood, allowing it to clot, and spinning out the solids to obtain a yellow liquid that contains only soluble components such as antibodies. Serum is generally also heat-treated prior to testing in order to inactivate complement and eliminate contaminating microorganisms. On one occasion, I inadvertently used samples that were not heat-treated for a live-virus neutralization assay, and upon adding virus to the serum sample, the whole tube turned to a viscous gel presumably due to complement and/or activation of soluble clotting factors. Occasionally, studies will instead use plasma, which is whole blood that has anticoagulant added to it and spun carefully to obtain three layers: the plasma layer on top with antibodies and soluble

proteins, the buffy layer containing live and intact white blood cells including B cells, and the red blood cell layer on the bottom. This technique is used by laboratories that want to collect B cells from patient samples for further analysis such as antibody gene sequencing.

Beyond aggregate binding and neutralization from serum that contains an unknown mixture of antibodies, visualizing individual antibodies requires more sophisticated techniques. These techniques primarily involve collecting antibody producing cells from peripheral blood samples and testing them individually for SARS-CoV-2 reactivity[202,233,234]. Sequencing of the antibody gene from these clones provides another level of detail that can help answer questions like which V(D)J combinations result in the best antibodies, and how quickly memory cells are mutating over time in response to variant antigens[235,236]. However, sequencing of antibodies is not straightforward because they are composed of two distinct proteins: the heavy and light chains, which are produced from different transcripts. Labs have designed several techniques for isolating and barcoding input DNA in order to preserve their association on a per cell basis[237,238].

Some questions can still only be answered using animal infection models as we are not yet capable of simulating an intact immune system in a dish, and not every important research question is suitable for a human subject study. Relatively few model systems were available early in the pandemic[239], but at this point, many different approaches in many species have been designed to answer specific questions[240]. Many studies of viral transmission, pathology, and cellular responses to SARS-CoV-2 have led to valuable insights including the value of mask wearing as a preventative measure and the origin of COVID-19 symptoms such as anosmia (loss of smell)[240]. The wide variety of vaccines, drugs, and antibodies that were developed at lightning speed were all also tested for safety and efficacy in pre-clinical animal models prior to human trials, ensuring the safety of human research subjects. Organoid and organ-on-chip technologies have advanced

tremendously in recent years, and there may come a day when these in vitro systems can sufficiently recapitulate the complexity of the human immune system, but significant technical hurdles remain, and animal models are likely to be necessary for several decades to come[241,242]. However, not even animal models can fully capture the idiosyncrasies of the human immune system, and the highest quality of data possible are generated by carefully designed human challenge models. A few brave souls have stepped up to volunteer in two COVID-19 human challenge studies that have given us valuable insights into the true risk of infection from a controlled level of exposure[89,243].

Section 1.4: Vaccines

1.4.1 A brief history of vaccines

Attempting to avoid disease is a natural instinct that exists in nearly all animals and does not even require a brain[244]. But, to make the counterintuitive decision to intentionally expose oneself to all or part of a pathogen takes a level of critical thinking found so far only in humans. The earliest form of this intentional self-exposure was called inoculation and was performed to protect from smallpox by taking material from the boils on infected persons and giving it to healthy individuals. This was practically guaranteed to make the healthy person ill, but was safer than acquiring smallpox naturally, and provided some immunity against future infections. This practice was based on the observation that those who previously recovered from smallpox were much less likely to die during subsequent outbreaks. Historical documents suggest that this practice was perhaps being performed as early as 200 BCE in what is now China[245], though it seems very likely that its first use would predate its first written account. Despite being somewhat safer than naturally acquired smallpox, this process of inoculation often proved fatal and sometimes initiated localized outbreaks[246,247].

The next real advancement didn't come until Edward Jenner showed in 1796 that inoculation with cowpox and/or horsepox viruses, which cause much milder illness in humans, can confer similar protection against smallpox[248,249]. This was the first true vaccine, and it showed that it was possible to immunize against a disease using a method that carries minimal risk. This breakthrough discovery would ultimately lead to the eradication of smallpox. Nearly a century later, in 1881, Louis Pasteur discovered the process of attenuation, which involves damaging a pathogen enough to weaken but not kill it[250]. Pasteur started by making vaccines against rabies and anthrax using this method, and attenuation became the catalyst for a revolution in vaccine design. This led to vaccines being developed for tuberculosis and yellow fever using a different kind of attenuation in which human pathogens are passaged repeatedly in live animals until they no longer cause serious disease in humans[246].

The next major advancement was cell culture, which enabled the growth of cells and viruses outside of living animals, allowing for more rapid research, more flexibility in process design, and cleaner production methods. Jonas Salk's polio vaccine was the first major vaccine to use this technology by producing large quantities of virus in human cell cultures and inactivating it with formaldehyde. It was used in conjunction with a live attenuated polio vaccine that was developed by Albert Sabin[246,251,252]. However, inactivated vaccines were not a new concept; they had first been used in the late 1800s against typhoid, cholera, and plague[253]. Like Salk's polio vaccine, these earlier vaccines also used whole inactivated organisms; however, effective immune responses do not always require the whole organism, and other vaccine types were developed that used individual parts of pathogens such as toxoids, polysaccharides, or proteins[246].

As the field of biochemistry developed further, recombinant protein expression techniques made it possible to produce specific proteins on demand. The first vaccine to take advantage of

this was the hepatitis B vaccine, which consisted solely of purified recombinant HBsAg protein that was produced in yeast and purified by affinity chromatography[254]. Protein subunit vaccines like this often require an immunostimulatory component called an adjuvant, which helps convince the immune system that the foreign protein is a sufficient threat to warrant a full immune response. An entire field of study has emerged around finding better adjuvants that stimulate more robust and longer-lived immune responses[255]. Protein subunit vaccines are now widely used, are generally easier to make than live vaccines, and can be used in immunocompromised individuals, but it is not always possible to produce stable recombinant proteins that can survive manufacturing and storage conditions. Another approach that has been used successfully is VLP vaccines. The first VLP vaccine was against human papilloma virus (HPV), which is composed of recombinant proteins that assemble into particles resembling native virus that can be more immunostimulatory than individual soluble proteins[256,257]. Other VLP vaccines made with proteins that do not self-assemble are also being explored using different strategies[258,259].

Given the success of protein subunit vaccines, two new vaccine types are being explored that result in the production of antigens within the body instead of externally: nucleic acid vaccines and viral vector vaccines. Viral vector vaccines use avirulent versions of well-known viruses as a backbone to which genetic material encoding a target antigen is added[260]. There are several advantages to this strategy such as strong immune stimulation by the vector and rapid production using well established cell culture techniques, but steps will need to be taken to address immunity against viral backbones and how that will impact future vaccinations. Nucleic acid vaccines, the second new vaccine type, have taken the world by storm since the COVID-19 pandemic. These vaccines involve isolating DNA/RNA that codes for an antigen of interest and introducing it into the body in such a way that it enters the vaccinee's cells and is expressed. There are many ways

that this can be accomplished, but the most well-known method at this point is RNA delivered via lipoparticle (acting as both vehicle and adjuvant), which is the technology that was used to make the first COVID-19 vaccines. Both viral vector- and nucleic acid-based vaccines are still very new technologies, and it is exciting to think what may be accomplished with them in the not-so-distant future. It is not unreasonable to think that either of these technologies could be used to design a common delivery system with well characterized safety and immunogenicity that can be rapidly adapted to immunize against nearly any pathogen, and even against non-infectious diseases like cancer.

1.4.2 COVID-19 vaccines

There are currently three vaccines fully approved in the United States for prevention of COVID-19: Pfizer-BioNTech's Comirnaty (previously BNT162b2), Moderna's Spikevax (previously mRNA-1273), and Novavax (previously NVX-CoV2373). An additional vaccine, Janssen's Jcovden (previously Ad26.COV2.S), remains approved for emergency use only. Comirnaty and Spikevax are both mRNA-lipoparticle vaccines that encode for the spike protein and together were the first COVID-19 vaccines to be approved for emergency use; they both received emergency use authorization less than one year after the start of the pandemic in December 2020[261–263]. Novavax is a subunit vaccine which contains recombinant spike protein and was approved in October of 2022[264,265]. Jcovden is an adenoviral vector vaccine which encodes for the spike protein[266]. Numerous other vaccines have been developed around the world as well, using these and different technologies (Table 1.1).

In addition to these vaccines, several updated boosters have been released that use spike protein from an updated variant. The Vidprevtyn Beta vaccine from Sanofi was originally designed against the Beta variant and was intended to be used as a booster. The Beta variant has not been in

significant circulation since July 2021, but it represented the most vaccine-resistant variant up until the emergence of Omicron BA.1, which will be discussed further in later chapters. More recently, both Pfizer and Moderna released updated versions of their vaccines, respectively renamed Comirnaty and Spikevax. These updated versions are targeted at the Omicron BA.5, which was still actively circulating when the updated boosters were released at the end of August 2022[267]. At that point in time, publicly available data on these updated boosters were sparse, leading to some questioning the rationale behind the decision to approve the updated boosters so soon[268]. One of the main advantages of the mRNA system is ostensibly the ability to rapidly update the nucleic acid to account for variants, and early data showed no significant change in the safety profile of the updated boosters[269]. The decision to roll out the updated boosters was further vindicated when follow up studies showed significant improvements in vaccine efficacy against circulating variants for the updated boosters relative to the original vaccine[270].

Name	Technology	Company	Efficacy[a]	Fully approved[b]	Emergency use[c]
Comirnaty[262]	mRNA	Pfizer-BioNTech	95%	41	145
Vaxzevria/ Covishield[214]	Adenoviral vector	Oxford/ AstraZeneca	74.0%	35	162
Spikevax[263]	mRNA	Moderna	94.1%	35	107
Vidprevtyn (Beta)[271]	Subunit	Sanofi-GSK	64.70%	30	0
BBIBP-CorV[272]	Whole inactivated	Sinopharm	78.10%	4	121
Novavax[265]	Subunit (VLP)	Novavax	90.4%	4	67
Jcovden[266]	Adenoviral vector	Janssen	66.9%	3	152
Sputnik V[273]	Adenoviral vector	GRIEM[d]	91.6%	3	78
CoronaVac[274]	Whole inactivated	Sinovac	83.5%	2	80
Covaxin[275]	Whole inactivated	Bharat Biotech	77.8%	1	59
VLA2001[276]	Whole inactivated	Valneva SE/ Dynavax	Vaxzevria[e]	1	32
Convidecia/ PakVac[277]	Adenoviral vector	CanSino Biologics	63.7%	1	9
WIBP-CorV[272]	Whole inactivated	Sinopharm	72.80%	1	5
EpiVacCorona[278]	Peptide	Vector Institute	Ineffective[f]	1	4
Covifenz[279]	VLP	Medicago	69.5%	1	0

Table 1.1 COVID-19 vaccines with full approval in at least one country

[a] Efficacy against symptomatic COVID-19 reported by the developing company in initial press release or initial peer-reviewed article describing a phase 3 clinical trial. This does not control for the variant distribution during the timeframe in which the study was performed.

[b] Number of national governmental agencies that granted full approval for commercial sale.

[c] Number of national governmental agencies that granted temporary emergency approval for use.

[d] Gamaleya Research Institute of Epidemiology and Microbiology.

[e] VLA2001 was only tested for non-inferiority to Vaxzevria (ChAdOx1) and was found to elicit higher neutralizing responses with non-inferior seroconversion rates. This was done because the study designers felt it was unethical to include a non-vaccinated control group.

[f] Official clinical trial results not available; third-party peer reviewed clinical trial found no measurable protection.

1.4.3 A deeper look at mRNA vaccines

Most of this dissertation will concern itself with the immune responses to mRNA vaccines, particularly the Pfizer vaccine. As the majority of this work was published prior to the full approval and subsequent name change to Comirnaty, BNT162b2 will be the most common name referenced by most chapters. The first thing to consider are the ingredients and their purpose. According to the package insert, each 0.2 mL dose of the original monovalent BNT162b2 vaccine contains: 3 µg of modRNA encoding the S glycoprotein of the SARS-CoV-2 Wuhan-Hu-1 strain (Original), lipids (0.04 mg ((4-hydroxybutyl)azanediyl)bis(hexane-6,1-diyl)bis(2-hexyldecanoate), 0.005 mg 2[(polyethylene glycol)-2000]-N,N-ditetradecylacetamide, 0.01 mg 1,2-distearoyl-sn-glycero-3-phosphocholine, and 0.02 mg cholesterol), 3.2 mg sucrose, 0.006 mg Tris, and 0.04 mg Tris-HCl. The diluent (sterile 0.9% Sodium Chloride Injection, USP) contributes 1.52 mg sodium chloride per dose.

The most important component is the modRNA, which takes advantage of a huge amount of development work that was well underway before the start of the pandemic[280,281]. It consists of a single positive sense RNA molecule encoding the full S protein with several key modifications that allow it to be efficiently translated in the cells of a vaccinated person[282,283]. First, the mRNA contains N1-methyl-pseudouridine (m1Ψ) (in place of standard uridine), which dampens the innate immune response, allowing more protein to be produced before the cells producing the protein are attacked by the adaptive immune system. Second, the protein contains two mutations (K986P, V987P) that lock it in the prefusion state, stabilizing important epitopes and preventing it from fusing host membranes[280]. Third, the gene itself is codon optimized, which means that silent mutations were made that take advantage of the natural abundance of tRNAs to enhance expression, and it contains the native signal sequence, ensuring proper localization and processing of the nascent protein through the ER. This codon optimization must also take the m1Ψ modification into account because of its different properties in the wobble position[283]. Fourth, it contains a modified 5′ cap molecule, ($m_2^{7,3'\text{-O}}$)Gppp($m^{2'\text{-O}}$)ApG, which is an analog of Cap 1 and has been shown to reduce innate immune response to mRNAs[284,285]. Fifth, the 5′ and 3′ UTRs were selected from human proteins with high expression rate (α-globin), with a slightly modified Kozak sequence for 5′ and a 3′ UTR that combines elements from two other highly expressed proteins (AES and mtRNR1)[283,286]. As a result of these features, BNT162b2 can drive expression of high levels of prefusion-stabilized S trimer for the adaptive immune system to recognize and respond to.

The lipids form the structure of the lipoparticle and are essential for the effectiveness of the vaccine. The formulation of the lipids contains four components, each with important roles[287]. ((4-hydroxybutyl)azanediyl)bis(hexane-6,1-diyl)bis(2-hexyldecanoate) is an ionizable lipid with a

positively charged tertiary amine that offsets the charge of the modRNA, allowing it to incorporate into the lipoparticles and helping it facilitate membrane fusion once the particles are taken up by cells[288]. 2-[(polyethylene glycol)-2000]-N,N-ditetradecylacetamide contains a bulky polyethylene glycol (PEG) group which enhances solubility and keeps the particles from aggregating during storage[289]. 1,2-distearoyl-sn-glycero-3-phosphocholine (DSPC) and cholesterol both act as structural lipids, providing the necessary curvature and flexibility for the formation of appropriately sized lipoparticles[287]. The actual processes for forming these particles (including conditions of temperature, time, and mixing rates) are not published, although general protocols for making lipoparticles do exist[289].

The remaining ingredients are minor components that are present as buffers (Tris and Tris-HCl) which keep the components at the correct pH, and an excipient (sucrose) which adds bulk that further prevents lipoparticle aggregation and adds to stability in storage. There are no preservatives included in BNT162b2. This is likely because the -80°C storage requirement gives no opportunities for microorganismal growth. Also note the distinct lack of adjuvants, because the protein being expressed inside cells is able to mimic viral infection to an extent that no additional adjuvants are necessary for a response; however, there is evidence indicating that the charged lipids used in mRNA vaccines can act as adjuvants by activating Toll-like receptors once internalized[290]. Finally, just prior to injection, the instructions call for addition of a measured quantity of normal saline (0.9% NaCl) which adjusts the osmolarity and dilutes the lipoparticles to enhance their distribution within the body.

1.4.4 Immune response to mRNA vaccines

What is clear above all else is that mRNA vaccines such as Comirnaty (BNT162b2) and Spikevax generate robust humoral and cellular immune responses. The precise mechanisms by

which this occurs are still being worked out[291,292], some of which is the subject of this dissertation, but a tremendous amount has already been established.

Once injected, the lipoparticles are taken up stochastically by the cells that they come into contact with, though the distribution of cell types that express S protein after vaccination has not been described. Those cells which do productively interact with a lipoparticle will take it up into the endocytic pathway, where a largely unknown process results in the RNA entering the cytoplasm to be expressed. The many features of the Pfizer and Moderna modRNAs then allow expression of the S protein with minimal activation of innate immune pathways, which would normally rapidly degrade foreign mRNA[292]. The relatively stable modRNA can produce substantial quantities of S protein without the need for self-replication but will eventually be degraded. For reference, a typical mRNA for a highly expressed protein would have a half-life of around 10 hours, while other RNA transcripts generally have an half-life under 2 hours; however, estimates of these value vary considerably[293,294]. The protein that is made during this time provides a reservoir of antigen to which the immune system can respond, much as it would to an actual viral infection. The gradual introduction of antigen may also play an important role in the ultimate immune response[295]. This process requires coordination of the different arms of the immune system in order to work properly. Antigen presenting cells must acquire either fragmented or whole S proteins that must be delivered to GCs, which themselves require activation of T_{FH} cells. CD8 killer T cell responses also form simultaneously via a separate pathway[292]. The modRNA provided by the vaccine is designed to be less immunostimulatory than unmodified mRNA, but it still activates endosomal innate immune receptors such as Toll-like receptors 3, 7, and 8, which trigger inflammatory pathways like type-I interferon[292]. After entering the cytoplasm, the mRNA (and modRNA) can trigger other innate sensing pathways such as inflammasome components like

MDA5, RIG-I, and NOD2. Thus, while the cell is producing antigen from the delivered modRNA, multiple pathways are also activated which trigger release of inflammatory cytokines and promote cell death[296]. These signals result in recruitment of immune cells that include antigen presenting cells, which take up antigen in these inflammatory environments before trafficking back to the spleen and lymph nodes where they can promote antibody development and production. Antigen presenting cells like DCs can also take up vaccine particles directly and produce antigen for presentation to the adaptive immune system[296].

While we know that all of these events must be occurring because of the robust vaccine responses observed in clinical trials, there are still open questions about how exactly many of these steps occur and in what ways they might be optimized. For example, it is well established that this first generation of COVID-19 mRNA vaccines gives relatively poor durability compared to some live attenuated vaccines like the smallpox vaccine, which confers nearly lifelong immunity from a single dose[297,298]. This low durability is likely to be improved by continued development of better antigen engineering and adjuvants. Further, while most research on waning immune responses to the COVID-19 vaccines has focused on neutralizing antibody responses, other components of the immune response (such as T cells and non-neutralizing antibodies) may provide longer term protection from severe disease. However, in line with previously discussed findings that SARS-CoV-2 can inhibit T cell responses among naïve individuals[100,113], the robust T cell responses induced by vaccination can also be weakened by subsequent COVID-19 infection[299].

We also have a poor understanding of what is causing the rare but sometimes serious complications that are seen after vaccination; however, new data suggests that the reason for the rare post-vaccination myocarditis in young men may be linked to soluble spike proteins being released into circulation[300]. The ideal mRNA vaccine against SARS-CoV-2 would also provide

immunity that would broadly cover variants, which we know is also a current weakness of existing designs that will hopefully become clear through the studies I present here. This is further compounded by the combination of vaccinations with natural infections (i.e., hybrid immunity or super immunity), which is one of the primary topics covered here. Finally, there exists a chasm in knowledge surrounding the quality of humoral immunity generated by vaccination. I will also attempt to probe this issue by exploring which populations generate better or worse antibody responses, in terms of both quantity and quality. It is my hope that the work presented here represents a concrete step towards improved vaccines for SARS-CoV-2 and beyond.

Chapter 2: Cross-reactivity of SARS-CoV structural protein antibodies against SARS-CoV-2

Timothy A. Bates,[1,3] Jules B. Weinstein,[1,3] Scotland Farley,[1,3] Hans C. Leier,[1] William B. Messer,[1,2] and Fikadu G. Tafesse[1,4,*]

[1]Department of Molecular Microbiology & Immunology, OHSU, Portland, OR 97239, USA

[2]Department of Medicine, Division of Infectious Diseases, OHSU, Portland, OR 97239, USA

[3]These authors contributed equally

[4]Lead contact

*Correspondence: tafesse@ohsu.edu

Cell Reports, Volume 34, Issue 7. February 16, 2021.

DOI: https://doi.org/10.1016/j.celrep.2021.108737

Section 2.1: Abstract

2.1.1 Graphical Abstract

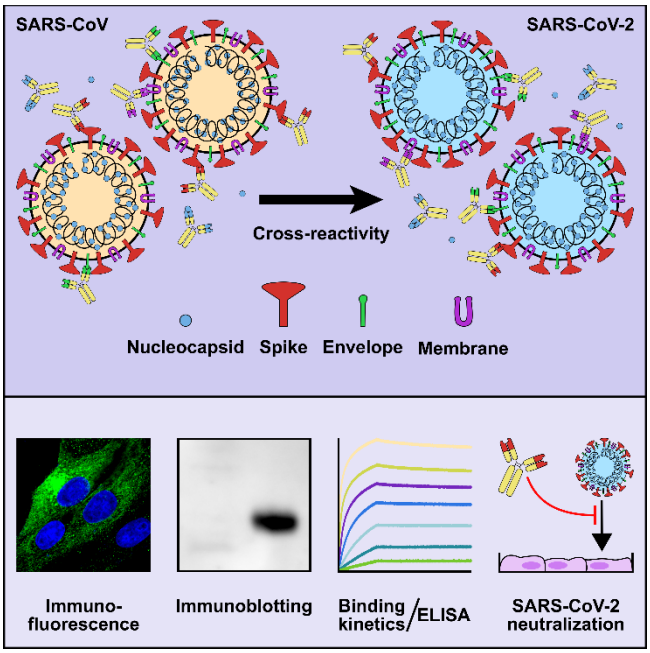

2.1.2 Summary

In the ongoing coronavirus disease 2019 (COVID-19) pandemic, there remain unanswered questions regarding the nature and significance of the humoral immune response toward other coronavirus infections. Here, we investigate the cross-reactivity of antibodies raised against the first severe acute respiratory syndrome coronavirus (SARS-CoV) for their reactivity toward SARS-CoV-2. We extensively characterize a selection of 10 antibodies covering all of the SARS-CoV structural proteins: spike, membrane, nucleocapsid, and envelope. Although nearly all of the examined SARS-CoV antibodies display some level of reactivity to SARS-CoV-2, we find only partial cross-neutralization for the spike antibodies. The implications of our work are two-fold. First, we establish a set of antibodies with known reactivity to both SARS-CoV and SARS-CoV-2, which will allow further study of both viruses. Second, we provide empirical evidence of the

high propensity for antibody cross-reactivity between distinct strains of human coronaviruses, which is critical information for designing diagnostic and vaccine strategies for COVID-19.

Section 2.2: Introduction

The recent emergence of the novel severe acute respiratory syndrome coronavirus 2 (SARS-CoV-2) in late 2019 has led to an ongoing worldwide coronavirus disease 2019 (COVID-19) pandemic and public health crisis[301]. At the time of writing, there are over 65 million confirmed infections and 1.5 million fatalities worldwide[80]. SARS-CoV-2 has been designated as a strain of the same species as the original SARS coronavirus (SARS-CoV) because of a high degree of sequence similarity[9]. SARS-CoV-2 falls within the family Coronaviridae and can be further subcategorized as a Betacoronavirus of lineage B[9]. There is an urgent need for tools to study this novel CoV, as part of the effort to quickly and safely develop vaccines and treatments. One avenue that merits exploration is the repurposing of reagents that were developed for use with SARS-CoV, because many are both extremely effective and commercially available.

CoVs are enveloped, positive-sense, single-stranded RNA viruses with exceptionally large genomes of up to 32 kb on a single RNA molecule. The genomes of most CoVs, including SARSCoV-2, contain two large open reading frames (which collectively code for 16 nonstructural proteins) in addition to several other open reading frames that are individually responsible for expression of four structural proteins (spike [S], nucleocapsid [N], membrane [M], and envelope [E]) and nine accessory proteins[19]. Coronaviridae are a large and diverse family of viruses, with several genera further divided into several lineages, and human (HCoV) and animal CoVs are intermixed within each of these categories[302]. Of the HCoVs, the SARS-CoVs are most closely related to the lineage C beta-CoV MERS, followed by the lineage A beta-CoVs HCoV-HKU1 and

HCoVOC43, and then the alpha CoVs HCoV-NL63 and HCoV-229E. The lineage A beta-CoVs and the alpha-CoVs are distributed worldwide with seroprevalence exceeding 90% in some studies, although they cause relatively mild disease compared with the rarer acute respiratory syndrome CoVs[112,303].

The four SARS-CoV-2 structural proteins are critical for shaping the physical form of the virion, but most available information about them has been extrapolated from other CoVs. Generally, the CoV M protein is involved in shaping the viral envelope membrane[24], the N protein complexes with the viral RNA[28], the S protein mediates receptor recognition and membrane fusion[304,305], and the E protein contributes to the structure of the viral envelope[25]. Furthermore, several of these CoV structural proteins have been shown to have intracellular functions unrelated to their role as structural proteins[28]. There are limits to the utility of extrapolation; it is known, for example, that the topology of the CoV E protein varies dramatically among various viruses[25], and the differences among the receptor binding domains (RBDs) of the S protein can be dramatic. Therefore, tools to interrogate the specific functions of each of the SARS-CoV-2 structural proteins would be of immense and immediate use.

CoV-specific antibodies are one type of tool used in such studies. Antibodies against the SARS-CoV-2 structural proteins could be used as reagents in microscopy and western blotting, as structural tools to probe functional epitopes, and even as antiviral therapies. The protein that produces the greatest SARS-CoV-2-specific antibody response in humans is the viral S protein[306], but it is known that antibodies are produced against the N, M, and E proteins as well[303,306]. Because SARS-CoV and SARS-CoV-2 are such markedly similar viruses, as discussed below, it is reasonable to assume that there may be some cross-reactivity between SARS-CoV antibodies

against their cognate SARS-CoV-2 structural proteins, and, indeed, there is already some evidence that this is the case[307–310].

SARS-CoV and SARS-CoV-2 S proteins share 76% amino acid sequence homology, and both rely on cellular angiotensin-converting enzyme 2 (ACE2) as an attachment receptor, as well as the TMPRSS2 protease for priming[29]. Recent reports have identified cross-reactive antibodies that bind to the S protein of both SARS-CoV and SARS-CoV-2; however, no such cross-reactive antibodies have been identified for the remaining structural proteins[307–310]. A non-human-primate model of SARS-CoV-2 DNA vaccination found that a polyclonal antibody response to S alone is sufficient to protect from SARS-CoV-2 challenge, similar to results from a human S-only vaccine trial for SARS-CoV[311,312]. Additionally, convalescent plasma from recovered COVID-19 cases has been broadly shown to reduce mortality of individuals with serious disease[313,314]. The sequence similarities between SARS-CoV and CoV2 N, M, and E proteins are high, at 91%, 90%, and 95%, respectively, making it likely that any individual antibody may be crossreactive. Indeed, there are reports of human antibodies against the S, N, and M proteins for which the epitopes are identical between SARS-CoV and SARS-CoV-2, further supporting the possibility of cross-reactivity, although none has been experimentally verified[306].

If cross-reactivity with SARS-CoV-2 is a common feature of SARS-CoV antibodies, then many recovered SARS-CoV patients may still possess SARS-CoV-2 reactive antibodies; antibody responses were shown to remain at high levels for at least 12 years according to a recent preprint[315]. Although sequence conservation is lower for more common HCoVs, their high prevalence may lead to widespread antibodies with cross-reactivity to SARS-CoV-2. Furthermore, antibodies promoting antibody-dependent cellular phagocytosis have been shown to assist in elimination of

SARS-CoV infection, showing that cross-reactive antibodies need not be neutralizing to play a productive role in resolution of CoV infection[316].

This report characterizes a series of SARS-CoV monoclonal antibodies for cross-reactivity, experimental utility, and neutralization of the live SARS-CoV-2 virus. Information about how antibodies from different CoV infections interact is critical for several reasons. It is an important factor to consider during the design of antibody-based CoV tests, particularly for those as closely related as SARS-CoV and SARS-CoV-2. New treatments for SARS-CoV-2 that interact with a patient's immune system will also need to take into account the prevalence of cross-reactive antibodies as a result of previous CoV infections. Further, information about the basic biology of this novel virus will be critical in developing such tailored treatments, and cross-reactive antibodies could be extremely useful in such studies.

Section 2.3: Results

2.3.1 Sequence similarities of the structural proteins of HCoVs

To begin to evaluate structural potential for cross-reactivity, we compared the amino acid sequences of each SARSCoV-2 structural protein with the homologous protein from the other HCoVs (Figure 2.1A). We first looked at the amino acid homology among the S proteins of the common HCoVs and found that other human beta-CoVs (MERS-CoV, HCoVHKU1, and HCoV-OC43) show only about 30% similarity to the SARS-CoV-2 S protein, and human alpha-CoVs (HCoV229E and HCoV-NL63) show only about 24% similarity to SARS-CoV-2 S protein. The S protein of the original SARSCoV, however, is much more closely related, showing 77% similarity between SARS-CoV and SARS-CoV-2, which lends support to the idea that anti-SARS-CoV S antibodies could be cross-reactive with the SARS-CoV-2 S protein. The E, M, and N protein

sequences show striking similarity between SARS-CoV and SARS-CoV-2; they are 96%, 91%, and 91% similar, respectively (Figure 2.1A).

The Biodefense and Emerging Infections (BEI) Research Resources Repository has available several types of antibodies and immune sera against each of the structural SARS-CoV proteins, as well as whole virus (summarized in Table 2.1). Eight of these are mouse monoclonal antibodies (240C, 341C, 540C, 154C, 472C, 19C, 283C, 42C) of either the IgM, IgG2a, or IgG1 class, recognizing either the SARS-CoV E, M, N, or S proteins. Of these, only two are neutralizing, 341C and 540C[317]. There are also polyclonal rabbit sera against the SARS-CoV S protein and an anti-S monoclonal human IgG1 antibody (CR3022) isolated from a SARS-CoV patient[318], all of which are neutralizing.

Although antibodies that recognize each of the structural proteins are of interest as experimental tools, antibodies that recognize the S protein are particularly so because of their potential to neutralize infectious virus. Structural information about the specific biochemical interactions between S-specific antibodies and the S protein is of great value. For the anti-S monoclonal antibodies (through BEI Resources) described in Table 2.1, the epitopes can be traced to one of three regions of the RBD. Whereas 240C, 341C, and 540C all bind within a region at the end of the RBD (epitope S_A)[317], the 154C antibody binds to a region at the beginning of the RBD (epitope S_B); and the human monoclonal antibody CR3022 binds to specific residues in a broad region in the middle of the RBD (epitope S_C)[310]. These epitopes are indicated in Figure 2.1B, along with the alignment of the SARS-CoV and SARS-CoV-2 RBDs. Although not identical, these regions do show some level of similarity between the two virus strains. The three-dimensional structure of the S protein in both monomeric and the functional trimeric form is displayed to illustrate the general accessibility of each portion of the protein (Figure 2.1C).

Figure 2.1 Sequence similarity between SARS-CoV and SARS-CoV-2

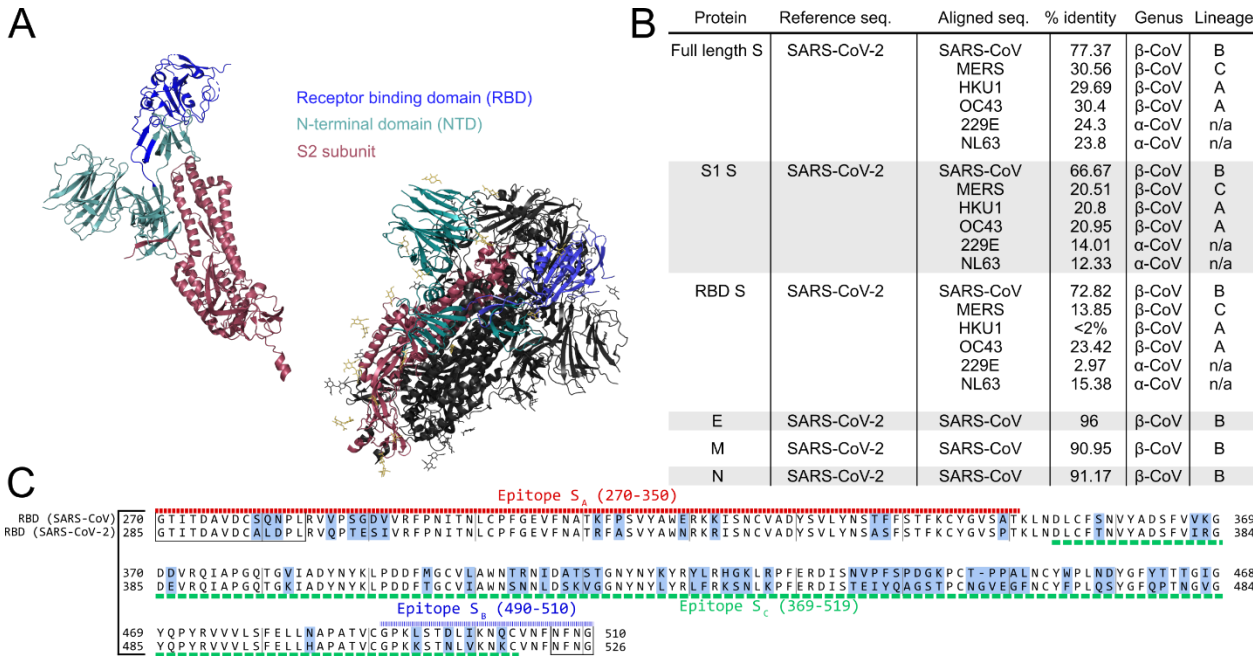

Protein	Reference seq.	Aligned seq.	% identity	Genus	Lineage
Full length S	SARS-CoV-2	SARS-CoV	77.37	β-CoV	B
		MERS	30.56	β-CoV	C
		HKU1	29.69	β-CoV	A
		OC43	30.4	β-CoV	A
		229E	24.3	α-CoV	n/a
		NL63	23.8	α-CoV	n/a
S1 S	SARS-CoV-2	SARS-CoV	66.67	β-CoV	B
		MERS	20.51	β-CoV	C
		HKU1	20.8	β-CoV	A
		OC43	20.95	β-CoV	A
		229E	14.01	α-CoV	n/a
		NL63	12.33	α-CoV	n/a
RBD S	SARS-CoV-2	SARS-CoV	72.82	β-CoV	B
		MERS	13.85	β-CoV	C
		HKU1	<2%	β-CoV	A
		OC43	23.42	β-CoV	A
		229E	2.97	α-CoV	n/a
		NL63	15.38	α-CoV	n/a
E	SARS-CoV-2	SARS-CoV	96	β-CoV	B
M	SARS-CoV-2	SARS-CoV	90.95	β-CoV	B
N	SARS-CoV-2	SARS-CoV	91.17	β-CoV	B

(**A**) Crystal structure of the S protein color coded by domain both as monomer and in the functional homotrimeric form in which one of the monomers is colored, while the other two are shown in white. As shown, the NTD and RBD compose the majority of the S1 region. See also Figure S2.1. (**B**) Similarity scores for each of the SARS-CoV-2 structural proteins compared with SARS-CoV and other common coronaviruses. Similarity in the S protein is substantially lower than for the other structural proteins. (**C**) Sequence alignment of the receptor binding domain (RBD) of SARS-CoV and SARS-CoV-2. Regions of difference are highlighted in blue, while the epitopes of the antibodies used in this study are underlined according to their designations in Table 2.1. The boxed regions fall outside of the canonical RBD sequence but are included because of overlap with the above epitope regions.

Table 2.1 SARS-CoV antibodies utilized by this study

Antibody	Reference	Protein Specificity	Species	Class	Neutralization of SARS-CoV	Epitope
240C	Tripp et al.	S	Mouse	IgG2a	No	S_A (490-510)
341C	Tripp et al.	S	Mouse	IgG2a	Yes	S_A (490-510)
540C	Tripp et al.	S	Mouse	IgG2a	Yes	S_A (490-510)
154C	Tripp et al.	S	Mouse	IgM	No	S_B (270-350)
CR3022	Ter Meulen et al. (GenBank DQ168569, DQ168570)	S	Human	IgG1	Yes	S_C (369-519)
NRC-772	Made by BEI	S	Rabbit	serum	Yes	
472C	Tripp et al.	E	Mouse	IgM	No	
19C	Tripp et al.	M	Mouse	IgM	No	
283C	Tripp et al.	M	Mouse	IgG1	No	
42C	Tripp et al.	N	Mouse	IgM	No	

2.3.2 Antibodies of the SARS-CoV structural proteins show cross-reactivities with SARS-CoV-2 by microscopy

To assess SARS-CoV antibodies against SARS-CoV-2, we first performed immunofluorescence (IF) staining of Vero E6 cells infected with live SARS-CoV-2 virus (Figure 2.2). The S-specific antibodies NRC-772, CR3022, and 240C all showed strong staining, whereas 540C and 154C showed weak staining. Antibody 341C showed no staining. The E-specific (472C), M-specific (19C and 283C), and N-specific (42C) antibodies all displayed robust staining. We confirmed the presence of SARS-CoV-2-infected cells by co-staining with human convalescent

serum, which demonstrates that negative 341C staining is not due to a lack of infection. To further validate the utility of these antibodies for IF, we performed staining of 293T cells transiently transfected with Strep-tagged constructs of each of the individual SARSCoV-2 structural proteins[20]. We compared the staining of the strep-tag within each structural protein in IF against that of the experimental antibodies, finding that the staining pattern of a majority of these antibodies is detectable, with some being highly similar to the strep-tag antibody (Figure S2.2). These results match our findings for the live SARS-CoV-2 infection; however, 42C (N-specific) showed markedly reduced staining of transiently transfected cells. Together, these antibodies provide complete coverage of SARS-CoV-2 structural proteins, showing their utility for SARS-CoV-2 experiments involving microscopy.

Figure 2.2 Immunofluorescence of SARS-CoV-2 structural proteins using SARS-CoV antibodies

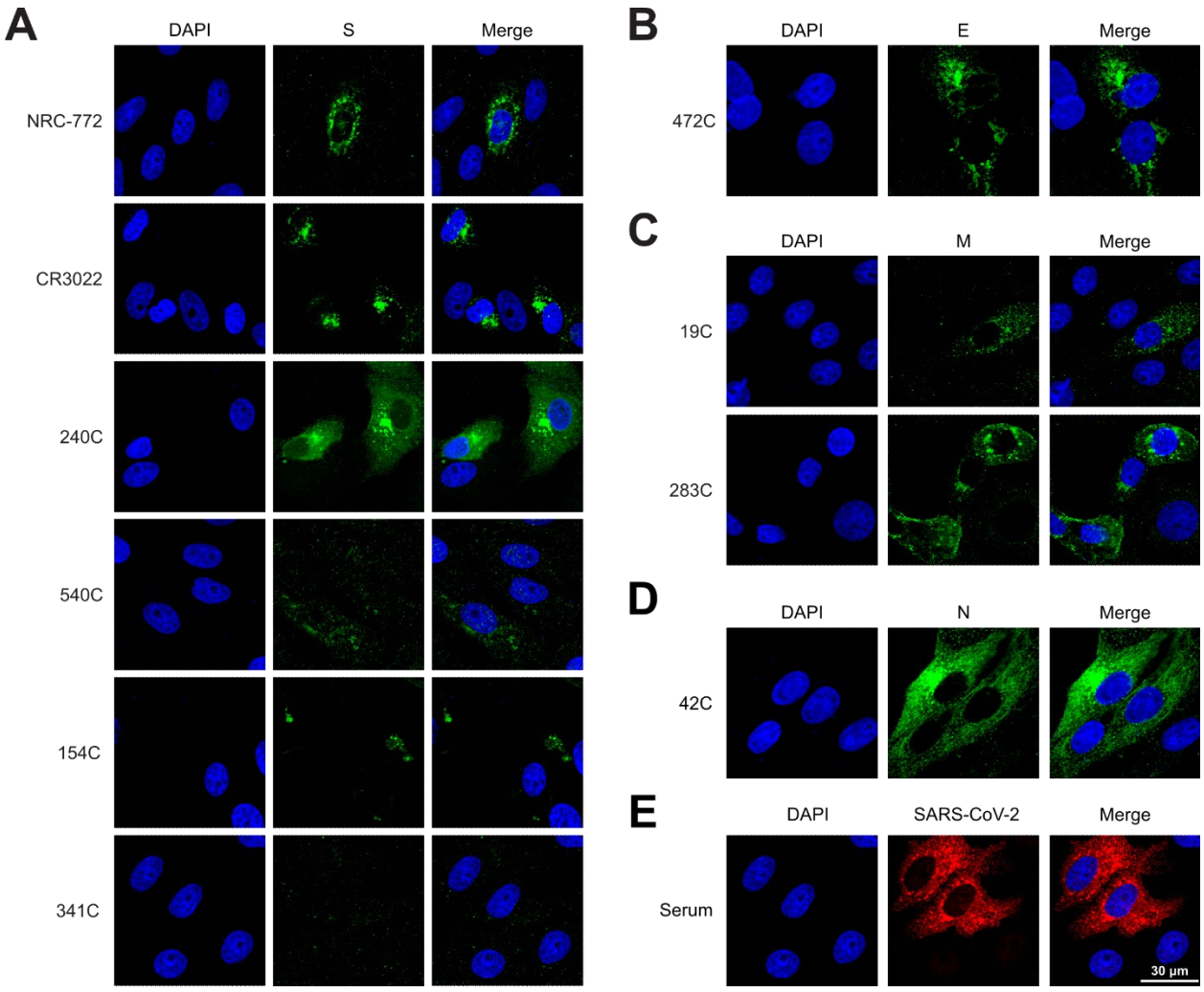

(**A–D**) Representative immunofluorescence images of Vero cells infected with SARS-CoV-2. 24 h post-infection, cells were fixed and stained with the listed SARSCoV antibodies (green): (**A**) spike, (**B**) envelope, (**C**) membrane, and (**D**) nucleocapsid. (**E**) 341C was co-stained with human convalescent serum (red) to confirm the presence of infected cells. Scale bars, 30 mm. DAPI (blue) was used to visualize cell nuclei. See also Figure S2.

2.3.3 Antibodies of the SARS-CoV structural proteins show cross-reactivities with SARS-CoV-2 by immunoblotting

We next evaluated these antibodies by western blot. His6tagged RBD from SARS-CoV-2 was produced in HEK293 cells and purified by Ni-NTA chromatography (Figure S2.3A). The purified RBD was then used for a western blot with each of the mouse monoclonal antibodies (Figures 2.3A and 2.3B). Anti-His6 antibody demonstrates high purity of the RBD protein. The staining produced by each experimental antibody was compared with lysate from untransfected 293T cells to assess background. Of these antibodies, 240C and NR-772 produced strong signal with little background, whereas the other monoclonal antibodies (CR3022, 154C, 341C, and 540C) did not produce detectable signal.

We also performed western blots on SARS-CoV-2 (Isolate USA-WA1/2020)-infected and uninfected Vero E6 cell lysates. Probing with human convalescent serum revealed bands at the expected size for each of the structural SARS-CoV-2 proteins: S, N, M, and E (Figure S2.3D). The 42C, 540C, NRC-772, 240C, and 283C antibodies each developed bands unique to the SARS-CoV-2-infected samples; however, not all of the bands were at the expected molecular weight. Previous reports have shown that SARS-CoV-2 proteins, including S, N, M, and E, all produce bands at several different molecular weights when expressed exogenously in HEK293T cells, and it is not surprising that these bands also exist in our blots[20]. What is unexpected is that for S monoclonal antibodies 240C, 540C, and 283C, we detect the lower molecular weight band (~50 kDa) and not the band at the expected molecular weight (Figure S2.3). This could be because of masking of the epitope by glycosylation absent from the truncated protein or specific recognition of proteolytically cleaved peptides. For instance, proteolytic cleavage of the S protein is known to be important for proper maturation of SARS-CoV-2 particles[29,319]. The N monoclonal antibody

42C is able to detect a band at the correct molecular weight (~46 kDa); however, there is a moderate level of background (Figure 2.3D). The M monoclonal antibody 283C detects a band at the expected molecular weight (~25 kDa) but also detects a lower molecular weight band similar to what has been shown in previous reports that showed that the M protein is particularly prone to proteolytic degradation in western blots, as well as a high molecular weight smear[20]. The M monoclonal antibody 19C shows similar staining, but weaker, and both display a high level of background staining. The E monoclonal antibody 472C displays a weak band at the expected molecular weight (~8 kDa), but the intensity is similar to that of background, so a positive determination cannot be made.

Figure 2.3 Biochemical characterization of SARS-CoV antibodies for their cross-reactivity with SARS-CoV-2 proteins

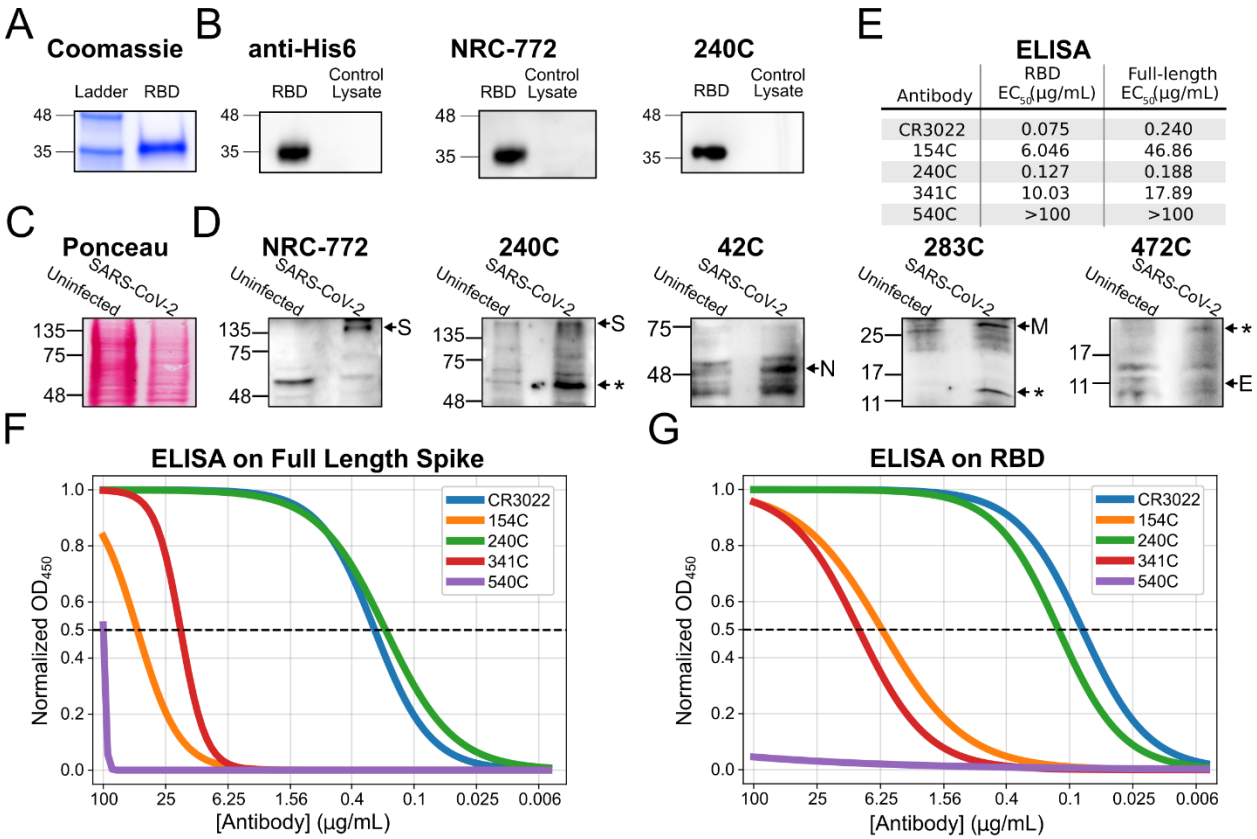

Characterization of the S-specific antibodies by western blot and ELISA. (**A**) Coomassie stain of in-house-purified His6-tagged RBD protein produced in HEK293-F suspension cells and purified by Ni-NTA chromatography. (**B**) Western blot of purified RBD with anti-His6 antibody and SARS-CoV S-specific antibodies. (**C**) Ponceau stain of SARS-CoV-2-infected and uninfected Vero E6 cell lysate. (**D**) Western blot of SARS-CoV-2-infected lysate probed with SARS-CoV structural protein-specific monoclonal antibodies. Shown are representative images of two to three independent experiments. (**E**) Summary table of observed EC50 values from both sets of ELISAs. (**F**) ELISA on purified full-length spike coated at 2 mg/mL. (**G**) ELISA on purified RBD coated at 2 mg/mL. n = 3 (each done in triplicates). Asterisks indicate an expected alternate band. See also Figures S3 and S4.

2.3.4 S antibodies show cross-reactivity in binding

The fact that the S glycoprotein is responsible for virus binding and entry into host cells makes it an attractive target for antibody generation because some of these antibodies may be neutralizing. Because of the potential functional role for these antibodies, and because of the number of different antibody clones, we decided to examine the S-protein-specific antibodies more thoroughly. We assessed the binding of the S-protein-specific antibodies to both the full-length SARS-CoV-2 S protein and the purified RBD by ELISA (Figures 2.3F, 2.3G, and S2.4; summarized in Figure 2.3E). The CR3022 and 240C antibodies showed strong binding to both the full-length S and the RBD (EC_{50} 75 and 127 ng/mL, respectively, to the RBD). 154C and 341C showed weak but detectable binding (6.046 and 10.03 mg/mL, respectively, to the RBD), whereas 540C did not demonstrate binding at all. The trend for these antibodies is generally similar to what was seen in the previous studies, where the antibodies were tested against recombinant SARS-CoV S protein[317]. The original report of CR3022 did not perform a direct ELISA for us to compare

with our results; however, our data agree with studies of CR3022 on SARS-CoV-2 showing that it binds strongly to both full-length S and the RBD[310]. Although CR3022 appears to be the strongest binder to RBD, 240C is marginally better on the full-length S protein.

To assess the binding kinetics of the antibody-RBD interaction in more detail, we measured the antibody-epitope interactions using biolayer interferometry (BLI). The three monoclonal antibodies that showed the strongest binding with the ELISA displayed high affinity for the SARS-CoV-2 RBD: CR3022 showed the strongest binding with a calculated K_D of 758 pM (Figure 4A), while 240C demonstrated a 1.36 nM K_D (Figure 2.4B) and 154C a 481 nM K_D (Figure 2.4C). As summarized in Figure 4D, these antibodies showed fast-on/slow-off kinetics in agreement with a previous report of CR3022 binding kinetics on RBD[310]. The other antibodies we tested displayed no measurable binding at the highest concentration used (Figure S2.5). Importantly, BLI does not account for the avidity of these antibodies, and it is likely that the interaction of each epitope/paratope pair is substantially lower than that of the intact antibody; however, the intact antibody more closely resembles the interaction that is likely to occur in most in vitro assays, or indeed in vivo. Our K_D is substantially lower than reported in Tian et al.[308]; however, this is likely due to differences in the reagents used. Tian et al.[308] expressed their RBD in E. coli, preventing glycosylation, while our RBD was produced in mammalian cells. Additionally, their CR3022 was produced as a single-chain variable fragment (scFv) in E. coli, which would contain only a single paratope and may fold differently from our full CR3022 antibody, which was produced in a plant expression system, is bivalent, and contains intact constant domains.

Figure 2.4 Binding kinetics and functional testing of Spike-specific antibodies against the RBD of the SARS-CoV-2

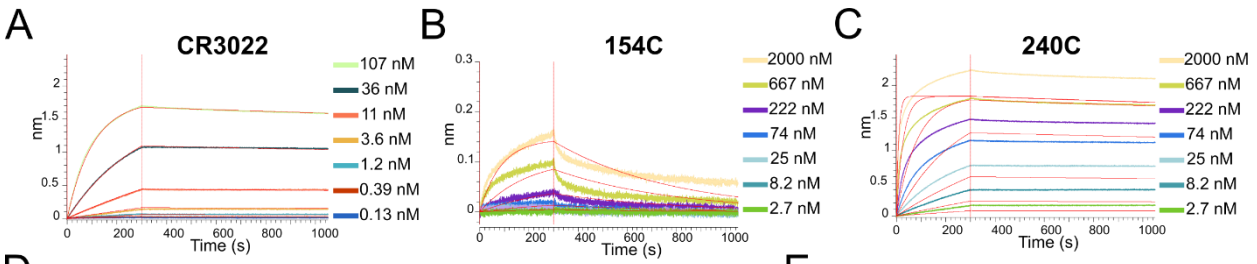

D

BLI affinity

Antibody	K_D (nM)	K_{ON} ($M^{-1}s^{-1}$)	K_{OFF} (s^{-1})
CR3022	0.758 ± .003	9.0×10^4 (± 2.8×10^1)	6.8×10^{-5} (± 3.0×10^{-7})
154C	481 ± 4	3.7×10^3 (± 2.6×10^1)	1.8×10^{-3} (± 6.8×10^{-6})
240C	1.36 ± 0.06	5.4×10^4 (± 2.0×10^2)	7.3×10^{-5} (± 3.3×10^{-6})
341C	ND	ND	ND
540C	ND	ND	ND

E

EC_{50} of neutralization (dilution factor)

Antibody	Live SARS-CoV-2	SARS-CoV-2 Spike Pseudovirus
CR3022	>1:1	>1:1
154C	1:8.2	1:17.5
240C	1:8.5	1:16.8
341C	1:5.6	1:8.1
540C	>1:1	1:6.3
1v6	1:4200	1:272

(**A–C**) Biolayer interferometry curves for CR3022, 154C, and 240C with 3-fold dilutions. Streptavidin biosensors were coated with biotinylated RBD, then blocked with 1 mM D-Biotin in kinetics buffer. Negative binding curves for 341C and 540C shown in Figure S5. Curve fitting was performed using 1:1 binding model in ForteBio Analysis HT 10.0 software. (**D**) Summary of quantified binding kinetics of Spike monoclonal antibodies from BLI experiment. (**E**) Neutralization assay 50% neutralization values against live SARS-CoV-2 by focus-forming assay and SARS-CoV-2 spike pseudotyped lentivirus by fluorescence microscopy. EC50 values represent triplicate experiments (n = 3). 1v6 is positive control from COVID-19 patient convalescent serum collected at day 14. The concentration of all monoclonal antibody stocks was 1 mg/mL. 154C and 240C showed only partial neutralization at the highest concentration tested (1:10 dilution), whereas 341C, 540C, and CR3022 failed to reliably neutralize pseudotyped virus at this dilution. See also Figures S2.5 and S2.6.

2.3.5 S antibodies of SARS-CoV show limited cross-neutralization of SARS-CoV-2

Finally, we assessed the neutralizing capabilities of these S protein-specific monoclonal antibodies. We set up a neutralization assay using a Lentivirus GFP-reporter pseudotyped with the SARS-CoV-2 S protein[226]. Neutralization was assessed by quantitative fluorescent microscopy, using the area of GFP expression compared with that of an antibody-untreated control. Serial dilutions of antibodies were used to generate neutralization curves and estimate the antibody concentration necessary for 50% neutralization. This readout was used because the monoclonal antibodies displayed only partial neutralization at the highest concentration used in our assay. To validate our assay, we used human convalescent serum from a SARS-CoV-2-positive patient. This anti-serum demonstrated 50% neutralization at a dilution of 1:270 (Figure 2.4E). Consistent with a previous report, CR3022 failed to show any neutralization at 100 mg/mL despite its potent binding in every other assay[310]. 154C and 240C both showed partial neutralization, with a 50% reduction in GFP area at 57.8 and 61.3 mg/mL, respectively. Consistent with the BLI results, 341C and 540C did not show substantial neutralization. We were surprised to see 154C perform the best in this assay, particularly because the original report of these antibodies on SARS-CoV showed 341 and 540 as the only antibodies with neutralizing capabilities. One unique aspect of 154C is that it is the only IgM antibody from this selection of S-specific antibodies; however, it is not clear how this might affect neutralization[310].

To further validate our pseudotyped lentivirus neutralization data, we set up focus-forming assay (FFA)-based neutralization studies using live SARS-CoV-2 (Isolate USA-WA1/2020) as previously described[222]. The virus was titrated such that each well received 30 plaque-forming units (PFUs)/ well, which was pre-incubated for 1 h with antibody dilutions starting at 1:10 down

to 1:1,280. The results from this assay were broadly similar with those seen in the pseudovirus neutralization assay, with 240C and 154C showing partial neutralization, and 341C, 540C, and CR3022 showing minimal neutralization (Figures 4E and S6). The human convalescent serum from a SARS-CoV-2 patient (1v6) performed better in the FFA, whereas the monoclonal antibodies each performed slightly less well than in the pseudotype neutralization assay. The reasons for this variation may be because of the substantial differences between the design of these two assays, including the cell type, virus type and quantity, and detection method. Despite these differences, the similar neutralizing trends in both assays show limited cross-neutralization of SARS-CoV-2 by the S monoclonal antibodies of SARS-CoV.

2.3.6 Summary of cross-reactivity of SARS-CoV structural protein-specific antibodies to SARS-CoV-2 structural proteins in various assays

The utility of each of the antibodies used in this study has been summarized in Table 2.2. In particular, the S protein-specific 240C performed well in every assay we performed, excluding neutralization. In contrast, 540C showed no detectable binding in any of our assays. The other S protein-specific monoclonal antibodies 154C, 341C, and CR3022 showed mixed utility in different assays (Table 2.2). The rabbit polyclonal antibody NRC772 also worked in every assay in which it was tested; however, polyclonal sera is limited to experiments where structural information about particular epitopes is not important due to the unknown admixture of the contained antibody clones. The antibodies against E, M, and N demonstrated utility in IF and showed some success in western blots in the case of the 42C and 283C antibodies (Table 2.2). Further studies could explore these antibodies in greater detail by producing purified E, M, and N proteins for use in biochemical assays, such as the ones we used to characterize the S protein-specific antibodies in this report.

Table 2.2 Summary of reagent quality in assays

Antibody	Protein target	Immunofluorescence	ELISA	Western blot	Biolayer interferometry	Neutralization
240C	S	+++	+++	+++	+++	partial
154C	S	-	++	-	+	partial
341C	S	-	++	-	-	-
540C	S	+	-	++	-	-
CR3022	S	++	+++	-	+++	-
NRC-772	S	+++	ND	+++	+++	ND
42C	N	+++	ND	++	ND	ND
427C	E	++	ND	-	ND	ND
19C	M	++	ND	+	ND	ND
283C	M	+++	ND	++	ND	ND

Section 2.4: Discussion

Our results demonstrate measurable cross-reactivity from a majority of the SARS-CoV structural protein-targeted antibodies that we evaluated against SARS-CoV-2 S, N, M, and E proteins. These tools can be readily obtained from BEI Resources and utilized by labs to study the properties of untagged SARS-CoV-2 structural proteins. These antibodies can serve the unmet need for more resources enabling the study of SARS-CoV-2. It is critical to understand the basic biology of SARS-CoV-2 in order to inform efforts toward improved diagnostics and treatments. Further, information about cross-reactivity of antibodies between SARS-CoV and SARS-CoV-2 may assist bioinformaticians in developing computational tools for predicting cross-reactivity of other antibodies, or even guiding rational design of improved CoV antibodies and small-molecule therapeutics.

We have shown that these publicly available antibodies are of potential use in several different types of assays with SARSCoV-2 proteins. We found that several of these SARS-CoV structural protein antibodies demonstrated good staining in IF of SARS-CoV-2-infected cells and in an overexpression system (240C, NRC-772, and CR3022 against S; 42C against N; 283C

against M; 472C against E). The anti-S antibodies, 240C and NRC-772, also give clear signal in western blot with minimal background. Several S antibodies show potent binding to fulllength S and the RBD by ELISA, as well as binding to the RBD by BLI (240C, CR3022, and NRC-772). This wide range of uses substantially broadens our ability to investigate the biochemical properties of SARS-CoV-2 structural proteins.

The neutralization experiments we performed showed that antibodies that were previously shown to be neutralizing against SARS-CoV were actually less likely to be strongly cross-reactive with SARS-CoV-2. This may be because of a phenomenon well described among rapidly evolving viruses, such as HIV and influenza, wherein neutralizing antibodies are more likely to bind to highly variable epitopes lying on the host-interacting surfaces of the viral proteins[320,321]. It is likely that the specific amino acid substitutions present in the RBD of the SARS-CoV-2 S protein compared with that of SARS-CoV were selected for, in part, because of their ability to avoid binding by existing SARS-CoV antibodies among the wild animal populations from whence SARS-CoV-2 emerged. It is then, perhaps, unsurprising that 240C and 154C retained partial neutralizing ability, whereas 341C and 540C seem to have lost their capacity to neutralize when faced with SARS-CoV-2. There are ongoing efforts to determine the evolutionary forces that are shaping the continued change of the SARS-CoV-2 S protein in response to more widespread antibody-based immunity in the worldwide population; it may even be possible to anticipate mutations that could give rise to more virulent strains[59]. Although these antibodies only partially neutralized a SARS-CoV-2 model infection, they are still of interest for their potential to elucidate the structure and function of their protein targets.

Antibodies have been critical tools in structure determination and in the mapping of proteins' functional regions. Having a wide array of antibodies that recognize varying epitopes is

of great help in this endeavor. Additionally, with the current dearth of knowledge regarding the life cycle and pathogenesis of SARS-CoV-2, particularly regarding the understudied M, N, and E proteins, we believe that these antibodies could be used in experiments to better understand the nuances of their functions beyond their obvious structural roles.

Our results also speak to the high proportion of SARS-CoV antibodies that display substantial cross-reactivity to SARS-CoV-2 structural proteins. Anecdotal evidence supports the efficacy of convalescent plasma treatment for COVID-19, indicating that cross-reactive antibodies generated during previous CoV infections may prove beneficial for emerging CoV infections[322]. Another recent study found that following recovery from infection with SARS-CoV-2, patients expressed increased levels of antibodies capable of binding to peptides from more distantly related HCoVs, such as HCoV-OC43 and HCoV-229E[323]. Conversely, studies of COVID-19 patients have found neutralizing antibody titers to be directly proportional to disease severity, suggesting a more complicated relationship between antibodies and COVID-19[324,325]. Some have hypothesized that this may be because of high concentrations of virus and neutralizing antibodies acting together to drive greater immune pathology[135,326]. A better understanding of the functions of individual antibody isotypes against different antigenic targets will be critical to predicting the utility of a particular antibody against SARS-CoV-2.

Further studies could also investigate possible cooperation between antibodies recognizing different epitopes, especially because CR3022 neutralization was shown to have synergy with another anti-S antibody that recognized a different epitope on the protein[318]. A recent study[327], for example, characterized a neutralizing monoclonal antibody that did not bind the RBD at all, and instead recognized an epitope in the NTD of the S protein. Knowledge about the variety of vulnerable epitopes, and possible synergy between antibodies that target them, brings us ever

closer to being able to design and deploy effective therapeutics and vaccines in this time of urgent need.

Section 2.5: Methods

Sequence alignment

Protein sequences were obtained from uniprot and aligned using the T-Coffee multiple sequence alignment server.

Cell transfection

Transfections were carried out in 293T cells seeded at 70%–90% cell density using Lipofectamine 3000 (ThermoFisher Scientific) as per manufacturer's instructions. For immunofluorescence, the SARS-CoV2 structural protein plasmids pTwist-EF1alpha-nCoV2019-S-2xStrep, pLVX-EF1alpha-nCoV-2019-E-IRES-Puro, pLVX-EF1alpha-nCoV-2019-M-IRES-Puro, or pLVX-EF1alpha-nCoV2019-N-IRES-Puro were transfected using 2 mg of plasmid per well of a 24-well plate. Structural SARS-CoV-2 protein plasmids were a kind gift from the Krogan Lab at UCSF and are described previously[20]. For pseudotyped lentivirus production, lentivirus packaging plasmids, HDM_Hgpm2, HDM_tat1b, PRC_CMV_Rev1b, SARS_CoV-2 S plasmid HDM_IDTSpike_fixK, and LzGreen reporter plasmid pHAGE2_CMV_ZsGreen_W were transfected using 0.44 mg for packaging, 0.68 mg for S, and 2 mg for reporter plasmids per 6 cm dish. Packaging, SARS-CoV-2 S, and reporter plasmids were a kind gift from Jesse D. Bloom from University of Washington, and are described previously[226]. Transfection media was carefully removed 6 hours post transfection, and replaced with DMEM.

Pseudotyped lentivirus production

293T cells were seeded at 2 million cells/dish in 6cm TC-treated dishes. The following day, cells were transfected as described above with lentivirus packaging plasmids, SARS-CoV-2 S plasmid, and lzGreen reporter plasmid[226]. After transfection, cells were incubated at 37C for 60 hours. Viral media was harvested, filtered with 0.45 mm filter, then frozen before use. Virus transduction capability was then tittered on 293T-Ace2 cells treated with 50 mLof5mg/ml polybrene (Sigma-Aldritch LLC). LzGreen titer was determined by fluorescence using BZ-X700 all-in-one fluorescent microscope (Keyence), a 1:16 dilution was decided as optimal for following neutralization assays due to broad transduced foci distribution.

SARS-CoV-2 virus propagation

One tube of frozen SARS-CoV-2 (BEI Resources) was thawed and diluted 1:10 for inoculation in minimal volume onto 70% confluent Vero E6 cells. The cells were incubated for 1 hour at 37°C, rocking every 15 minutes to ensure even coverage. Additional media was added up to the manufacturer's recommended culture volume, and the cells were incubated for 72 hours at 37°C. Supernatant was collected and spun at 3,000 3×g for 5 minutes, then aliquoted for storage at -80°C.

SARS-CoV-2 infection

A 96-well plate of 50% confluent Vero cells was inoculated with 50 mL frozen SARS-CoV-2 virus stock for 1 hour at 37°C with rocking every 15 minutes. Added an additional 50 mL of fresh media and incubated for 24 hours at 37°C. Fixed plate by submerging in 4% PFA in PBS for 1 hour, then brought into BSL-1 for immunofluorescence staining.

Immunofluorescence

293T cells were seeded on 24-well plates containing glass coverslips coated with poly-lysine solution; 100,000 cells were seeded per well. Cells were transfected with SARS-CoV-2 structural protein plasmids as described above. After 48 hours post transfection, cells were fixed with 4% PFA in PBS. Cover slips with transfected 293T cells and the 96-well plate with SARS-CoV-2 infected Vero cells were permeabilized with 2% BSA, 0.1% Triton-X-100 in PBS. Transfected cells were incubated for 3 hours at RT with the following anti-SARS-CoV structural protein monoclonal or polyclonal antibodies at a 1:250 dilution for transfected 293T cells, or 1:200 for infected Vero cells: mouse anti-SARS-CoV S monoclonal IgM 154C, mouse anti-SARS-CoV S monoclonal IgG2a 240C, mouse anti-SARS-CoV S monoclonal IgG2a 341C, mouse anti-SARS-CoV S monoclonal IgG2a 540C, mouse anti-SARS-CoV N monoclonal IgM 19C, mouse anti-SARS-CoV M monoclonal IgG1 283C, mouse anti-SARS-CoV E monoclonal IgM 472C, mouse anti-SARS-CoV N monoclonal IgM 42C, human anti-SARS-CoV S monoclonal IgG1 CR3022, and rabbit anti-SARS-CoV S polyclonal sera (BEI Resources) and mouse anti-2xStrep-tag antibody (Sigma-Aldrich). Anti-mouse IgG AF555, anti-rabbit IgG AF555, or anti-mouse IgM AF488 conjugated secondary antibodies were added at 1:500 dilution for 1 hour at RT (Invitrogen). Confocal imaging was performed with a Zeiss LSM 980 using a 63x Plan-Achromatic 1.4 NA oil immersion objective. Images were processed with Zeiss Zen Blue software. Maximum intensity *z*-projections were prepared in Fiji. All antibody stain images were pseudocolored for visual consistency.

Pseudovirus neutralization assay

Neutralization protocol was based on previously reported neutralization research utilizing SARS-CoV-2 S pseudotyped lentivirus[226]. 293T-Ace2 cells were seeded on tissue culture treated,

poly-lysine treated 96-well plates at a density of 10,000 cells per well. Cells were allowed to grow overnight at 37°C. LzGreen SARS-COV-2 S pseudotyped lentivirus were mixed with 2-fold dilutions of the following monoclonal or polyclonal anti-SARS-CoV-2 S antibodies: mouse anti-SARS-CoV S monoclonal IgM 154C, mouse anti-SARS-CoV S monoclonal IgG2a 240C, mouse anti-SARS-CoV S monoclonal IgG2a 341C, mouse anti-SARS-CoV S monoclonal IgG2a 540C, rabbit anti-SARS-CoV S polyclonal sera, Guinea pig anti-SARS-CoV S polyclonal sera, human monoclonal anti-SARS-CoV S CR3022 (BEI Resources). Human patient sera from a SARS-CoV-2 patient was used as positive neutralization control, while virus alone was used as negative control. Sera and antibody dilutions ranged from 1:10 to 1:1048. Virus-antibody mixture was incubated at 37°C for 1 hour after which virus was added to 293T-Ace2 treated with 5µg/ml polybrene. Cells were incubated with neutralized virus for 44 hours before imaging. Cells were fixed with 4% PFA for 1 hour at RT, incubated with DAPI for 10 minutes at RT, and imaged with BZ-X700 all-in-one fluorescent microscope (Keyence). Estimated area of DAPI and GFP fluorescent pixels was calculated with built in BZ-X software (Keyence).

Focus forming assay (FFA) for live SARS-CoV-2 virus neutralization measurement

The FFA was performed as previously described[222]. In brief, Vero E6 cells were plated into 96 well plates at 24,000 cells/well and incubated overnight. Previously propagated SARS-CoV-2 stocks were titrated by plaque forming unit (PFU) assay and diluted to 30 pfu in 15 µL. To the virus, 15 µL of antibody dilutions were added such that the final antibody dilution was 1:10 to 1:1280 in two-fold dilutions and this was incubated at 37°C for 1 hour. All virus and antibody dilutions were prepared in Opti-MEM media with 2% FBS. 30 µL of neutralized virus was then added to the confluent Vero E6 cells and incubated for 1 hour at 37°C. 150 µL of overlay media (Opti-MEM, 2% FBS, 2% Methylcellulose) was then added to each well and incubated for 48

hours at 37°C. Following infection, the plates were fixed using formaldehyde and subsequently blocked for 30 minutes with perm buffer containing 0.1% bovine serum albumin and 0.1% saponin. SARS-CoV-2 RBD and N protein immunized alpaca polyclonal serum was used as primary antibody at 1:5,000 dilution in perm buffer, and anti-Llama-HRP secondary was used at 1:20,000 dilution. Plates were developed with TrueBlue (SeraCare) substrate and imaged with an Immunospot analyzer.

Enzyme-linked immunosorbent assay (ELISA)

ELISA plates, Nunc MaxiSorp (Invitrogen), were coated with purified recombinant SARS-COV-2 RBD domain (BEI resources, NR-52306) at 2µg/ul in PBS. Coating was carried out overnight at 4°C. Protein was blocked in 2% BSA, 1% tween-20 in PBS for 30 minutes at RT. The following anti SARS-CoV-2 S monoclonal and polyclonal antibodies were serially diluted by 2-fold dilutions in blocking buffer: mouse anti-SARS-CoV S monoclonal IgM 154C, mouse anti-SARS-CoV S monoclonal IgG2a 240C, mouse anti-SARS-CoV S monoclonal IgG2a 341C, mouse anti-SARS-CoV S monoclonal IgG2a 540C, human monoclonal anti-SARS-CoV-S CR3022 (BEI Resources). Human patient sera from a SARS-CoV-2 patient was used as a positive control. Dilutions ranged from1:10 to 1:10480, and were incubated for 1 hour at RT. Anti-mouse HRP, and anti-human-HRP secondary antibodies were used at 1:4000 concentration in blocking buffer, and were incubated 1 hour at RT. 50 µL of TMB HRP substrate (ThermoFisher Scientific) was added, and following incubation for 10 minutes at RT, 50µL of 2N H2SO4 was added as a stopping solution. Plate absorbance at 405nm was measured using a CLARIOstar® Plus plate fluorimeter (BMG Labtech).

RBD protein purification and biotinylation

Purified SARS-CoV-2 S-RDB protein was prepared as described previously[328]. Breifly, codon optimized His-tagged RBD in pInducer-20 was used to make lentivirus in HEK 293T cells which was then used to infect HEK 293-F suspension cells. The suspension cells were allowed to grow for 3 days with shaking at 37°C at 8% CO_2. Cell supernatant was collected, sterile filtered, and purified by Ni-NTA chromatography. The purified protein was then buffer exchanged into PBS and concentrated. For use in BLI, purified RBD was biotinylated using the ChromaLINK biotin protein labeling kit according to the manufacturer's instructions with 5x molar equivalents of labeling reagent to achieve 1.92 biotins/protein.

Biolayer interferometry (BLI)

Streptavidin biosensors (ForteBio) were soaked in PBS for at least 30 minutes prior to starting the experiment. Biosensors were prepared with the following steps: equilibration in kinetics buffer (10 mM HEPES, 150 mM NaCl, 3mM EDTA, 0.005% Tween-20, 0.1% BSA, pH 7.5) for 300 seconds, loading of biotinylated RBD protein (10ug/mL) in kinetics buffer for 200 seconds, and blocking in 1 μM D-Biotin in kinetics buffer for 50 seconds. Binding was measured for seven 3-fold serial dilutions of each monoclonal antibody using the following cycle sequence: baseline for 300 seconds in kinetics buffer, association for 300 seconds with antibody diluted in kinetics buffer, dissociation for 750 seconds in kinetics buffer, and regeneration by 3 cycles of 20 seconds in 10 mM glycine pH 1.7, then 20 seconds in kinetics buffer. All antibodies were run against an isotype control antibody at the same concentration. Data analysis was performed using the ForteBio data analysis HT 10.0 software. Curves were reference subtracted using the isotype control and each cycle was aligned according to its baseline step. K_Ds were calculated using a 1:1

binding model using global fitting of association and dissociation of all antibody concentrations, excluding dilutions with response below 0.005 nm.

RBD Western blot

293T cells were seeded in 10 cm dishes at a density of 3.5 million cells per dish. After overnight growth, cells were transfected using lipofectamine 3000 as described above. Plasmids pTwist-EF1alpha-nCoV-2019-S-2xStrep, pLVX-EF1alpha-nCoV-2019-E-IRES-Puro, pLVX-EF1alpha-nCoV-2019-M-IRES-Puro, or pLVX-EF1alpha-nCoV-2019-N-IRES-Puro were transfected using 90 µg of DNA per 10 cm dish. Cells were scraped 48 hours post-transfection, then lysed in RIPA buffer (EMD Millipore). Cell lysates were diluted with reducing Laemmli buffer, incubated for 10 minutes at 37°C, then ran on 4–20% Mini-PROTEAN® TGX™ Precast Protein Gels (BIO-RAD). Additionally, 1µg of purified recombinant S RBD-His_6 was diluted in PBS and Laemmli buffer to a final volume of 20 µL and added to a 7.5% Mini-PROTEAN® TGX™ Precast Protein Gel (BIO-RAD). Resolved proteins were then transferred to a PVDF membrane, blocked in TBS with 2% BSA 0.1% Tween-20, then incubated with the following antibodies diluted to 1:500 in blocking buffer: mouse anti-SARS-CoV N monoclonal IgM 19C, mouse anti-SARS-CoV M monoclonal IgG1 283C, mouse anti-SARS-CoV E monoclonal IgM 472C, and mouse anti-2xStrep-tag antibody, and anti-His-HRP. Blots were stained with SuperSignal™ West Pico PLUS Chemiluminescent Substrate (ThermoFisher Scientific) using an ImageQuant LAS 4000 imager (GE Life Sciences).

SARS-CoV-2 infected lysate Western blot

Around 10^6 Vero E6 cells were infected with SARS-CoV-2 at MOI of 0.1. At 72 hours post infection, cells were washed with PBS and lysed with 8M urea + 1x RIPA buffer + 1x Laemmli buffer. The cell lysates were then removed from the BSL-3 for further analysis. An equal

quantity of uninfected Vero E6 cells were processed similarly. The cell lysates were heated to 42°C for 30 minutes, then run on a 15% SDS-PAGE gel and transferred to a PVDF membrane. A sample membrane was stained with Ponceau to assess loading quantities. The remaining membranes were blocked for 30 minutes at room temperature with 2% bovine serum albumin, 1% polyvinylpyrrolidone, 0.1% tween-20 in PBS (PBS-T). 1v6 and NRC-772 were used at 1:1000 while 154C, 240C, 341C, 540C, 19C, 42C, 283C, and 472C were used at 1:100. The primary antibodies diluted in blocking buffer and incubated with the membranes at room temperature for 4 hours before being washed thrice with PBS-T. Secondary antibodies were anti-Human-HRP (SAB3701359) for 1v6 and CR3022 at 1:5000; anti-rabbit-HRP (7074) for NRC-772 at 1:5000; anti-mouse-IgG-HRP (7076) for 240C, 341C, 540C, and 283C at 1:1000; anti-mouse-IgM-HRP (62-6820) for 154C, 19C, 42C, and 472C. Blots were stained with SuperSignal™ West Pico PLUS Chemiluminescent Substrate (ThermoFisher Scientific) using an ImageQuant LAS 4000 imager (GE Life Sciences).

Quantification and Statistical Analysis

Sequence alignments and identity scores were calculated using the T-Coffee software package via the online portal. The EC_{50} values for ELISA and live virus neutralization were calculated using a three-parameter logistic regression model in Python using the SciPy statistics library. Each EC_{50} includes data from three replicate experiments and unless otherwise noted, three technical replicates within each experiment. K_D values were calculated in Fortebio Data Analysis HT software and fit to a 1:1 binding model and globally fit to both the association and dissociation curves of all concentrations with response values above 0.005 nm.

Section 2.6: Supplemental Figures

Figure S2.1 Alignment of structural proteins for SARS-CoV and SARS-CoV-2

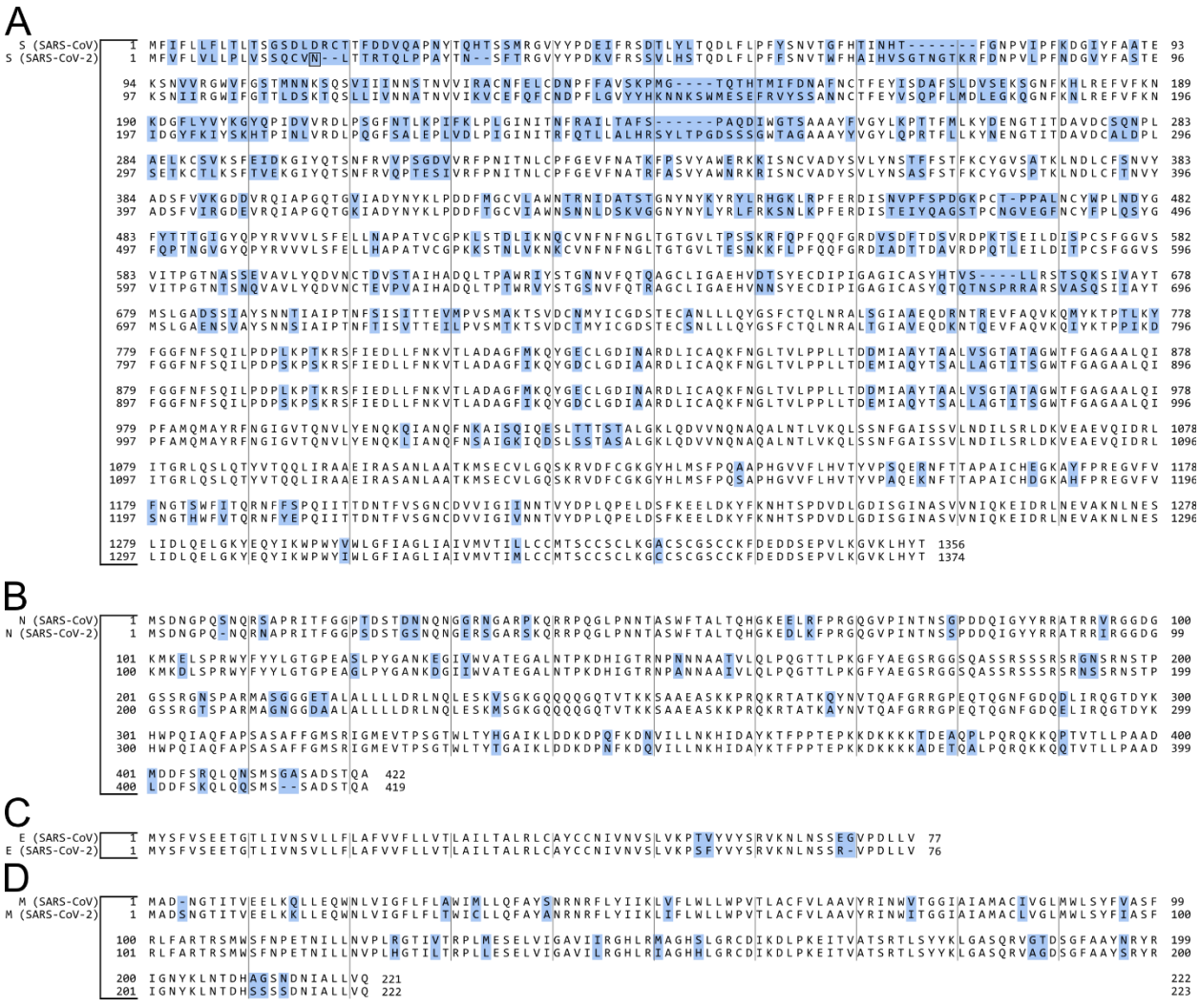

Protein sequences were obtained from Uniprot. Differences are highlighted in blue. Grey lines are spaced every 10 characters. For each pair, SARS-CoV is on the top and SARS-CoV-2 is on the bottom. (**A**) Spike, (**B**) Nucleocapsid, (**C**) Envelope, and (**D**) Membrane proteins.

Figure S2.2 Immunofluorescence of SARS-CoV-2 structural proteins using SARS-CoV antibodies at 63× magnification.

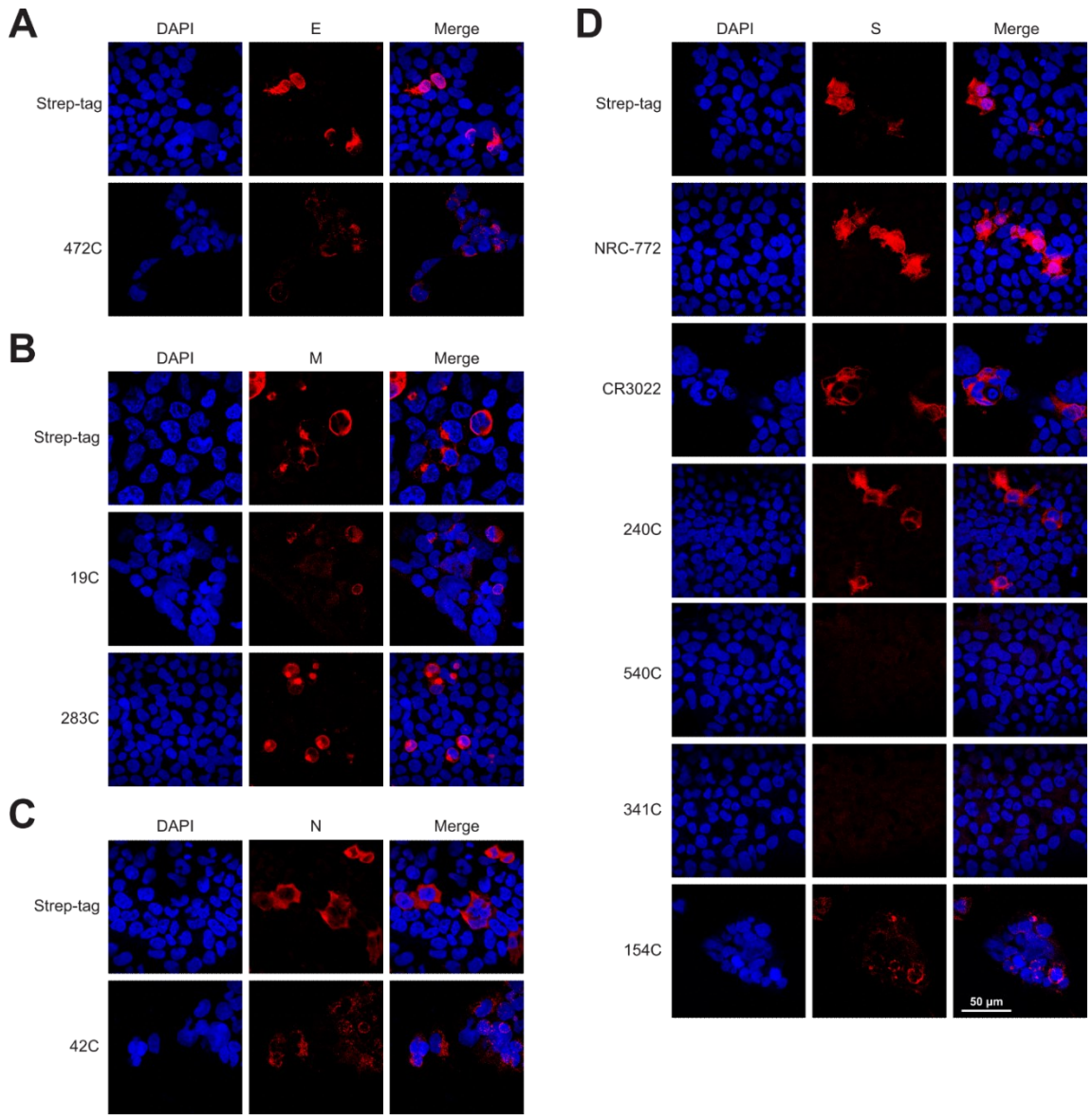

Representative immuno-fluorescence images of HEK 293T cells transiently transfected with SARS-CoV-2 structural proteins. 24 h post-transfection, cells were fixed and stained with the listed SARS-CoV antibodies: (**A**) Envelope, (**B**) Membrane, (**C**) Nucleocapsid, and (**D**) Spike proteins. All proteins are strep-tagged and control stained with anti-strep-tag antibody or the indicated antigen-specific antibody (Red). DAPI (Blue) was used to visualize cell nuclei.

Figure S2.3 Complete western blot and gel images.

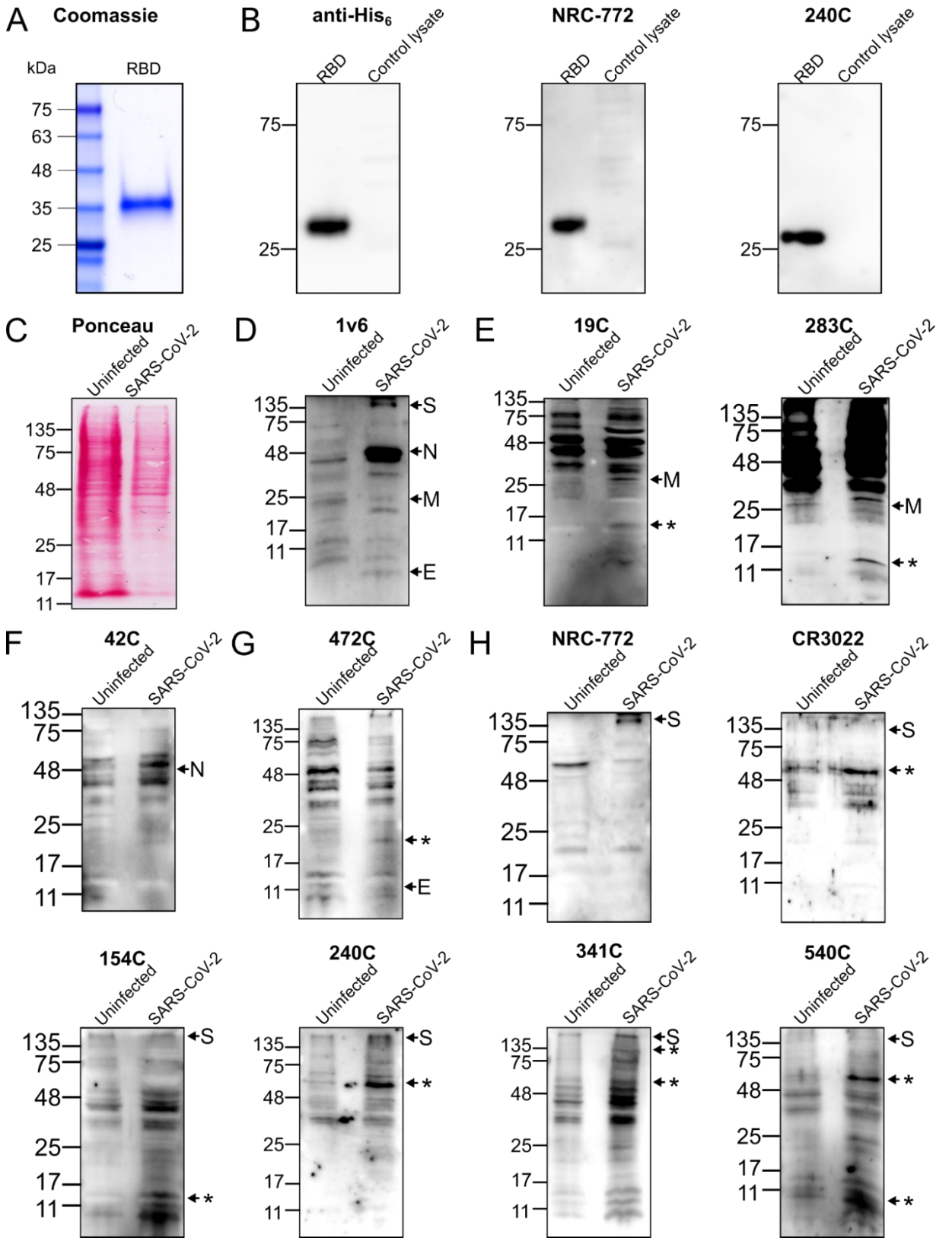

(**A**) Coomassie stain of purified RBD used in B. (**B**) purified SARS-CoV-2 spike RBD protein and control wild-type HEK 293T lysate probed with anti-S monoclonal antibodies. (**C**) Ponceau staining of SARS-CoV-2 infected and uninfected Vero E6 cell lysate. Western blots with SARS-CoV-2 lysates stained with (**D**) convalescent human serum (**E**) anti-M (**F**) anti-N (**G**) anti-E and (**H**) anti-S SARS-CoV monoclonal antibodies. Arrows indicate expected molecular weight and * indicates expected alternate bands based on western blot results from previous reports[20].

Figure S2.4 ELISA extended data.

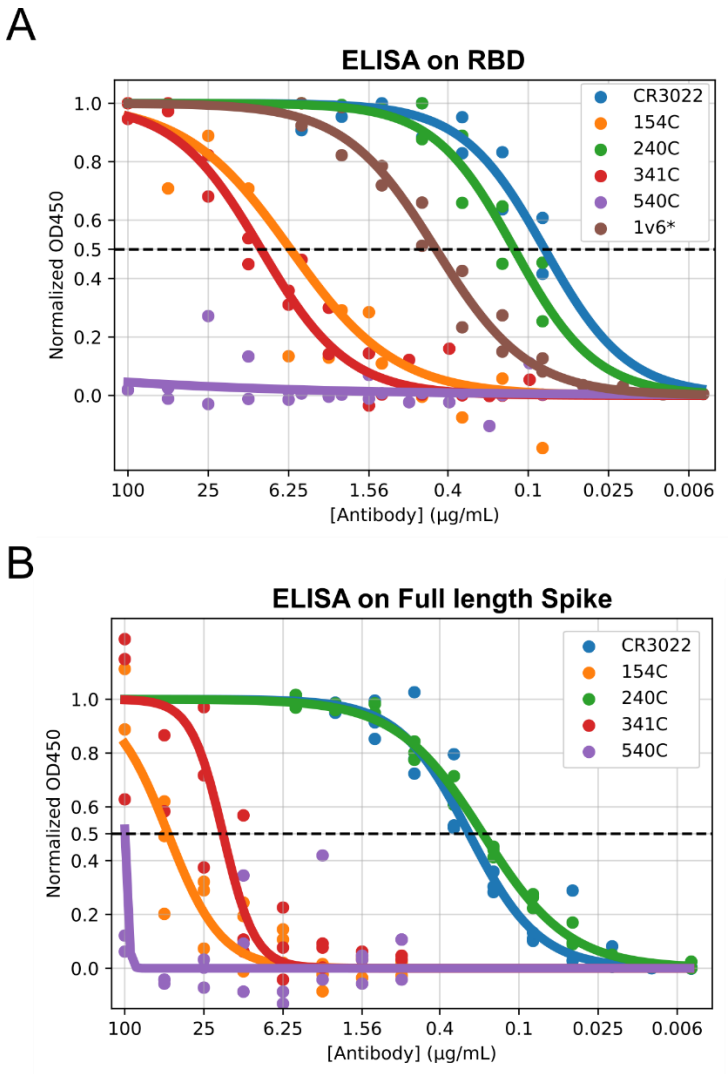

ELISA against (**A**) RBD coated at 2 µg/mL and (**B**) full length spike coated at 2 µg/mL and then probed with the indicated monoclonal antibody, or 1v6 human convalescent serum. Each point represents the mean of 2 or 3 technical replicates from a single experiment. Data were normalized according to the maximum signal seen for each secondary antibody in each experiment. *1v6 is convalescent serum used to validate the assay. A stock concentration of 1 mg/mL was used to facilitate calculations for reference purposes, but this does not represent an accurate EC_{50} value.

Figure S2.5 BLI extended data.

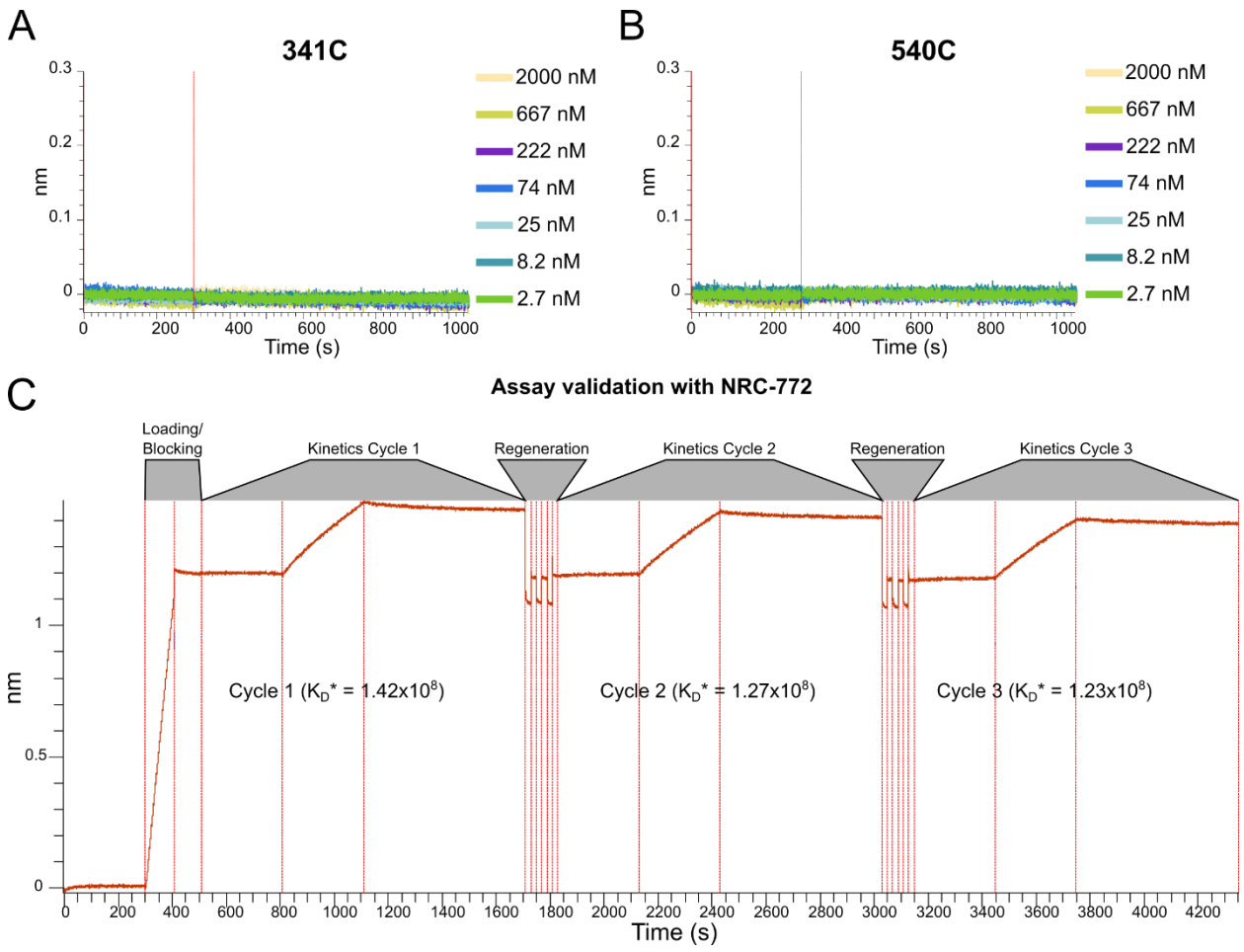

Negative binding curves for antibodies (**A**) 341C and (**B**) 540C. (**C**) NRC-772 rabbit polyclonal antibody used for method validation. Curves show minimal loss of signal with multiple regeneration cycles as well as stable K_D values, demonstrating stability of RBD under regeneration conditions. NRC-772 serum used at 1:50 dilution in kinetics buffer. *K_D values assume 1 mg/mL initial concentration in order to facilitate K_D calculation only as a reference between cycles and does not represent an accurate affinity measurement.

Figure S2.6 SARS-CoV-2 neutralization extended data.

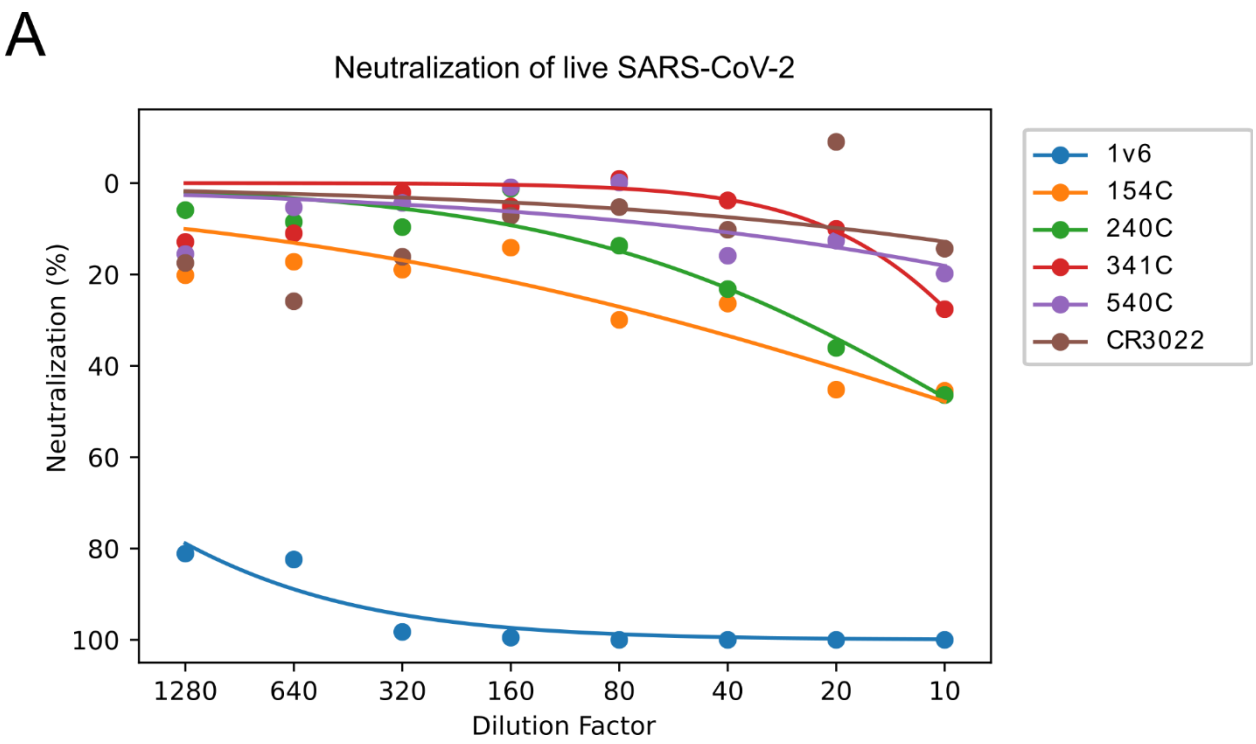

(**A**) Vero E6 cells were infected with approximately 30 pfu/well of live SARS-CoV-2 which was pre-incubated for 1 hour with the indicated final dilutions of antibodies before the addition of overlay media and 48 hours of incubation. Each point represents the average of three biological replicates, each in technical triplicate.

Section 2.7: Acknowledgments

2.7.1 Acknowledgments

This work was supported by NIH training grant T32AI747225 on Interactions at the Microbe-Host Interface and OHSU Innovative IDEA grant 1018784. BLI data were generated on an Octet Red 384, which is made available and supported by OHSU Proteomics Shared Resource facility and equipment grant number S10OD023413. We acknowledge the support of the members of the Messer lab who performed collection of patient samples and the patients who agreed to donate samples for scientific research.

2.7.2 Author contributions

Conceptualization: F.G.T. and T.A.B.; methodology, formal analysis, and investigation: T.A.B., J.B.W., S.F., H.C.L., and F.G.T.; resources: W.B.M.; writing – original draft: T.A.B., J.B.W., and S.F.; writing – review and editing: all authors; visualization: T.A.B., J.B.W., S.F., H.C.L., and F.G.T.; supervision: F.G.T.; project administration: F.G.T.; fund acquisition: F.G.T.

Chapter 3: Neutralization of SARS-CoV-2 variants by convalescent and BNT162b2 vaccinated serum

Timothy A. Bates[1,8], Hans C. Leier[1,8], Zoe L. Lyski[1], Savannah K. McBride[1], Felicity J. Coulter[1], Jules B. Weinstein[1], James R. Goodman[2], Zhengchun Lu[1], Sarah A. R. Siegel[3], Peter Sullivan[3], Matt Strnad[3], Amanda E. Brunton[3], David X. Lee[1], Andrew C. Adey[4,5], Benjamin N. Bimber[6], Brian J. O'Roak[4], Marcel E. Curlin[7,*], William B. Messer[1,3,7,*], & Fikadu G. Tafesse[1,*]

[1]Department of Molecular Microbiology & Immunology, Oregon Health & Science University (OHSU), Portland, OR, USA.

[2]Medical Scientist Training Program, OHSU, Portland, OR, USA.

[3]OHSU-PSU School of Public Health, Program in Epidemiology, Portland, OR, USA.

[4]Department of Molecular & Medical Genetics, OHSU, Portland, OR, USA.

[5]Knight Cardiovascular Institute, OHSU, Portland, OR, USA.

[6]Vaccine and Gene Therapy Institute, OHSU, Beaverton, OR, USA.

[7]Department of Medicine, Division of Infectious Diseases, OHSU, Portland, OR, USA.

[8]These authors contributed equally: Timothy A. Bates, Hans C. Leier.

*Correspondence: curlin@ohsu.edu; messer@ohsu.edu; tafesse@ohsu.edu

Nature Communications, Volume 12, Article 5135. August 26, 2021.

DOI: https://doi.org/10.1038/s41467-021-25479-6

Section 3.1: Abstract

SARS-CoV-2 and its variants continue to infect hundreds of thousands every day despite the rollout of effective vaccines. Therefore, it is essential to understand the levels of protection that these vaccines provide in the face of emerging variants. Here, we report two demographically balanced cohorts of BNT162b2 vaccine recipients and COVID-19 patients, from which we evaluate neutralizing antibody titers against SARS-CoV-2 as well as the B.1.1.7 (alpha) and B.1.351 (beta) variants. We show that both B.1.1.7 and B.1.351 are less well neutralized by serum from vaccinated individuals, and that B.1.351, but not B.1.1.7, is less well neutralized by convalescent serum. We also find that the levels of variant-specific anti-spike antibodies are proportional to neutralizing activities. Together, our results demonstrate the escape of the emerging SARS-CoV-2 variants from neutralization by serum antibodies, which may lead to reduced protection from re-infection or increased risk of vaccine breakthrough.

Section 3.2: Introduction

Since its emergence in Wuhan, China in late 2019, severe acute respiratory syndrome coronavirus 2 (SARS-CoV-2) has spread worldwide, causing widespread illness and mortality from coronavirus 2019 disease (COVID-19)[329]. Continued SARS-CoV-2 transmission has led to the emergence of variants of concern (VOC) that show evidence of increased transmissibility or resistance to prior immunity[46,330]. By early 2021, three major VOCs were widely recognized: B.1.1.7, also called variant alpha[331]; B.1.351, also called variant beta; and P.1, also called variant gamma[331,332]. These VOCs were associated with increases in infections and hospitalizations in their countries of origin, and all have increased in frequency in other regions, suggesting a competitive fitness advantage over existing lineages[333].

Though a relatively small number of nonsynonymous mutations and deletions distinguish VOCs from earlier lineages (Table S3.1), many of these encode residues in the spike protein, which interacts with the SARS-CoV-2 cellular receptor, angiotensin-converting enzyme 2 (ACE2), via its receptor-binding domain (RBD)[334,335]. RBD mutations could potentially increase transmissibility by enhancing binding to ACE2, or promote immune escape by altering epitopes that are the primary target of potently neutralizing antibodies[335]. In fact, the most prominent mutation that appeared early in the pandemic and rose to near-fixation in new strains was a substitution at spike residue position 614 (D614G) which positions the RBD in a more accessible configuration and confers greater infectivity but also greater susceptibility to neutralizing antibodies[57,336].

In addition to sharing D614G and a N501Y substitution which is associated with greater ACE2 affinity[337], VOCs have acquired other spike mutations, some of which are associated with resistance to antibody neutralization. These include E484K and K417N/T, both of which arose independently in the B.1.351 and P.1 lineages[61,338,339]. Epidemiological reports suggest that natural immunity to earlier SARS-CoV-2 lineages may confer limited protection from reinfection by B.1.351 or P.1[331,340], and prior analyses using relatively small numbers of vaccinee sera against pseudotyped or chimeric viruses showed reduced neutralization of B.1.351 and P.1[339,341].

In this study, we use clinical virus isolates of SARS-CoV-2, the B.1.1.7 variant, and the B.1.351 variant to examine the potency of the antibody response to both BNT162b2 vaccination and natural infection. We find that vaccinated serum is less effective at neutralizing B.1.1.7 and B.1.351 than early lineage SARS-CoV-2, and that convalescent serum is less neutralizing against B.1.351, but B.1.1.7 is similarly neutralized compared to early lineage SARS-CoV-2. Further, we find that age correlates negatively with vaccine response against both variants, and that following

natural infection, neutralizing antibody titers wane to undetectable levels within 6 months to a year after infection.

Section 3.3: Results

3.3.1 Antibody response to BNT162b2 vaccination

The three COVID-19 vaccines authorized for emergency use by the U.S. Food and Drug Administration (BNT162b2 [Pfizer–BioNTech], mRNA-1273 [Moderna], and Ad26.COV2.S [Janssen]) elicit immunity using a spike protein antigen derived from early isolates such as USA_WA1/2020 (WA1)[342]. Numerous reports have shown that the mutant spike proteins expressed by the VOCs may bind less strongly to antibody repertoires induced by these vaccines[50,227,343]. RBD-binding antibody levels in adults who had received two doses of the BNT162b2 mRNA vaccine were determined by ELISA using recombinant RBD from WA1 (RBD-WA1) and RBDs with all amino acid substitutions possessed by each B.1.1.7 (N501Y) and B.1.351 (N501Y, E484K, K417N) (Table S3.1). Compared to that of RBD-WA1, vaccinated patient sera had a geometric mean 50% effective concentrations (EC_{50}) which were 1.4-fold lower (P=0.0089) for RBD-B.1.1.7 and 1.5-fold lower (P=0.0351) for RBD-B.1.351 (Figure 3.1A). BNT162b2-elicited antibodies also displayed potent neutralizing activity against WA1 in a 50% focus reduction neutralization tests ($FRNT_{50}$) (geometric mean titer (GMT) 1:393 +/- 2.5) but decreased neutralization of B.1.1.7 (GMT 1:149 +/- 2.4) and B.1.351 (GMT 1:45 +/- 2.3), representing 2.6-fold (P<0.0001) and 8.8-fold (P<0.0001) reductions, respectively (Figures 3.1B and Supplementary Figure S3.1). The positive correlation between serum EC_{50} and NT_{50} was consistent for each matched variant-RBD pair, indicating that variant-specific RBD-targeted antibody concentration is proportional to live virus neutralization capacity against each lineage (Figure 3.1C).

We next compared the $FRNT_{50}$ values of each patient for WA1 to their $FRNT_{50}$ values for each of the variants, finding that neutralizing titers for WA1 and B.1.1.7 were highly correlated at the individual level (Figure 3.1D). In contrast, WA1 and B.1.351 $FRNT_{50}$ titers correlated weakly at the individual level, with some individuals' sera able to potently neutralize WA1 while simultaneously failing to neutralize B.1.351 at the highest concentration used in our assay (1:20) (Figure 3.1E). The lower correlation between B.1.351 with WA1 $FRNT_{50}$ values likely indicates that a larger proportion of the epitopes recognized by WA1 neutralizing antibodies are functionally altered in B.1.351 than in B.1.1.7.

Older adults make up the most vulnerable population to COVID-19 and therefore have been prioritized for vaccination[50]. We found similar age-dependent decline in FRNT50 titers against each lineage in our study (Figures 3.1F-3.1H and Table S3.1). These differences were highly significant for all three variants between subgroups of younger (20-50 y.o. n=25) and older (>50 y.o. n=25) adults in our cohort (Figure 3.1I). There was no correlation between gender and neutralization titers after vaccination (Figure S3.3).

Figure 3.1 Serum antibody levels of BNT162b2 vaccine recipients and potency of sera to neutralize SARS-CoV-2 variants.

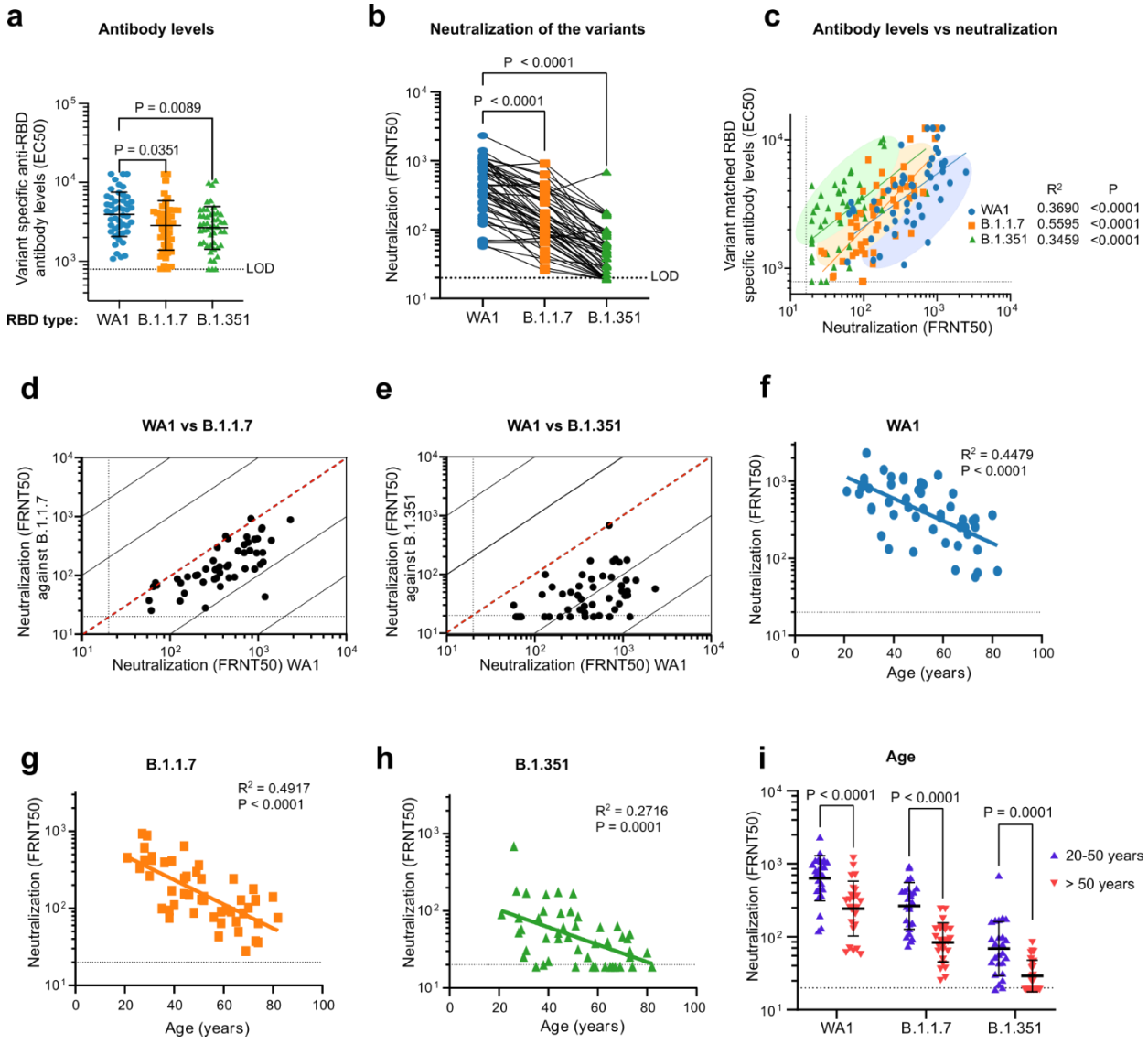

(**a**) Serum antibody levels (EC_{50}) that recognize the spike RBD of the wild-type USA-WA1/2020 (WA1) (Blue circles), B.1.1.7 (Orange squares), and B.1.351 (Green triangles) variants are shown. The RBD-B.1.1.7 carries the N501Y mutation, the only RBD mutation present in the B.1.1.7 variant. The RBD-B.1.351 has the K417N, E484K, and N501Y mutations which are the only three RBD mutations present in the B.1.351 variant. n = 51 biologically independent

samples. (**b**) Comparison of neutralization titers (FRNT50) between WA1, B.1.1.7 (P = 0.0351) and B.1.351 (P = 0.0089) for BNT162b2 vaccinee sera. n = 50 biologically independent samples. (**c**) Correlation of variant matched RBD-specific antibody levels and neutralization titers ($FRNT_{50}$) of the WA1 virus and the two variants. (**d**), (**e**) Correlations between neutralization titers of the B.1.1.7 (**d**) and B.1.351 (**e**) variants with the WA1 virus. The dotted diagonal lines indicate identical neutralization, and the solid diagonal black lines indicate 10-fold differences in neutralization. (**f**)–(**h**) Correlation between participant age and neutralization titer against WA1 (**f**) (P < 0.0001), B.1.1.7 (**g**) (P < 0.0001), and B.1.351 (**h**) (P < 0.0001). n = 50 biologically independent samples. (**i**) Effect of age range 20–50 years (blue triangle) and >50 years (red inverted triangle) on the neutralization potency among the BNT162b2 vaccine recipients (WA1, B.1.1.7 P < 0.0001, B.1.351 P = 0.0001). n = 25 biologically independent samples per age group. For (**a**), (**b**), (**f**)–(**i**), data are presented as the mean ± SD of log transformed values; P values are two-sided and include a Šidák multiple comparison correction. All experiments were performed in duplicate.

3.3.2 Antibody response to natural SARS-CoV-2 infection

In contrast to the spike-specific antibody repertoire raised by BNT162b2 vaccination, the antibody response to SARS-CoV-2 infection is more antigenically diverse[7]. Overall, RBD binding activities against all lineages were significantly lower in convalescent sera compared to vaccinee sera across all sample timepoints (1-301 days post-PCR positive) (Figures 3.1A and 3.2A). Moreover, there was no observable difference in convalescent serum EC50 between RBD-WA1, RBD-B.1.1.7, and RBD-B.1.351 (Figure 3.2A). In convalescent sera, there was also no clear correlation between variant-specific RBD binding and neutralization (Figure 3.2C). To better capture the reduced antibody levels, we modified our ELISA protocol to reduce the limit of

detection to 1:200 (compared with 1:1600 for vaccinee ELISAs). Differences in FRNT50 titer against WA1 and the VOCs were similarly reduced overall compared to vaccinee sera (WA1, GMTs 1:52.1 +/- 4.3; B.1.1.7, 1:36.8 +/- 3.0; B.1.351, 28.8 +/- 2.3) but showed substantially less variability with a 1.8-fold drop for B.1.351 and a 1.4-fold drop for B.1.1.7 relative to WA1 (Figures 3.2B and Figure S3.2). Many convalescent sera fell below the FRNT limit of detection (Figures 3.2D-E): for WA1, 43% of convalescent cohort sera failed to neutralize ≥50% of input virus at the lowest dilution, and this proportion was even greater for the VOCs (B.1.1.7, 54%; B.1.351, 64%).

It remains unclear which factors, if any, are predictive of protection following recovery from COVID-19, however at least one study has shown a link between disease severity and final neutralizing antibody titer[331]. While our convalescent cohort did not show any significant correlation between $FRNT_{50}$ and disease severity (Figure S3.4), this may be due to differences in average disease severity between our cohorts. We additionally saw no correlation between neutralizing titer for any lineage with patient age, sex, or hospitalization for COVID-19 (Figure S3.4). Looking at the entire convalescent cohort, we see no significant correlation between $FRNT_{50}$ and time between sample collection and first positive PCR test result for COVID-19 (Figure S3.4). However, subsetting the cohort into groups based on different ranges of days post PCR test, we see the median titer follow a similar trajectory to those reported in previous studies (Figure 3.2F). Median titer values for all variants start (1-13 days) at a low point, increase to a maximum at 14-90 days, then decrease over 300 days. These results are in agreement with previous reports indicating that immunity resulting from vaccination peaks around 14 days after receiving the second boost, then wanes with a half-life of 69 days[344]. Although serum neutralizing antibody titers apparently decrease over time, recent studies have shown that memory B cells can persist for at least a year following infection[345,346].

Figure 3.2 Neutralization of SARS-CoV-2 variants by convalescent serum.

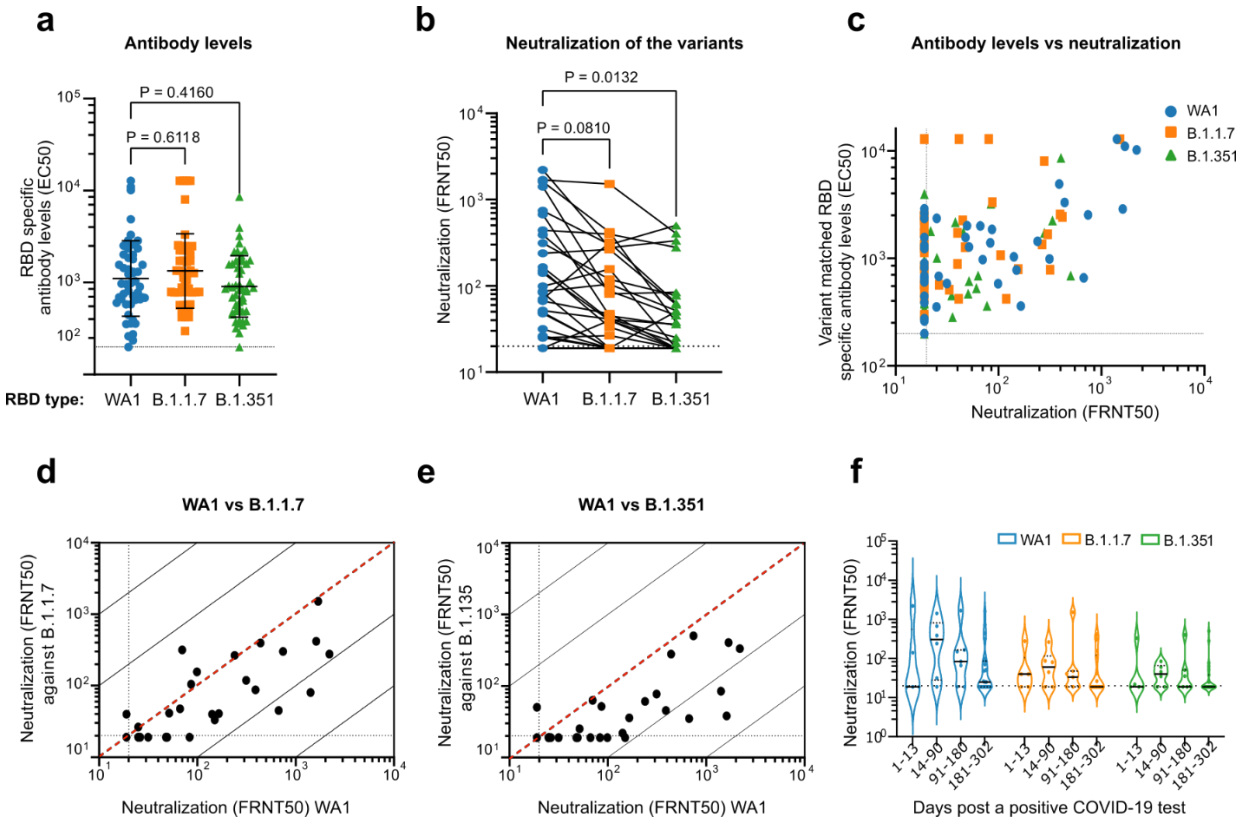

(**a**) Quantification of serum antibody levels (EC_{50}) that recognize RBD protein corresponding to the wild-type (WA1)(blue circles), B.1.1.7 (orange squares), and B.1.351 (green triangles) variants. n = 50 biologically independent samples. Data are presented as the mean ± SD of log transformed values. (**b**) Comparison of neutralization titers between WA1, B.1.1.7, and B.1.351 for convalescent sera. n = 44 biologically independent samples. (**c**) Relationship between convalescent antibody levels and neutralization ($FRNT_{50}$) of the different viral variants. (**d**), (**e**) Correlations between convalescent serum neutralization titer of the B.1.1.7 (**d**) and B.1.351 (**e**) variants with the WA1 virus. The dotted diagonal lines indicate identical neutralization, and the solid diagonal black lines indicate 10-fold differences in neutralization. (**f**) Violin plots indicating $FRNT_{50}$ values for WA1 (blue), B.1.1.7 (orange), and B.1.351 (green), stratified by

the number of days between the date of confirmatory COVID-19 PCR test and the date of serum sample collection. Black bars indicate median $FRNT_{50}$ for each group. For (**a**), (**b**), (**f**) P values are two-sided and include a Šidák multiple comparison correction. All experiments were performed in duplicate.

Section 3.4: Discussion

In this study we provide evidence of reduced antibody-mediated immunity to newly emerging SARS-CoV-2 variants B.1.1.7 and B.1.351 after immunization with the Pfizer-BioNTech COVID-19 vaccine or following natural infection. Our study involves a relatively large cohort, provides data well-balanced for gender and age distribution, controls for time since vaccination, and directly compares early-type and two newly emerging SARS-CoV-2 variants of global concern. Critically, we use authentic clinical isolates that display the native antigenic landscape of the virus, an approach that provides the best possible examination of antibody activity against these viruses.

While it is likely that the resistance of some VOCs to neutralization is driven by accumulated mutations in the RBD and the rest of the spike protein, and there is evidence that high levels of RBD-binding antibodies is a meaningful correlate of protection from isogenic lineages[335,347], other features of host immunity may contribute to protection. Specifically, the neutralization titers seen in our convalescent subjects, while lower overall, have a smaller gap in neutralizing activity between WA1 and VOCs than in BNT162b2 vaccinees. This difference between convalescents and vaccinees suggests that SARS-CoV-2 infection may elicit more broadly cross-reactive and potentially cross-neutralizing antibodies, even with reduced affinity for mutant RBDs. This notion has a strong foundation in coronavirus research, as there is substantial cross-reactivity of anti-SARS-CoV spike antibodies with SARS-CoV-2 spike[348]. Indeed, risk of

reinfection by VOCs may be driven by generally low serological responses in most COVID-19 patients, rather than the presence of RBD mutations that allow immune escape. Other arms of the adaptive immune response that we did not explore here, such as T cell immunity, could also contribute to cross-lineage immunity[349].

A particularly significant finding was the negative correlation between age and neutralizing antibody titer against VOCs in vaccinees, given that age is the predominant risk factor for severe COVID-19[350] and patients of advanced age stand to benefit the most from vaccination. Longitudinal studies of this and other cohorts could examine the durability of vaccine-induced immune responses and should be designed to resolve the nature of antibody responses induced by vaccination or natural infection that may correlate with broad cross-neutralization. At least one new study attempts answer this by estimating the minimum protective antibody titer using data from various published SARS-CoV-2 studies combined with validated influenza models[125]. At the same time, others have begun quantifying rates of vaccine breakthrough infections for various VOCs[351]. Our data suggests that protection from natural infection-derived immunity wanes considerably by 6 months to a year post infection, and that vulnerability to the B.1.1.7 and B.1.351 viruses is likely higher than for the original SARS-CoV-2 lineage. Further work is needed to identify more precisely the protective antibody titer threshold, which will be particularly important for developing vaccines that will be effective in vulnerable populations, including those of advanced age, against future SARS CoV-2 variants.

Section 3.5: Methods

3.5.1 Ethics statement

This study was conducted in accordance with the Oregon Health & Science University Institutional Review Board (IRB#00022511 & #21230). Written informed consent was obtained for all study participants.

3.5.2 Serum collection

Vaccinated cohort - IRB#00022511:

Subjects were enrolled at Oregon Health & Science University immediately after receiving their first dose of the Pfizer-BioNTech COVID-19 vaccine. After written obtaining informed consent, 4-6 mL of whole blood were collected (BD Vacutainer® Plus Plastic Serum Tubes) and centrifuged for 10 minutes at 1000 x g. A second blood sample was obtained 14-15 days after subjects received their second dose of the Pfizer-BioNTech COVID-19 vaccine. Samples were stored at -20°C until sera were collected for neutralization assay. A subset of serological samples (n=51) was randomly selected while maintaining equal gender representation, balanced age distribution, time between vaccination doses equal to 21 days +/- 1 day, and time from boost to blood sampling equal to 14 days +/- 1 day. Randomization was performed using R version 4.0.3 in RStudio version 1.2.5001.

Natural infection cohort - IRB#21230:

Subjects with confirmed COVID-19 infection were part of a larger cohort of COVID-19 individuals at the Oregon Health & Science University. After obtaining written informed consent, 10mL of whole blood was collected for serum (BD Vacutainer® Red Top Serum Tubes), and 40mL of whole blood were collected for PBMCs and plasma (BD Vacutainer® Lavender Top EDTA Tubes). Serum tubes were centrifuged for 10 minutes at 1000 x g. Samples were heat-

inactivated for 30 minutes at 56°C and stored at -20°C until needed. A subset of serological samples (*n*=50) from individuals with time post infection (determined by date of first positive PCR) ranging from 1 day – 10 months, a spectrum of disease severity scores and clinical disease ranging from asymptomatic to severe (hospitalized in the ICU) were chosen for this analysis.

3.5.3 Cell culture

Vero E6 monkey kidney epithelial cells (CRL-1586) were obtained from the ATCC. Unless otherwise stated, cells were maintained at all times in standard tissue culture-treated vessels in complete media (DMEM, 10% FBS, 1% nonessential amino acids, 1% penicillin-streptomycin) at 37°C and 5% CO_2.

3.5.4 SARS-CoV-2 growth and titration

SARS-CoV-2 isolates USA/CA_CDC_5574/2020 [lineage B.1.1.7] (NR-54011), hCoV-19/South Africa/KRISP-K005325/2020 [lineage B.1.351] (NR-54009), and USA-WA1/2020[352] [lineage A] (NR-52281) were obtained through BEI Resources and sequenced following a single passage: (WA1/2020 isolate GenBank: SAMN18527778 and p1 GenBank: MZ344995; B.1.1.7 isolate GenBank: SAMN18527802 and p1 GenBank: MZ344998; B.1.351 isolate GenBank: SAMN18527801 and p1 GenBank: MZ344999). Sub-confluent monolayers of Vero E6 cells in 75 cm^2 flasks were inoculated with the p0 isolates and grown for 72 h, at which time significant cytopathic effect was observed for all strains. Culture supernatants were removed, centrifuged 10 min at 1,000 x g, and stored in aliquots at -80°C. To determine titer, confluent monolayers of Vero E6 cells in 96-well plates were inoculated with tenfold serial dilutions of SARS-CoV-2 prepared in dilution media (Opti-MEM, 2% FBS) for 1 h at 37°C, then covered with overlay media (Opti-MEM, 2% FBS, 1% methylcellulose) and cultured an additional 24 h. Overlay media was then removed, and plates were fixed for 1 h in 4% paraformaldehyde in PBS. To

develop foci, cells were permeabilized for 30 minutes in perm buffer (0.1% BSA, 0.1% Saponin in PBS) and incubated with 1:5,000 polyclonal anti-SARS-CoV-2 alpaca serum, generated by immunization of an alpaca with recombinant SARS-CoV-2 S and N proteins (Capralogics Inc.), for 2 hours at room temperature. Plates were washed three times with wash buffer (0.01% Tween-20 in PBS), then incubated with 1:20,000 anti-alpaca-HRP (Novus #NB7242) for 2 hours at room temperature. Plates were again washed three times with wash buffer and 30µL of KPL TrueBlue substrate (Seracare #5510-0030) added to each well. Plates were incubated at room temperature for 20 minutes and imaged with a CTL Immunospot Analyzer, then foci were counted using CTL ImmunoSpot (7.0.26.0) Professional DC[348].

Additional SARS-CoV-2 isolates were propagated and titrated during the development of this assay. They included the three previously described clinical isolates: USA/CA_CDC_5574/2020 [lineage B.1.1.7] (NR-54011), hCoV-19/South Africa/KRISP-K005325/2020 [lineage B.1.351] (NR-54009), and USA-WA1/2020 [lineage A] (NR-52281) as well as two additional clinical isolates: hCoV-19/South Africa/KRISP-EC-K005321/2020 [lineage B.1.351] (NR-54008) and hCoV-19/England/204820464/2020 (NR-54000). Substantial differences were noted in the focus phenotypes of these strains (Figure S3.5).

3.5.5 SARS-CoV-2 Sequencing

Isolated viral RNA was subjected to first strand synthesis reverse transcription (RT) to produce single-stranded cDNA using Protoscript II (NEB), then amplified via pooled amplicon PCR using a 1,200 base pair overlapping amplicon strategy[353]. Individual sample PCR reactions were pooled, cleaned, and then subjected to shotgun sequencing library preparation[354,355]. Samples were then sequenced on a NextSeq500 using universal primers (Table S3.2) with a custom sequencing protocol (Read 1: 50 imaged cycles; Index Read 1: 8 imaged cycles, 27 dark cycles,

10 imaged cycles; Index Read 2: 8 imaged cycles, 21 dark cycles, 10 imaged cycles; Read 2: 50 imaged cycles)[355]. FASTQ reads were quality trimmed and aligned to the reference genome (GenBank: NC_045512), using BWA-mem. Quasispecies variant calling was performed using LoFreq[356]. Structural variant calling was conducted using Pindel[357]. Variant and coverage data were used to generate a per-sample consensus sequence, requiring a variant to be >50% of the total reads to be included. Consensus data used linage assignment using Pangolin[40]. Each cultured isolate consensus was compared to the original clinical isolate genome accessed from GISAID.

3.5.6 SARS-CoV-2 FRNT

Serial dilutions of patient sera and virus neutralization were carried out in duplicate, using separately prepared dilutions, in a 96-well plate format. Each sample was added in duplicate 1:10 to dilution media, and 4 four-fold serial dilutions were made spanning a range from 1:10 to 1:2560. An equal volume of dilution media containing 50 FFU of SARS-CoV-2 was added to each well (final dilutions of sera, 1:20 – 1:5120) and incubated 1 h at 37°C. The virus-sera mixtures were then added to monolayers of Vero E6 in corresponding 96-well plates, incubated 1 h at 37°C, and covered with overlay media. Fixation, foci development, and counting were carried out as described above in titration focus forming assay experiments. Focus counts were used to calculate percent neutralization by dividing by the average of positive control wells without patient serum treatment.

3.5.7 Production of variant RBDs

Site-directed mutagenesis was used to introduce mutations into Wild-type RBD (BEI resources #NR-52309). Purified SARS-CoV-2 WA1, B.1.1.7, and B.1.351 RBD protein was prepared by mammalian expression and Ni-NTA chromatography[348]. Sanger sequence confirmed (see Table S3.2 for primer sequences) recombinant RBD lentivirus was produced using

Lipofectamine 3000 (Invitrogen #L3000008) and used to generate stable HEK293F cells. Cells were allowed to grow for 3 days in Freestyle 293 expression media (Gibco # 12338018). Supernatant was collected by centrifugation at 1000×g for 10 minutes, then incubated with Ni-NTA beads for 1 hour at room temperature. The beads were washed with ten column volumes of 20mM imidazole in PBS, then eluted with 235mM imidazole in PBS. The purified protein was buffer exchanged into plain PBS and concentrated by 10 kDa cutoff column and purity was assessed by OD_{280} and SDS-PAGE.

3.5.8 ELISA

ELISAs were performed in biological duplicate 96-well plates (Nunc™ MaxiSorp™ #423501). Plates were coated 100 uL/well with purified wild-type SARS-CoV-2 RBD, RBD-501, or RBD-triple constructs at 1 ug/mL in PBS and incubated overnight at 4°C with rocking. Plates were then washed three times with wash buffer (0.05% Tween-20 in PBS) and blocked with 150 uL/well blocking buffer (5% nonfat dry milk powder and 0.05% Tween-20 in PBS) at RT for 1 hour with rocking. Convalescent and vaccinated patient sera were initially diluted in Opti-MEM in the 96-well plate format used above. For the ELISA, diluted vaccinated and infected patient sera were further diluted in blocking buffer on the plate (4×4-fold dilutions from 1:200 for infected patients; 4×2-fold dilutions from 1:1,600 for vaccinated patients). After incubating at RT for 1 hour with rocking, plates were washed three times. The secondary antibody Goat anti-Human IgG, IgM, IgA (H+L) (Invitrogen, #A18847) was diluted in blocking buffer (1:10,000) and applied to the plates 100 uL/well. Plates were protected from light and incubated at RT for 1 hour with rocking, then washed three times prior to the addition of the peroxidase activity detector 3,3',5,5'-tetramethylbenzidine (TMB, Thermo Scientific Pierce 1-Step Ultra TMB ELISA Substrate #34029). The reaction was stopped after 5 minutes using an equivalent volume of 1 M H_2SO_4;

optical density (OD) was measured at 450 nm using a CLARIOstar plate reader. OD_{450} readings were normalized by subtracting the average of negative control wells and finally dividing by the average maximum signal (95^{th} percentile) for each unique coating protein in each experiment.

3.5.9 $FRNT_{50}$ and EC_{50} calculation

Percent neutralization values for FRNT50 or normalized OD_{450} values for EC_{50} were compiled and analyzed using python (v3.7.6) with numpy (v1.18.1), scipy (v1.4.1), and pandas (v1.0.1) data analysis libraries. Data from biological replicates was combined and fit with a three-parameter logistic model. For $FRNT_{50}$s, values were simultaneously calculated for individual biological replicates and patients for whom individual replicate $FRNT_{50}$ values differed by more than 4-fold were excluded from further analysis. Final $FRNT_{50}$ values below the limit of detection (1:20) were set to 1:19. Final EC_{50} values below the limit of detection (1:1600 for vaccine cohort, 1:200 for natural infection cohort) were set to 1:1599 for the vaccine cohort and 1:199 for the natural infection cohort. EC_{50} and $FRNT_{50}$ curves were plotted using python with the Matplotlib (v3.1.3) data visualization library.

3.5.10 Statistical analysis

Aggregated EC_{50} and $FRNT_{50}$ values were analyzed in Graphpad Prism (v9.0.2). EC50 and FRNT50 data were log transformed and one-way ANOVA using the Šidák multiple comparison correction was used for columnated data while two-way ANOVA using the Šidák multiple comparison correction was used for grouped data. The reported statistical methods are indicated in the relevant figure legends. Comparison of fold reduction and 95% confidence intervals for EC_{50} and $FRNT_{50}$ were generated using one-way ANOVA. Linear model fitting was performed on log transformed EC_{50} and $FRNT_{50}$ data and statistical significance was determined by F test with a zero-slope null hypothesis. All *P*-values were two-tailed with a

significance cutoff of 0.05. Patient samples with missing data points or demographic information were excluded from individual analyses which utilized those values.

Section 3.6: Supplemental Tables and Figures

*Table S3.1 List of mutations in B.1.1.7 and B.1.351 SARS-CoV-2 clinical isolates**

Lineage	GISAID Clade	GISAID ID	Spike mutations	Non-Spike mutations
B.1.1.7	GR	EPI_ISL_683466	H69del, V70del, Y145del, #N501Y, A570D, D614G, P681H, T716I, S982A, D1118H	N D3L, N G204R, N R203K, N S235F, NS8 Q27stop, NS8 R52I, NS8 Y73C, NSP3 A890D, NSP3 A1305V, NSP3 I1412T, NSP3 T183I, NSP6 F108del, NSP6 G107del, NSP6 S106del, NSP12 P323L, NSP13 K460R, NSP14 E347G
B.1.351	GH	EPI_ISL_678570	D80A, D215G, L242del, A243del, L244del, #K417N, #E484K, #N501Y, D614G, Q677H**, A701V	E P71L, N T205I, NS3 Q57H, NS3 S171L, NSP2 T85I, NSP3 K837N, NSP5 K90R, NSP6 F108del, NSP6 G107del, NSP6 S106del, NSP12 P323L

Mutation within the RBD

* Obtained from BEI Resources

** Additional mutation not found in clinical isolate

Table S3.2 List of primers used in this study

Oligo	**Sequence**
M13 reverse (pCAGGS sequencing primer)	CAGGAAACAGCTATGAC
Tn5-i5-Adapter	TCGTCGGCAGCGTCTCCACGC [i5-Tn5-Index] GATCGAGGACGGCAGATGTGTATAAGAGACAG
Tn5-i7-Adapter	GTCTCGTGGGCTCGGCTGTCCCTGTCC [i7-Tn5-Index] CCGTCTCCGCCTCAGATGTGTATAAGAGACAG
Tn5-ME	5Phos/CTGTCTCTTATACACATCT
PCR-i5-Primer	AATGATACGGCGACCACCGAGATCTACAC [i5-PCR-Index] TCGTCGGCAGCGTC
PCR-i7-Primer	CAAGCAGAAGACGGCATACGAGAT [i7-PCR-Index] GTCTCGTGGGCTCGG
Read 1 Sequencing Primer	GATCGAGGACGGCAGATGTGTATAAGAGACAG
Read 2 Sequencing Primer	CCGTCTCCGCCTCAGATGTGTATAAGAGACAG
Index 1 Sequencing Primer	CTGTCTCTTATACACATCTGAGGCGGAGACGG
Index 2 Sequencing Primer	CTGTCTCTTATACACATCTGCCGTCCTCGATC

Figure S3.1 Vaccinee serum $FRNT_{50}$ curves.

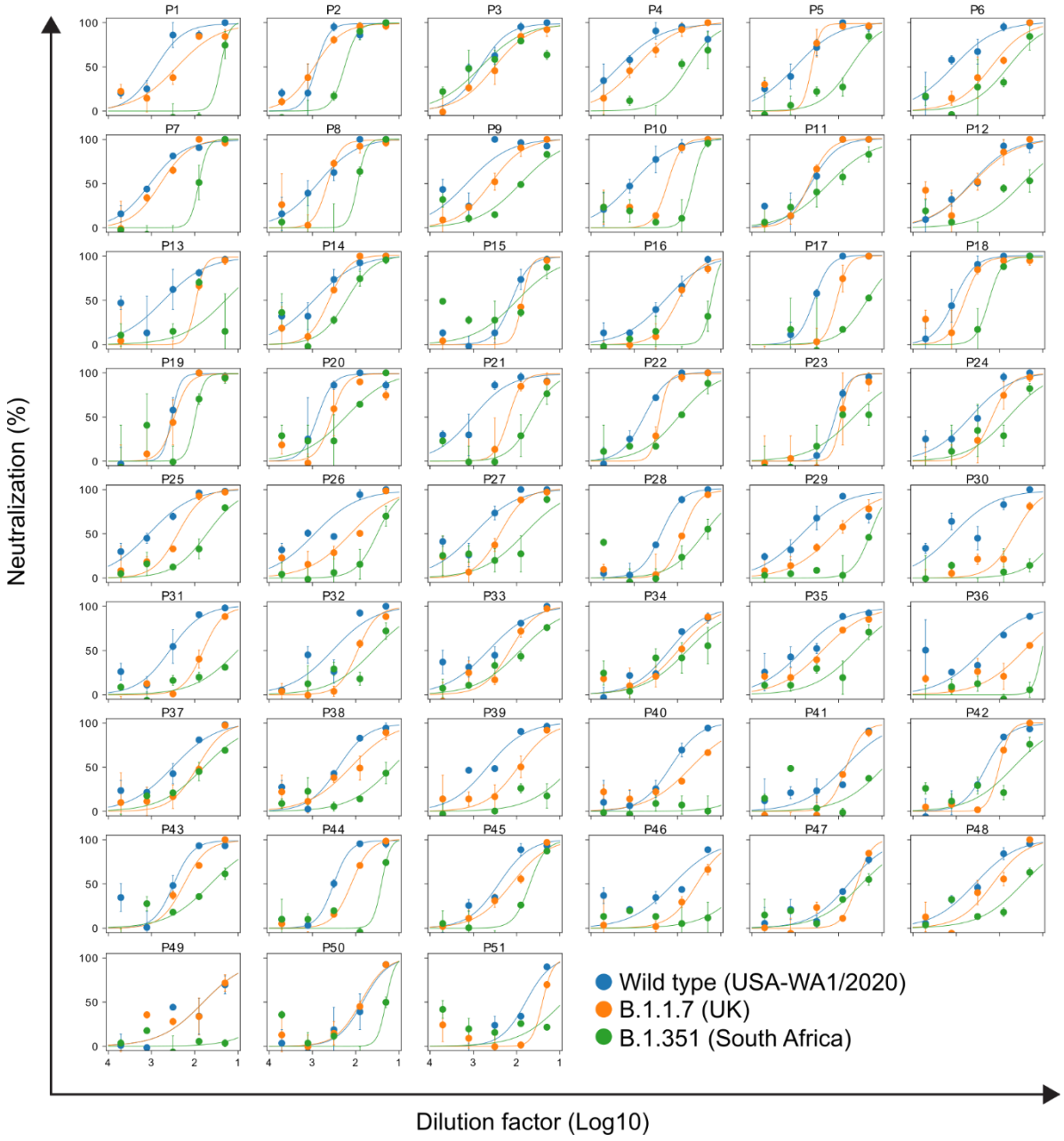

Neutralization curves of serum (n = 51) against the different strains of SARS-CoV-2 are shown. Serum was collected two weeks after the second dose of the BNT162b2 vaccine. Error bars represent SEM of biological replicates.

Figure S3.2 Convalescent serum FRNT50 curves.

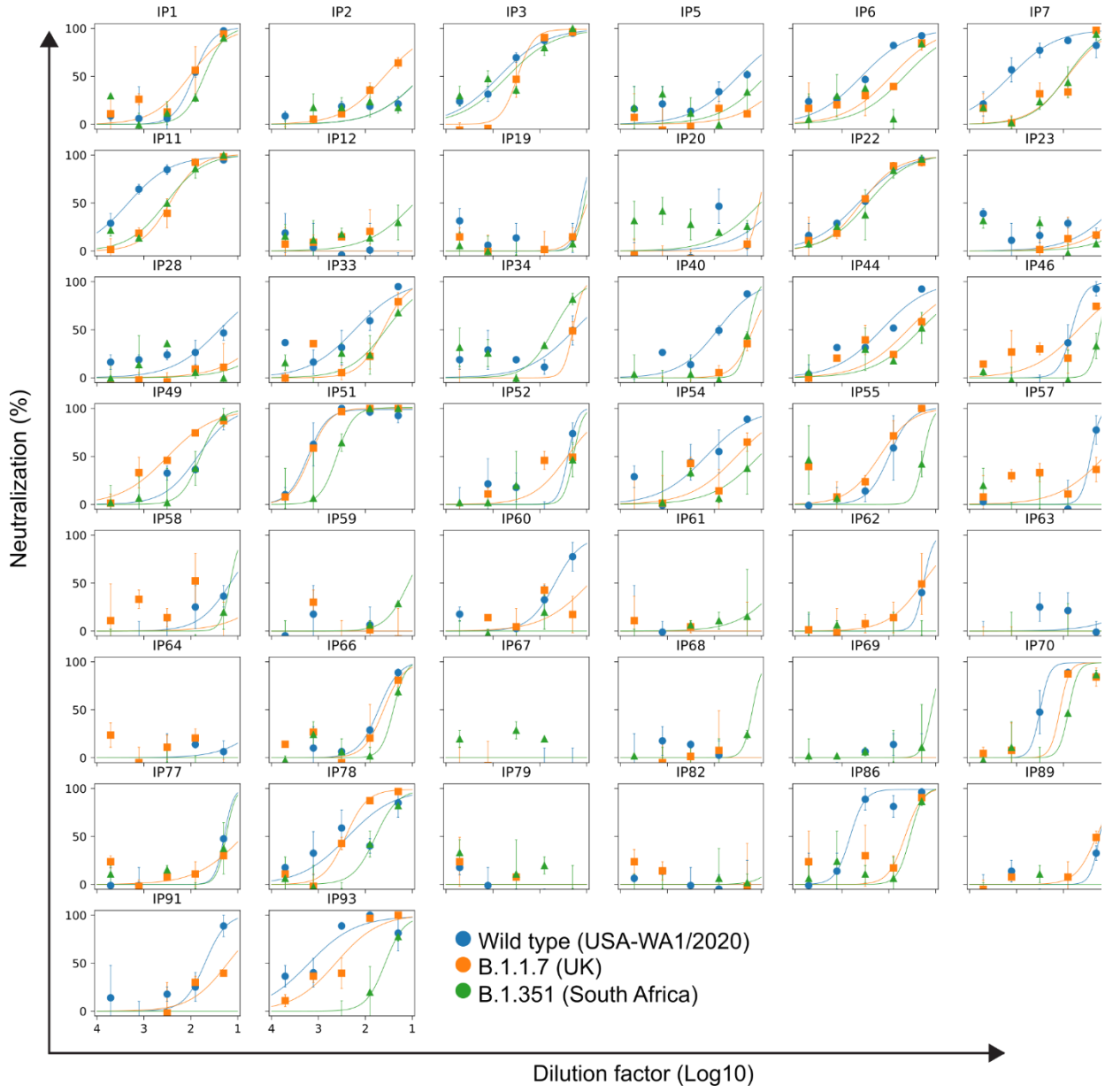

Neutralization plots of convalescent sera (n = 44) against the different strains of SARS-CoV-2 are shown. Error bars represent SEM of biological replicates.

Figure S3.3 Vaccine response by sex.

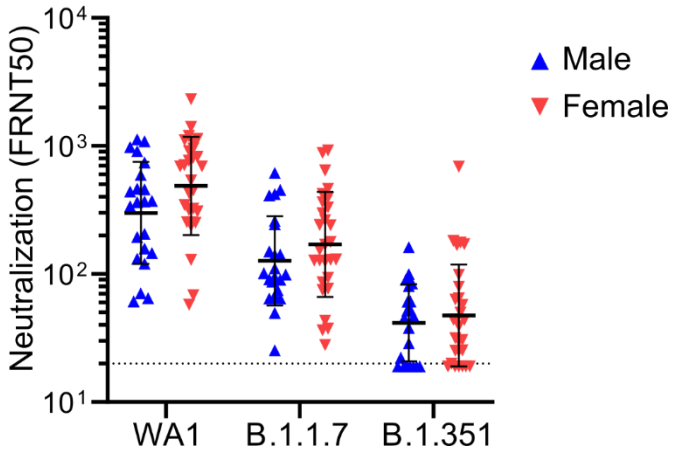

Comparison of vaccine sera neutralization titers ($FRNT_{50}$) of the different SARS-CoV-2 strains showing no correlation with sex. The male group contains n=22, and the female group contains n=28 independent biological samples. Data are presented as the geometric mean +/- SD with individual values shown. Statistical comparison was performed using a two-way ANOVA with the Šidák multiple comparison correction. There is no significance correlation between vaccine serum neutralization titers with sex.

Figure S3.4 Correlates of selected demographic and clinical factors with neutralization in the COVID-19 convalescent cohort.

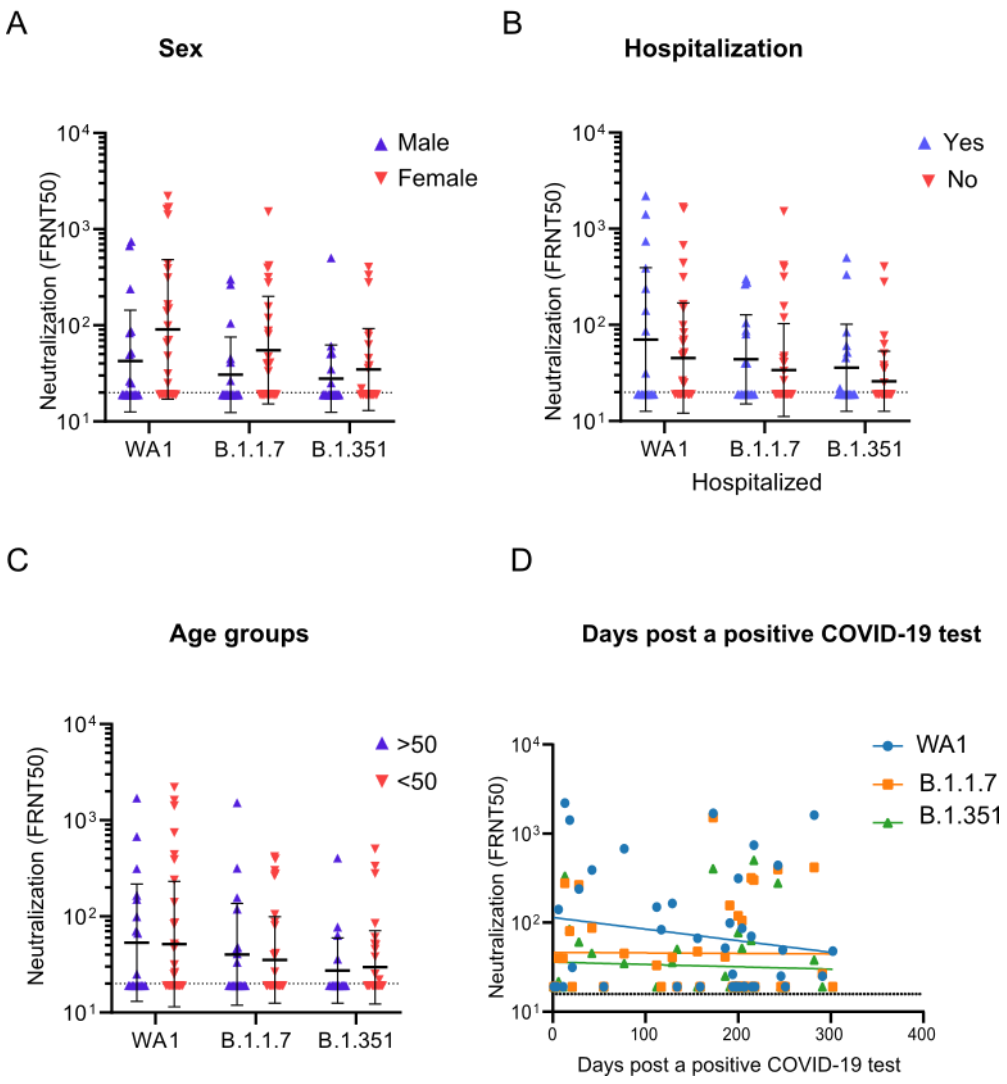

(**A-C**) Correlation of convalescent neutralization titers with sex (male n=19, female n=25 biologically independent samples) (**A**), hospitalization versus ambulatory care (yes n=17, no n=37 biologically independent samples) (**B**), and age of COVID-19 patients (>50 n=19, <50 n=35 biologically independent samples) (**C**). Data are presented at the geometric mean +/- SD with individual values shown. (**D**) comparison of $FRNT_{50}$ and the number of days between the

date of confirmatory COVID-19 PCR test and the date of serum sample collection. Statistical comparisons were performed using a two-way ANOVA with the Šidák multiple comparison correction. There is no significant correlation between convalescent neutralization titers and sex, hospitalization, age, or days after a positive COVID-19 test.

Figure S3.5 Variant focus forming assay phenotypes.

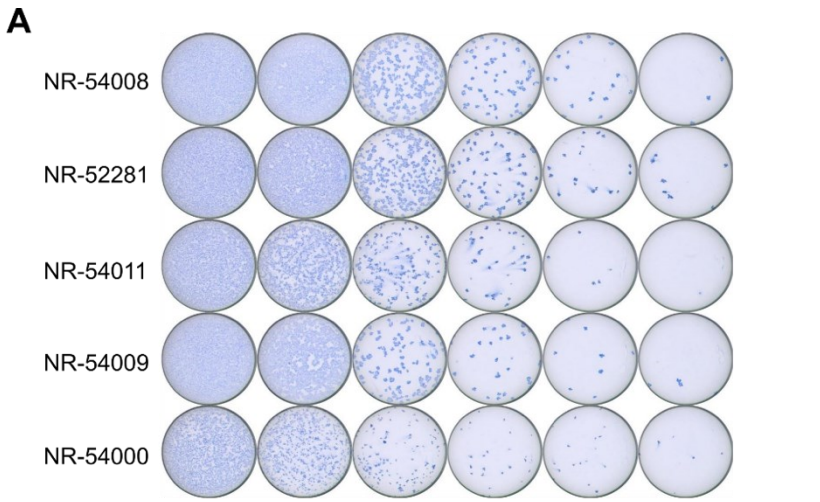

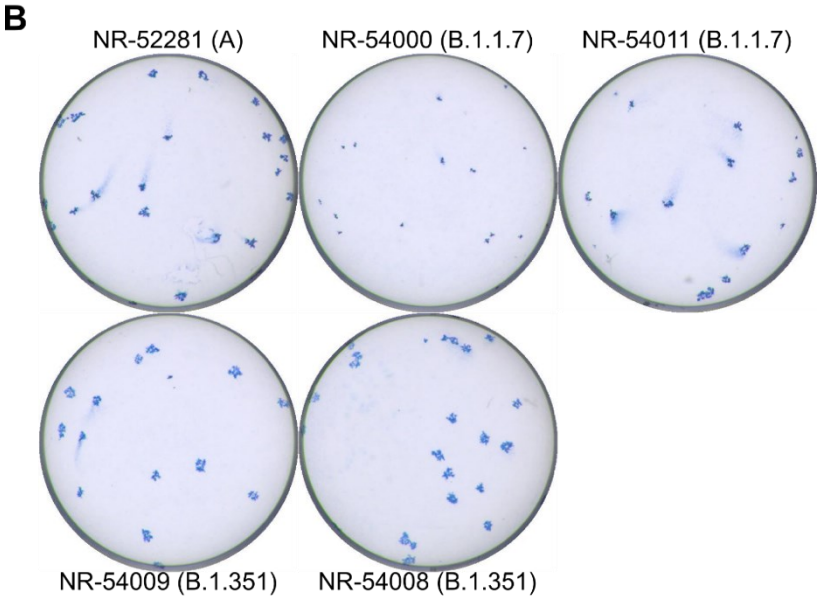

C

Lineage	BEI number	Average focus size (pixels)
A	NR-52281	193.7
B.1.1.7	NR-54000	51.9
B.1.1.7	NR-54011	212.8
B.1.351	NR-54009	303.8
B.1.351	NR-54008	309.4

Focus assay well images showing an example of the utilized titration curves for the clinical isolates tested during for assay development (**A**). Increased resolution of wells with individual foci (**B**). Average focus size for each isolate (**C**). Individual focus sizes were measured manually

using ImageJ using the images indicated in (**B**). The average size indicates the mean number of pixels across all foci in each image, excluding those contacting the edge of the well.

Section 3.7: Acknowledgments

3.7.1 Acknowledgments

The authors thank the generous contribution of the many patients and vaccinees who participated in this study. In addition, we gratefully acknowledge the efforts of the entire OHSU COVID-19 serology study team. We also want to thank the following members of the Oregon SARS-CoV-2 Genome Sequencing Center at OHSU for their help in sequencing our samples: Sonia N. Acharya, Cierra N. LaBlanc, Kayla I. Carter, Sally Grindstaff, Brendan L. O'Connell, and Ruth V. Nichols. This study was funded in part by an unrestricted grant from the M.J. Murdock Charitable Trust, by NIH training grant T32AI747225 on Interactions at the Microbe-Host Interface, and OHSU Innovative IDEA grant 1018784, and NIH R01AI145835.

3.7.2 Author Contributions

Concept and design: T.A.B., H.C.L., Z.L.L., M.E.C., W.B.M. and F.G.T.; acquisition, analysis, or interpretation of data: T.A.B., H.C.L., Z.L.L., S.K.M., F.J.C., J.B.W., J.R.G, Z.L., S.A.R.S., P.S., M.S., A.E.B., D.X.L., A.C.A., B.N.B., B.J.O., M.E.C., W.B.M. and F.G.T.; Drafting of the manuscript: T.A.B. and H.C.L.; critical revision of the manuscript for important intellectual content: T.A.B., H.C.L., Z.L.L., S.K.M., F.J.C., J.B.W., J.R.G, Z.L., S.A.R.S., P.S., M.S., A.E.B., D.X.L., A.C.A., B.N.B., B.J.O., M.E.C., W.B.M., and F.G.T.; statistical analysis: T.A.B., W.B.M. and A.E.B.; obtained funding: M.E.C., W.B.M. and F.G.T.

Chapter 4: Age-Dependent Neutralization of SARS-CoV-2 and P.1 Variant by Vaccine Immune Serum Samples

Timothy A. Bates[1], Hans C. Leier[1], Zoe L. Lyski[1], James R. Goodman[2], Marcel E. Curlin[3], William B. Messer[1], Fikadu G. Tafesse[1,*]

[1]Department of Molecular Microbiology & Immunology, Oregon Health & Science University, Portland.

[2]Medical Scientist Training Program, Oregon Health & Science University, Portland.

[3]Division of Infectious Diseases, Oregon Health & Science University, Portland.

*Correspondence: tafesse@ohsu.edu

JAMA, Volume 326, Issue 9, Pages 868-869. July 21, 2021.

DOI: https://doi.org/10.1001/jama.2021.11656

Section 4.1: Abstract

This study examines the relationship between age and neutralizing antibody titers against the SARS-CoV-2 USA-WA1/2020 strain and the P.1 variant after 2 doses of the BNT162b2 vaccine.

Section 4.2: Introduction

Vaccination with 2 doses of the BNT162b2 vaccine (Pfizer-BioNTech) reportedly provides 95% protection from COVID-19[262]. However, patient age is known to contribute to the risk of COVID-19 incidence and severity[358]. We examined the relationship between age and neutralizing antibody titers against the early SARS-CoV-2 USA-WA1/2020 strain and the P.1 variant of concern after 2 doses of the BNT162b2 vaccine.

Section 4.3: Results

A total of 50 individuals were enrolled in this study (27 [54%] women; median age, 50.5 [range, 21-82] years); prevaccination EC_{50} measurements were below the limit of quantification for all participants, indicating no prior exposures. Postvaccination EC_{50} measurements showed a significant negative association with age ($R^2 = 0.19$; $P = .002$) (Figure 4.1).

Figure 4.1 SARS-CoV-2–Specific Antibody Levels

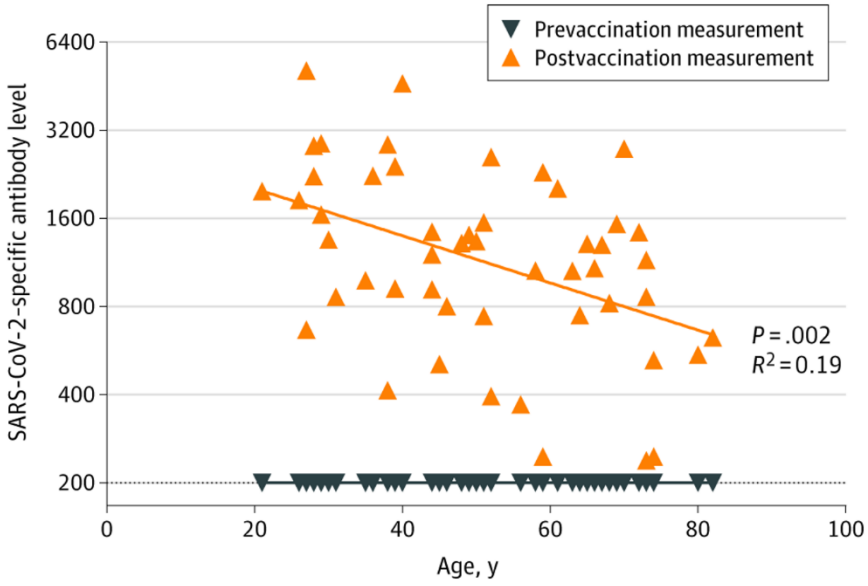

Enzyme-linked immunosorbent assay measurement of SARS-CoV-2 spike receptor–binding domain-specific antibody levels and association with age at time of vaccination for 50

participants 14 days after receiving their second vaccine dose. Prevaccination samples for all participants were below the limit of detection, indicating no prior exposure. Postvaccination samples displayed a significant negative association with age. The dotted line indicates the lower limit of quantification.

Robust neutralizing responses were observed in all participants against the original strain (USA-WA1/2020), with a geometric mean titer (GMT) serum dilution of 393 (95% CI, 302-510). Responses were lower against the P.1 variant, with a GMT of 91 (95% CI, 71-116), representing a 76.8% reduction. For both USA-WA1/2020 and P.1, age was significantly negatively correlated with $FRNT_{50}$ ($P < .001$ and $P = .001$) (Figure 4.2). For the USA-WA1/2020 strain, the youngest participants (20-29 years; n = 8) had a GMT of 938 (95% CI, 608-1447) and the oldest participants (70-82 years; n = 9) had a GMT of 138 (95% CI, 74-257), representing an 85% reduction ($P < .001$). For the P.1 variant, the youngest participants had a GMT of 165 (95% CI, 78-349) and the oldest participants had a GMT of 66 (95% CI, 51-86), representing a 60% reduction ($P = .03$).

Figure 4.2 Neutralization of Live SARS-CoV-2 Clinical Isolates

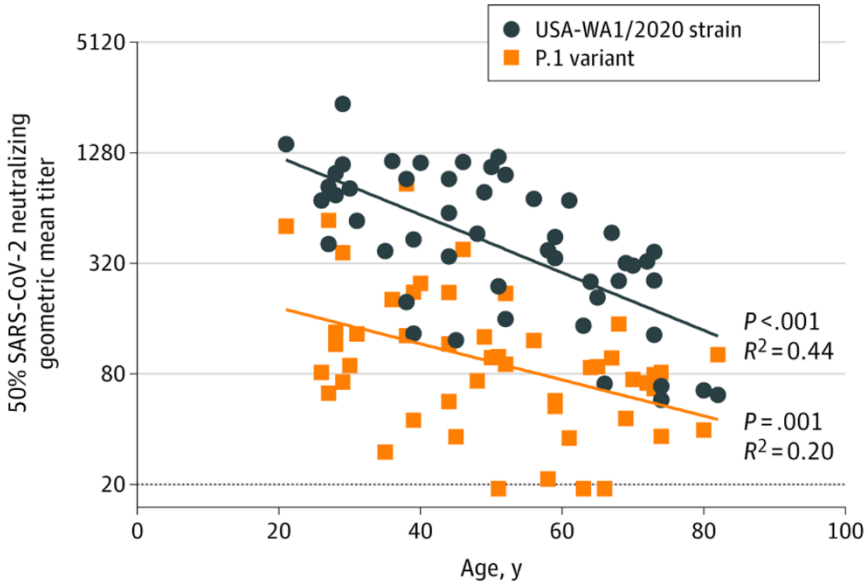

Live virus neutralization of participant serum samples collected 14 days after the second vaccine dose. Neutralization experiments were performed with the USA-WA1/2020 strain and P.1 variant. Both show a significant negative association with participant age. The dotted line indicates the lower limit of quantification.

Section 4.4: Discussion

In this study, initial vaccine-elicited neutralizing antibody titers were negatively associated with age, resulting in a diminished ability to neutralize SARS-CoV-2 in vitro. Neutralizing titers against P.1 were reduced across all ages, although the magnitude of the age-dependent difference was smaller. Interim clinical trial data did not identify age as a contributing factor to overall vaccine efficacy[262]. However, recent studies in vaccinated populations have found a measurable increase in COVID-19 cases among vaccinated older adults[263,359]. The data from the current study are consistent with neutralizing antibody levels playing an important role in this observation.

Neutralizing antibody titers are thought to be strongly correlated with protection from infection; however, the threshold of this protection has not yet been precisely determined[125]. Future studies should specifically address whether the reduced antibody levels seen among older vaccinated individuals lead to concomitantly diminished protection. Additionally, the emerging SARS-CoV-2 variants of concern, including P.1, B.1.1.7, and B.1.351, have been widely reported to be less well neutralized by vaccine-induced antibodies and are responsible for a majority of breakthrough infections, according to a May 2021 report[360]. The compounding effects of reduced neutralizing antibody titers due to both age and the variants of concern should be considered when designing policies around booster vaccinations. Limitations of this study include the small sample size and the possibility of unrecognized infection prior to vaccination.

Section 4.5: Methods

The Oregon Health & Science University conducted large-scale vaccination of all workforce members in accordance with Oregon vaccination guidelines between December 2020 and February 2021. Individuals were enrolled in this study during their first vaccination visit and serum samples were collected prior to receipt of the first dose and 14 days after receipt of the second dose of the BNT162b2 vaccine. Study participants were selected randomly from a larger vaccine study cohort to maintain equal sex and age distribution.

SARS-CoV-2 spike receptor–binding domain-specific antibody levels were measured by enzyme-linked immunosorbent assays, and 50% effective titers (EC50) were calculated. SARS-CoV-2 50% neutralizing titers were determined by focus reduction neutralization tests (FRNT50) using live clinical isolates of the original SARS-CoV-2 strain (USA-WA1/2020) and the P.1 variant. Associations between age and EC50 and FRNT50 were determined by fitting a linear model to log-transformed data in Graphpad Prism, version 9.0.2. Two-tailed P values were calculated by F test with a zero-slope null hypothesis and a significance cutoff of $P \leq .05$.

This study was performed in accordance with the institutional review board at Oregon Health & Science University. Written informed consent was obtained from participants. Additional method details of the serum collection and laboratory analyses can be found in the eAppendix in the Supplement.

Section 4.6: Supplemental Methods

4.6.1 Serum collection:

At the time of enrollment, 4-6 mL of whole blood were collected from each participant, centrifuged at 1000×g, and stored at -20°C as a pre-vaccination sample. Participants all received their second vaccine dose 21 +/- 1 days following the first dose. 14 +/- 1 days following their

second dose, 4-6 mL of whole blood were collected and similarly centrifuged and stored. All serum samples were heat inactivated before use. Randomized sample selection was performed using R version 4.0.3 in RStudio version 1.2.5001.

4.6.2 SARS-CoV-2 growth and titration:

SARS-CoV-2 clinical isolates were obtained from BEI Resources: [WA1] USA-WA1/2020 (NR-52281); [P.1] hCoV-19/Japan/TY7-503/2021 (NR-54982). Passage 1 virus were generated by inoculating subconfluent Vero E6 cells with p0 samples and grown for 72 hours until cytopathic effect was observed. Culture supernatants were decanted and centrifuged at 1,000×g for 10 min before freezing in aliquots at -80°C. Virus stocks were sequence verified prior to use. Titers were determined by focus forming assay using 10-fold dilutions. Confluent 96-well plates of Vero E6 cells were treated with viral dilutions produced in Opti-MEM, 10% FBS (dilution media) and incubated for 1 hour in a tissue culture incubator. Following infection, Opti-MEM, 2% FBS, 1% methylcellulose (overlay media) was added to each well and the plate was incubated for 24 hours. Overlay media was removed and cells were fixing for 1 hour in 1× phosphate buffered saline (PBS), 4% formaldehyde (fixing solution). The focus forming assay was developed and read as described previously[348].

4.6.3 SARS-CoV-2 FRNT and ELISA

Focus reduction neutralization assays were performed as previously described[361]. Briefly, participant serum samples were diluted in duplicate using dilution media to make 5×4-fold dilutions (1:10 – 1:2560). Equal volumes of diluted antibody and 2× virus stock were combined and incubated for 1 hour in a tissue culture incubator. Virus-serum solutions were then added to confluent Vero E6 cells in 96-well plates and again incubated for 1 hour in a tissue culture incubator before adding overlay media and incubating for 24 hours. Cells were treated with fixing

solution for 1 hour. Development, imaging, and counting were carried out identically to titration experiments (above). ELISAs were performed as previously described using purified SARS-CoV-2 spike receptor binding domain[361].

4.6.4 $FRNT_{50}$ and EC_{50} calculation

Percent neutralization values for $FRNT_{50}$ or normalized OD_{450} values for EC_{50} were calculated in python (v3.7.6) with numpy (v1.18.1), scipy (v1.4.1), Matplotlib (v3.1.3), and pandas (v1.0.1) data analysis libraries. Replicate data were consolidated and fit with a three-parameter logistic model. For $FRNT_{50}$ values, replicate curves were generated separately and participants for whom individual replicate $FRNT_{50}$ values differed by more than 4-fold were excluded from further analysis. Final $FRNT_{50}$ values below the lower limit of quantification of 20 were set to 19 while values above the upper limit of quantification of 5120 were set to 5121. Final EC_{50} values below the lower limit of quantification (200) were set to 199 while values above the upper limit of quantification (48,600) were set to 48601 respectively. Pre-vaccination samples were tested by ELISA at 1:200 and no samples showed signal more than 4-fold above background, so all samples were set to 199.

Section 4.7: Acknowledgments

4.7.1 Acknowledgments

We acknowledge the efforts of the Oregon Health & Science University COVID-19 serology research team for their assistance with sample acquisition, data collection, and statistical analysis, including Christopher Malibiran, BS; Cynthia Martinez, BS; David Xthona Lee, BA; Devin Schoen, BS; Felicity Coulter, MS; Haley Miller, BS; Hiro Ross, BS; Joseph Easly, BS; Kristin Bialobok, MSN; Laura Craft, BS; Madison Egan, BS-RD; Madison Wahl, BA; Marcus Curlin; Mari Tasche, BS; Matthew Strnad, BS; Maya Herzig, BS; Olivia Glatt, BA; Peter Sullivan,

BA; Rick Mathews, BE; Sara McCrimmon, MPH; Sarah Siegel, PhD; Taylor Anderson, MD; Teresa Xu, BA; and Zhengchun Lu, MBBS-PhD. We also thank Savannah McBride, BA (Department of Molecular Microbiology & Immunology, Oregon Health & Science University), for technical help and Endale Tafesse, PhD (Department of Plant Sciences, University of Saskatchewan), for advice on data analysis. None of these individuals were compensated for their contributions. We are deeply grateful for the Oregon Health & Science University faculty, staff, and patients who contributed to this study.

4.7.2 Funding

This study was funded in part by an unrestricted grant from the M.J. Murdock Charitable Trust, by National Institutes of Health training grant T32AI747225 on Interactions at the Microbe-Host Interface, Oregon Health & Science University Innovative IDEA grant 1018784, and National Institutes of Health grant R01AI145835.

The funders had no role in the design and conduct of the study; collection, management, analysis, and interpretation of the data; preparation, review, or approval of the manuscript; and decision to submit the manuscript for publication.

4.7.3 Author contributions

Dr. Tafesse had full access to all of the data in the study and takes responsibility for the integrity of the data and the accuracy of the data analysis. Mr Bates and Mr Leier contributed equally to this work. *Concept and design:* Bates, Leier, Lyski, Curlin, Messer, Tafesse. *Acquisition, analysis, or interpretation of data:* All authors. *Drafting of the manuscript:* Bates, Leier. *Critical revision of the manuscript for important intellectual content:* All authors. *Statistical analysis:* Bates, Messer. *Obtained funding:* Curlin, Messer, Tafesse. *Administrative, technical, or material support:* Bates, Lyski, Goodman, Curlin, Tafesse. *Supervision:* Curlin, Messer, Tafesse.

Chapter 5: Antibody Response and Variant Cross-Neutralization After SARS-CoV-2 Breakthrough Infection

Timothy A. Bates[1]; Savannah K. McBride[1]; Bradie Winders[2], Devin Schoen[2], Lydie Trautmann[3], Marcel E. Curlin[2], and Fikadu G. Tafesse[1,*]

[1]Department of Molecular Microbiology & Immunology, Oregon Health & Science University, Portland.

[2]Division of Infectious Diseases, Oregon Health & Science University, Portland.

[3]Vaccine and Gene Therapy Institute, Oregon Health & Science University, Portland.

*Correspondence: tafesse@ohsu.edu

JAMA, Volume 327, Issue 2, Pages 179-181. December 16, 2021.

DOI: https://doi.org/10.1001/jama.2021.22898

Section 5.1: Abstract

This study of fully vaccinated health care workers examines antibody levels and variant cross-neutralization after COVID-19 breakthrough infection.

Section 5.2: Introduction

Breakthrough infections after vaccination against SARS-CoV-2 are increasingly reported, possibly due to waning of vaccine-induced antibody levels[362]. Moreover, emerging variants of concern with diminished susceptibility to vaccine-induced antibodies are responsible for most new cases[363,364]. Studies have focused on determining the rate of vaccine breakthrough based on antibody levels after standard vaccination practices[365,366]. We assessed antibody levels and variant cross-neutralization after breakthrough infection.

Section 5.3: Results

Twenty-six participants with breakthrough infections (mean age, 38 years; 20 [77%] women; 24 [92%] were vaccinated with BNT162b2, sampled a median 28 days after PCR date and 213.5 days after final vaccination; 21 [81%] with mild symptoms) were matched to 26 controls (mean age, 39 years; 21 [81%] women; 26 [100%] were vaccinated with BNT162b2, sampled a median 28 days after final vaccination). Total receptor-binding domain–specific immunoglobulin increased in participants with breakthrough infection with a median EC_{50} of 2152 (95% CI, 961-3596) compared with 668 (95% CI, 473-892) in controls (322% increase; $P < .001$) (Figure 5.1A). Median serum dilutions increased for both IgG and IgA. For example, the median IgA EC_{50} after breakthrough infection was 120 (95% CI, 44-246), compared with 24 (95% CI, 24-24) for controls (502% increase; $P < .001$). IgM levels were not significantly different between groups (Figure 5.1B).

Figure 5.1 SARS-CoV-2 Spike Receptor-Binding Domain (RBD)–Specific Antibody Levels After Vaccination and Breakthrough Infection

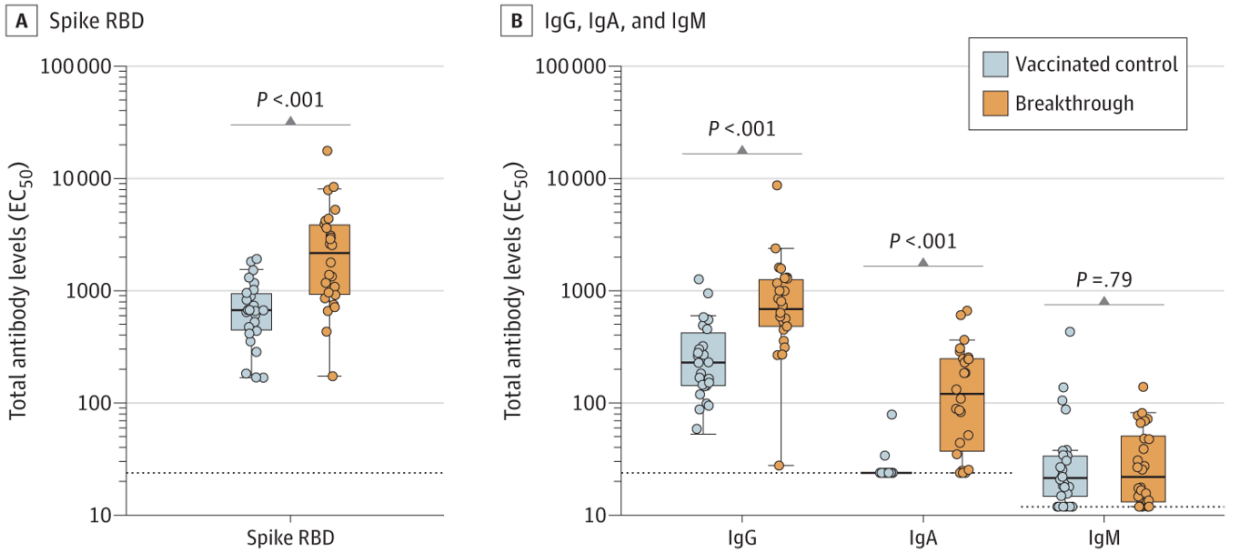

Enzyme-linked immunosorbent assay measurement of serum dilution titers with a 50% effective concentration (EC_{50}) of SARS-CoV-2 spike RBD-binding antibodies. The dotted lines indicate the assay limits of detection. Two-tailed *P* values were determined using the Wilcoxon matched-pairs signed rank test with the Holm-Šídák multiple comparison correction. Box plots were generated using the Tukey method. The large box displays the median and IQR. The error bars indicate 1.5 times the IQR or the furthest outlier, whichever is closer to the median. All individual data points are displayed as filled circles.

Among sequence-confirmed breakthrough cases, 10 were Delta and 9 were non-Delta infections. Among breakthrough cases, the median $FRNT_{50}$ against WA1 was 4646 (95% CI, 2283-7053) vs 489 (95% CI, 272-822) for controls (950% increase; $P < .001$). $FRNT_{50}$ results for Alpha, Beta, and Gamma variants are shown in (Figure 5.2A). In breakthrough cases, median $FRNT_{50}$ against the Delta variant was 2482 (95% CI, 1072-4923), compared with 243 (95% CI, 118-336) for controls (1021% increase; $P < .001$) (Figure 5.2A). Sera from Delta breakthrough

cases showed improved potency against the Delta variant at 99% (95% CI, 73-151) of WA1 neutralization for each participant, compared with 36% (95% CI, 33-52) for non-Delta cases and 41% (95% CI, 24-56) for controls (Figure 5.2B).

Figure 5.2 Live SARS-CoV-2 Variants Neutralization After Vaccination and Breakthrough Infection

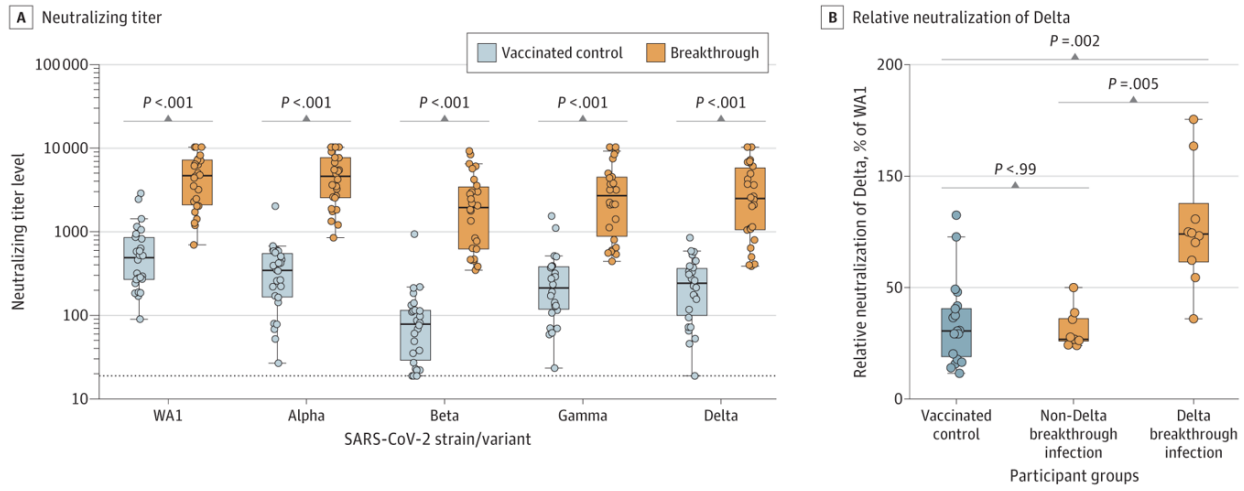

Live SARS-CoV-2 neutralization by focus-forming assay. A, The dotted line indicates the assay limit of detection. Two-tailed P values were determined using the Wilcoxon matched-pairs signed rank test with the Holm-Šídák multiple comparison correction. B, Participants with inconclusive sequencing information were excluded from this analysis. Two-tailed P values were determined using the Kruskal-Wallis test with the Dunn multiple comparison correction. Box plots were generated using the Tukey method. The large box displays the median and IQR. The error bars indicate 1.5 times the IQR or the furthest outlier, whichever is closer to the median. All individual data points are displayed as filled circles.

Section 5.4: Discussion

Results of this study showed substantial boosting of humoral immunity after breakthrough infection, despite predominantly mild disease. Boosting was most notable for IgA, possibly due to

the differences in route of exposure between vaccination and natural infection. In addition, breakthrough sera demonstrated improved variant cross-neutralization, and Delta breakthrough infections in particular exhibited improved potency against Delta vs WA1, suggesting that the protective immune response may be broadened through development of variant boosters with antigenic inserts matching the emerging SARS-CoV-2 variants. Limitations of this study include the small number of samples and the difference in time from initial vaccination to serum collection between the breakthrough and control groups, which emerging evidence suggests may contribute to the development of variant cross-neutralizing antibody responses[367].

Section 5.5: Methods

Fully vaccinated health care workers subsequently diagnosed with SARS-CoV-2 breakthrough infection based on a positive polymerase chain reaction (PCR) test result were sequentially recruited at the Oregon Health & Science University between January 31, 2021, and August 18, 2021. Only those with no history of previous infection whose test results were negative for nucleocapsid antibodies were included. Controls were fully vaccinated individuals without a breakthrough infection matched on sex, age, time between vaccine doses, and time between sample collection and most recent antigen exposure (PCR confirmation for those with breakthrough infection and final vaccine dose for controls). Full-length viral genomic sequencing was used to determine SARS-CoV-2 variant identity. Enzyme-linked immunosorbent assays were used to determine serum dilution titers with a 50% effective concentration (EC_{50}) of IgG, IgA, and IgM antibodies specific to the SARS-CoV-2 spike receptor–binding domain. Live SARS-CoV-2 neutralizing serum dilution titers were determined by 50% focus reduction neutralization tests ($FRNT_{50}$) against isolates of the original SARS-CoV-2 strain (WA1) and variants of concern (Alpha, Beta, Gamma, and Delta). Median breakthrough and control serum values were calculated

in GraphPad Prism and compared with the Wilcoxon matched-pairs signed rank test with the Holm-Šídák correction. Delta-neutralizing potency was determined by comparing Delta- and WA1-neutralizing titers for sequence-confirmed Delta variant breakthrough cases, non-Delta breakthrough cases, and controls using the Kruskal-Wallis test with Dunn correction. Statistical significance was defined as a 2-tailed $P < .05$. Additional laboratory methods are provided in the Supplement. The Oregon Health & Science University institutional review board approved this study. Written informed consent was obtained.

Section 5.6: Supplemental Methods

5.6.1 Cohort serum collection:

Among fully vaccinated participants with breakthrough infections, after recovery, whole blood (4-6 mL) was collected with a BD Vacutainer® Plus Plastic Serum Tube and centrifuged for 10 minutes at 1000xg. Serum samples were stored at -20°C. Full vaccination was defined as having received 2 doses of BNT162b2 or mRNA-1273, or 1 dose of Ad26.COV2.S.

5.6.2 SARS-CoV-2 variants sequencing:

SARS CoV-2 testing was performed as previously described[368]. Briefly, RNA extraction was performed using one of three methods (Maxwell RSC, MagNA Pure 96, or KingFisher Flex) according to manufacturer instructions using kit viral transport starting volumes of 300 µL, 200 µL or 200 µL, respectively. PCR tests were considered valid if internal control RNA (RNase P or MS2) was detected. PCR was validated to a lower limit of detection of ~5 genomic copies/reaction using known standards. Valid tests were interpreted as detected when 2 or 3 viral targets were reactive, inconclusive if a single viral target was reactive and otherwise negative.

SARS CoV-2 genomic sequencing was performed using the Ion AmpliSeq™ SARS-COV-2 Insight Research Panel Assay according to manufacturer instructions with residual RNA from

SARS-COV-2 testing. Reverse transcription was performed using the Ion Torrent™ NGS Reverse Transcription Kit. Sequence data were analyzed and aligned using plugins GenerateConsensus to generate FASTA files and SARS-CoV-2 Coverage Analysis for coverage depth. FASTA files were manually reviewed and uploaded into GISAID and NCBI.

5.6.3 Enzyme-linked immunosorbent assays (ELISA) and Focus reduction neutralization tests (FRNT):

ELISAs were performed as previously described[369]. The following proteins were used: SARS-CoV-2 RBD produced in Expi293F cells as described[370], N (SARS-CoV-2 Nucleocapsid-His, insect cell-expressed, SinoBio Cat: 40588-V08B, Item #NR-53797, lot #MF14DE1611). FRNT assays were carried out as previously described[370]. Duplicate 5x4.7-fold (1:10-1:4879) serial dilutions of participant sera were prepared in 96-well plates. SARS-CoV-2 and variant isolates.

Viral stocks were propagated in Vero E6 cells as previously described[370]. The following SARS-CoV-2 isolates were used: USA-WA1/2020 [lineage A] (NR-52281), USA/CA_CDC_5574/2020 [lineage B.1.1.7 – alpha] (NR-54011), hCoV-19/South Africa/KRISP-K005325/2020 [lineage B.1.351 – beta] (NR-54009), hCoV-19/Japan/TY7-503/2021 [lineage P.1 – gamma] (NR-54982), and hCoV-19/USA/PHC658/2021 [lineage B.1.617.2 – delta] (NR-55611) were obtained from BEI Resources.

5.6.4 Statistical analysis

$FRNT_{50}$ and EC_{50} values were calculated by fitting to a dose-response curve as previously described[370]. Final $FRNT_{50}$ values below the limit of detection (1:20) were set to 1:19. Final EC_{50} values below the limit of detection of 1:25 for N, Spike RBD, IgG, IgA were set to 1:24 and 1:12.5

for IgM was set to 1:12. Individuals for whom a breakthrough variant could not be determined were excluded from the delta potency analysis.

Section 5.7 Acknowledgments

5.7.1 Acknowledgments

We acknowledge the efforts of the OHSU COVID-19 serology research team for their assistance with sample acquisition and data collection. We also want to thank the Oregon SARS-CoV-2 Genome Sequencing Center at OHSU for their help in sequencing our samples, including Xuan Qin, PhD, Brian O'Roak, PhD, Andrew Adey, PhD, and Benjamin Bimber, PhD. None of the above individuals were compensated for their contributions. We are grateful for the Oregon Health & Science University faculty, staff, and patients who contributed to this study.

5.7.2 Funding

This study was funded in part by an unrestricted grant from the M. J. Murdock Charitable Trust, an unrestricted grant from the Oregon Health & Science University (OHSU) Foundation, National Institutes of Health training grant T32HL083808 on Multidisciplinary Research Training in Pulmonary Medicine, and OHSU Innovative IDEA grant 1018784.

The funders had no role in the design and conduct of the study; collection, management, analysis, and interpretation of the data; preparation, review, or approval of the manuscript; and decision to submit the manuscript for publication.

5.7.3 Author contributions

Dr Tafesse had full access to all of the data in the study and takes responsibility for the integrity of the data and the accuracy of the data analysis. *Concept and design:* Bates, McBride, Winders, Curlin, Tafesse. *Acquisition, analysis, or interpretation of data:* All authors. *Drafting of the manuscript:* Bates. *Critical revision of the manuscript for important intellectual content:* All

authors. *Statistical analysis:* Bates, McBride, Schoen. *Obtained funding:* Curlin, Tafesse. *Administrative, technical, or material support:* Bates, McBride, Schoen, Curlin, Tafesse. *Supervision:* Curlin, Tafesse.

Chapter 6: Vaccination before or after SARS-CoV-2 infection leads to robust humoral response and antibodies that effectively neutralize variants

Timothy A. Bates[1], Savannah K. McBride[1], Hans C. Leier[1], Gaelen Guzman[1], Zoe L. Lyski[1], Devin Schoen[2], Bradie Winders[2], Joon-Yong Lee[3], David Xthona Lee[1], William B. Messer[1,2,4,*], Marcel E. Curlin[2,*], Fikadu G. Tafesse[1,*]

[1]Department of Molecular Microbiology and Immunology, Oregon Health & Science University, Portland, OR 97239, USA.

[2]Division of Infectious Diseases, Oregon Health & Science University, Portland, OR 97239, USA.

[3]Biological Sciences Division, Pacific Northwest National Laboratory, Richland, WA 99354, USA.

[4]OHSU-PSU School of Public Health, Oregon Health & Science University, Portland, OR 97239, USA.

*Corresponding authors: messer@ohsu.edu (W.B.M.); curlin@ohsu.edu (M.E.C.); tafesse@ohsu.edu (F.G.T.)

Science Immunology, Volume 7, Issue 68. January 25, 2022.

DOI: https://doi.org/10.1126/sciimmunol.abn8014

Section 6.1: Abstract

Current COVID-19 vaccines significantly reduce overall morbidity and mortality and are vitally important to controlling the pandemic. Individuals who previously recovered from COVID-19 have enhanced immune responses after vaccination (hybrid immunity) compared to their naïve-vaccinated peers; however, the effects of post-vaccination breakthrough infections on humoral immune response remain to be determined. Here, we measure neutralizing antibody responses from 104 vaccinated individuals, including those with breakthrough infections, hybrid immunity, and no infection history. We find that human immune sera following breakthrough infection and vaccination following natural infection, broadly neutralize SARS-CoV-2 variants to a similar degree. While age negatively correlates with antibody response after vaccination alone, no correlation with age was found in breakthrough or hybrid immune groups. Together, our data suggest that the additional antigen exposure from natural infection substantially boosts the quantity, quality, and breadth of humoral immune response regardless of whether it occurs before or after vaccination.

Section 6.2: Introduction

Severe acute respiratory coronavirus 2 (SARS-CoV-2) is the causative agent of the ongoing coronavirus disease 2019 (COVID-19) pandemic. Globally, cases continue to increase despite worldwide vaccination campaigns[80]. Numerous safe and effective vaccines have been developed which effectively reduce the risk of infection, severe disease, and death including BNT162b2 (Pfizer), mRNA-1273 (Moderna), and Ad26.COV2.S (Janssen)[262,263]. However, variants of concern (VOC) with differing levels of increased transmissibility and resistance to existing immunity have sequentially emerged, spread widely and receded over time since the beginning of the pandemic[39,363,364,370]. Several studies have shown that antibody responses from the initial wave

of vaccines in early 2021 have waned over the six months following vaccination, possibly contributing to an increase in breakthrough infections[362,371–374]. Booster vaccine doses were first approved in Israel in July 2021, and have since been more widely adopted in other countries to address these concerns despite the concern that boosters campaigns may divert much needed vaccine doses away from lower income countries[372].

Vaccination following recovery from natural SARS-CoV-2 infection, or "hybrid immunity," has been reported to substantially increase both the potency and breadth of humoral response to SARS-CoV-2[204,346]. However, current studies on breakthrough infection occurring after vaccination have focused on identifying susceptibility factors such as virus neutralizing titer prior to infection[365]. The impact of breakthrough infection on the neutralizing antibody response and how this compares to the response elicited by hybrid immunity remains unclear; we therefore undertook the present study to directly address this gap in knowledge.

Section 6.3: Results

6.3.1 Cohort and study design

We recruited a total of 104 participants (Table 6.1) consisting of 31 fully vaccinated individuals with PCR-confirmed breakthrough infections, 31 individuals with one (6 individuals) or two vaccine (25 individuals) doses following recovery from COVID-19 (hybrid immunity), and 42 fully vaccinated individuals with no history of COVID-19 or breakthrough infection (Figure 6.1A). Ninety-six participants received BNT162b2, 6 received mRNA-1273, and 2 received Ad26.COV2.S. Serum samples were collected from each of the participants, which were then tested for 50% effective antibody concentrations (EC_{50}) by enzyme-linked immunosorbent assay (ELISA), and 50% live SARS-CoV-2 neutralizing titer with focus reduction neutralization tests ($FRNT_{50}$) against early lineage strain SARS-CoV-2 (WA1) and clinical isolates of three VOCs:

Alpha (B.1.1.7), Beta, (B.1.351), and Delta (B.1.617.2). We performed additional antibody-dependent cellular phagocytosis (ADCP) experiments to evaluate any functional differences in the antibody response of each group.

Table 6.1 Cohort demographics.

Characteristic	Vaccine Only N = 42	Hybrid Immunity N = 31	Breakthrough N = 31
Sex			
Female - N (%)	35 (83.3)	19 (61.3)	24 (77.4)
Male - N (%)	7 (16.7)	12 (38.7)	7 (22.6)
Age (yr)			
Median [Range]	40 [23-74]	50 [23-73]	38 [24-63]
Critical time periods (days) - Median [IQR]			
Latest vaccine dose to blood draw	24 [17.25-35.75]	25 [17.5-34]	N/A
PCR positivity to blood draw	N/A	N/A	35 [23-48.5]
PCR positivity to first vaccine dose	N/A	289 [124-334.5]	N/A
Second vaccine dose to PCR positive	N/A	N/A	139 [81.5-201.5]
Days between vaccine doses	21 [21-22]	22 [21-25]	21 [21-23]
Vaccine type - N (%)			
BNT162b2 (Pfizer)	42 (100)	25 (80.6)	29 (93.5)
mRNA-1273 (Moderna)	0 (0)	5 (16.1)	1 (3.2)
Ad26.COV2.S (Janssen)	0 (0)	1 (3.2)	1 (3.2)

We first analyzed the hybrid immunity of participants who received only a single vaccine dose compared to those who had received two doses (Figure S6.1). All measures of antibody levels, ADCP, and live virus neutralization revealed no significant difference between these two groups. For this reason, we combined these samples into a single group containing participants with both one and two vaccine doses following natural infection, which we henceforth refer to as the hybrid immune group.

6.3.2 Antibody levels following breakthrough infection, hybrid immunity, and vaccination alone

ELISA geometric mean titers (GMT) EC_{50} values for SARS-CoV-2 spike-specific antibodies were significantly elevated in both the breakthrough (2.5-fold, P = 0.005) and hybrid

immune (3.6-fold, $P < 0.0001$) groups compared to vaccination alone, but we saw no significant difference between the breakthrough and hybrid groups (Figure 6.1B). A similar trend was seen for EC_{50} values specific for the spike receptor binding domain (RBD) (Figure 6.1B). We additionally confirmed that none of the vaccine-only participants exhibited reactivity against the nucleocapsid (N) protein, supporting lack of previous infection, whereas the breakthrough and hybrid immune groups were 68 and 48 percent N responsive, respectively (Figure 6.1B). Opsonization with hybrid immune and breakthrough sera also induced phagocytosis of spike protein-coated particles in an ADCP assay significantly more than vaccination alone, but not compared to each other (Figure 6.1C). The levels of IgG and IgA antibodies specific to RBD protein displayed a similar trend to the total EC_{50} levels with significant increases for hybrid immunity and breakthrough compared to vaccination alone, but not compared with each other (Figure 6.1D). RBD-specific IgM values were notably low and did not differ significantly between groups. Consistent with previous reports[375], spike-specific antibody levels correlated negatively with age among vaccine-only participants. In contrast, neither the breakthrough nor hybrid immune group recapitulated this correlation, displaying no significant age-related trend (Figure 6.1E).

Figure 6.1 Antibody levels following breakthrough infection, hybrid immunity, and vaccination alone.

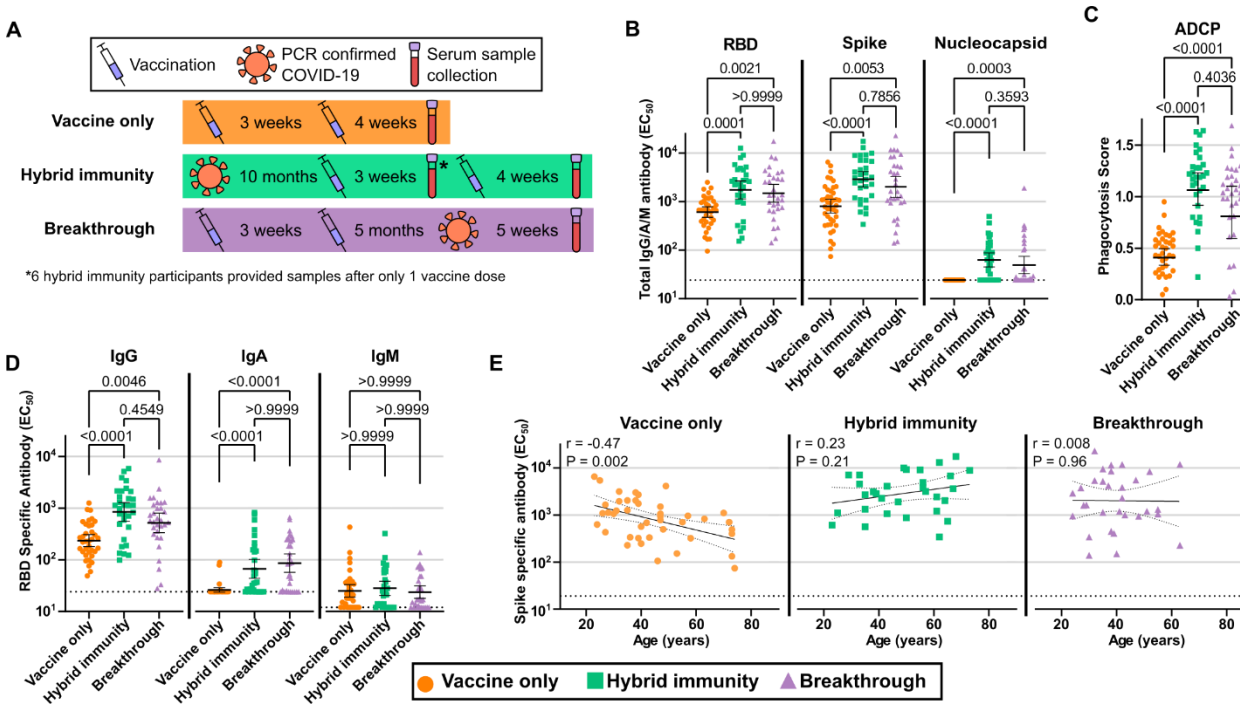

(**A**) Schematic depicting the order and approximate time scale of vaccination and natural infection for each group. The blue syringe indicates a dose of vaccine, the orange virus particle indicates PCR confirmed natural infection with SARS-CoV-2, and the purple capped vial indicates serum collection. The asterisk (*) indicates that 6 (out of 31) hybrid immune participants provided serum samples following only a single vaccine dose. (**B**) IgG/A/M inverse fold-dilution EC_{50} values for sera specific to RBD, full-length spike, and nucleocapsid proteins measured by ELISA. (**C**) Antibody dependent cellular phagocytosis scores. (**D**) RBD-specific EC_{50} values for IgG, IgA, and IgM class antibodies measured by ELISA. (**E**) Correlation between spike-specific EC_{50} values and participant age. Error bars in **B** and **D** indicate the geometric mean with the 95% confidence interval, while error bars in **C** indicate the arithmetic mean with the 95% confidence interval. P values in **B-D** were calculated with two-tailed

Kruskal-Wallis test with Dunn's multiple comparison correction. Scatter plots in **E** depict the simple linear fit of age and log transformed EC_{50} values with 95% confidence bands along with the Spearman rank correlation coefficient and two-tailed P value.

6.3.3 Neutralizing antibody titers against SARS-CoV-2 and the variants of concern

We next quantified the functional activity of participants' immune sera by comparing their neutralization titers against early (WA1) SARS-CoV-2 and selected VOCs. Against all viruses, the trend mirrored that of the antibody EC_{50} levels, with the vaccine-only group $FRNT_{50}$ titers significantly lower than both breakthrough and hybrid immunity, which were comparable with each other (Figure 6.2A). The $FRNT_{50}$ GMT of hybrid immune group participants were 10.8, 16.9, 32.8, and 15.7-fold higher than vaccination alone for WA1, Alpha, Beta, and Delta variants, while breakthrough group participants were 6.0, 11.8, 17.0, and 8.5-fold higher than vaccination alone, respectively, all with $P < 0.0001$. Among vaccine group participants, neutralization of the Beta variant was significantly reduced compared to WA1, while the difference seen for the hybrid immune and breakthrough groups was not significant (Figure S6.2).

Figure 6.2 Antibody levels following breakthrough infection, hybrid immunity, and vaccination alone.

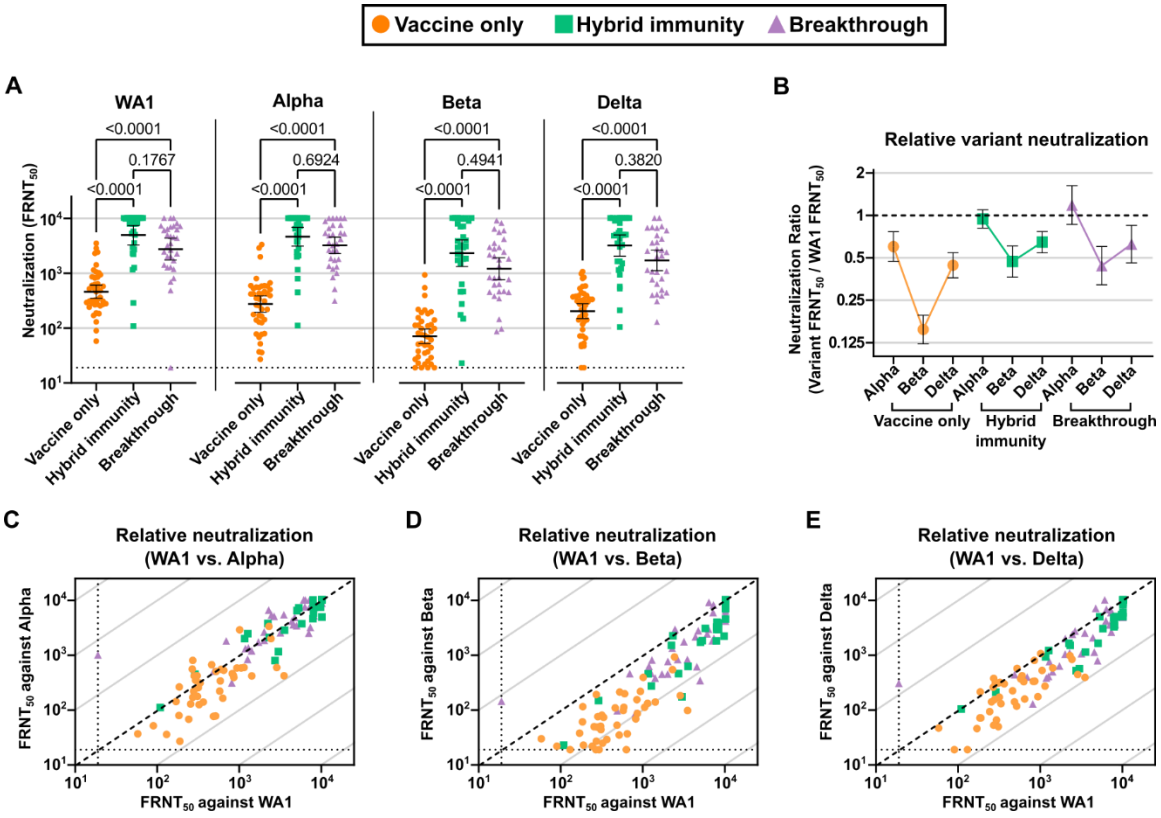

(**A**) Neutralizing antibody titers determined by focus forming assay with clinical isolates of the original strain of SARS-CoV-2 (WA1), Alpha, Beta, and Delta variants. (**B**) The ratio of Alpha, Beta, and Delta variant neutralization to WA1 neutralization. WA1 neutralizing titer versus Alpha (**C**), Beta (**D**), and Delta (**E**) variant neutralizing titer. The dotted line indicates equal neutralization. Error bars in **A** and **B** indicate the geometric mean with the 95% confidence interval. P values in **A** were two-tailed and calculated with the Kruskal-Wallis method with Dunn's multiple comparison correction.

In addition to eliciting immunity with greater breadth (Figure 6.2A), the serum antibody potency across the breadth of VOCs tested was greater for both hybrid immune and breakthrough groups, as measured by an increase in the ratio of variant neutralization over WA1 FRNT50 values

against Alpha and Beta for the hybrid immune and breakthrough groups, and against Delta for the hybrid immune group (Figure 6.2B and S6.3). Breakthrough and hybrid immune participants grouped more tightly and displayed variant neutralizing titers closer to that of WA1 (Figure 6.2C-E).

6.3.4 Quality of the neutralizing antibody response

We also found that hybrid immunity was associated with a remarkable improvement in the proportion of spike-specific antibodies that were also neutralizing. WA1 neutralizing titers correlated with spike-specific antibody levels for all three groups, but the hybrid immune and breakthrough groups correlated more strongly (Figure 6.3A). To analyze the efficiency of sera at neutralizing a given virus strain, we determined a neutralizing potency index by calculating the ratio of neutralizing titer ($FRNT_{50}$) to spike binding EC_{50} values[123]. The index expresses a ratio of fold-serum-dilution with 50% neutralization potency to fold-serum-dilution 50% spike binding capacity, or a relative neutralizing antibody to total antibody ratio for a given subject's serum. The neutralizing potency index was significantly higher among hybrid immune and breakthrough participants than after vaccination alone (Figure 6.3B). Lastly, we found that the relationship between age and total antibody levels also extends to neutralizing titer; vaccine-only participants displayed a clear negative correlation with age, while the hybrid immune and breakthrough participants showed no such correlation (Figure 6.3C). No association was seen between reported sex and neutralizing titer for any of the groups (Figure 6.3D).

Figure 6.3 Neutralizing efficiency and correlation with age.

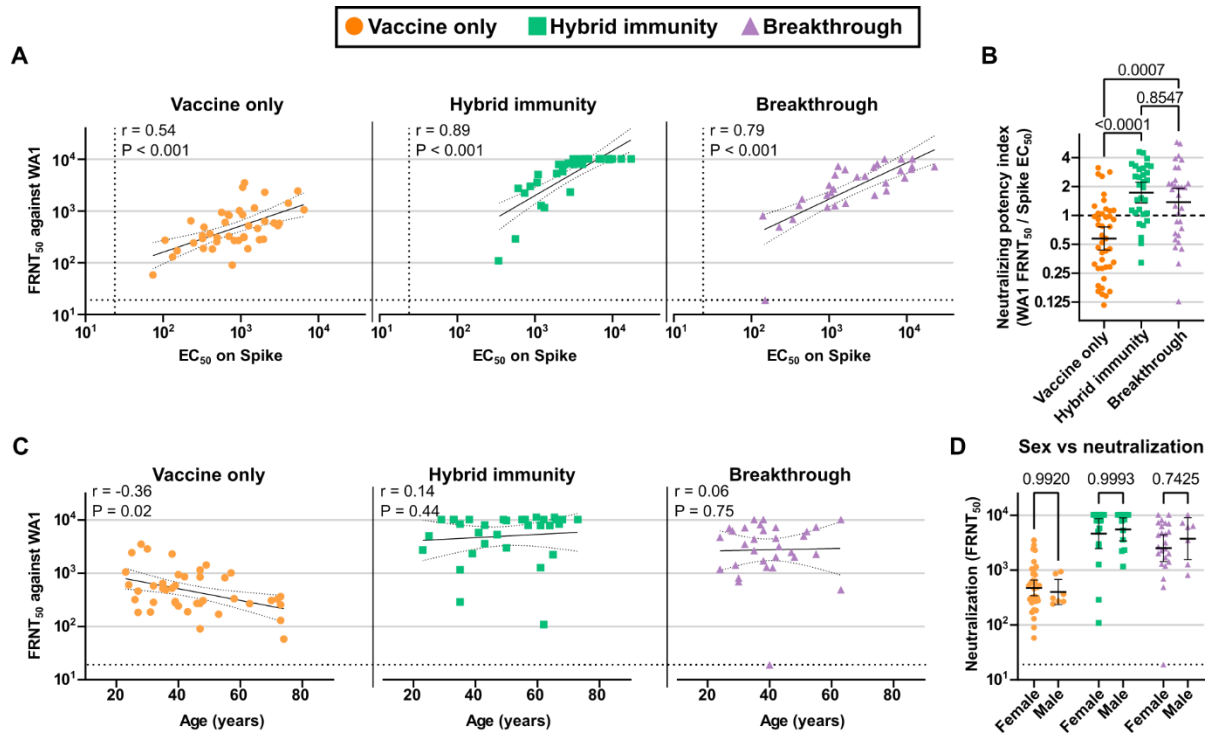

(**A**) Correlation between spike-specific EC_{50} vaules and WA1 neutralizing titers. (**B**) Serum neutralizing potency index was calculated as the ratio of WA1 neutralizing titer to spike-specific EC_{50} values. (**C**) Correlation between age and WA1 neutralizing titers. (**D**) WA1 neutralization by sex. Error bars in **B** and **D** indicate the geometric mean with the 95% confidence interval. P values in **B** were two-tailed and calculated with the Kruskal-Wallis method with Dunn's multiple comparison correction. P values in **D** were two-tailed and calculated with using a two-way ANOVA with the Šidák multiple comparison correction. Scatter plots in **A** depict the simple linear fit of log transformed $FRNT_{50}$ versus log transformed EC_{50} values with 95% confidence bands. Scatter plots in **C** depict the simple linear fit of log transformed $FRNT_{50}$ versus age with 95% confidence bands. Correlations in **A** and **C** show spearman rank correlation coefficients and two-tailed P values.

Section 6.4: Discussion

Overall, our results show that SARS-CoV-2 infection before or after vaccination gives a significantly larger boost to the neutralizing antibody response compared to two doses of vaccine alone. More importantly, the potency and breadth of the antibody response appears to improve concomitantly. It has been well established that natural infection alone provides short-lived protection from infection[375], showing the importance of vaccination, regardless of infection history. Because vaccination protects against severe disease and death[376], it is safer for individuals to be vaccinated before rather than after natural infection.

The negative correlation between age and neutralizing antibody levels following vaccination alone is an effect that has been previously identified[369]. The relationship between age and antibody levels following natural infection is markedly more complex, with a peak in antibody levels seen between the ages of 60 and 80[377]. The exact reasons for this association remain to be determined, but one hypothesis is that the greater disease severity among individuals of advanced age leads to an overall greater humoral response[123]. These two opposing trends may obscure any age dependence of antibody levels in the present study among patients with humoral responses resulting from both vaccination and natural infection.

Recent studies have suggested that the humoral response continues to develop long after vaccination, with memory B cells at late time points after vaccination showing improved quality and breadth compared to early time points[202,204,378]. Our data cannot separate the contribution of mixed boosting due to the combination of vaccination with natural infection, from the contribution of ongoing memory B cell development during the time between first antigen exposure and most recent boosting, whether from vaccination or breakthrough infection. Future studies with individuals who have been vaccinated and boosted may be able to distinguish between these

possibilities, and an early study suggests that booster vaccination 8 months following a second dose leads to improved overall Delta variant neutralizing titers by 6 to 12-fold[367]. This appears consistent with the 8.5-fold and 15.7-fold improvements against the Delta variant for the breakthrough and hybrid immune groups, respectively, compared to two vaccine doses alone. This suggests that the magnitude of improvement for booster vaccinations may be similar to those seen with combined vaccination and natural infection, including hybrid immunity with a single dose of mRNA vaccine. This would point to the importance of the memory B cell compartment in generating a robust and variant cross-neutralizing humoral response. While this study focuses on the humoral response, it is known that the cellular response by T cells plays an important role in the responding to SARS-CoV-2 vaccination and infection[379].

COVID-19 vaccines using mRNA technology, including BNT162b2 and mRNA-1273 are the most commonly administered vaccines in the United States, where this study took place, and most of this study's participants received the BNT162b2 vaccine. However, some participants received the Ad26.COV2.S adenovirus-based vaccine. The majority of hybrid immunity research has focused on mRNA vaccination, but research on adenovirus vaccine hybrid immunity has shown similar improvements to neutralizing titers and variant cross-neutralization[380]. While this study was not designed to compare the effectiveness of different vaccination technologies, we do not anticipate any substantial effect due to differences in vaccine types.

Vaccination is highly effective at preventing the most severe outcomes from COVID-19 and should be provided regardless of prior infection status and age. A single dose of vaccine may provide sufficient protection for many individuals with previous SARS-CoV-2 infection. Vaccine availability remains limited in many regions and the shortest path to broad global immunity may

be to prioritize administering at least one vaccine dose to as many individuals as possible with a confirmed history of SARS-CoV-2 infection.

Section 6.5: Methods

6.5.1 Study design

The purpose of this study was to directly compare the humoral immune response among individuals who received COVID-19 vaccines either prior to or following naturally acquired SARS-CoV-2 infection. Serum samples were collected from participants, which were analyzed using enzyme-linked immunosorbent (ELISA) assays, focus reduction neutralization tests, and measurement of antibody dependent cellular phagocytosis. Study participants were selected for inclusion based on a history of both vaccination and previous SARS-CoV-2 infection. Vaccinated controls with no history of previous infection were selected on the basis of sex, age, days between vaccine doses, and the time period since the most recent vaccination.

6.5.2 Cohort selection and serum collection

Health care workers at Oregon Health & Science University were recruited and enrolled in the study belonging to three groups: Vaccine-only, hybrid immunity, and breakthrough infection. Written informed consent was obtained at the time of enrollment and study approval was obtained from the OHSU institutional review board (IRB#00022511). Vaccine-only participants were fully vaccinated, defined as having received 2 doses of BNT162b2 or mRNA-1273, or 1 dose of Ad26.COV2.S. Serum samples were collected at least 14 days after the final vaccine dose. Hybrid immune participants had a history of PCR-confirmed diagnosis of COVID-19 at least 10 days prior to vaccination with at least one dose of BNT162b2, mRNA-1273, or Ad26.COV2.S and serum samples were collected at least 10 days after the final vaccine dose. Breakthrough participants were fully vaccinated as defined for the vaccine only group at least 10 days prior to PCR confirmed

diagnosis of COVID-19 and serum samples were collected at least 10 days after the date of diagnosis. Sera were obtained by collecting 4-6 mL of whole blood in a BD Vacutainer Plus Plastic Serum Tube, which was centrifuged for 10 min at 1000xg before serum was aliquoted and stored at -20°C. Hybrid immune and breakthrough infection participants were selected based on availability while vaccine-only participants were selected to most closely match the average sex, age, and time since most recent vaccination (or infection for breakthrough) of the other two groups. Participants in these cohorts are previously described[369,381].

6.5.3 Enzyme-linked immunosorbent assays (ELISA)

ELISAs were performed as previously described[369]. In 96-well plates (Corning Incorporated, EIA/RIA High binding, Ref #359096). Plates were coated with 100 µL/well of the following proteins at 1 µg/mL in PBS and incubated overnight at 4°C with rocking: SARS-CoV-2 RBD (produced in Expi293F cells and purified using Ni-NTA chromatography), Full-length SARS-CoV-2 spike (Recombinant Spike, SARS-CoV-2 stabilized protein, produced in Expi293F cells, BEI resources #NR-52724), Nucleocapsid (SARS-CoV-2 Nucleocapsid-His, insect cell-expressed, SinoBio Cat: 40588-V08B, Item #NR-53797, lot #MF14DE1611). Plates were washed three times with 0.05% v/v Tween-20 in PBS (wash buffer) and blocked with 150 µL/well 5% nonfat dry milk powder in wash buffer (blocking buffer) at room temperature of approximately 20°C (RT) for 1 hour with rocking. Breakthrough and control sera were aliquoted and frozen in dilution plates then resuspended in blocking buffer; sera were diluted and added to ELISA plates 100 µL/well (6 × 4-fold dilutions from 1:50 to 1:51,200), except for IgM (6 × 3-fold dilutions from 1:25 to 1:6075). Sera was incubated for 1 hour at RT before plates were filled three times with wash buffer. Secondary antibodies were added to plates at 100 µL/well depending on the intended readout: Goat anti-human IGG/A/M-HRP at 1:10,000 (Invitrogen, Ref #A18847), anti-human

IgA-HRP at 1:3,000 (BioLegend, Ref #411002), Mouse anti-human IgG-HRP Clone G18-145 at 1:3,000 (BD Biosciences, Ref #555788), Goat anti-human IgM-HRP at 1:3,000 (Bethyl Laboratories, Ref #A80-100P). Plates were incubated protected from light with secondary at RT for 1 hour with rocking, then filled three times with wash buffer prior to the development with o-phenylenediamine dihydrochloride (OPD, Thermo Scientific #34005) according to the manufacturer's instructions. The reaction was stopped after 25 min using an equivalent volume of 1 M HCl; optical density was measured at 492 nm using a CLARIOstar plate reader. Normalized A_{492} values were calculated by subtracting the average of negative control wells and dividing by the 99th percentile of all wells from the same experiment. A dilution series of positive control serum was included on each plate to verify appropriate performance of the assay.

6.5.4 Cell culture

Vero E6 monkey kidney epithelial cells (CRL-1586) were obtained from ATCC and maintained in tissue culture-treated vessels in Dulbecco's Modified Eagle Medium (DMEM), 10% fetal bovine serum (FBS), 1% nonessential amino acids (NEAA), 1% penicillin-streptomycin (PS) (complete media) in tissue culture conditions (TCC) of 100% relative humidity, 37°C, and 5% CO_2. THP-1 (ATCC, TIB-202) human monocyte cells were obtained from ATCC and maintained in suspension culture in tissue culture treated vessels in Roswell Park Memorial Institute medium (RPMI-1640) supplemented with 10% FBS, 1% NEAA, and 1% PS (THP-1 media).

6.5.5 SARS-CoV-2 growth and titration

SARS-CoV-2 isolates USA-WA1/2020 [lineage A] (NR-52281), USA/CA_CDC_5574/2020 [lineage B.1.1.7 – alpha] (NR-54011), hCoV-19/South Africa/KRISP-K005325/2020 [lineage B.1.351 – beta] (NR-54009), hCoV-19/USA/PHC658/2021 [lineage B.1.617.2 – delta] (NR-55611) were obtained from BEI Resources. Viral stocks were propagated

as previously described[370]. Sub-confluent Vero E6 cells were infected at an MOI of 0.05 in a minimal volume (0.01 mL/cm2) of Opti-MEM + 2% FBS (dilution media) for 1 hour at TCC then 0.1 mL/cm2 additional complete media was added and incubated for 24 hours at TCC. Culture supernatant was centrifuged for 10 min at 1000xg and frozen at -80°C in aliquots. Titration was performed on clear 96 well tissue culture plates containing 70–90% confluent (at the time of infection) Vero E6 cells. 8 × 10-fold dilutions were prepared in dilution media and 30 µL/well of diluted virus was incubated with the cells for 1 hour at TCC before further addition of Opti-MEM, 2% FBS, 1% methylcellulose (overlay media) and incubation for 24 hours at TCC. Plates were then fixed by soaking in 4% formaldehyde in PBS for 1 hour then removing from BSL-3 following institutional biosafety protocols. Cells were permeabilized in 0.1% bovine serum albumin and 0.1% saponin in PBS (perm buffer) for 30 min, then with polyclonal anti-SARS-CoV-2 alpaca serum (Capralogics Inc.) (1:5000 in perm buffer) overnight at 4°C. Plates were washed three times with 0.01% Tween-20 in PBS (focus wash buffer), then incubated for 2 hours at RT with 1:20,000 anti-alpaca-HRP (Novus #NB7242). Plates were filled three times with focus wash buffer, then incubated with TrueBlue (Sera Care #5510-0030) for 30 min or until sufficiently developed for imaging. Well images were captures with a CTL Immunospot Analyzer and counted with Viridot (1.0) in R (3.6.3)[382]. Viral stock titers in focus forming units (FFU) were calculated from the dilution factor and volume used during infection.

6.5.6 Focus reduction neutralization test (FRNT)

FRNT assays were carried out as described[370]. Duplicate 5x4.7-fold (1:10-1:4879) serial dilutions of participant sera were prepared in 96-well plates. An equal volume of dilution media containing approximately 50 FFU of SARS-CoV-2 or variant was added to each well (final dilutions of sera, 1:20 – 1:9760) and incubated 1 hour at TCC. Virus-serum mixtures were used to

infect Vero E6 cells in 96-well plates as described above in the titration assay. Each plate contained 16 virus-only control wells, one for each serum dilution series. Fixation, development, and counting of FRNT plates was carried out as described above in the titration assay. Percent neutralization values were calculated for each well as the focus count divided by the average focus count of virus-only control wells from the same plate.

6.5.7 Antibody Dependent Cellular Phagocytosis (ADCP)

ADCP assay was adapted from a protocol described previously[383]. Biotinylated RBD incubated at 1µg/ml with fluorescent neutravidin beads (Invitrogen, F8775) for 2 hours at RT; beads were washed twice with 1% BSA in PBS (dilution buffer) and resuspended at a final dilution of 1:100 in dilution buffer. In a 96-well plate, 10µL of resuspended bead solution was incubated with 10µL of diluted serum from study subjects for 2 hours at 37°C. After serum pre-treatment, $2x10^4$ THP-1 cells were added to each well in 80µL THP-1 media and incubated overnight in TCC. The following morning, 100 µL of 4% paraformaldehyde was added to each well and incubated at least 30 min at RT before analysis on a CytoFLEX flow cytometer (Beckman Coulter). Samples were mixed for 3 s prior to analysis and samples were injected until at least 2500 cell events were recorded per sample. Phagocytosis scores are reported as the product of percent bead-positive cells and mean fluorescence intensity of bead-positive cells, then divided by 10^6 for presentation. Three replicate experiments were performed for each participant serum sample, the average of which was used for further analysis. The gating strategy with representative data are presented in Fig. S4.

6.5.8 Statistical analysis

$FRNT_{50}$ and EC_{50} values were calculated by fitting percent neutralization or normalized A_{492} values to a dose-response curve as previously described[370]. Final $FRNT_{50}$ values below the limit of detection (1:20) were set to 1:19. Final EC_{50} values below the limit of detection of 1:25

for N, Spike, RBD, IgG, IgA were set to 1:24 and values below 1:12.5 for IgM was set to 1:12. Aggregated EC_{50} and $FRNT_{50}$ values were analyzed and plotted in Graphpad Prism (9.2.0). Dot plots of EC_{50} and $FRNT_{50}$ values were generated on a log transformed axis with error bars showing the geometric mean and 95% confidence interval. Phagocytosis score and Neutralization ratio were plotted on a linear axis with error bars showing the arithmetic mean and 95% confidence interval. P values for dot plots were two-tailed and calculated using the Kruskal-Wallis test with Dunn's multiple comparison correction. P values for reported sex versus neutralization were two-tailed and calculated by group using a two-way ANOVA with the Šidák multiple comparison correction. Scatter plots were prepared by first log transforming $FRNT_{50}$ and EC_{50} data then performing simple linear fitting and plotting the 95% confidence bands. Correlations were calculated using Spearman's correlation and two-tailed P values were calculated for the 95% confidence interval.

Section 6.6: Supplemental Figures

Figure S6.1 One versus two vaccine dose hybrid immunity.

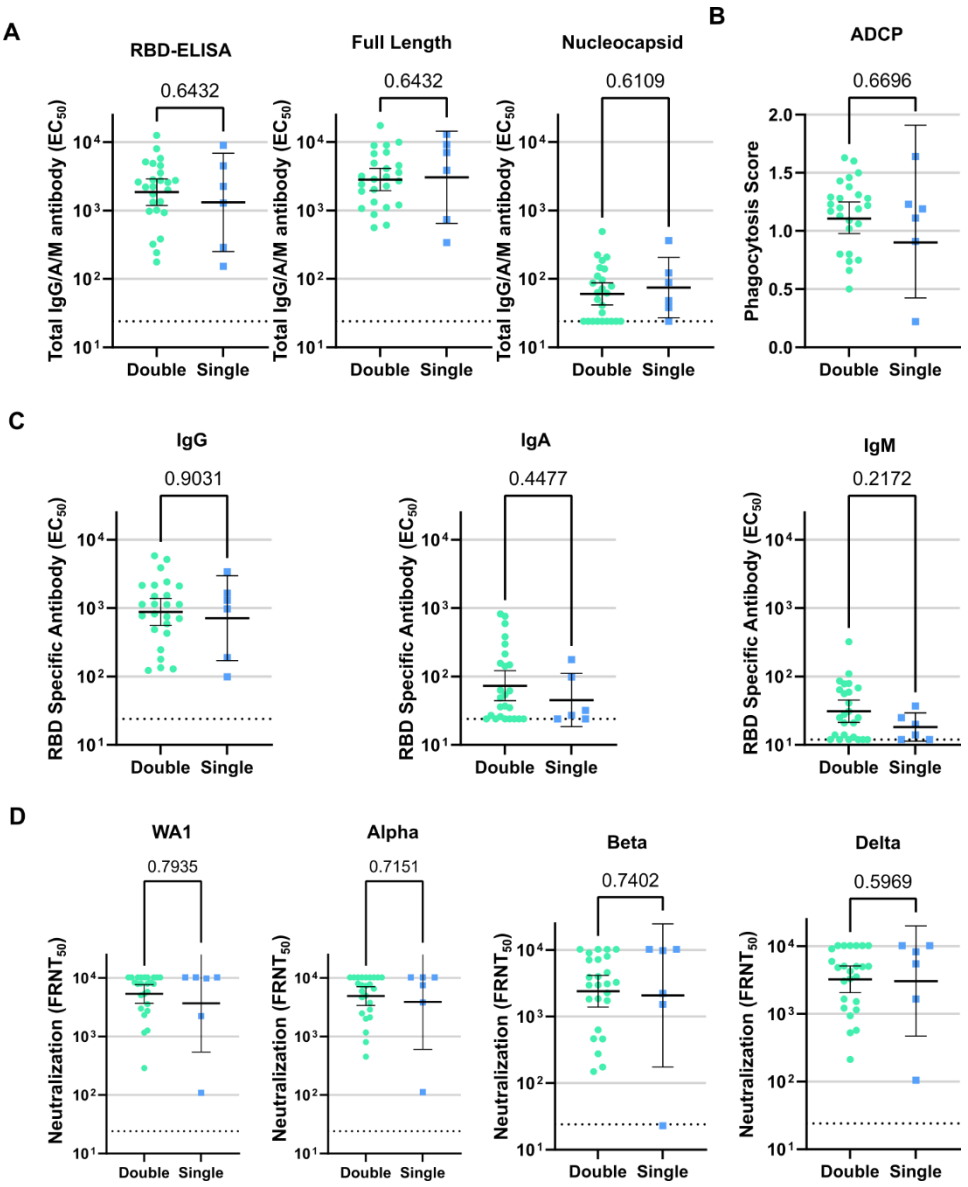

(**A**) Total IgG/A/M antibody levels determined by ELISA. (**B**) Antibody dependent phagocytosis scores. (**C**) RBD-specific antibody levels by class. (**D**) Live virus neutralization by variant. Error bars show the geometric mean (arithmetic mean for ADCP) with 95% confidence intervals. P values are two-tailed and were calculated using the Kruskal-Wallis test.

Figure S6.2 Neutralization by variant.

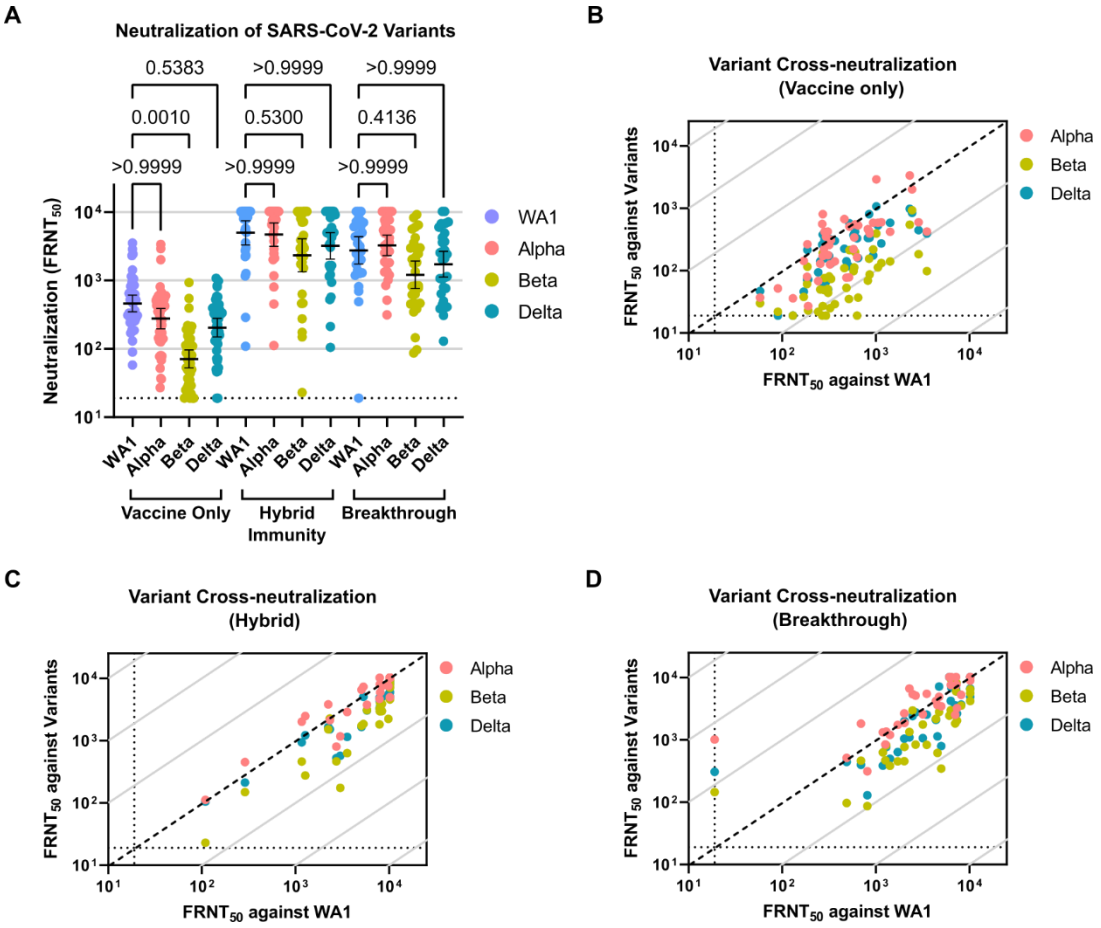

(**A**) Neutralization of live SARS-CoV-2 clinical isolates organized by group. WA1 neutralizing titer versus each variant for vaccine only (**B**), hybrid immunity (**C**), and breakthrough (**D**) groups. The dotted line indicates equal neutralization of variants and WA1 for each participant.

Figure S6.3 Variant neutralization ratios.

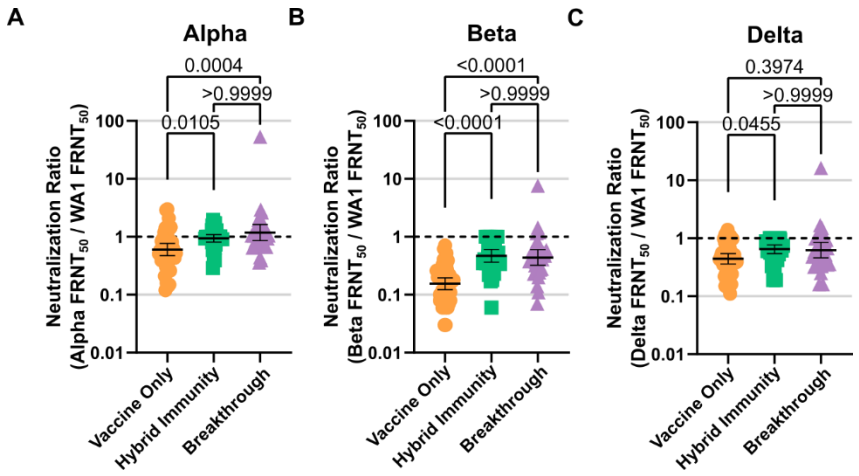

Ratio of variant neutralization over WA1 neutralization titers for Alpha (**A**), Beta (**B**), and Delta (**C**). The dotted lines indicate equal neutralization of variant and WA1. Error bars indicate the geometric mean and 95% confidence interval. P values are two-tailed and were calculated with the Kruskal-Wallis method with Dunn's multiple comparison correction.

Figure S6.4 ADCP flow gating scheme.

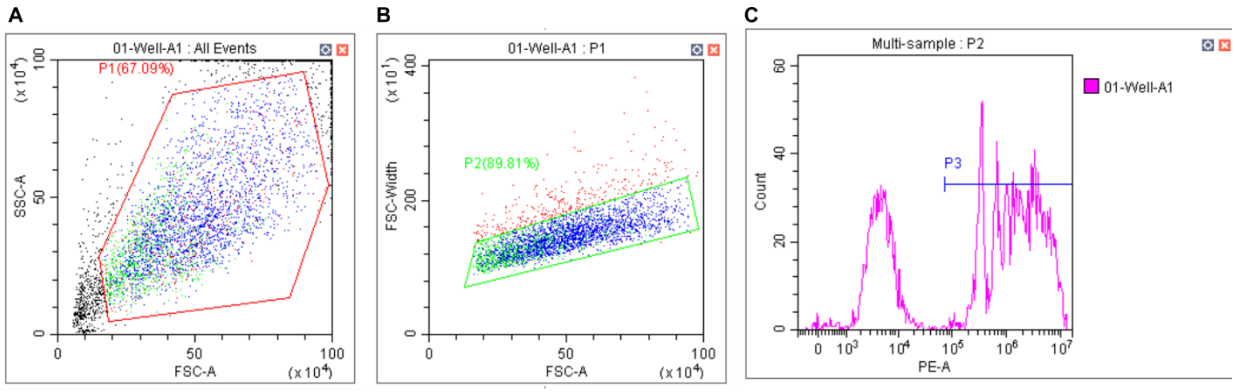

(**A**) Intact cells were isolated from free beads and cell debris based on forward and side scatter. (**B**) Singlet cells were isolated from doublets/aggregates by forward scatter width. (**C**) Group P3 indicates cells which have phagocytosed at least one fluorescent bead, whereas group P2 represents all single cells including those which have not taken up any beads.

Section 6.7: Acknowledgments

6.7.1 Acknowledgments

We acknowledge the study participants for their generous contributions; the OHSU COVID-19 serology study team and the OHSU occupational health department for recruitment and sample acquisition; and the OHSU clinical laboratory under the direction of Dr. Donna Hansel and Xuan Qin for SARS-Co-2 testing and reporting.

6.7.2 Funding

This study was funded by a grant from the M.J. Murdock Charitable Trust (MEC), an unrestricted grant from the Oregon Health & Science University (OHSU) Foundation (MEC), the National Institutes of Health training grant T32HL083808 (TAB), Oregon Health & Science University Innovative IDEA grant 1018784 (FGT), and National Institutes of Health grant R01AI145835 (WBM).

6.7.3 Author contributions

Conceptualization: TAB, HCL, ZLL, WBM, MEC, FGT. Cohort recruitment: ZLL, DS, BW, WBM, MEC. Sample acquisition and preparation: ZLL, DXL, DS, BW, JYL, WBM, MEC. Laboratory analysis: TAB, SKM, GG. Statistical analysis and visualization: TAB, JYL. Funding acquisition: TAB, WBM, MEC, FGT. Supervision: WBM, MEC, FGT. Writing – original draft: TAB. Writing – review and editing: all authors

Chapter 7: Omicron neutralizing antibody response following booster vaccination compared with breakthrough infection

Marcel E. Curlin[1,4,5], Timothy A. Bates[2,4], Gaelen Guzman[2], Devin Schoen[1], Savannah K. McBride[2], Samuel D. Carpenter[3], Fikadu G. Tafesse[2]

[1]Department of Medicine, Division of Infectious Diseases, Oregon Health & Science University, Portland, OR, USA

[2]Department of Molecular Microbiology & Immunology, Oregon Health & Science University; Portland, Oregon, USA

[3]Department of Psychiatry, Oregon Health & Science University; Portland, Oregon, USA

[4]These authors contributed equally

[5]Lead contact

Med, Volume 3, Issue 12. September 21, 2022.

DOI: https://doi.org/10.1016/j.medj.2022.09.001

Section 7.1: Abstract

7.1.1 Background

The spread of the vaccine-resistant Omicron SARS-CoV-2 variants threatens unvaccinated and fully vaccinated individuals, and accelerated booster vaccination campaigns are underway to mitigate the ongoing wave of Omicron cases. The immunity provided by standard vaccine regimens, boosted regimens, and immune responses elicited by vaccination plus natural infection remain incompletely understood. The magnitude, quality and durability of serological responses, and likelihood of protection against future SARS-CoV-2 variants following these modes of exposure are poorly characterized but are critical to the future trajectory of the COVID-19 pandemic.

7.1.2 Methods

Ninety-nine individuals were semi-randomly selected from a larger vaccination cohort following vaccination and in some cases breakthrough infection. We analyzed spike receptor-binding domain-specific IgG, IgA, and IgM by enzyme-linked immunosorbent assay, neutralizing antibody titers against live SARS-CoV-2 variants, and antibody-depended cell-mediated phagocytosis.

7.1.3 Findings

In 99 vaccinated adults, compared with responses after two doses of an mRNA regimen, the immune responses three months after a third vaccine dose and one month after breakthrough infection due to prior variants show dramatic increases in magnitude, potency, and breadth, including increased antibody dependent cellular phagocytosis and robust neutralization of the currently circulating Omicron BA.2 variant.

7.1.4 Conclusions

Boosters and natural infection substantially boost immune responses. As the number of Omicron subvariant cases rise and as global vaccination and booster campaigns continue, an increasing proportion of the world's population will acquire potent immune responses that may be protective against future SARS-CoV-2 variants.

Section 7.2: Introduction

Since 2020, the global coronavirus disease 2019 (COVID-19) pandemic has been punctuated by episodic waves of increased incidence associated with the emergence of new severe acute respiratory syndrome coronavirus 2 (SARS-CoV-2) variants with progressively greater transmissibility and resistance to immune responses elicited by currently approved vaccines. The most epidemiologically important variants have been classified as variants of concern (VOCs) by the World Health Organization and include Alpha, Beta, Gamma, Delta, and Omicron. The Omicron variant includes several competing sub-lineages including BA.1, BA.2, BA.4, BA.5, and BA.2.12.1, the latter four of which are presently responsible for most new cases. All Omicron sub-lineages are notable for their high transmissibility and resistance to neutralization by vaccine-induced antibodies[384–386]. Each contain more than 60 amino acid changes relative to the founding strain, with more than 30 in the spike protein, and 15–17 falling within the receptor-binding domain (RBD) responsible for binding to the human cell surface receptor angiotensin-converting enzyme 2 (ACE2)[51]. All known neutralizing antibodies bind to the spike protein, with the vast majority targeting the RBD[387–389]. Mutations within this region have caused a dramatic decrease in susceptibility to neutralization by several therapeutic monoclonal antibodies, resulting in substantial loss of clinical efficacy and, consequently, revocation of emergency use authorization for the treatment of COVID-19[390].

It is known that the additional antigenic exposure from boosters and breakthrough infections bolster serological immunity, and third-dose vaccine booster campaigns are underway worldwide to mitigate the ongoing wave of Omicron cases[391,392]. Vaccine breakthrough infections can directly train the immune system against variant spike proteins but come with medical risks including prolonged illness (long COVID) and death[365,393]. Conversely, booster vaccination is generally safe and has been shown to effectively increase the neutralizing response against Omicron BA.1[394–396]. The durability of responses due to boosting and breakthrough infection are unknown, but antibody levels have been shown to decrease over time following primary vaccination, suggesting that waning of the augmented immunity following additional exposure is likely[374,397]. It is also unknown whether recovery from breakthrough infection or booster vaccination provide greater protection from reinfection with Omicron sub-variants and any future variants, which will likely affect the future trajectory of the pandemic. To address these knowledge gaps, we examined serological immune responses and antibody-dependent cell-mediated phagocytosis in individuals who had received either two doses of a standard vaccine regimen, a standard regimen followed by a booster, or breakthrough infection following vaccination.

Section 7.3: Results

7.3.1 Cohort

A total of 99 individuals were studied (Table 7.1). Participants from the two-dose group provided serum samples a median of 24 days after the second dose. The three-dose group received a third vaccine dose a median of 253 days after the second and then provided serum samples a median of 86 days after the third dose (Figure 7.1A). Both two- and three-dose groups reported no history of SARS-CoV-2 infection and displayed a lack of nucleocapsid antibodies (Figure 7.1B). Breakthrough group participants had infection confirmed by a positive PCR-based COVID-19 test

at a median of 159.5 days after their final vaccine dose and provided serum samples a median of 29 days after the date of PCR testing. Among the breakthrough infections, 10 of 30 participants were infected with the Delta variant.

Table 7.1 Cohort demographics and clinical data

Characteristic	Two-dose	Three-dose	Breakthrough
Cohort characteristics			
N	42	27	30
Female - N (%)	35 (83.3)	19 (70.4)	23 (76.7)
Male - N (%)	7 (16.7)	8 (29.6)	7 (23.3)
Age (year) – median [range]	40 [23-74]	47 [26-74]	38 [24-63]
Time intervals (days) – median [interquartile range]			
Last vaccine to blood draw	24 [17.25-35.75]	86 [79.5-93.5]	N/A
PCR positivity to blood draw	N/A	N/A	29 [23-47]
2nd vaccine to positive PCR	N/A	N/A	159.5 [81.25-202.25]
Time between 1st and 2nd vaccines	21 [21-22]	21 [21-22]	21 [21-23]
Time between 2nd and 3rd vaccines	N/A	253 [249-263.5]	N/A
Vaccine type – N (%)			
BNT162b2 (Pfizer)	42 (100)	27 (100)	28 (93.3)
mRNA-1237 (Moderna)	0 (0)	0 (0)	1 (3.3)
Ad26.COV2.S (Janssen)	0 (0)	0 (0)	1 (3.3)
Breakthrough infection strain – N (%)			
Alpha (B.1.1.7)	N/A	N/A	5 (16.7)
Beta (B.1.351)	N/A	N/A	1 (3.3)
Gamma (P.1)	N/A	N/A	3 (10)
Delta (B.1.617.2)	N/A	N/A	10 (33.3)
Unknown*	N/A	N/A	11 (36.7)

*All breakthrough cases occurred between January 1, 2021, and August 18, 2021 (pre-Omicron).

Figure 7.1 Cohort design

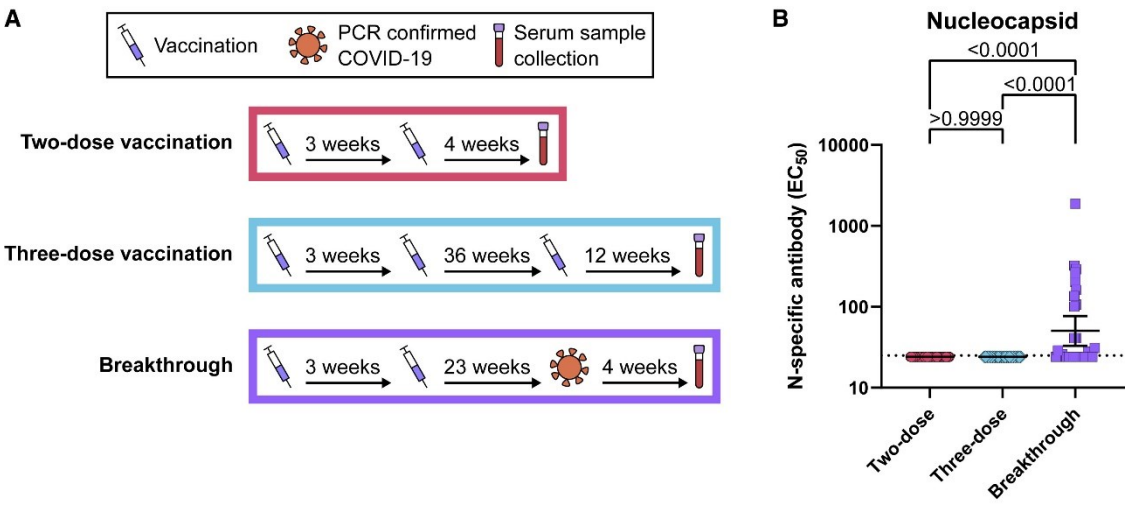

(**A**) Schematic describing median cohort vaccine dose, PCR-confirmed natural infection, and sample collection timing. (**B**) Serum dilutions with half-maximal binding (EC_{50}) of IgG/A/M antibodies to SARS-CoV-2 nucleocapsid protein. Error bars indicate the geometric mean and 95% confidence intervals. p values show the results of a two-tailed Kruskal-Wallis test with Dunn's multiple comparison correction.

7.3.2 Approach

In each sample, we analyzed the spike RBD-specific immunoglobulin G (IgG), IgA, and IgM antibody levels by enzyme-linked immunosorbent assay (ELISA). We also measured the ability of each serum sample to neutralize authentic wild-type SARS-CoV-2 (WA1) and clinical isolates of the Delta (B.1.617.2) and Omicron (BA.1 and BA.2) variants with focus reduction neutralization tests (FRNTs). Finally, we examined the ability of serum in each group to trigger antibody-dependent cell-mediated phagocytosis (ADCP) of spike protein-coated beads.

7.3.3 Binding antibody responses

Compared with two-dose vaccination, the geometric mean of serum dilutions with half-maximal binding in ELISA (EC_{50}) to full-length SARS-CoV-2 spike protein was 2.23-fold higher in the three-dose group and 2.78-fold higher in the breakthrough group; the three-dose and breakthrough groups were not significantly different from each other (Figure 7.2A). Spike RBD-specific antibodies did not significantly increase in the three-dose group but did in the breakthrough group, which was 2.8-fold higher than in the two-dose group (Figure 7.2B). Spike-specific IgG and IgA levels showed similar increases relative to the two-dose group, with 2.2- and 2.5-fold higher IgG levels and 2.2- and 2.9-fold higher IgA levels in the three-dose and breakthrough groups, respectively (Figure 7.2C and D). IgM levels were not significantly different between any of the groups (Figure 7.2E).

Figure 7.2 Antibody response to two-dose vaccination, three-dose vaccination, and breakthrough infection

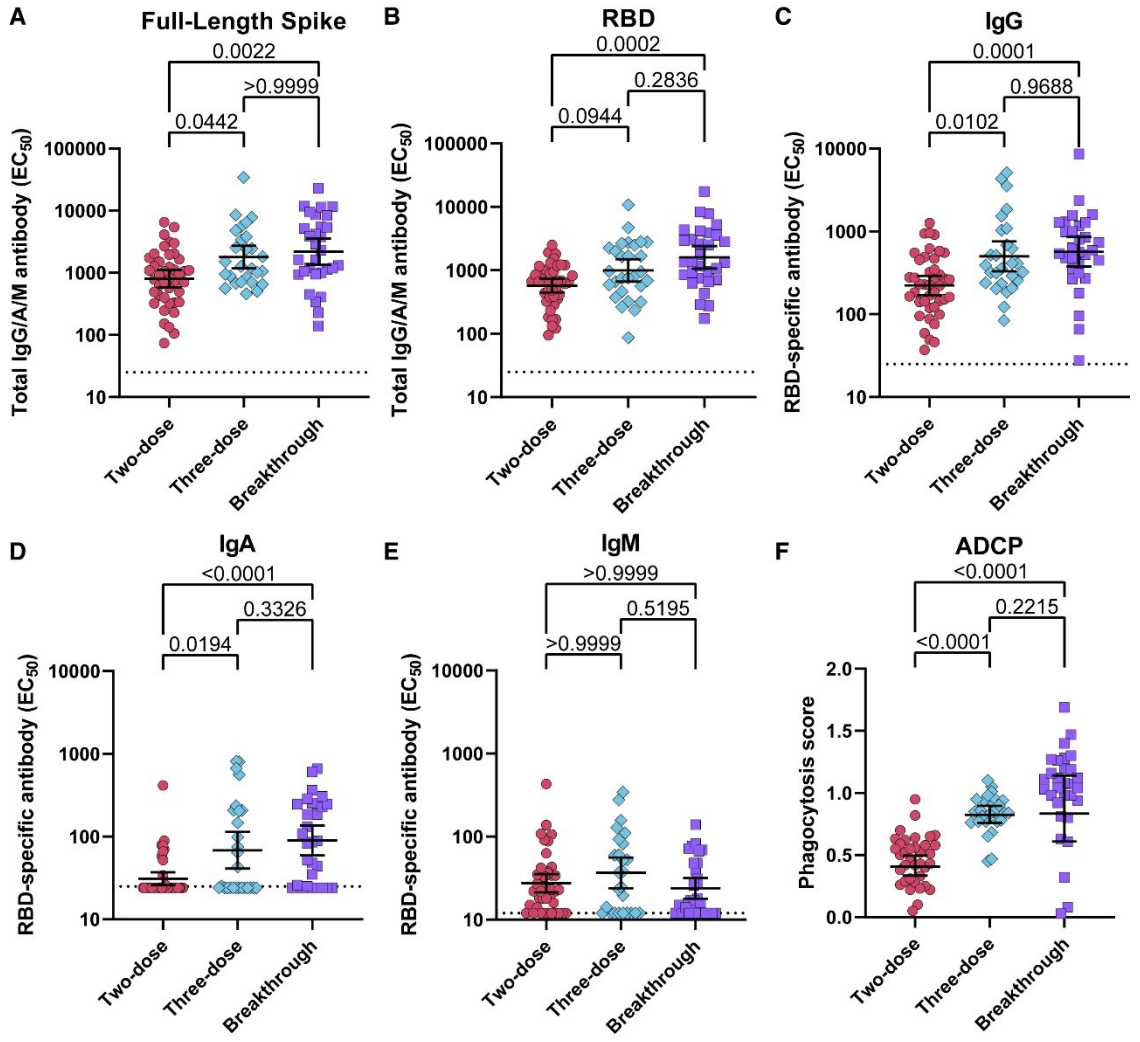

(**A**) Serum dilutions with EC_{50} of IgG/A/M antibodies to full-length SARS-CoV-2 spike protein. (**B**) Serum IgG/A/M antibody EC_{50} to spike receptor-binding domain (RBD). (**C–E**) Serum (**C**) IgG-, (**D**) IgA-, and (**E**) IgM-specific antibody EC50s to RBD. (**F**) Antibody-dependent cellular phagocytosis scores indicate the increase in uptake of RBD-coated beads caused by sera. Error bars indicate the geometric mean and 95% confidence intervals. p values show the results of two-tailed Kruskal-Wallis tests with Dunn's multiple comparison correction.

7.3.4 Antibody-dependent cell-mediated phagocytosis

Similar to neutralizing antibody responses, ADCP also increased in the three-dose (1.8-fold) and breakthrough (2.2-fold) groups compared with two-dose vaccination; here, as well, the three-dose and breakthrough groups were not significantly different from each other (Figure 7.2F).

7.3.5 Neutralizing antibody responses

Consistent with previous reports, neutralization of live SARS-CoV-2 improved to a greater degree than the observed rise in binding antibody levels[392,398]. The geometric mean titers (GMTs) showing 50% neutralization of the original SARS-CoV-2 virus (WA1) in FRNT assays were 4.6- and 7.1-fold higher for the three-dose and breakthrough groups, respectively, compared with two-dose vaccination, but were not significantly different from each other (Figure 7.3A). The GMT of the breakthrough group to neutralize the Delta variant increased 9.0-fold, while the three-dose group increased only 4.2-fold, compared with two-dose vaccination. However, the difference between the three-dose and breakthrough groups did not rise to the level of statistical significance (Figure 7.3B). Against Omicron BA.1, 25 of 42 (59%) sera in the two-dose group fell below the limit of detection for neutralization, while all three-dose and breakthrough participants showed detectable neutralization, with 11.6- and 16.8-fold higher neutralizing GMTs, respectively, which were not significantly different from each other (Figure 7.3C). Against Omicron BA.2, 50% of sera in the two-dose group fell below the limit of detection, while all three-dose and breakthrough participants showed detectable neutralization with 5.4- and 12.3-fold higher GMTs than the two-dose group, respectively, but were not significantly different from each other (Figure 7.3D).

Figure 7.3 Live SARS-CoV-2 neutralization by two-dose vaccination, three-dose vaccination, and breakthrough infection cohorts

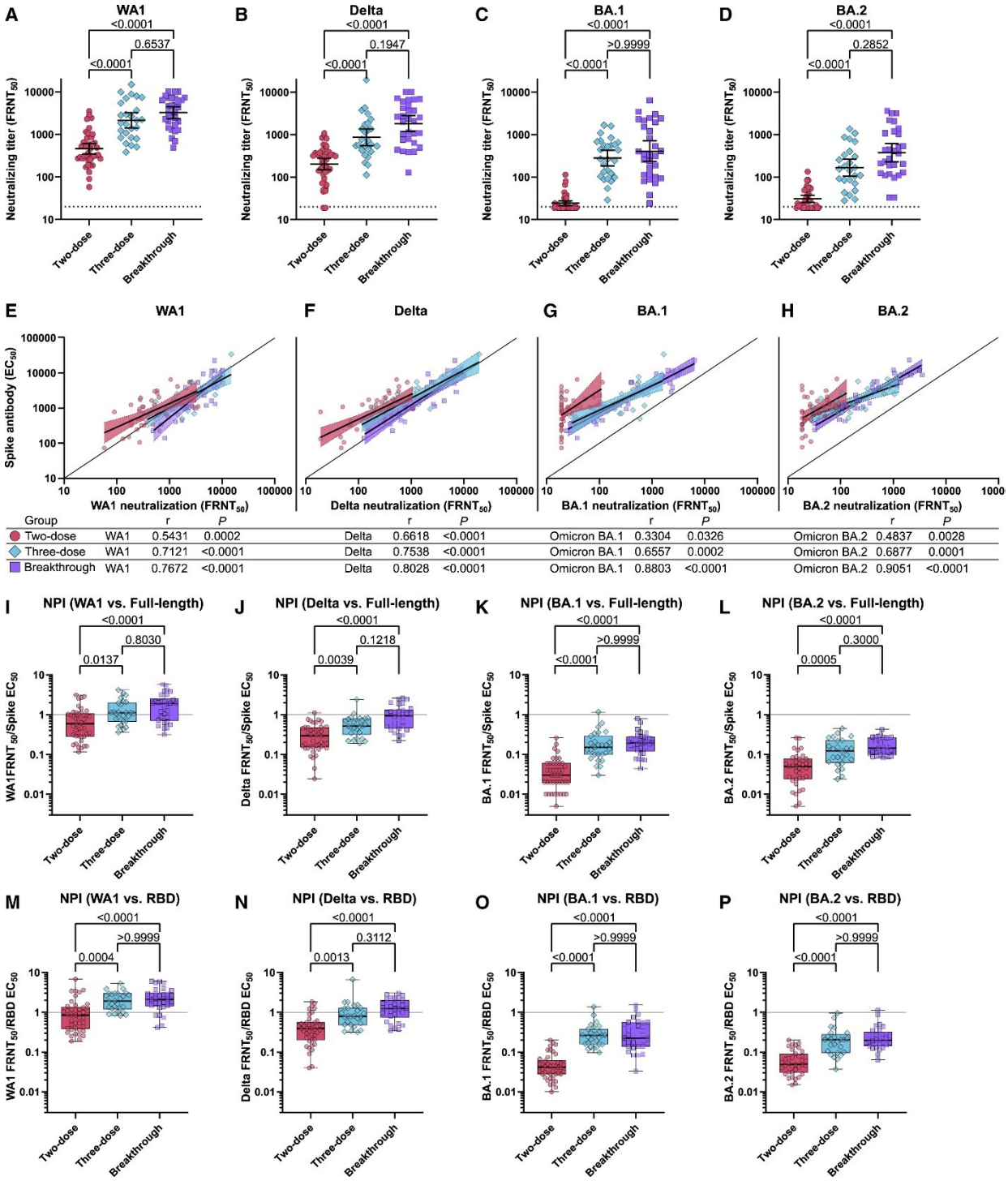

(**A–D**) Wild-type SARS-CoV-2 (WA1) (**A**), Delta (**B**), Omicron BA.1 (**C**), and Omicron BA.2 (**D**) neutralizing activity determined by 50% focus reduction neutralization test ($FRNT_{50}$). (**E–H**) Correlation of serum full-length spike-binding antibody EC_{50} with (**E**) WA1 $FRNT_{50}$, (**F**) Delta $FRNT_{50}$, (**G**) Omicron BA.1 $FRNT_{50}$, and (**H**) Omicron BA.2 $FRNT_{50}$. The solid line indicates equal EC_{50} and $FRNT_{50}$ values. (**I–L**) Neutralizing potency indexes show the ratio of (**I**) WA1, (**J**) Delta, (**K**) Omicron BA.1, and (**L**) Omicron BA.2 $FRNT_{50}$ over full-length spike-specific antibody EC_{50}. (**M–P**) Neutralizing potency indexes calculated instead with RBD-specific antibody EC_{50}s for (**M**) WA1, (**N**) Delta, (**O**) Omicron BA.1, and (**P**) Omicron BA.2. The solid gray lines indicate equal $FRNT_{50}$ and EC_{50}. Error bars in (**A**–**D**) indicate the geometric mean and 95% confidence intervals. Box plots in (**I–P**) show the median, interquartile range, and full range. p values in (**A–D**) and (**I–P**) show the results of two-tailed Kruskal-Wallis tests with Dunn's multiple comparison correction.

7.3.6 Antibody response quality

The relationship between spike-binding antibody level and neutralizing titer gives an indication of the quality of the antibody response by controlling for the total quantity of antibodies present. In all three groups, binding antibody titer correlated strongly with neutralization of WA1 and Delta. However, the correlations were weaker for the two-dose group against Omicron BA.1 and BA.2, largely due to the high proportion of samples below the detection limit (Figure7.3E–H). We explored this association further by calculating the neutralizing potency index (NPI) as the ratio of live-virus neutralization to spike-specific antibody EC_{50} for WA1, Delta, Omicron BA.1, and Omicron BA.2. For WA1, the median NPI was 0.60 for two dose, 1.10 for three dose, and 1.91 for breakthrough, showing an increase in the ratio of neutralizing activity to spike-binding EC_{50} (Figure7.3I). The median Delta NPI was 0.30, 0.52, and 0.94; the median Omicron BA.1 NPI

was 0.03, 0.15, and 0.20; and the median Omicron BA.2 NPI was 0.05, 0.12, and 0.14 for the two-dose, three-dose, and breakthrough groups, respectively (Figure7.3J–L). NPI values were significantly increased in the three-dose and breakthrough groups relative to the two-dose group for all viruses tested but were not significantly different from each other. A similar trend was seen when calculating the NPI using RBD-specific antibody levels instead of those for full-length spike (Figure7.3M−P).

7.3.7 Relative loss of strain-specific neutralizing capacity

Comparing the neutralization of Delta and Omicron BA.1 and BA.2 with that of WA1 clearly showed a greater extent of resistance by Omicron sub-variants, with some individuals displaying a nearly 100-fold reduction in neutralization of Omicron compared with WA1 (Figure 7.4A–C). To quantify the relative loss of neutralizing activity against the Delta and Omicron (BA.1 and BA.2) variants compared with WA1, we calculated the ratio of neutralization for each variant to WA1 neutralization in each participant. For Delta, the median ratio was 0.42 for two dose, 0.43 for three dose, and 0.55 for breakthrough, none of which were significantly different (Figure 7.4D). Against Omicron BA.1, however, the median ratio was 0.06 for two dose, 0.12 for three dose, and 0.13 for breakthrough, and here, the three-dose and breakthrough groups were significantly higher than the two-dose group. The corresponding Omicron BA.2 median ratios were 0.07, 0.10, and 0.10, respectively, and no groups were significantly different from each other (Figure 7.4E and F).

Figure 7.4 Quality of the neutralizing antibody response to two-dose vaccination, three-dose vaccination, and breakthrough infection

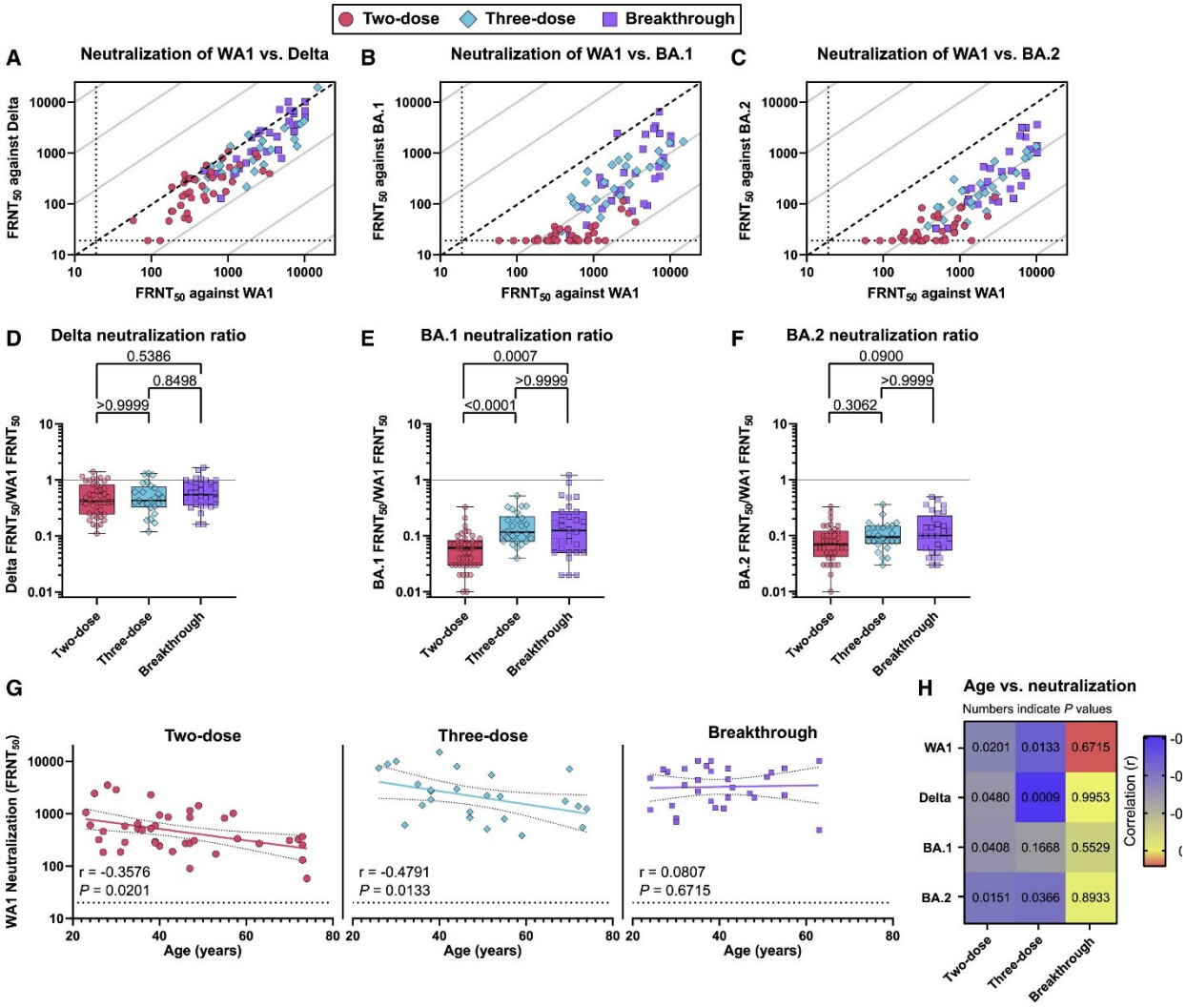

(**A–C**) Scatter plots depicting (**A**) Delta, (**B**) Omicron BA.1, and (**C**) Omicron BA.2 $FRNT_{50}$ versus WA1 $FRNT_{50}$. The broken lines indicate equal neutralization of variants and WA1, while gray lines signify 10-fold differences. (**D–F**) Relative neutralization of (**D**) Delta, (**E**) Omicron BA.1, and (**F**) Omicron BA.2 $FRNT_{50}$ over WA1 $FRNT_{50}$. The solid line indicates equal neutralization of WA1 and variants. (**G**) Correlation of WA1 $FRNT_{50}$ with age at the time of study enrollment. (**H**) Heatmap showing correlation between age and $FRNT_{50}$ for WA1, Delta,

Omicron BA.1, and Omicron BA.2 for two-dose, three-dose, and breakthrough groups. Box plots in (**D**–**F**) show the median, interquartile range, and full range, while p values show the results of two-tailed Kruskal-Wallis tests with Dunn's multiple comparison correction. r values in (**G**) indicate the Spearman correlation coefficients with corresponding two-tailed p values. Linear best-fit lines with 95% confidence bands were determined by simple linear regression of log-transformed $FRNT_{50}$ and non-transformed age values. Colors in (**H**) indicate Spearman correlation coefficients, and values indicate the corresponding p values. See also Figure S7.1.

7.3.8 Antibody response versus age and gender

Previous studies have established a negative correlation between antibody response and age among vaccinated individuals[369]. Among study participants, we observed a negative correlation between age and WA1 neutralizing titer for the two-dose and also the three-dose groups but not for the breakthrough group (Figure 7.4G). We then calculated the correlation between age and neutralizing titer against WA1 as well as Delta, Omicron BA.1, and Omicron BA.2, which is depicted in a heatmap (Figure 7.4H and Figure S7.1A–C). We found no difference in neutralizing titer based on gender (Figure S7.2A–D).

Section 7.4: Discussion

7.4.1 Discussion

We compared SARS-CoV-2-specific serological and sero-dependent immune responses in individuals receiving two standard vaccine doses and three vaccine doses and individuals experiencing breakthrough infection. We found that despite the reliance of the vaccine on the original SARS-CoV-2 spike protein sequence, both booster vaccination and breakthrough infection enhance serological responses to a similar degree. In each of these re-exposure groups,

we observed significant increases in IgG binding levels, antibody-dependent cell-mediated phagocytosis, and neutralizing titers. Further, we observed improved breadth of the humoral response, as seen by improved Delta and Omicron BA.1 and BA.2 variant neutralization and an increased ratio of variant to WA1 neutralizing titers, and improved antibody quality, as reflected in an improvement in the amount of neutralizing activity for a given spike-binding antibody titer.

Thus, while two doses of the currently available mRNA vaccines provide robust antibody responses correlating with strong protection against symptomatic infection due to the original SARS-CoV-2 and early variants, serological immunity against the Omicron BA.1 and BA.2 variants is substantially reduced[399] but is restored both by booster vaccination and breakthrough infection. This is consistent with a previous study indicating that hybrid immunity from SARS-CoV-2 infection followed by one or two mRNA vaccine doses provides similar antibody responses to breakthrough infection[392]. Interestingly, the negative correlation between age and antibody levels seen in those exposed through vaccination alone is not seen in those who have experienced breakthrough infection.

Despite the augmented immune responses seen with additional exposure after receipt of a primary series, our data also highlight a progressive loss of susceptibility to neutralizing responses with the emergence of new variants, consistent with recent reports[51,385]. This is most clearly evident in the declining NPI (degree of neutralization for a given amount of antibody), the declining ratio of variant neutralization to WA1 neutralization in the progression from Delta to the Omicron sub-variants, and subtle differences in this ratio suggesting further loss between BA1 and BA2.

The similarity seen between immune responses to three-dose regimens and breakthrough infection suggests that vaccines based on the original WA1 variant continue to provide neutralizing

antibody responses conferring at least partial protection against currently circulating variants, including early Omicron sub-lineages. However, the progressive loss in neutralizing capacity suggests that boosting with updated vaccine inserts will likely take on an important role in developing effective prophylaxis against future SARS-CoV-2 variants. Both Pfizer and Moderna have both recently pursued bivalent vaccine approaches; Moderna has studied a bivalent vaccine containing inserts corresponding to the original strain and B.1.351, and both Pfizer and Moderna are developing similar vaccines pairing original-strain and Omicron-adapted inserts[269,400,401]. While reports suggest improved immunogenicity for each of these, peer-reviewed data are not yet available, and doubts remain about the relevance of these vaccines to the emerging BA.4/5 sub-variants and anticipated future variants[402].

This debate highlights the inherent difficulty in evaluating immune responses to vaccination in the face of such a highly prevalent and rapidly evolving viral pandemic, since the emergence of new strains continually challenges our current understanding of the minimum requirements for a broadly effective vaccine. While we provide additional data on early Omicron variants, ongoing work will be required to understand the impact of BA.4/5 and future lineages and whether periodic vaccine updates, multivalent vaccines, or perhaps vaccines focusing on relatively invariant portions of the spike protein will be the key to finding an effective long-term vaccine strategy against SARS-CoV-2.

7.4.2 Limitations of the study

One limitation of this study is the slightly longer time to sampling in the three-dose group compared with the other groups. The protection from three-dose vaccination is known to decrease measurably over the first 3 months[403], and therefore neutralizing antibody levels may be underestimated in our data relative to the other groups. In addition, age distributions were not

perfectly matched in the three groups studied, though the trends we observed persisted even in a sub-analysis of those <65 years of age (Figure S7.3). Lastly, participants were recruited from among healthcare workers self-reporting infection or otherwise volunteering for the study, and it was not possible to recruit a cohort broadly representative of diverse ethnic groups.

Section 7.5: Methods

7.5.1 Cohort selection and serum collection

Two- and three-dose group participants were selected from a larger cohort of vaccinated health care workers at Oregon Health & Science University recruited at the time of their first vaccine dose. Participants were asked to return after either their second or third vaccine dose to provide whole blood samples. Breakthrough group participants were recruited and enrolled at Oregon Health & Science University from among fully vaccinated health care workers receiving positive results during PCR-based diagnostic testing for SARS-CoV-2 infection, at which time participants provided information on symptoms of illness by direct interview. Whole blood (4–6 mL) was collected with a BD Vacutainer® Plus Plastic Serum Tube and centrifuged for 10 min at 1000xg, then stored at −20°C. Two- and three-dose group participants confirmed no history of COVID-19 by direct interview and validated by nonreactivity in a SARS-CoV-2 N protein ELISA. The vaccines used in this study were BNT162b2 (Pfizer), mRNA-1273 (Moderna), or Ad26.COV2.S (Janssen) and only individuals with no reported immunocompromising conditions were included. Participants information on sex, and age, was self-reported. Information on race, gender and socioeconomic status was not collected.

7.5.2 Ethics statement

This study was conducted with approval of the Oregon Health and Sciences University Institutional review board (IRB# 00022511). All participants were enrolled following written informed consent.

7.5.3 Enzyme-linked immunosorbent assays (ELISA)

ELISAs were performed as previously described[369]. In 96-well ELISA plates. Plates were coated with SARS-CoV-2 RBD (produced in Expi293F cells and purified using Ni-NTA chromatography), N at 100 µL/well at 1 µg/mL in PBS and incubated overnight at 4°C with rocking. Plates were washed three times with 0.05% Tween 20 in PBS (wash buffer) and blocked with 150 uL/well with 5% nonfat dry milk powder and 0.05% Tween 20 in PBS (blocking buffer) at room temperature (RT) for 1 h with rocking. Breakthrough and control sera were aliquoted and frozen in dilution plates then resuspended in blocking buffer; sera were diluted and added to ELISA plates 100 µL/well (6 x 4-fold dilutions from 1:50 to 1:51,200, except for IgM (6 x 4-fold dilutions from 1:25 to 25,600). Sera was incubated in coated plates for 1 h at RT, then washed three times with wash buffer. Plates were incubated with anti-human IgA-HRP at 1:3,000, Mouse anti-human IgG-HRP at 1:3,000, or Goat anti-human IgM-HRP at 1:3,000 at RT for 1 h with rocking, then washed three times with wash buffer prior to developing with o-phenylenediamine dihydrochloride (OPD) according to manufacturer instructions. The reaction was stopped after 25 min using an equivalent volume of 1 M HCl; optical density was measured at 492 nm using a CLARIOstar plate reader.

7.5.4 Antibody dependent cellular phagocytosis (ADCP)

ADCP was assessed as described previously[392]. Biotinylated SARS-CoV-2 RBD protein was incubated with neutravidin beads for 2 h at room temperature then washed with PBS with 1%

BSA (dilution buffer) two times. 10 µL of 1:100 diluted RBD beads were incubated with an equal volume of diluted serum for 2 h at 37°C. Bead-serum mixtures were then incubated with 20,000 THP-1 cells in a final volume of 100 uL overnight in a tissue culture incubator. 100 µL of PBS with 4% formaldehyde was then used to fix each well for 30 min prior to flow cytometry. Triplicate, samples were flowed on a CytoFLEX flow cytometer. 2500 events were recorded per replicate. Phagocytosis scores were calculated as the product of percent bead-positive cells and mean fluorescence intensity of bead-positive cells, then divided by 10^6.

7.5.5 SARS-CoV-2 growth and titration

SARS-CoV-2 isolates USA-WA1/2020 [lineage A], hCoV-19/USA/PHC658/2021 [lineage B.1.617.2 – Delta], hCoV-19/USA/MD-HP20874/2021 [lineage B.1.1.529 – Omicron BA.1], and hCoV-19/USA/CO-CDPHE-2102544747/2021 [lineage B.1.1.529 – Omicron BA.2] were obtained from BEI Resources. Viral stocks were propagated as previously described[370]. Sub-confluent Vero E6 cells grown in Dulbecco's Modified Eagle Medium (DMEM), 10% fetal bovine serum (FBS), 1% nonessential amino acids, 1% penicillin-streptomycin (complete media) were infected at an MOI of 0.05 in a minimal volume (0.01 mL/cm^2) of Opti-MEM + 2% FBS (dilution media) for 1 h at TCC then 0.1 mL/cm^2 additional complete media was added and incubated until at least 20% cytopathic effect (CPE) was observed, typically 72–96 h. Culture supernatant was centrifuged for 10 min at 1000xg and frozen at −80°C. Titration was performed by focus forming assay on sub-confluent Vero E6 cells. 10-fold dilutions were prepared in dilution media and incubated for 1 h, then covered with Opti-MEM, 2% FBS, 1% methylcellulose (overlay media) and incubated for 24 h (48 h for Omicron BA.1 and BA.2). Plates were then fixed in 4% formaldehyde in phosphate buffered saline (PBS) for 1 h then removed from BSL-3 following institutional guidelines. Cells were permeabilized in 0.1% bovine serum albumin (BSA), 0.1%

saponin in PBS (perm buffer) for 30 min, and were then incubated with polyclonal anti-SARS-CoV-2 alpaca serum (1:5000 in perm buffer, or 1:2000 for Omicron) overnight at 4°C. Plates were washed three times with 0.01% Tween 20 in PBS (wash buffer), then incubated for 2 h at RT with 1:20,000 anti-alpaca-HRP, or 1:5000 for Omicron. Plates were washed three times with wash buffer, then incubated with TrueBlue for 30 min or until sufficiently developed for imaging. Foci images were captures with a CTL Immunospot Analyzer and counted with Viridot (1.0) in R (3.6.3)[382]. Viral stock titers in focus forming units (FFU) were calculated based on the dilution factor and volume used for infection.

7.5.6 Focus reduction neutralization test (FRNT)

FRNT assays were carried out as previously described[370]. We prepared 5 × 4.7-fold (1:10–1:4879) serial dilutions in duplicate for each serum sample. An equal volume of viral stock was added to each well (final dilutions of sera, 1:20–1:9760) such that approximately 50 FFU were added to each well. Virus-serum mixtures were incubated for 1 h before being used to infect sub-confluent Vero E6 cells in 96-well plates for 1 h, then covering with 150 µL/well overlay media. Each 5-point serum dilution series was accompanied by a virus only control well. Fixation, development, and counting of FRNT plates was carried out as described in SARS-CoV-2 growth and titration. Percent neutralization values were calculated for each well as focus count divided by the average of virus-only wells from the same plate.

7.5.7 Statistical analysis

$FRNT_{50}$ and EC_{50} values were calculated by fitting to a dose-response curve as previously described[370]. Final $FRNT_{50}$ values below the limit of detection (1:20) were set to 1:19. Final EC_{50} values below the limit of detection of 1:25 for N, full-length Spike, Spike RBD, IgG, IgA were set to 1:24 and 1:12.5 for IgM was set to 1:12. Aggregated EC_{50} and $FRNT_{50}$ values were analyzed in

Graphpad Prism (9.3.1). Significance was determined using Kruskal-Wallis tests with Dunn's multiple comparison correction, p-values were two-tailed. Correlations were calculated with log-transformed EC_{50} and/or $FRNT_{50}$ values with the Spearman method, with corresponding two-tailed p values. Best fit lines were calculated via simple linear regression.

Section 7.6: Supplemental Figures

Figure S7.1 Variant neutralization correlation with age

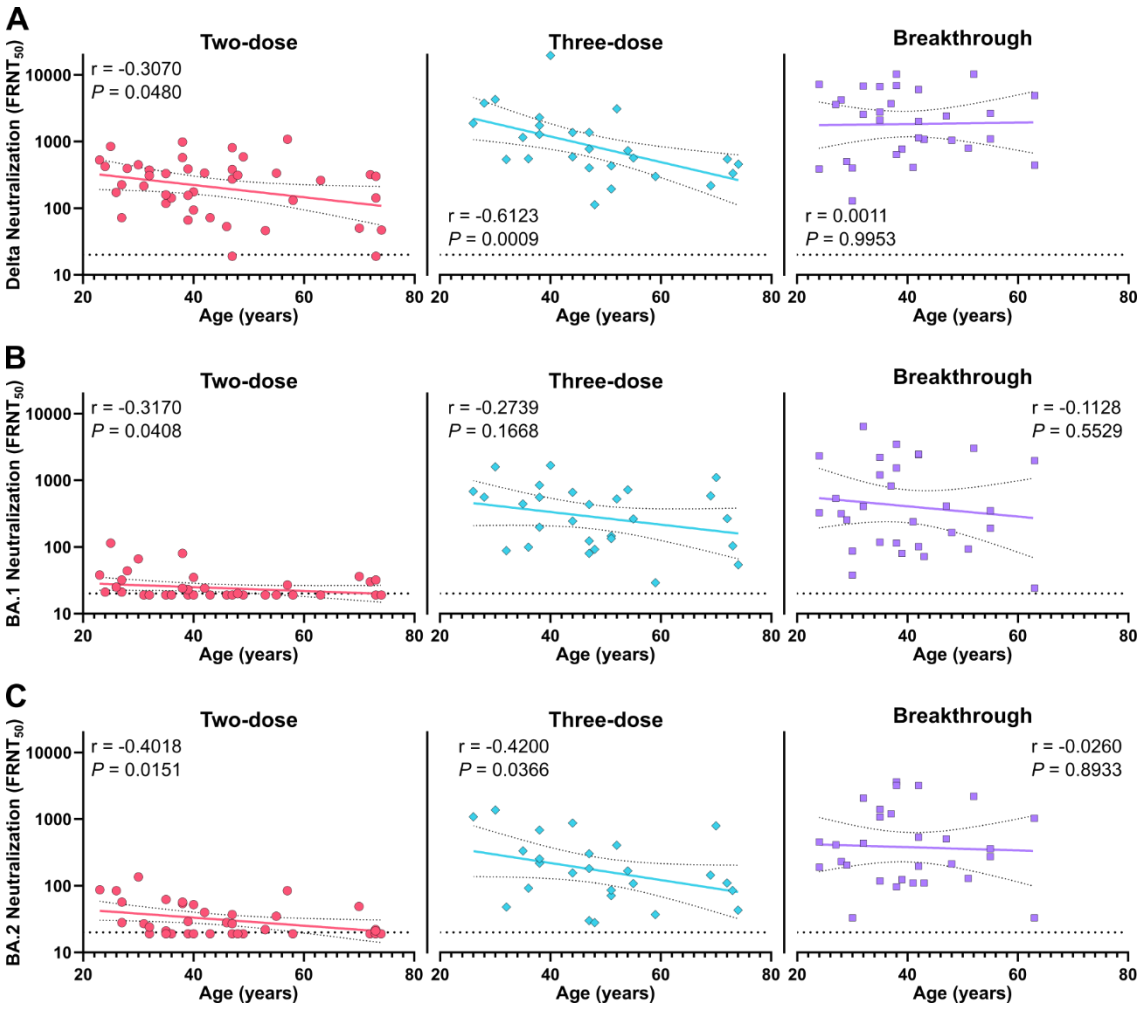

Correlation of (**A**) Delta, (**B**) Omicron BA.1, and (**C**) Omicron BA.2 FRNT50 with age at the time of study enrollment. r values indicate the Spearman correlation coefficients with corresponding two-tailed P values. Linear best fit-lines with 95% confidence bands were

determined by simple linear regression of log transformed FRNT50, and non-transformed Age values.

Figure S7.2 Relationship between sex and variant neutralization

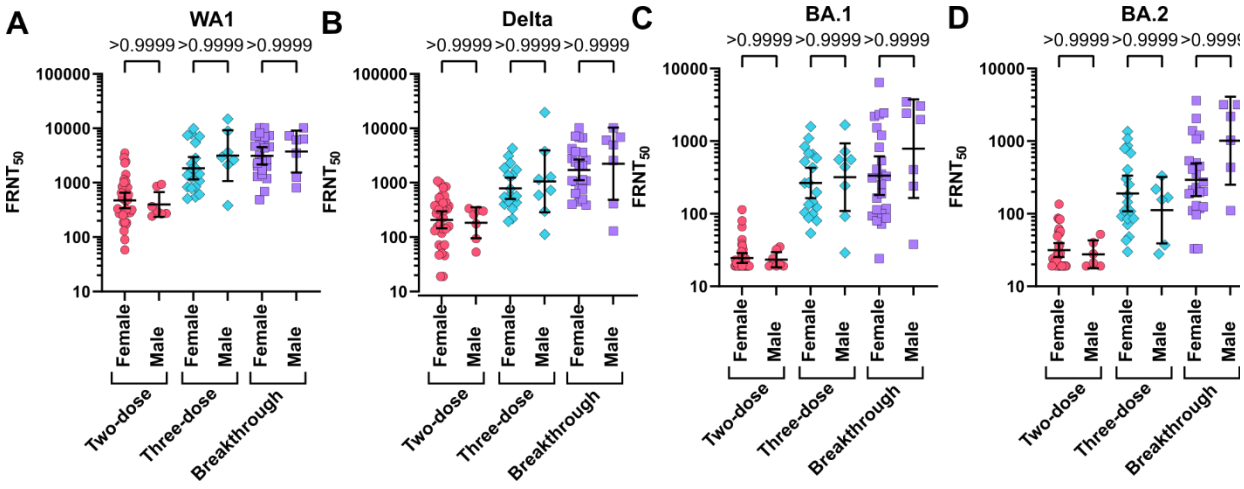

Two-dose, three-dose, and breakthrough groups divided by sex showing FRNT50 values against (**A**) WA1, (**B**) Delta, (**C**) Omicron BA.1, and (**D**) Omicron BA.2. Error bars indicate geometric mean and 95% confidence intervals. P-values show the results of two-tailed Kruskal-Wallis tests with Dunn's multiple comparison correction.

Figure S7.3 Correlation between neutralization and age for individuals <65 years of age

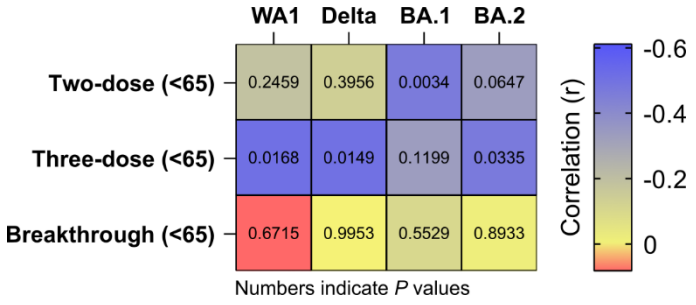

Magnitude of Pearson correlation coefficients against WA1, Delta, BA.1 and BA.2 for each group.

Section 7.7: Acknowledgments

7.7.1 Acknowledgments

We gratefully recognize the OHSU faculty and staff who participated in this study, the OHSU COVID-19 serology study team and the OHSU occupational health department for recruitment and sample acquisition, Dr. William Messer and research team for sample handling, the OHSU clinical laboratory under the direction of Dr. Donna Hansel and Dr. Xuan Qin for SARS-CoV-2 testing and reporting, and BEI Resources for providing clinical viral isolates. This study was funded by a grant from the M. J. Murdock Charitable Trust (to M.E.C.), an unrestricted grant from the OHSU Foundation (to M.E.C.), NIH training grant T32HL083808 (to T.A.B.), and OHSU Innovative IDEA grant 1018784 (to F.G.T.). The funders had no role in the conceptualization, conduct, or interpretation of this work.

7.7.3 Author contributions

Conceptualization, M.E.C., F.G.T., and T.A.B.; recruitment and sample collection, M.E.C., D.S., and S.D.C.; experimental design, M.E.C., F.G.T., and T.A.B.; laboratory analysis, F.G.T., T.A.B., G.G., and S.K.M.; statistical analysis, T.A.B.; supervision: M.E.C. and F.G.T.; manuscript drafting, M.E.C. and T.A.B.; manuscript review and editing, M.E.C., T.A.B., D.S., S.D.C., and F.G.T.

Chapter 8: BNT162b2 induced neutralizing and non-neutralizing antibody functions against SARS-CoV-2 diminish with age

Timothy A. Bates[1, 7], Pei Lu[2, 7], Ye jin Kang[2], Devin Schoen[3], Micah Thornton[4], Savannah K. McBride[1], Chanhee Park[4], Daehwan Kim[4], William B. Messer[1], Marcel E. Curlin[3, 8], Fikadu G. Tafesse[1, 8], Lenette L. Lu[2, 5, 6, 8, 9]

[1]Department of Molecular Microbiology and Immunology, OHSU, Portland, OR, 97239, USA

[2]Division of Infectious Diseases and Geographic Medicine, Department of Internal Medicine, UTSW Medical Center, Dallas, TX, 75390, USA

[3]Department of Occupational Health, OHSU, Portland, OR, 97239, USA

[4]Lyda Hill Department of Bioinformatics, UTSW Medical Center, Dallas, TX 75390, USA

[5]Department of Immunology, UTSW Medical Center, Dallas, TX 75390, USA

[6]Parkland Health & Hospital System, Dallas, TX, 75235, USA

[7]These authors contributed equally

[8]Corresponding authors

[9]Lead contact

Cell Reports Volume 41, Issue 4. October 25, 2022.

DOI: https://doi.org/10.1016/j.celrep.2022.111544

Section 8.1: Abstract

Each severe acute respiratory syndrome coronavirus 2 (SARS-CoV-2) variant renews concerns about decreased vaccine neutralization weakening efficacy. However, while prevention of infection varies, protection from disease remains and implicates immunity beyond neutralization in vaccine efficacy. Polyclonal antibodies function through Fab domains that neutralize virus and Fc domains that induce non-neutralizing responses via engagement of Fc receptors on immune cells. To understand how vaccines promote protection, we leverage sera from 51 SARS-CoV-2 uninfected individuals after two doses of the BNT162b2 mRNA vaccine. We show that neutralizing activities against clinical isolates of wild-type and five SARS-CoV-2 variants, including Omicron BA.2, link to FcγRIIIa/CD16 non-neutralizing effector functions. This is associated with post-translational afucosylation and sialylation of vaccine-specific antibodies. Further, polyfunctional neutralizing and non-neutralizing breadth, magnitude, and coordination diminish with age. Thus, studying Fc functions in addition to Fab-mediated neutralization provides greater insight into vaccine efficacy for vulnerable populations, such as the elderly, against SARS-CoV-2 and novel variants.

Section 8.2: Introduction

Neutralizing antibody responses are among the core measures of vaccine efficacy in the COVID-19 pandemic[396,404]. Yet, even when neutralization is compromised in the setting of new severe acute respiratory syndrome coronavirus 2 (SARS-CoV-2) variants[405,406] and cases of vaccine breakthrough infections rise, protection from hospitalization remains relatively high[407–410]. Thus, the continued emergence of new variants highlights the need to understand vaccine efficacy through protection from disease in addition to prevention of infection.

Though one of the key components of immune protection, the complexity of polyclonal antibody responses and its roles in disease remain only partially understood. For SARS-CoV-2, attention has focused on leveraging direct neutralization of virus by antigen recognition via the Fab domain. However, the overall magnitude of neutralizing responses in patients with severe COVID-19 is higher compared with mild disease, suggesting that neutralizing activity alone poorly captures the capacity to protect from serious illness[411,412]. Independently, data from multiple large clinical trials have demonstrated that convalescent plasma carrying neutralizing activity does not prevent infection or disease in humans[413–415], suggesting that passive transfer of neutralizing polyclonal antibodies is insufficient to confer protection. These lines of evidence show that in SARS-CoV-2 infection, more nuanced evaluations of neutralizing responses with respect to potency[123] and dynamics[411] and immune responses beyond neutralization are vital in understanding pathogenesis.

Antibodies function through the combination of the Fab domain, which directs neutralizing activity against microbial targets, and the Fc domain, which induces non-neutralizing functions[139]. Through binding Fc receptors expressed on innate and adaptive immune cells as well as activation of complement, antibody Fc domains have the ability to induce a spectrum of host responses directed against an antigen recognized by the Fab domain[416]. Thus, antibody Fc effector functions have the potential to impact outcomes of SARS-CoV-2 infection and protection in vaccines.

Studies using monoclonal antibodies targeting SARS-CoV-2 show that Fc effector functions can be protective. Passive transfer of monoclonal antibodies with mutations that abrogate Fc domain binding to Fc receptors result in increased SARS-CoV-2 viral load and decreased survival in multiple animal models when compared with intact antibodies[134,417–419]. This effect is more pronounced with therapeutic than with prophylactic administration[420]. Thus, monoclonal

antibody Fc functions support neutralizing activity to prevent viral entry. Moreover, even after viral infection, Fc functions can inhibit disease progression.

Conversely, several lines of evidence show that Fc effector functions in polyclonal responses during SARS-CoV-2 infection could be pathogenic. Post-translational immunoglobulin G (IgG) glycosylation is altered with disease severity in many ways[421–423], but one consistent observation across several studies is that decreased IgG fucosylation correlates with worsening clinical symptoms and hospitalization[424–426]. The proposed mechanism of pathology is through increased binding to the activating Fc receptor FcγRIIIa/CD16a. In an *in vitro* poly I:C-stimulated human macrophage model with FcγRIIIa/CD16a expression, addition of afucosylated, compared with fucosylated, IgG from patients infected with SARS-CoV-2 enhances secretion of the pro-inflammatory cytokine interleukin-6 (IL-6)[426,427]. In monocytes, FcγR-mediated activation can cause pyroptosis[428]. In a human Fc receptor transgenic mouse model, passive transfer of afucosylated polyclonal IgG from individuals with severe COVID-19 increases production of IL-6 and tumor necrosis factor α (TNFα) but not the anti-inflammatory IL-10[425]. Consistent with these data, FcγRIIIa/CD16a natural killer (NK) cell activation that leads to antibody-dependent cellular cytotoxicity (ADCC) is enhanced with symptom severity and normalizes upon convalescence[424]. The low-affinity activating FcγRIIa/CD32a and inhibitory FcγRIIb/CD32b along with the high-affinity FcγRI/CD64 mediate the non-neutralizing Fc effector functions of antibody-dependent cellular phagocytosis (ADCP) by monocytes. Neutrophils express antibody receptors for both IgG, the activating high-affinity FcγRI, and low-affinity FcγRIIa and FcγRIIIB, as well as IgA, the low-affinity FcαRI. These, along with complement receptors CR1 and CR3, contribute to neutrophil phagocytosis. Finally, C1q binding to IgG and IgM Fc domains activates complement pathways through C3 deposition[429–432]. In contrast to FcγRIIIa/CD16a activities, the implications of

FcγRIIa/CD32a- and FcγRIIb/CD32b-mediated phagocytosis and complement activation in SARS-CoV-2 are less clear given the variability in cohort populations with respect to clinical outcomes, demographics, and co-morbidities[433–437]. However, that multiple Fc effector functions in infection and disease are detectable suggest that these responses, if induced by vaccines, could influence outcomes.

For COVID-19 vaccines, neutralizing titers are often used to extrapolate protective efficacy[438]. While antibody-dependent NK cell activation (ADNKA), ADCC, ADCP by monocytes, antibody-dependent neutrophil phagocytosis (ADNP) by neutrophils, and complement activation are also elicited[439–441], it is unclear whether these Fc effector functions are protective, inert, or pathogenic. Moreover, how non-neutralizing antibody functions impact direct neutralization of live virus is not known. To assess the relationships between Fab and Fc domain functions in polyclonal responses from vaccination, we evaluated immune sera from SARS-CoV-2-uninfected healthcare workers who received two doses of the BNT162b2 mRNA vaccine. We assessed neutralization against SARS-CoV-2 wild-type virus (WA.1) and five clinical variants: Alpha (B.1.1.7), Beta (B.1.351), Gamma (P.1), Delta (B.1.617.2), and Omicron (BA.2). We measured vaccine-specific antibody Fc features of isotype, Fc receptor binding, Fc effector functions, and IgG glycosylation. We found heterogeneous neutralizing and non-neutralizing antibody responses. Neutralization across variants correlated with FcγRIIIa/CD16a effector functions in an age-, but not sex-, dependent manner. Post-translational afucosylation and sialylation of vaccine-specific antibodies associated with enhanced FcγRIIIa/CD16a activity. Neutralizing and non-neutralizing functions independently and collectively diminished with age, limiting polyfunctional breadth, magnitude, and coordination in those ≥65 years old compared with those <65. Our results show that assessment of vaccine efficacy against SARS-CoV-2 and

novel variants is enhanced by the addition of diverse Fc functions to traditional Fab functions, particularly in vulnerable populations such as the elderly.

Section 8.3: Results

8.3.1 Study Subjects

To evaluate polyclonal antibody responses to mRNA COVID-19 vaccines, sera were collected from 51 adults who received two doses of the BNT162b2 vaccine between December 2020 and February 2021 (Table 8.1)[369]. These individuals spanned a spectrum of ages from 21 to 82 years. To limit confounding variables, samples were selected to minimize variations in time between vaccine doses 1 and 2 (20–22 days, variation of 2 days) and dose 2 to sample collection (14–15 days, variation of 1 day); sex distribution was balanced. To avoid the complicating factor of hybrid immunity due to SARS-CoV-2 infection, we excluded individuals with report of prior infection or active symptoms and performed confirmatory testing to verify the absence of detectable SARS-CoV-2 nucleocapsid specific antibodies (Figure S8.1A).

Table 8.1 Demographics and vaccination status

BNT162b2-vaccinated donors	
Characteristic	**total (n = 51)**
Median age (range), years	50 (21-82)
Sex	
Female (%)	28 (54.9)
Male (%)	23 (45.1)
Median time between vaccine doses (range), days	21 (20-22)
Median time between second dose and sample collection (range), days	14 (14-15)

8.3.2 Neutralizing antibody titers of wild type and SARS-CoV-2 variants

Using the SARS-CoV-2 receptor-binding domain (RBD) antigen encoded by BNT162b2[282], we found that 100% of individuals after two doses of the vaccine had detectable antigen-specific IgG compared with 51% with IgA (Figure S8.1A). Thus, consistent with other

studies, the primary isotype mediating antibody function 2 weeks after a second BNT162b2 dose was IgG[442,443]. To assess direct neutralization, we performed focus reduction neutralization tests using live wild-type SARS-CoV-2 (isolate WA1/2020) virus (Figure S8.1B). Consistent with the generation of RBD-specific IgG, all individuals had detectable capacity to neutralizing activity. Linear regression showed that neutralization was dependent on RBD-specific antibodies, specifically IgG and not IgA (Figure 8.1A).

Figure 8.1 BNT162b2-induced IgG mediates age-dependent neutralization of WT and SARS-CoV-2 clinical variants

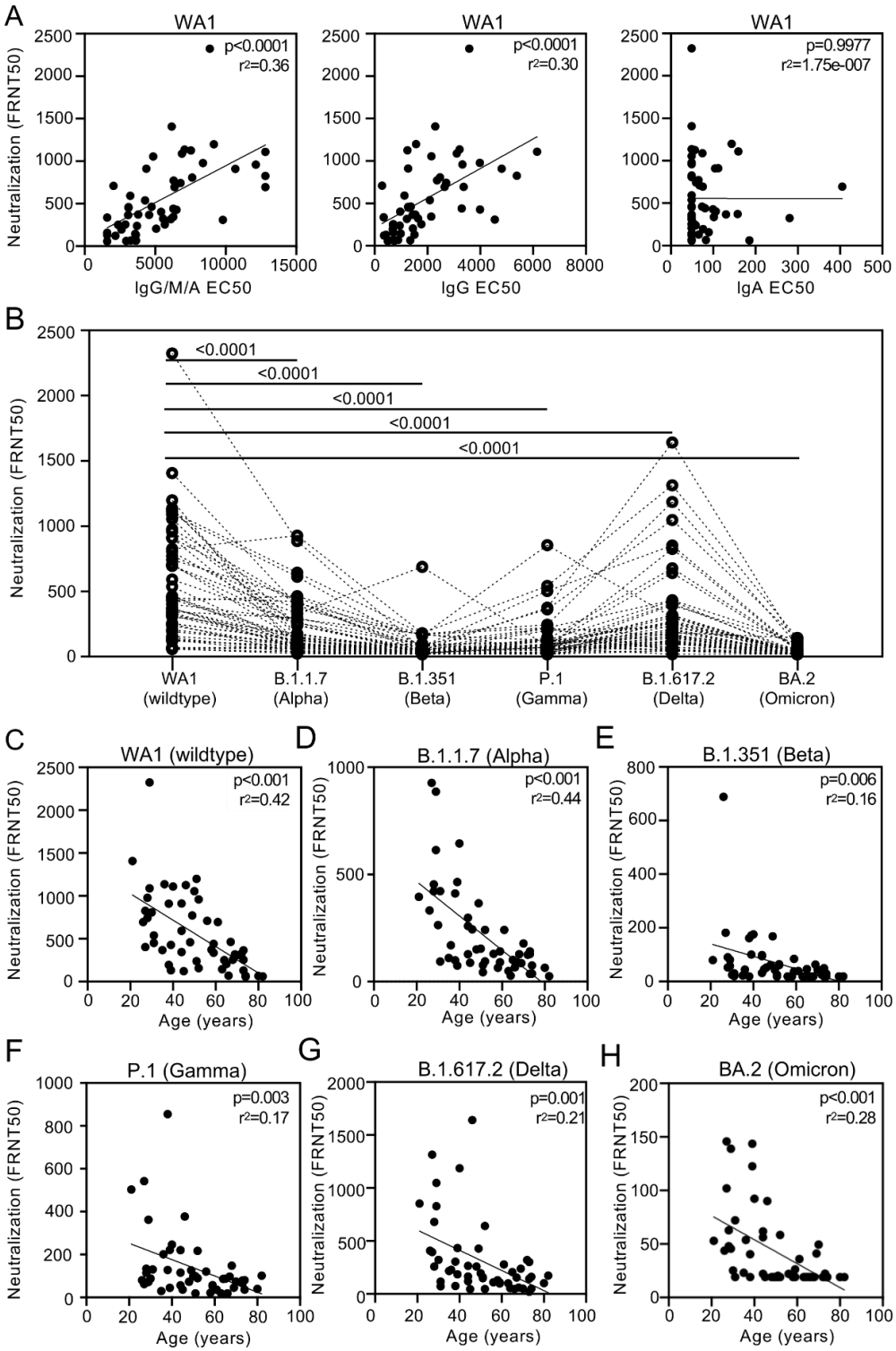

(**A**) Live SARS-CoV-2 neutralization (FRNT50) wild-type WA1 and receptor-binding domain (RBD)-specific IgG/M/A, IgG, and IgA EC50 values (Figure S8.1A) are plotted with relationship assessed by linear regression. (**B**) Neutralization of live SARS-CoV-2 wild-type WA1 and variants (Figure S8.1B) are depicted, with each dotted line representing a single individual and statistical significance calculated by Wilcoxon matched pair signed rank test. (**C–H**) Live SARS-CoV-2 neutralization (FRNT50) for (**C**) WT and variants (**D**) B.1.1.7 (Alpha) (n = 50), (**E**) B.1.351 (Beta) (n = 50), (**F**) P.1 (Gamma) (n = 50), (**G**) B.1.617.2 (Delta), and (**H**) BA.2 (Omicron) and age in years are plotted, with relationship assessed by linear regression and p values adjusted for sex. Data show the average of technical duplicates for n = 51 individuals' serum samples. See also Figure S8.1.

We next measured the neutralizing activity of vaccinee sera against SARS-CoV-2 clinical isolates of the viral variants Alpha (B.1.1.7), Beta (B.1.351), Gamma (P.1), Delta (B.1.617.2), and Omicron (BA.2)[53], (Figure S8.1B). We used live virus instead of pseudovirus to more effectively model physiological ratios and spectrum of SARS-CoV-2 antigens during infection and replication[230]. We found that neutralization of variants was diminished relative to wild type and varied by viral variant and individual (Figure 8.1B), with the lowest levels detected against Omicron (BA.2), consistent with other studies[53,444,445]. More specifically, while all individuals had detectable neutralization against wild type and Alpha (B.1.1.7), only 57% had detectable responses against Omicron (BA.2), which were lower on average than for other variants. While sex can impact immune responses[446], we observed no sex-based difference in neutralization (Figure S8.1C). However, we did detect a negative correlation between age and neutralization (Figure S8.1D). To incorporate both age and sex into our evaluations, we used multivariable regression to assess the relationships with neutralization. We found that neutralization of wild type and variants

was negatively correlated with age (Figure 8.1C–1H), but the correlation with sex remained non-significant. Upon review of the 43% of individuals with no detectable neutralizing activity against Omicron (BA.2), we observed that the median age of this subgroup was 63.5 years, above the median age of 50 for all individuals in this study. Consistent with other reports, these data showed that BNT162b2 induced RBD IgG neutralized SARS-CoV-2 wild-type virus and multiple variants in an age-, but not sex-, dependent manner[369,443,447].

8.3.3 Vaccine-specific Fc effector functions

Because IgG was the predominant vaccine-specific isotype, we focused on RBD-specific IgG effector functions to evaluate the relationship between viral neutralization via by the Fab domain and non-neutralizing Fc activity. We began by measuring RBD-specific antibody binding to the activating receptors FcγRIIIa/CD16a and FcγRIIa/CD32a and the sole inhibitory receptor FcγRIIb/CD32b because engagement of these low-affinity Fc receptors is modifiable by dynamic changes in subclass and post-translational glycosylation[416,448,449]. We found that RBD-specific IgG binding to FcγRIIIa/CD16a (Figure 8.2A), FcγRIIa/CD32a (Figure 8.2B), and FcγRIIb/CD32b (Figure 8.2C) positively correlated with SARS-CoV-2 neutralization in varying degrees.

Figure 8.2 Vaccine-specific IgG induction of FcγRIIIa/CD16a effector functions correlate with neutralization of WT and SARS-CoV-2 clinical variants

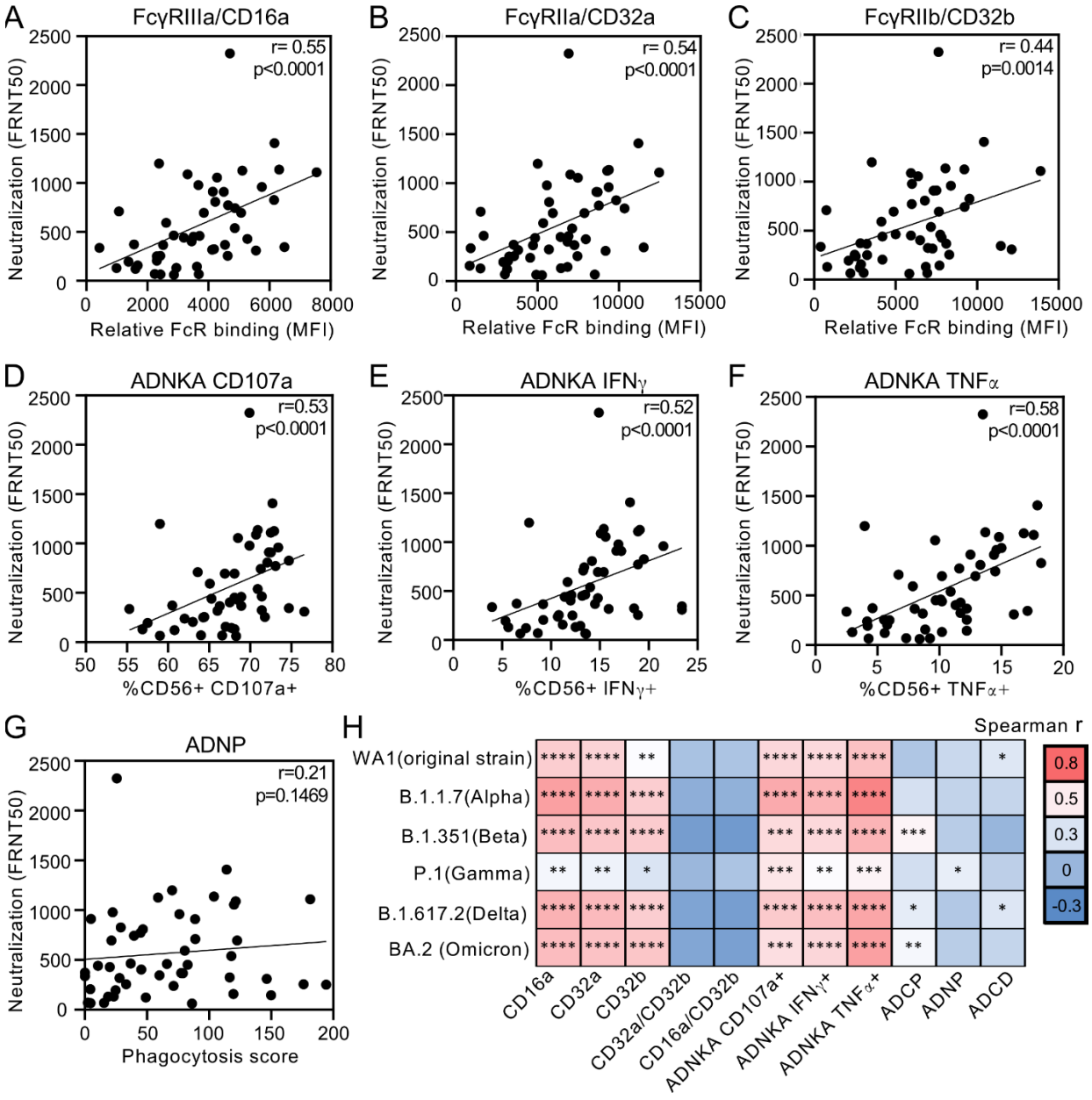

(**A–G**) Relationships between live SARS-CoV-2 WA1 neutralization (FRNT50) and RBD-specific relative binding to (**A**) FcγRIIIa/CD16a, (**B**) FcγRIIa/CD32a, and (**C**) FcγRIIb/CD32b, RBD-specific antibody-dependent natural killer cell activation (ADNKA) determined by (**D**) CD107a expression, (**E**) IFNγ production, (**F**) TNF-α secretion, and (**G**) RBD-specific antibody-

dependent neutrophil phagocytosis (ADNP) are shown. (**H**) Heatmap summarizes Spearman correlations (Figure S8.2) between neutralization of SARS-CoV-2 WT WA1 and variants with relative binding of RBD-specific IgG to activating (FcγRIIIa/CD16a and FcγRIIa/CD32a), inhibitory (FcγRIIb/CD32b), and ratios of activating:inhibitory FcγR (FcγRIIIa/CD16a:FcγRIIb/CD32b and FcγRIIa/CD32a:FcγRIIb/CD32b) binding and Fc effector functions ADNKA, antibody-dependent cellular phagocytosis (ADCP), ADNP, and antibody-dependent complement deposition (ADCD). $^{*}p \leq 0.05$; $^{**}p \leq 0.01$; $^{***}p \leq 0.001$; $^{****}p \leq 0.0001$. Depicted here are data representing one of three dilutions with the highest signal to noise ratio for n = 51 individuals' serum samples. See also Figure S8.2.

Because Fc domain engagement is only the first step in signaling and initiation of effector functions, we examined the downstream consequences of activation by measuring RBD ADNKA, which leads to ADCC[450], ADCP and ADCP, and antibody-dependent complement deposition (ADCD). We found that neutralization titers positively correlated with all three markers of ADNKA: CD107a degranulation and intracellular interferon gamma (IFNγ) and TNF-α production (Figure 8.2D–2F). This association was not observed with ADNP (Figure 8.2G) and ADCP (Figure S8.2A) and was less statistically significant with C3 deposition in ADCD (Figure S8.2A). Because the primary Fc receptor that induces ADNKA is FcγRIIIa/CD16a, these findings corroborated data with respect to binding (Figure 8.2A). In contrast, the combinatorial engagement of low- and high-affinity FcγRs and the FcαR on neutrophils in ADNP did not correlate with neutralization (Figure 8.2G). Along these lines, the ratio of activating FcγRIIa/CD32a and, to a lesser degree, FcγRIIIa/CD16a to the inhibitory FcγRIIb/CD32b involved in ADCP in THP-1 monocytes did not relate to neutralization (Figure S8.2A and S8.2H). The link between FcγRIIIa/CD16a NK cell activation and neutralization was sustained across variants, though fits again varied (Figure 8.2H

and S8.2B). These data together demonstrated that in contrast to FcγRIIa/CD32a and FcγRIIb/CD32b, vaccine-specific IgG induction of FcγRIIIa/CD16a functions associated with neutralization.

8.3.4 IgG glycosylation

As in many infectious and non-infectious processes, post-translational glycosylation of polyclonal IgG has been shown to mediate binding affinity to Fc receptors in SARS-CoV-2 infection[424–427]. A core biantennary structure on the conserved asparagine residue N297 on the Fc domain is modified by the addition and subtraction of galactose (G), sialic acid (S), fucose (F), and bisecting N-acetylglucosamine (GlcNAc) to generate glycoform diversity (Figure 8.3A)[451]. Monoclonal and polyclonal antibody studies have shown that changes in glycoform composition have the potential to impact binding and downstream effector functions (Figure S8.3A)[430–432,449,451]. To evaluate the impact of glycosylation on vaccine-induced antibodies, we measured the relative abundance of N-glycans on total non-antigen- and RBD-specific IgG (Figure S8.3B). For each individual, non-antigen- compared with RBD-specific IgG glycoforms were distinct (Figure 8.3A and 8.3B). Glycoforms (Figure S8.3C) containing fucose (Figure 8.3C), total sialic (Figure 8.3D) composed of di-sialic (Figure 8.3E) and mono-sialic (Figure 8.3F) acids, galactose (di-galactosylated in Figure 8.3G and agalactosylated and mono-galactosylated in Figure S8.3D), and bisecting GlcNAc (Figure S8.3E) were significantly different between total non-antigen- and RBD-specific IgG.

Figure 8.3 Differential fucose and sialic acid on vaccine-specific IgG link to FcγRIIIa/CD16a effector functions

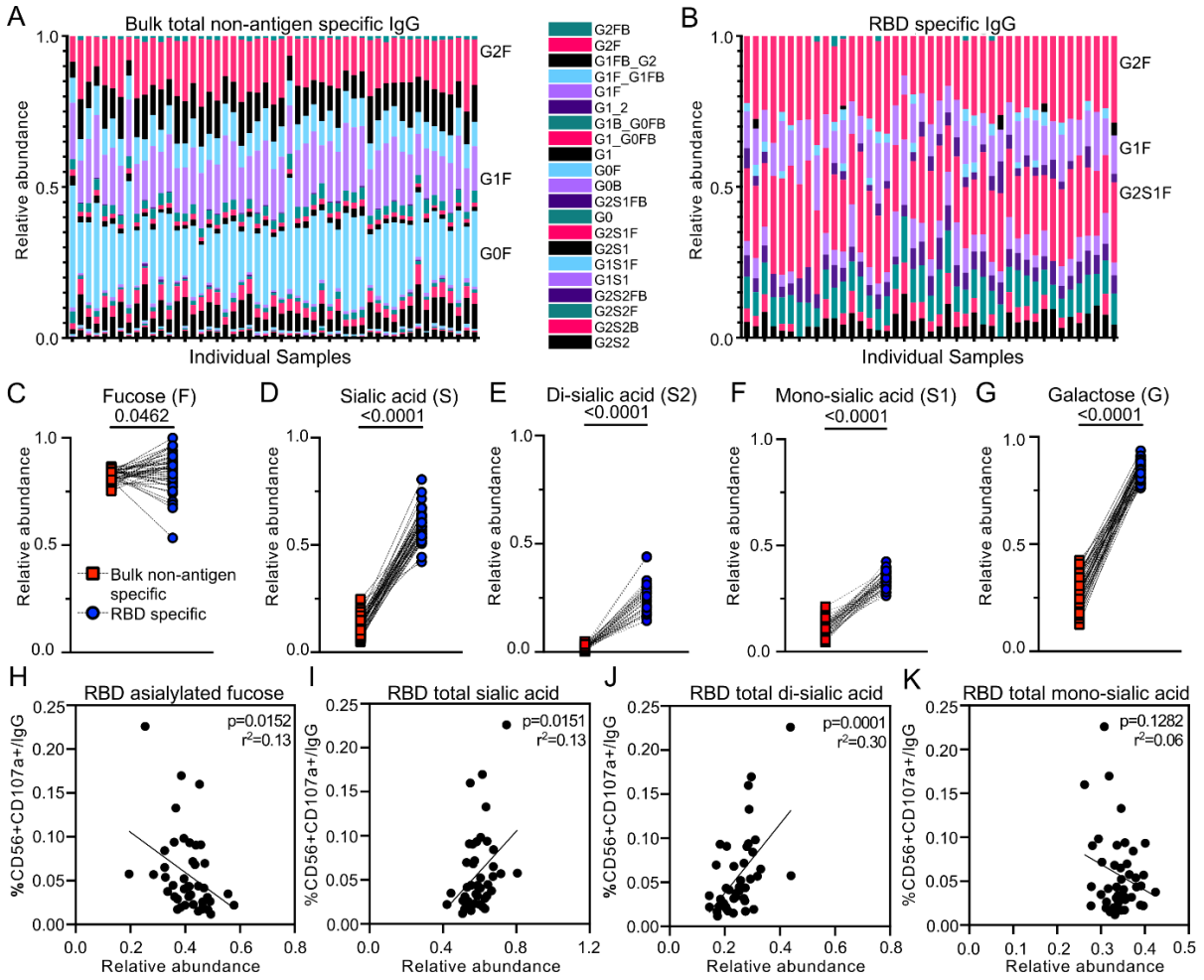

(**A** and **B**) Stacked column graphs depict the relative abundance of individual glycoforms (Figure S8.3A and S8.3B) with respect to (**A**) total bulk non-antigen-specific and (**B**) RBD-specific IgG. Each column represents one individual study participant. (**C**–**G**) Dot plots summarize differences between bulk non-antigen-specific and RBD-specific IgG in the collective relative abundance of all individual glycoforms (Figure S8.3C and S8.3D) containing (**C**) fucose, (**D**) total sialic acid, (**E**) di-sialic acid, (**F**) mono-sialic acid, and (**G**) di-galactose, with statistical significance calculated by Wilcoxon matched-pairs signed rank test. (**H**–**J**) Data

for (**H**) asialylated fucosylated, (**I**) total sialic acid, and (**J**) total di-sialic acid, the three RBD-specific glycoforms that have a statistically significant relationship across all markers of ADNKA are plotted with CD107a expression per RBD-specific IgG, as well as IFNγ and TNF-α (Figure S8.4). (**K**) For comparison, data for total mono-sialic acid are plotted. Depicted here are data representing one of three dilutions with the highest signal-to-noise ratio for n = 51 individuals' serum samples. See also Figures S8.3 and S8.4.

To evaluate if differential antibody glycosylation impacted effector functions associated with neutralization, we investigated which glycoforms lead to FcγRIIIa/CD16a-mediated NK cell activation by linear regression. We found that relative levels of RBD-, and not total non-antigen-, specific IgG glycoforms significantly correlated with CD107a degranulation and intracellular IFNγ and TNF-α production at varying levels (Figure S8.4A–D). Relative levels of IgG glycoforms that contained fucose without sialic acid (asialylated fucosylated) and glycoforms that contained sialic acid (specifically di-sialic and not mono-sialic acid) correlated with all three markers of NK cell activation (Figure 8.3H–K). The negative relationship between asialylated fucosylated species on RBD-specific IgG with ADNKA indicated an inhibitory effect of the presence of fucose. This contrasted with sialic acid, where the absence negatively (Figure 8.3H and S8.4E–H) and the presence positively (Figure 8.3I–J, S8.4F–G, and S8.4I–J) associated with ADNKA. Taken together, these data showed that fucose and sialic acid on vaccine-specific IgG influence FcγRIIIa/CD16a NK cell activation in opposing manners.

8.3.5 Impact of age on antibody Fc effector functions

We next investigated if Fc domain features were dependent on age as we had observed with Fab domain-mediated neutralization. We observed a negative relationship between RBD-specific IgG binding to FcγRIIIa/CD16a, FcγRIIa/CD32a, and FcγRIIb/CD32b with age (Figure

8.4A–C) by linear regression, taking sex into account (Figure 8.4D). In contrast, no statistically significant relationships between age and Fc receptor binding to antibodies targeting control antigens from the other pulmonary viruses respiratory syncytial virus (RSV) and influenza (flu) and the negative control *Bacillus anthracis* (anthrax) were seen (Figure 8.4D). Consistent with neutralization data, we observed that age negatively correlated with RBD-specific IgG-mediated NK cell CD107a degranulation (Figure 8.4E) and intracellular IFNγ and TNF-α production at varying levels (Figure 8.4F and S8.5). In comparison, the relationships between age and RBD-specific ADCP (Figure 8.4G) and ADNP (Figure 8.4H), as well as ADCD (Figure S8.5), were non-significant. Consistent with differential IgG glycosylation linked to NK cell activation (Figure 8.3), asialylated fuosylated glycoforms in RBD-, compared with non-antigen-, specific IgG were increased in those ≥65 years old (Figure 8.4I). These data showed that age negatively impacted some, but not all, Fc effector functions, as it did for neutralization, which is likely due to the combination of decreased antibody levels and reduced antibody quality in differential glycosylation and altered FcR engagement.

Figure 8.4 Age influences some, but not all, vaccine-specific antibody FcγR functions

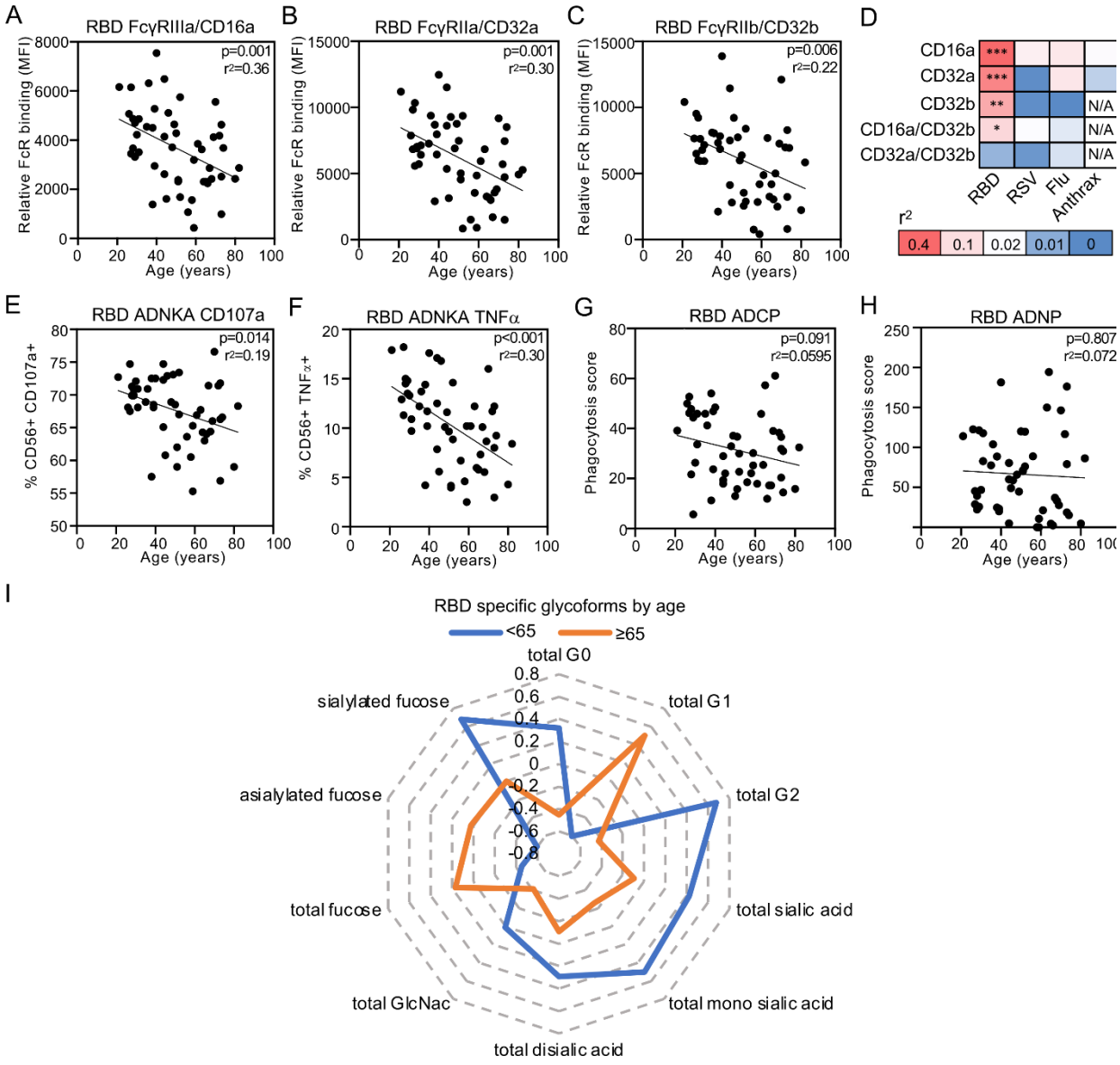

(**A–C**) The relationships between relative binding of RBD-specific IgG to (**A**) FcγRIIIa/CD16a, (**B**) FcγRIIa/CD32a, and (**C**) inhibitory FcγRIIb/CD32b and age are shown. (**D**) Heatmap of the coefficient of determination (r^2) summarizes the goodness of fit across RBD and control respiratory syncytial virus (RSV), influenza (flu), and anthrax antigens in FcγR binding and age. $^{*}p \leq 0.05$; $^{**}p \leq 0.01$; $^{***}p \leq 0.001$; N/A, not available given absence of significant detectable levels. (**E–H**) The relationship between age and RBD ADNKA as measured by (**E**) CD107a and

(**F**) TNF-α and (**G**) ADCP and (H) RBD ADNP are shown. Linear regression with p values adjusted for sex are reported. (I) Radar plots depict vaccine-specific IgG glycoforms calculated from the *Z* scored data for each individual RBD-specific IgG glycoform relative to bulk non-antigen-specific IgG glycoforms, with lines representing the median for each age group. Depicted here are data representing one of three dilutions with the highest signal-to-noise ratio for n = 51 individuals' serum samples. See also Figure S8.5.

8.3.6 Polyclonal functional breadth and magnitude

Polyclonal antibody responses consist of multiple Fab and Fc domain features that interact to influence disease outcomes. To begin to assess the collective functionality for each vaccinee sample, we calculated the breadth of neutralization across all five SARS-CoV-2 isolates tested (Figure S8.5A). In addition, we *Z* score-transformed data from Fc assays to enable comparisons between effector functions and summarization of the cumulative Fc functional magnitude for each individual (Figure S8.5B). To assess how Fc functionality related to Fab activity, we grouped individuals by their neutralization breadth. We found that neutralization of all variants (100%) was detectable in 28 of the 51 individuals, and those remaining demonstrated 50%–83% breadth (Figure 8.5A). Of those with <100% neutralization breadth, the cumulative Fc functional scores were low or negative. Of those with 100% neutralization breadth, both positive and negative cumulative Fc functional scores were detected. Thus, high neutralization breadth and potent Fc effector functions are linked. Moreover, Fc functionality represented a source of immune variation in the presence of broad Fab-mediated neutralization.

Figure 8.5 Enhanced BNT162b2 induced polyfunctional antibody breadth and magnitude against SARS-CoV-2 in younger, compared with older, adults

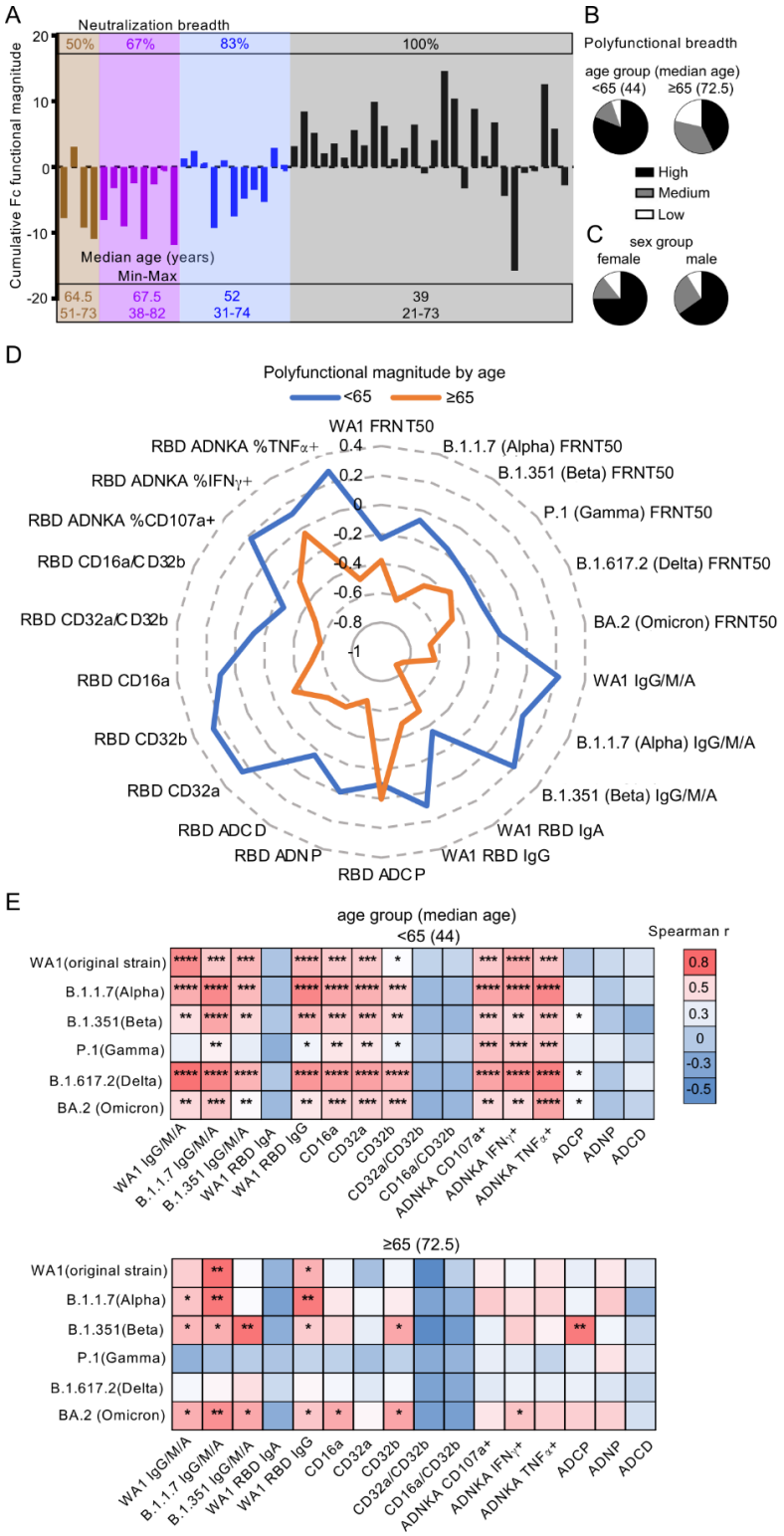

For each individual, the neutralization breadth across variants (Figure S8.6A) and cumulative vaccine-specific Fc functional magnitude from the sum of the *Z* scores for each of the individual effector functions (Figure S8.6B) were calculated. (**A**) Grouped by neutralization breadth (top), each column shows the cumulative Fc functional score for one individual. Median, minimum, and maximum ages characterizing each neutralization breadth group are shown (bottom). Polyfunctional antibody breadth was calculated for each individual (Figure S8.6C) and used to categorize individuals into high (90%–100%), medium (80%–90%), or low (<80%) responders. (**B** and **C**) The proportions of high, medium, and low responders are grouped by (**B**) age and (**C**) sex. (**D**) Radar plots depict vaccine-specific polyfunctional antibody magnitude calculated from the *Z* scored data for each antibody function (Figure S8.6C), with lines representing the median for each age group. (**E**) Heatmap summarizes Spearman correlations (Figure S8.2) between neutralization of SARS-CoV-2 WT WA1 and variants with RBD-specific IgG/M/A, IgG, and IgA levels, relative binding of RBD-specific IgG to activating (FcγRIIIa/CD16a and FcγRIIa/CD32a), inhibitory (FcγRIIb/CD32b), and ratios of activating:inhibitory FcγR (FcγRIIIa/CD16a:FcγRIIb/CD32b and FcγRIIa/CD32a:FcγRIIb/CD32b) binding, and Fc effector functions ADNKA, ADCP, ADNP, and ADCD for each age group. $^{*}p \leq 0.05$; $^{**}p \leq 0.01$; $^{***}p \leq 0.001$; $^{****}p \leq 0.0001$. Depicted here are data representing one of three dilutions with the highest signal-to-noise ratio for n = 51 individuals' serum samples. See also Figure S8.2 and S8.6.

Because we observed that both neutralizing (Figure 8.1) and non-neutralizing (Figure 8.4) antibody functions were dependent on age, we assessed age with respect to neutralization breadth. We found that the median age for those with 100% neutralization was younger (39 years) compared with those with <100% (64.5, 67.5, and 52 years for 50%, 67%, and 83% neutralization,

respectively) (Figure 8.5A). Thus, both antibody Fab- and Fc-mediated breadth and potency diminished with age.

To focus on age categorically, we grouped individuals into those <65 and ≥65. The cutoff of 65 years was chosen for three reasons: (1) 63.5 is the median age of the subgroup of individuals with no detectable neutralization against Omicron (BA.2), the variant with the lowest overall activities (Figure 8.1B), (2) the median ages of the two groups with the lowest neutralization breadths are 64.5 and 67.5 (Figure 8.5A), and (3) ≥65 is the definition of older adults used by the Center for Disease Control and Prevention with respect to COVID-19 vaccine administration guidelines[452]. We calculated the polyfunctional breadth for each vaccinee by enumerating the proportion of detectable SARS-CoV-2 neutralizing and non-neutralizing responses to categorize individuals as high, medium, and low responders (Figure S8.5C). We observed that most individuals <65 had high polyfunctional breadth while those ≥65 had low or medium (Figure 8.5B). This difference in breadth was not noted with groupings by sex (Figure 8.5C). In addition to antibody breadth, we evaluated polyfunctional magnitude using vaccine-specific neutralizing and non-neutralizing antibody *Z* score data. We found that the extent of all antibody functions, except for ADCP, was diminished in the ≥65, compared with the <65, group (Figure 8.5D). Because polyfunctional antibody responses are comprised of multiple activities that potentially occur concurrently to influence outcomes of infection, we assessed the coordination between antibody features and functions in these two age groups. We found more coordination in those <65 compared with those ≥65 (Figure 8.5E). Thus, the breadth, magnitude, and coordination of BNT162b2-induced neutralizing and non-neutralizing antibody polyfunctionality diverge with respect to the age of 65 years.

Section 8.4: Discussion

In this study, we show that two doses of the BNT162b2 mRNA vaccine elicited coordinated neutralizing and non-neutralizing antibody functions. The presence of vaccine-specific antibodies is critical, but neutralizing and non-neutralizing antibody functions are driven by quality as well as quantity. Thus, titers correlated with neutralizing activity (Figure 8.1A) and vaccine-induced neutralizing responses against live clinical isolates of SARS-CoV-2 and five distinct variants decreased with age (Figure 8.1B). Neutralization correlated with FcγRIIIa/CD16a activation of NK cells that leads to cellular cytotoxicity but not phagocytosis or complement deposition (Figure 8.2). Engagement with FcγRIIIa/CD16a was associated with post-translational vaccine-specific IgG afucosylation and sialylation (Figure 8.3H–K), which diverge with age (Figure 8.4I). Antibody functions were diminished among those aged ≥65: neutralization breadth across variants, overall Fc functional potency, and coordination between neutralizing and non-neutralizing antibody activities (Figures 8.5B, 8.5D, and 8.5E), demonstrating compromised vaccine-induced polyfunctionality. Neutralizing activity and antibody titers are measured in vaccine studies to gauge effectiveness at blocking infection. The findings from this study show that non-neutralizing antibody effector functions are immune correlates that could inform on the potential of vaccines to prevent disease, a target that is of growing importance with the continual emergence of new variants that subvert neutralization.

Non-neutralizing antibody functions are mediated by immune complexing and binding between the Fc domain and Fc receptors. Thus, even with reduced Fab domain avidity for mutated viral proteins such as spike, vaccine-induced non-neutralizing Fc functions could remain robust. Our data show that neutralizing activities across all variants are lower compared with wild-type virus (Figure 8.1B), suggesting that effectiveness in preventing infection is significantly

compromised. However, even with increased case numbers of infection due to variants, epidemiological data show relatively strong vaccine protection against disease and hospitalization[407–410,453]. Our data show that the correlation between titers and neutralizing activities was decreased across different variants and that the relationships with non-neutralizing functions, specifically ADNKA, partially overlapped (Figure 8.5E).

In line with these observations from human studies, data from animal models demonstrate that *in vitro* neutralization does not uniformly correlate with *in vivo* protection against disease[417]. Moreover, enhancement of non-neutralizing Fc effector functions delay viral spread synergistically with neutralizing activity in mice[454]. In humans, our results show that many non-neutralizing Fc effector functions are elicited by vaccination but ADNKA, which leads to cellular cytotoxicity, is specifically linked to neutralization across wild type and SARS-CoV-2 variants (Figure 8.2). Thus, along with inhibiting viral entry by neutralization, vaccine-specific antibodies via FcγRIIIa/CD16a-expressing NK cells, monocytes, and macrophages could target cytotoxicity against airway epithelial cells already infected with SARS-CoV-2 to prevent viral spread and disease.

In natural infection, FcγRIIIa/CD16a is associated with disease severity[424–428]. While our data here do not include individuals with severe COVID-19 disease, the nature of polyclonal antibodies generated during natural infection diverge from vaccination. First, the antigenic repertoire after natural infection likely contains non-RBD-specific antibody responses that are absent after vaccination. Second, antibody titers are likely diminished with exposure to lower amounts of antigen from mild and asymptomatic infection compared with severe disease and vaccination[455]. Thus, FcγRIIIa/CD16a activities from immunity generated after natural infection could confer different downstream consequences compared with vaccination.

Post-translational IgG glycosylation influences Fc receptor binding and activation. Along with afucosylation, which enhances FcγRIIIa/CD16a engagement that is also observed in severe COVID-19 disease, our data from whole vaccine-specific IgG show that sialic acid could also contribute (Figures 8.3H and 8.5). As such, sialylation on vaccine-specific IgG could further modify FcγRIIIa/CD16a activation. The study of IgG glycosylation has focused primarily on N297 of the Fc domain[421,424–427], not accounting for the 20% of polyclonal IgG modified on the Fab domain[456]. Our evaluation of whole IgG suggests that glycans from both Fab and Fc domains contribute to Fc effector functions by indirectly and directly affecting Fc receptor interactions[148,457,458]. Thus, how an Fc receptor is activated by differential antibody glycosylation could be critical in determining the outcomes of downstream immune responses.

The factors that predict vaccine response at an individual level are the subject of intense study. Several lines of evidence support that age is one important factor[369,421,443]. Our study was designed to look specifically at the contribution of age to non-neutralizing antibody activities from vaccination. In the elderly, compared with younger individuals, virus-specific memory B cells and antibody titers persist longer than neutralizing activity[459]. Thus, loss of neutralization with a shift toward more dependence on non-neutralizing antibody activity could be a hallmark of immunosenescence. As such, monitoring non-neutralizing, in addition to neutralizing, functions could help determine the need and dose of booster vaccinations for this population. Moreover, approaches using adjuvants to enhance vaccine-mediated non-neutralizing antibody functions such as FcγRIIIa/CD16a could be beneficial[460].

With respect to the broader population, analyses of longitudinal and cross-sectional studies involving vaccination and infection show that non-neutralizing functions including NK cell activity and ADCC are sustained longer than neutralization[461–463]. Modeling of neutralization

decay predicts that protection from infection is lost but protection from severe disease is retained[125]. This divergence between neutralizing titers and immune protection is likely due to multiple factors including viral fitness[338,464,465] and T cell activities[466], as well as non-neutralizing responses such as the FcγRIIIa/CD16a functions observed here. Thus, enhancing non-neutralizing activities elicited by vaccines could provide longer-lasting protection against disease independent of altering vaccine antigens to target each new variant.

Current CDC vaccine recommendations for healthy adults <50 involve three total doses and, for those ≥50, four doses. At the time of this writing, 91.8% of the US population ≥65 have received two doses, 70.4% three, and 39.1% four[467]. Outside the US, many parts of the world still have limited access to vaccine and have lower rates of vaccination. Our data support the assertion that for those elderly individuals with two doses of BNT162b2, immunity is suboptimal because neutralizing and non-neutralizing antibody activities are restricted. The effects of additional doses of vaccines using antigens from the original SARS-CoV-2 strain or Omicron and infection on top of vaccination that generates hybrid immunity remain to be fully defined but likely encompass enriched neutralization breadth and Fc potency[421,443,468]. How much protection is enhanced is a subject of active discourse[217,394]. Evaluating the breadth, magnitude, and coordination of polyclonal antibody functions (Figure 8.5) will enhance resolution of correlates of protection, particularly in the context of variants where the effect of neutralizing activity is likely limited. There is growing evidence that adjuvants and antigens can be used to skew immune responses, including antibody glycosylation and Fc effector functions, for rational vaccine design[469–472]. Approaches that leverage the collaboration between antibody Fab and Fc domain functions could improve vaccine efficacy against variants for all and specifically for vulnerable populations with difficulty generating neutralizing responses such as the elderly.

Section 8.5: Limitations of the Study

Limitations to this study include sample size, a lack of ethnicity, race, and clinical data, and the homogeneity of the population examined, with all participants being employees of a local healthcare system. These cohort characteristics limited the ability to resolve more subtle differences and extrapolate across a diverse array of individuals but also minimized potential sources of confounding variables, likely facilitating the discovery of relationships between antibody features that would otherwise be difficult to discern due to the complexity and heterogeneity of polyfunctional antibodies. The absence of infection was not determined by molecular microbiological diagnostics but rather serologically by the lack of detectable nucleocapsid (Figure S8.1A), RBD-specific antibodies prior to vaccination[369], and clinical history. As such, it is plausible that individuals with asymptomatic infections are included. However, the dominant immune responses measured were likely due to vaccination given the narrow window between the second vaccine dose and sample collection time (14–15 days). As the cohort was sex balanced, the major known phenotypic variation in this group was age (21–82 years).

Section 8.6: Methods

8.6.1 Cohort

Study participants (n = 51) were enrolled between December 2020 and February 2021 at Oregon Health & Science University immediately after receiving their first dose of BNT162b2 vaccine. Cohort age and sex distributions are described in Table 8.1. Participants received a second vaccine dose between 21 ± 1 day following the first dose, then returned 14-15 days later for follow up. Whole blood was collected in serum tubes (BD) and serum isolated by centrifugation 1000xg for 10min. Sera were heat inactivated at 65°C for 30min then frozen at −20°C. This study was conducted in accordance with the Oregon Health & Science University Institutional Review Board

with written informed consent from all participants, and approved by the UT Southwestern Medical Center Institutional Review Board. Written informed consent was received from all study participants prior to participation.

8.6.2 Cell lines

Vero E6 cells were purchased from ATCC (ATCC VERO C1008), grown at 37C, 5% CO2 and maintained in Dulbecco's Modified Eagle Medium supplemented with 10% fetal bovine serum, 1% penicillin/streptomycin, 1% non-essential amino acids. THP-1 cells were purchased from ATCC (ATCC TIB-202), grown at 37C, 5% CO2 and maintained in RPMI-1640 supplemented with 10% fetal bovine serum, 2mM L-glutamine, 10mM HEPES, and 0.05 mM β-mercaptoethanol. CD16.NK-92 were purchased from ATCC (ATCC PTA-6967), grown at 37C, 5% CO2 and maintained in in MEM-α supplemented with 12.5% FBS, 12.5% horse serum, 1.5g/L sodium bicarbonate, 0.02mM folic acid, 0.2mM inositol, 0.1 mM 2-β-mercaptoethanol, 100U/mL recombinant IL-2.

8.6.3 Primary immune cells

Fresh peripheral blood was collected at UT Southwestern from healthy volunteers. All were over 18 and de-identified prior to blood processing. Neutrophils isolated from peripheral blood were maintained at 37C, 5% CO2 in RPMI with 10% fetal bovine serum, L-glutamine, and HEPES. The study was approved by the UT Southwestern Medical Center Institutional Review Board. Written informed consent was received from all study participants prior to participation.

8.6.4 Virus

SARS-CoV-2 clinical isolates were passaged once before use in neutralization assays: USA-WA1/2020 [original strain] (BEI Resources NR-52281); USA/CA_CDC_5574/2020 [B.1.1.7] (BEI Resources NR-54011); hCoV-54 19/South Africa/KRISP-K005325/2020 [B.1.351]

(BEI Resources NR-54009); hCoV-19/Japan/TY7-503/2021 [P.1] (BEI Resources NR-54982); hCoV-19/USA/PHC658/2021 [B.1.617.2] (BEI Resources NR-55611); and hCoV-19/USA/CO-CDPHE-2102544747/2021 [B.1.1.529 - BA.2] (BEI Resources NR-56520). Isolates were propagated in Vero E6 cells for 24 to 72hrs until cultures displayed at least 20% cytopathic effect (CPE), as previously described.

8.6.5 Enzyme linked immunosorbent assays (ELISA)

ELISAs were performed as described[370]. Plates were coated overnight at 4°C with 1 mg/mL recombinant SARS-CoV-2 spike receptor binding domain (RBD) protein[348] (BEI Resources NR-52309) or recombinant SARS-CoV-2 nucleocapsid (N) protein (BEI Resources NR-53797). Serum dilutions (6 x 3-fold for RBD, 6 x 4-fold for N) in duplicate were prepared in 5% milk powder, 0.05% Tween 20, in phosphate buffered saline (PBS), starting at 1:1600 (pan-Ig), 1:50 (IgA), 1:200 (IgG). The secondary antibodies used were pan-Ig (1:10,000 anti-human GOXHU IgG/A/M-HRP, A18847 Invitrogen), IgA (1:3,000 anti-human IgA-HRP, 411,002 Biolegend), and IgG (1:3,000 anti-human IgG-HRP 555788, BD Biosciences). Plates were developed with o-phenylenediamine (OPD) (ThermoScientific). Absorbance at 492nm was measured on a CLARIOstar plate reader and normalized by subtracting the average of negative control wells and dividing by the highest concentration from a positive control dilution series. ELISA EC50 values were calculated by fitting normalized A492 as described[370]. The limit of detection (LOD) was defined by the lowest dilution tested for RBD and half of the lowest dilution for N. Values below the LOD were set to LOD – 1.

8.6.6 Focus reduction neutralization test (FRNT)

Focus forming assays were performed as described[370]. Sub-confluent Vero E6 cells were incubated for 1 h with 30 µL of diluted sera (5 x 4-fold starting at 1:20) which was pre-incubated

for 1 h with 100 infectious viral particles per well. Samples were tested in duplicate. Wells were covered with 150 µL of overlay media containing 1% methylcellulose and incubated for 24hrs, 48hrs for Omicron. Plates were fixed by soaking in 4% formaldehyde in PBS for 1 h at room temperature. After permeabilization with 0.1% BSA, 0.1% saponin in PBS, plates were incubated overnight at 4°C with primary antibody (1:5,000 anti-SARS-CoV-2 alpaca serum, 1:2,000 for Omicron) (Capralogics Inc)[370]. Plates were then washed and incubated for 2hrs at room temperature with secondary antibody (1:20,000 anti-alpaca-HRP, 1:5,000 for Omicron) (NB7242 Novus) and developed with TrueBlue (SeraCare) for 30min. Foci were imaged with a CTL Immunospot Analyzer, enumerated using the viridot package[382] and percent neutralization calculated relative to the average of virus-only wells for each plate. FRNT50 values were determined by fitting percent neutralization to a 3-parameter logistic model as described previously[370]. The limit of detection (LOD) was defined by the lowest dilution tested, values below the LOD were set to LOD – 1. Duplicate FRNT50 values were first calculated separately to confirm values were within 4-fold. When true, a final FRNT50 was calculated by fitting to combined replicates.

8.6.7 Fc receptor binding assays

Fc receptor binding assays were performed as described with modifications[473]. Carboxylated microspheres (Luminex) were coupled with recombinant SARS-CoV-2 RBD[348] (BEI Resources NR-52309) by covalent NHS-ester linkages via EDC (1-Ethyl-3-[3-dimethylaminopropyl]carbodiimide hydrochloride, Thermo Scientific Pierce) and Sulfo-NHS (N-hydroxysulfosuccinimide) (Thermo Scientific) per the manufacturer's instructions. A mixture of influenza antigens from strain H1N1 (NR-20083 and NR-51702, BEI Resources), H5N1 (NR-12148, BEI Resources), H3N2, B Yamagata lineage, and B Victoria lineage (NR-51702, BEI

Resources) was used as a control. A mixture of recombinant *Bacillus anthracis* antigens (Anthrax Protective Antigen, NR-36208 BEI Resources; Anthrax Lethal Factor, NR-28544 BEI Resources; Anthrax Edema Factor, NR-36210 BEI Resources) and a separate mixture of recombinant Respiratory Syncytial Virus antigens (G protein from strain B1, NR-31098 BEI Resources; F protein from strain B1, NR-31097 BEI Resources; G protein from strain A2, NR-31096 BEI Resources) were also used as controls. Antigen-coupled microspheres (1250 beads per well) were incubated with serially diluted sera (1:100, 1:1000, 1:10,000) in 96-well Bioplex Pro Flat Bottom plates (Bio-Rad) at 4°C for 16hrs. Recombinant Fc receptors (FcγRIIIa/CD16a, FcγRIIa/CD32a, FcγRIIb/CD32b, R&D Systems) were fluorescently labeled with PE (Abcam) before addition to bead bound antigen specific immune complexes. After 2hrs of incubation at room temperature, the beads were washed with PBS with 0.05% Tween 20 and antigen specific antibody bound Fc receptor measured on a on a MAGPIX instrument containing xPONENT4.2 software (Luminex). The background signal, defined as MFI of microspheres incubated with PBS, was subtracted. Representative data from one dilution was chosen by the highest signal to noise ratio for further analyses.

8.6.8 Non-antigen and RBD-specific IgG glycosylation

Non-antigen and RBD specific IgG glycans were purified and relative levels quantified as described with modifications[474,475]. Recombinant RBD protein (BEI Resources NR-52309)[348] was biotinylated with sulfosuccinimidyl-6-[biotinamido]-6-hexanamido hexanoate (sulfo-NHS-LC-LC biotin; ThermoScientific) and coupled to streptavidin beads (New England Biolabs). Patient sera were incubated with RBD-coupled beads and excess sera washed with PBS (Sigma). Bead-bound RBD-specific antibodies then eluted using 100mM citric acid (pH 3.0) and neutralized with 0.5M potassium phosphate (pH 9.0). Non-antigen specific or RBD-specific IgG were purified from

the serum or eluted RBD-specific antibodies respectively by protein G beads (Millipore). Purified IgG was denatured and treated with PNGase enzyme (New England Biolabs) for 12hrs at 37°C to release glycans.

To isolate bulk IgG glycans, proteins were removed by precipitation using ice-cold 100% ethanol at −20°C for 10min. To isolated RBD-specific IgG glycans, Agencourt CleanSEQ beads (Beckman Coulter) were used to bind glycans in 87.5% acetonitrile (Fisher Scientific). The supernatant was removed, glycans eluted from beads with HPLC grade water (Fisher Scientific) and dried by centrifugal force and vacuum (CentriVap). Glycans were fluorescently labeled with a 1.5:1 ratio of 50mM APTS (8-aminoinopyrene-1,3,6-trisulfonic acid, ThermoFisher) in 1.2M citric acid and 1M sodium cyanoborohydride in tetrahydrofuran (Fisher Scientific) at 55°C for 3hrs. The labeled glycans were dissolved in HPLC grade water (Fisher Scientific) and excess unbound APTS was removed using Agencourt CleanSEQ beads and Bio-Gel P-2 (Bio-rad) size exclusion resin. Glycan samples were run with a LIZ 600 DNA ladder in Hi-Di formamide (ThermoFisher) on an ABI 3500xL DNA sequencer and analyzed with GlycanAssure Data Acquisition Software v.1.0. Each glycoform was separated by peaks and identified based on glycan standard libraries (GKSP-520, Agilent). The relative abundance of each glycan for each individual sample was determined as (area under curve of each glycan)/(sum of area under curve of all individual glycans).

8.6.9 Antibody dependent cellular phagocytosis (ADCP)

The THP-1 (TIB-202, ATCC) phagocytosis assay of antigen-coated beads was conducted as described with modifications[476]. SARS-CoV-2 RBD recombinant protein (BEI Resources NR-52309)[348] was biotinylated with Sulfo-NHS-LC Biotin (Thermo Fisher), then incubated with 1 μm fluorescent neutravidin beads (Invitrogen) at 4°C for 16hrs. Excess antigen was washed away and

RBD-coupled neutravidin beads were resuspended in PBS-0.1% bovine serum albumin (BSA). RBD-coupled beads were incubated with serial dilutions of sera (1:100, 1:500 and 1:2500) for 2hrs at 37°C. THP1 cells (1×10^5 per well) were then added. Plasma opsonized RBD-coupled beads and THP1 cells were incubated at 37°C for 16hrs. Cells were then washed once and fixed with 4% PFA. Bead uptake was measured on a BD LSRFortessa (SCC) equipped with high-throughput sampler and analyzed by FlowJo10. Phagocytic scores were calculated as the integrated median fluorescence intensity (MFI) (% bead-positive frequency × MFI/10,000)[477]. Representative data from one dilution was chosen by the highest signal to noise ratio for further analyses.

8.6.10 Antibody dependent neutrophil phagocytosis (ADNP)

The neutrophil phagocytosis assay of antigen-coated beads was conducted as described with modifications[476]. Whole healthy donor blood was mixed with equal volume 3% dextran-500 (Thermo Fisher) and incubated for 25 min at room temperature to lyse and pellet the red blood cells. Leukocytes were removed and washed in endotoxin-free sterile water (Cytiva), followed by 1.8% NaCl (Thermo scientific) and then Hanks' balanced salt solution without calcium and magnesium (Thermo Fisher). RBD conjugated beads, as described above, were incubated with serial dilution of sera (1:100, 1:500 and 1:2500) in duplicate for 2hrs at 37°C. Isolated neutrophils (1×10^5 per well) were added and incubated for 2hrs at 37°C. Bead uptake was measured on a BD LSRFortessa (SCC) equipped with high-throughput sampler and analyzed by FlowJo10. Phagocytic scores were calculated as the integrated median fluorescence intensity (MFI) (% bead-positive frequency × MFI/1,000). The purity of neutrophils was confirmed by staining with CD66b (BioLegend). Sera samples were tested in two independent experiments with neutrophils from two different HIV negative healthy donors. The mean of the data from both donors was used for further

analysis. Representative data from one dilution was chosen by the highest signal to noise ratio for further analyses.

8.6.11 Antibody dependent complement deposition (ADCD)

The ADCD assay was performed as described with modifications[478]. Carboxylated microspheres (Luminex) were coupled with SARS-CoV-2 RBD protein[348] (NR-52309 BEI Resources) by covalent NHS-ester linkages via EDC (1-Ethyl-3-[3-dimethylaminopropyl]carbodiimide hydrochloride, Thermo Scientific Pierce) and Sulfo-NHS (N-hydroxysulfosuccinimide, Thermo Scientific) per manufacturer instructions. A mixture of influenza antigens from strains H1N1 (NR-20083 and NR-51702, BEI Resources), H5N1 (NR-12148, BEI Resources), H3N2, B Yamagata lineage, and B Victoria lineage (NR-51702, BEI Resources) was used as a control. Serum samples were heated at 56°C for 30min. Antigen-coated microspheres (1250 per well) were added to a 96-well Bioplex Pro Flat Bottom plates (Bio-Rad) and incubated with serial dilutions of sera (1:10, 1:50 and 1:250) at 4°C for 16hrs. Freshly resuspended lyophilized guinea pig complement (Cedarlane) diluted 1:60 was added to the plate for 20min at 37°C. After washing off excess complement three times with15mM EDTA, anti-C3 PE-conjugated goat polyclonal IgG (MP Biomedicals) was added. The beads were then washed and C3 deposition quantified on a MAGPIX instrument containing xPONENT4.2 software (Luminex). The background signal, defined as MFI of microspheres incubated with PBS, was subtracted. Representative data from one dilution was chosen by the highest signal to noise ratio for further analyses.

8.6.12 Antibody dependent NK cell activation (ADNKA)

ADNKA assay was performed as described with modifications[479]. ELISA plates were coated with recombinant RBD antigen (300 ng/well)[348] (BEI Resources NR-52309). Wells were

washed, blocked, and incubated with serial dilutions of sera (1:10, 1:30, 1:90) for 2hrs at 37°C prior to adding CD16a.NK-92 cells (PTA-6967, ATCC) (5×10^4 cells/well) for 5hrs with brefeldin A (Biolegend), Golgi Stop (BD Biosciences) and anti-CD107a (clone H4A3, BD Biosciences). Cells were stained with anti-CD56 (clone 5.1H11, BD Biosciences) and anti-CD16 (clone 3G8, BD Biosciences) and fixed with 4% PFA. Intracellular cytokine staining to detect IFNγ (clone B27, BD Biosciences) and TNFα (clone Mab11, BD Biosciences) was performed in permeabilization buffer (Biolegend). Markers were measured using a BD LSRFortessa and analyzed by FlowJo10. CD16 expression was confirmed in all cells. NK cell degranulation and activation were calculated as percent of CD56+NK cells positive for CD107a, or IFNγ or TNFα expression. Representative data from one dilution was chosen by the highest signal to noise ratio for further analyses.

8.6.13 Quantification and statistical analysis

Statistical analysis and graphing were performed using Stata17 and GraphPad Prism9.0. Data are summarized using the descriptive measures median, minimum, maximum and percent (%). Wilcoxon matched pair signed rank tests were used to compare neutralization of live SARS-CoV-2 variants (Figure 8.1B) and glycoforms between antigen non-specific and RBD specific IgG (Figure 8.3C–F, S8.3D, and S8.3E). Mann-U-Whitney tests were used to compare the neutralization of live SARS-CoV-2 variants between male and female (Figure S8.1C). Spearman rank correlations were used to examine bivariate associations between variables (Figure 8.2 and 8.5E, S8.1D and S8.2). Simple linear regression was used to examine the relationship between IgG glycoforms as the independent and Fc functional profiles as the dependent variables (Figure 8.3H–K and S8.4). Multiple robust regression models were used to adjust for the effect of age and sex when comparing the study variables between individuals (Figure 8.1A, 8.1C–H, 8.4, and S8.5). Z

scores of each individual Fc feature was calculated and then summed to generate the cumulative Fc functional magnitude (Figure 8.5A and S8.6B). For the radar plots (Figure 8.4I), Z scores of each individual RBD specific IgG glycoforms relative to bulk non-antigen specific IgG glycoforms were calculated and the median values for each age group were plotted. For the radar plots (Figure 8.5D), Z scores of each feature for each individual were calculated and the median values for each group were plotted. All p values are two-sided, and $p < 0.05$ was considered significant. In figures, asterisks denote statistical significance ($*p \leq 0.05$; $**p \leq 0.01$; $***p \leq 0.001$; $***p \leq 0.0001$) with comparisons specified by connecting lines.

Section 8.7: Supplemental Figures

Figure S8.1 BNT162b2 vaccination induces IgG mediated neutralization of SARS-CoV-2 wildtype (WT) and clinical variants that diminish with age but are not altered by sex

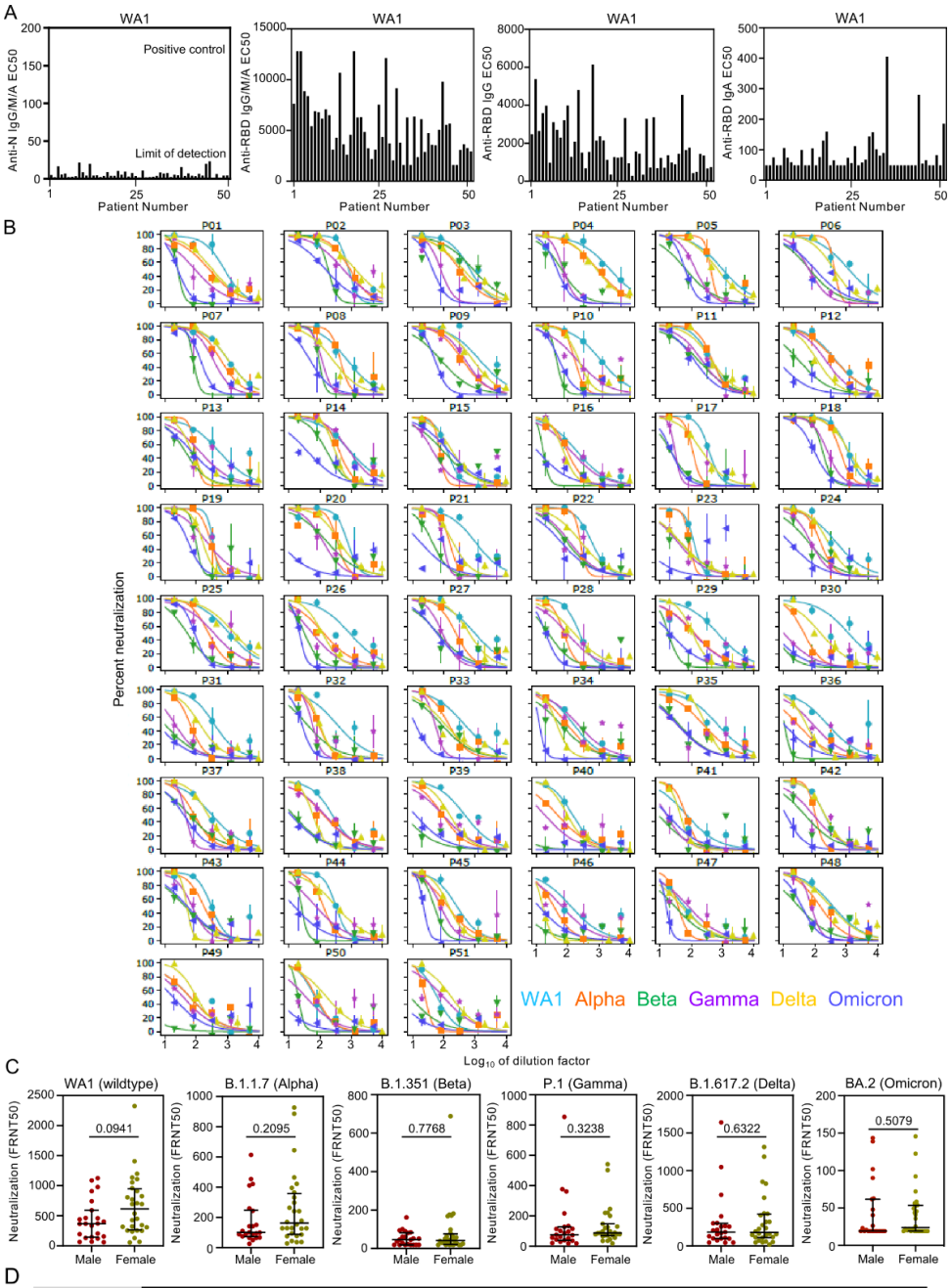

D

	WA1 (wildtype) FRNT50	B.1.1.7 (Alpha) FRNT50	B.1.351 (Beta) FRNT50	P.1 (Gamma) FRNT50	B.1.617.2 (Delta) FRNT50	BA.2 (Omicron) FRNT50
Spearman r	-0.6411	-0.6858	-0.5416	-0.4234	-0.5227	-0.6119
p	<0.0001	<0.0001	<0.0001	0.0022	<0.0001	<0.0001

(**A**) EC50 values are depicted for each individual for Nucleocapsid (N) specific antibodies, receptor binding domain (RBD) specific antibodies, IgG and IgA. Each column represents one individual. (**B**) Neutralization graphs from focus forming assays to calculate FRNT50 for each SARS-CoV-2 WT and clinical variants are shown. Each graph shows the data for one individual. (**C**) Dot plots show the distribution of neutralization for SARS-CoV-2 WT and variants by sex with statistical significance calculated by Mann-U-Whitney. (**D**) Spearman correlation coefficients and statistical significance between age and neutralization for SARS-CoV-2 WT and clinical variants are shown. Related to Figure 8.1.

Figure S8.2 Vaccine specific IgG induction of FcγRIIIa/CD16 effector functions correlate with neutralization of SARS-CoV-2 variants

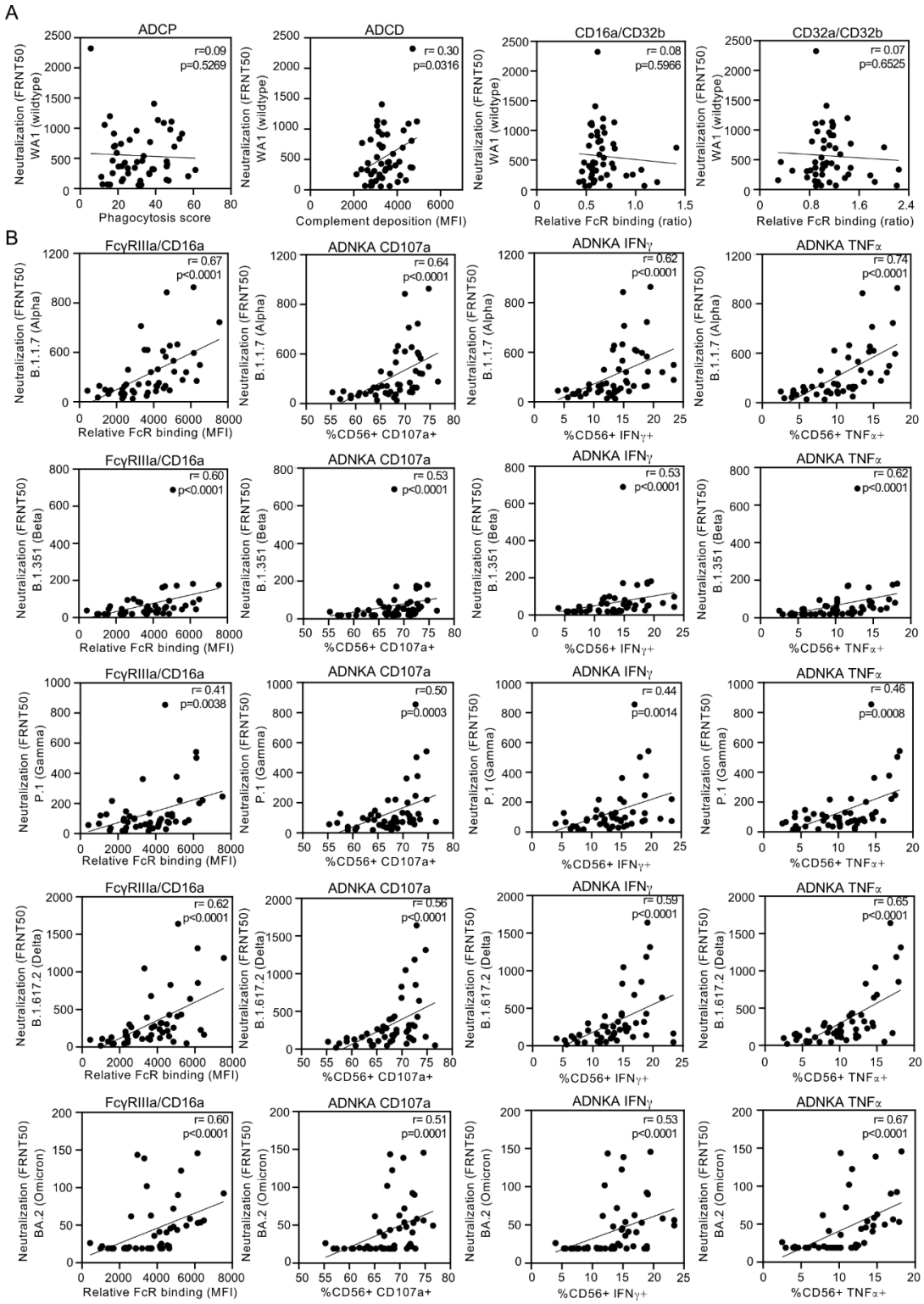

(**A**) The relationships between live SARS-CoV-2 WA1 wildtype neutralization and RBD specific antibody dependent cellular phagocytosis (ADCP), and RBD specific antibody dependent complement deposition (ADCD), and receptor binding domain (RBD) specific relative binding ratios of activating:inhibitory FcγR FcγRIIIa/CD16a:FcγRIIb/CD32b, FcγRIIa/CD32a:FcγRIIb/CD32b are shown. (**B**) The relationships between live SARS-CoV-2 variants neutralization and RBD specific FcγRIIIa/CD16a binding and effector function antibody dependent natural killer cell activation (ADNKA) are depicted. Statistical significances were determined by Spearman correlation. Related to Figure 8.2.

Figure S8.3 Bulk total non-antigen and vaccine specific IgG glycosylation patterns diverge

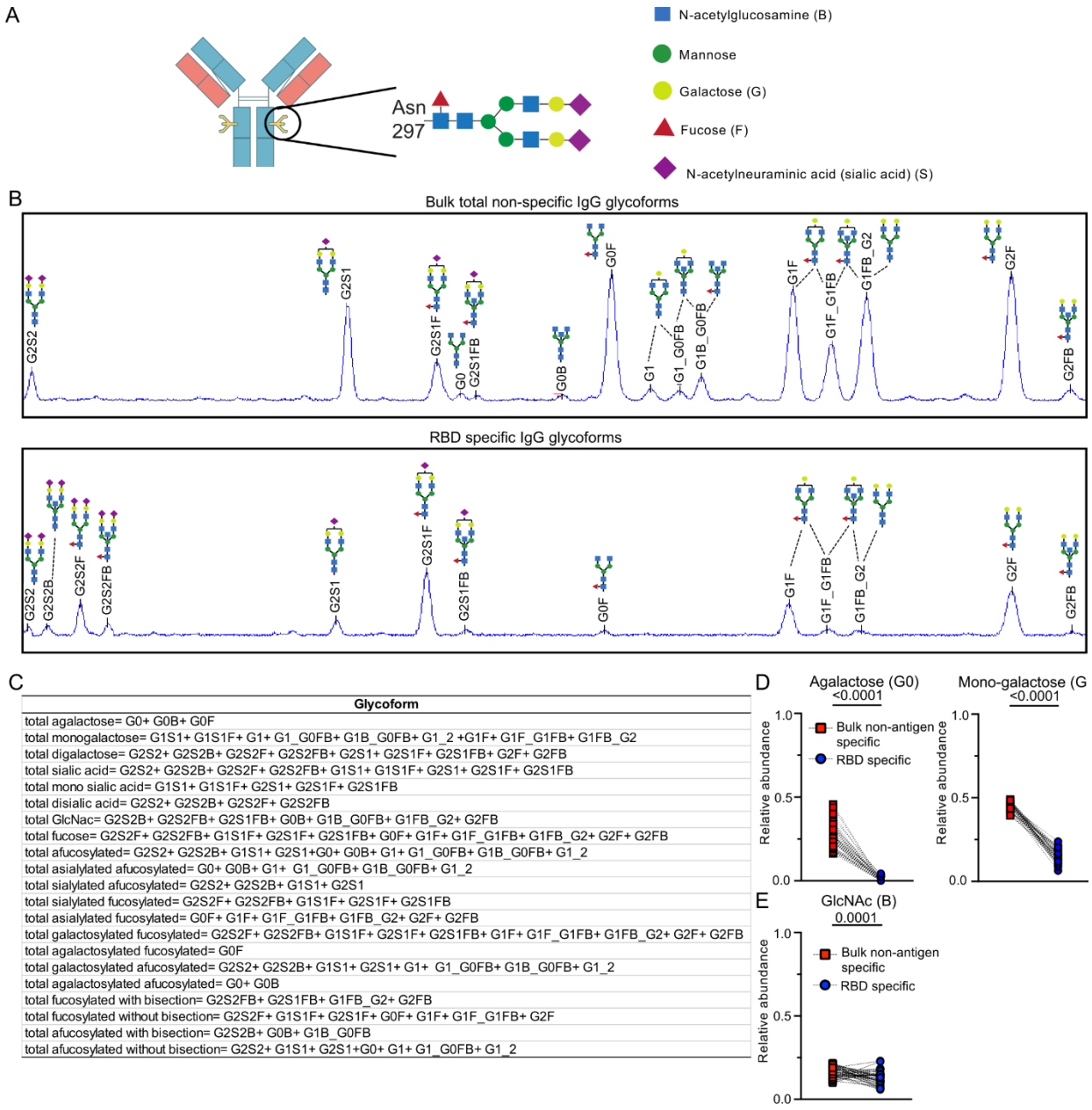

(**A**) Human IgG1 contains a conserved Fc domain N297 residue on which a bi-antennary structure of N-acetylglucosamine (GlcNAc) and mannose resides. The subsequent addition and subtraction of galactose (G), fucose (F), N-acetylneuraminic acid (sialic acid) (S) and bisecting GlcNAc (B) contributes to post translational diversity that develops with antibody maturation through the Golgi and ER. (**B**) Capillary electrophoresis chromatographs for bulk total non-

antigen and receptor binding domain (RBD) specific IgG glycans captured from one individual are shown. Quantification of each peak determines the relative abundance of each glycoform depicted. (**C**) The collective relative abundance of all individual glycoforms with fucose (F), sialic acid (S), galactose (G) and bisecting GlcNAc (B) are calculated for bulk total non-antigen and RBD specific IgG. Differences between bulk total non-antigen and RBD specific (**D**) agalactosylated and mono-galactosylated and (**E**) bisecting GlcNAc structures are shown. Statistical significances were calculated by Wilcoxon matched-pairs signed rank test. Related to Figure 8.3.

Figure S8.4 Differential fucose and sialic acid on vaccine specific IgG link FcγRIIIa/CD16a mediated IFNg and TNFa production.

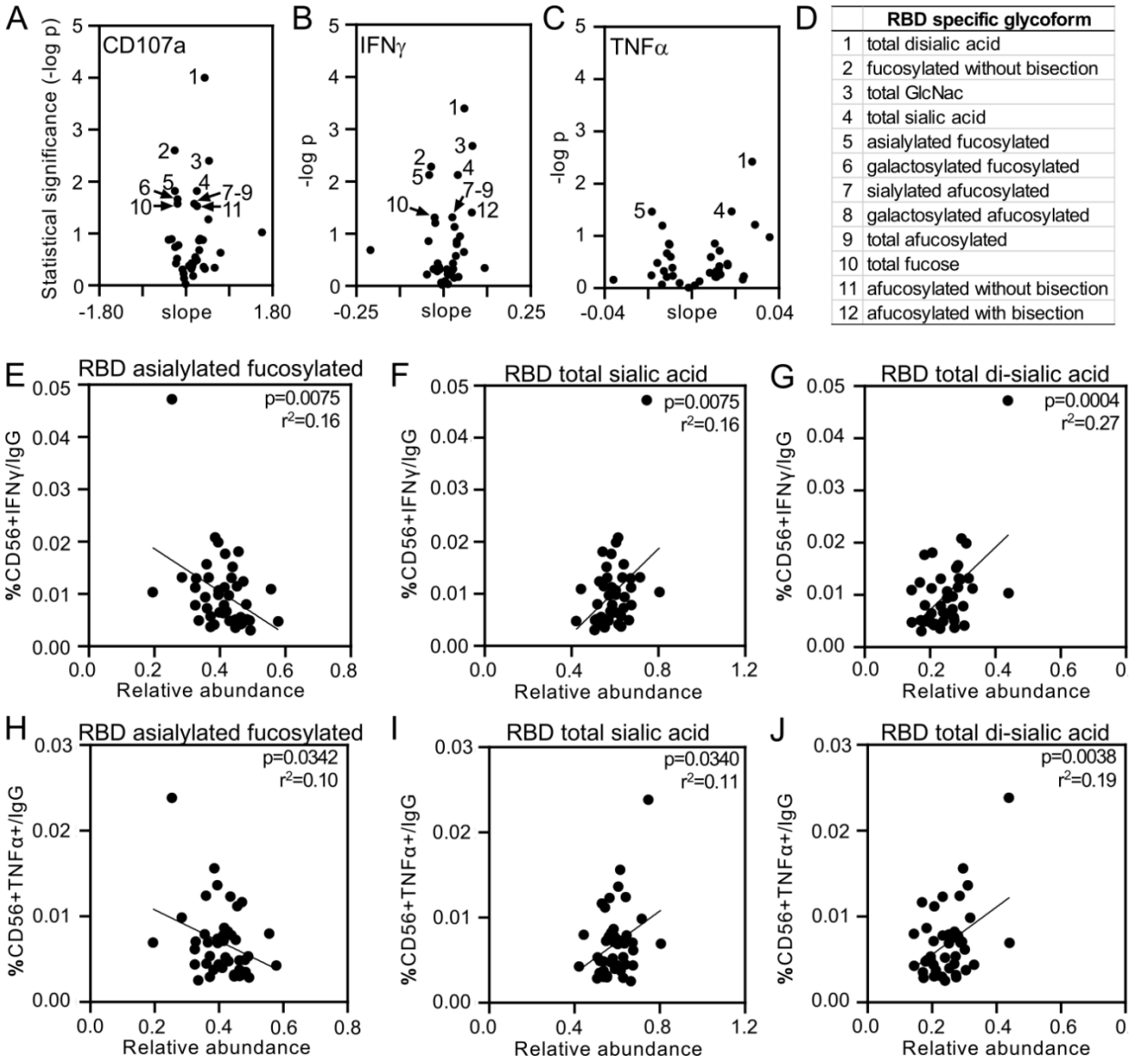

Volcano plots depict slope and statistical significance (-log p) from linear regression assessing the dependency of receptor binding domain (RBD) ADNKA by (**A**) % CD56 CD107a, (**B**) IFNγ and (**C**) TNFα on different RBD specific IgG glycans. (**D**) Relationships where $p<0.05$ are enumerated and identified. Data for antibody dependent natural killer cell activation (ADNKA) markers of IFNγ (middle row) and TNFα (bottom row) per RBD IgG and relative abundance of

RBD specific (**E** and **H**) asialylated fucosylated, (**F** and **I**) total sialic and (**G** and **J**) total di-sialic acid are plotted. Statistical significances were evaluated by linear regression. Related to Figure 8.3.

Figure S8.5 Minimal relationship between age and vaccine specific antibody dependent complement deposition (ADCD)

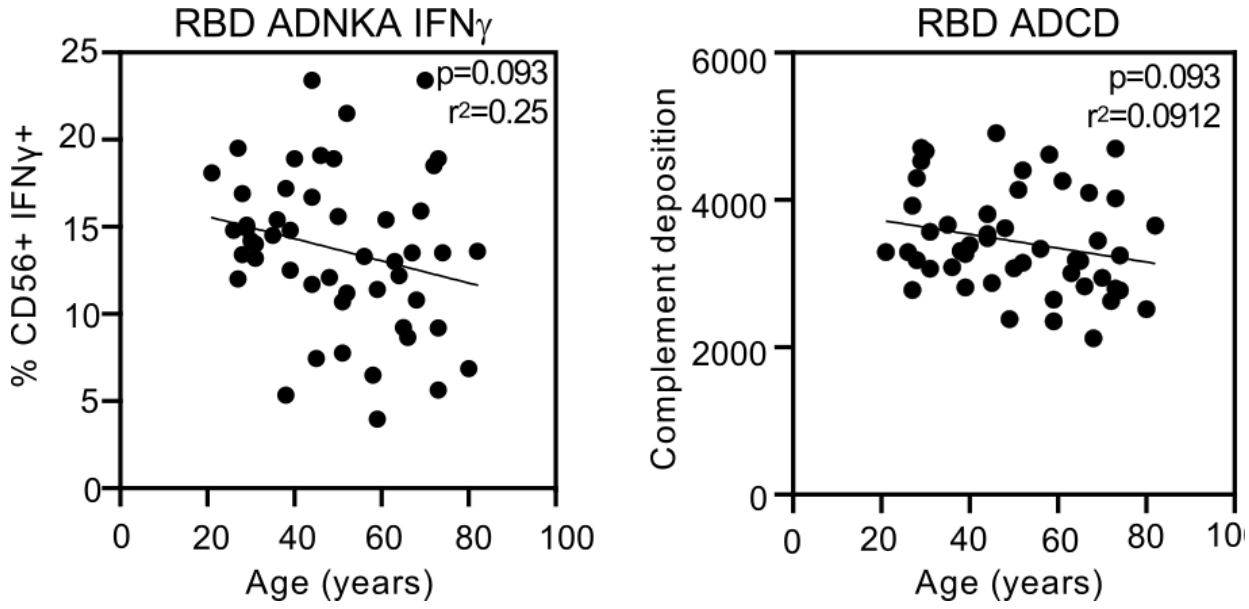

Receptor binding domain (RBD) specific C3 deposition and age are plotted (right panel). The relationship between age and RBD antibody dependent natural killer cell activation (ADNKA) as measured by IFNγ are shown (left panel). Linear regression with p value adjusted for sex is reported. Related to Figure 8.4.

Figure S8.6 Antibodies function by the combination of Fab and Fc domains

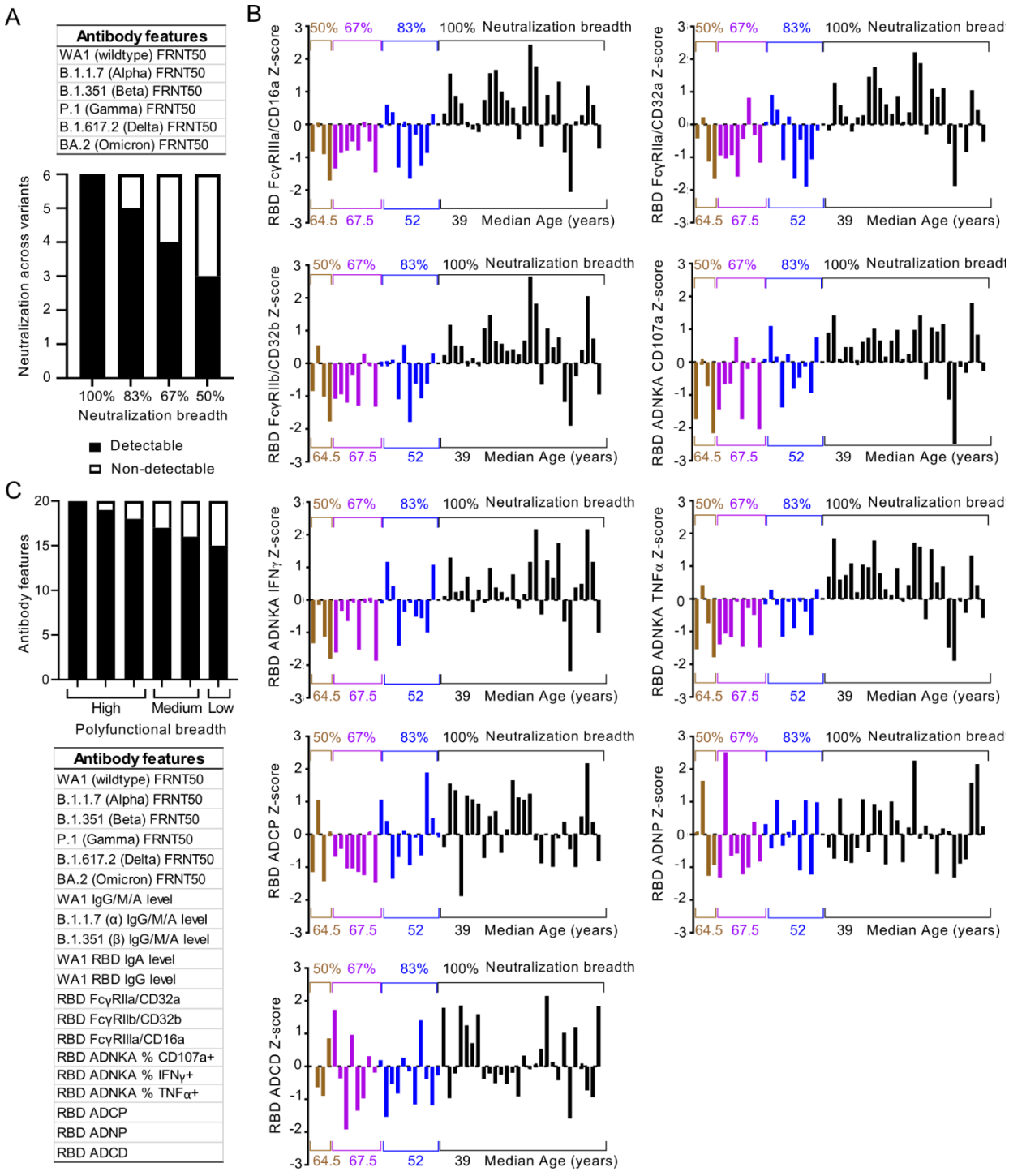

(**A**) Neutralization breadth across all 6 SARS-CoV-2 wildtype and clinical variants was calculated for each individual. In this cohort, individual responses fell into four main categories:

those with detectable neutralizing activity for 100% of viruses tested, 83%, 67% and 50%. (**B**) Histograms depict the Z scored data for each vaccine specific Fc effector function tested. Each column represents one individual. Groupings are by neutralization breadth categories described in (**A**). (**C**) Vaccine specific polyfunctional breadth was calculated for each individual with all 20 vaccine specific features listed. In this cohort, individual responses fell into three main categories: those with high (90-100%), medium (80-90%) and low (<80%) of functions detected. Related to Figure 8.5.

Section 8.8: Acknowledgments

8.8.1 Acknowledgments

This study was funded by a grant from the M. J. Murdock Charitable Trust (to M.E.C.); an unrestricted grant from the OHSU Foundation (to M.E.C.); NIH training grant T32HL083808 (to T.A.B.); NIH grant R011R01AI141549-01A1 (to F.G.T.); OHSU Innovative IDEA grant 1018784 (to F.G.T.); NIH grant R01AI145835 (to W.B.M.); Burroughs Wellcome Fund UT Southwestern Training Resident Doctors as Innovators in Science (to Y.J.K.); and a pilot project grant from the UT Southwestern Department of Internal Medicine and Disease Oriented Scholars Award (to L.L.L.). We gratefully acknowledge the OHSU workforce members who participated in this study; the OHSU COVID-19 serology study team and the OHSU occupational health department for their efforts in recruitment and sample acquisition; and the OHSU clinical laboratory under the direction of Donna Hansel and Xuan Qin for SARS-CoV-2 testing and reporting. We thank UTSW healthy volunteers who donated their blood for neutrophil studies; Dawn Wetzel for efforts in recruitment; Gabrielle Lessen for phlebotomy assistance; and Ann McDonald, Gabrielle Lessen, and Joshua Miles for graphical assistance. We are grateful for the support of the M.J. Murdock Charitable

Trust and the OHSU Foundation. The funders of the study had no role in study design, execution, analysis, interpretation, or writing of this manuscript.

8.8.2 Author Contributions

L.L.L. and F.G.T. conceived, designed, and supervised the work. T.A.B. and P.L. designed, conducted, and analyzed experiments. M.E.C., W.B.M., D.S., and S.K.M. coordinated sample and reagent collection. S.K.M. acquired and analyzed data. Y.J.K., M.T., C.P., and D.K. analyzed the data. L.L.L., F.G.T., T.A.B., and P.L. wrote the manuscript. Y.J.K., M.T., S.K.M., D.K., W.B.M., and M.E.C. contributed to manuscript revisions.

Chapter 9: An extended interval between vaccination and infection enhances hybrid immunity against SARS-CoV-2 variants

Timothy A. Bates[1], Hans C. Leier[1], Savannah K. McBride[1], Devin Schoen[2], Zoe L. Lyski[1], David X. Lee[1], William B. Messer[1,2,3,#], Marcel E. Curlin[2,#], Fikadu G. Tafesse[1,#]

[1]Department of Molecular Microbiology & Immunology, Oregon Health & Science University; Portland, OR 97239, United States.

[2]Division of Infectious Diseases, Oregon Health & Science University; Portland, OR 97239, United States.

[3]OHSU-PSU School of Public Health, Oregon Health & Science University; Portland, OR 97239, United States

[#]Corresponding authors

JCI Insight Volume 8, Issue 5, March 8, 2023.

DOI: https://doi.org/10.1172/jci.insight.165265

Section 9.1: Abstract

As the COVID-19 pandemic continues, long-term immunity against SARS-CoV-2 will be globally important. Official weekly cases have not dropped below 2 million since September of 2020, and continued emergence of novel variants have created a moving target for our immune

systems and public health alike. The temporal aspects of COVID-19 immunity, particularly from repeated vaccination and infection, are less well understood than short-term vaccine efficacy. In this study, we explore the impact of combined vaccination and infection, also known as hybrid immunity, and the timing thereof on the quality and quantity of antibodies elicited in a cohort of 96 health care workers. We find robust neutralizing antibody responses among those with hybrid immunity against all variants, including Omicron BA.2, and significantly improved neutralizing titers with longer vaccine-infection intervals up to 400 days. These results indicate that anti-SARS-CoV-2 antibody responses undergo continual maturation following primary exposure by either vaccination or infection for at least 400 days after last antigen exposure. We show that neutralizing antibody responses improved upon secondary boosting with greater potency seen after extended intervals. Our findings may also extend to booster vaccine doses, a critical consideration in future vaccine campaign strategies.

Section 6.2: Introduction

Since the emergence of severe acute respiratory syndrome coronavirus 2 (SARS-CoV-2) in late 2019, the coronavirus disease 2019 (COVID-19) pandemic has continued to expand and contract at regular intervals, and it remains an ongoing threat to global public health. As of August 2022, the number of officially recognized cases is approaching 600 million[80], and the true number of people with at least one previous infection is likely much higher with estimates upwards of 3.4 billion, 44% of the global population, even before the emergence of the Omicron variants[480]. Due to ongoing transmission and the continued emergence of novel SARS-CoV-2 variants, it is likely that this number will continue to rise despite large-scale public health control efforts. Nevertheless, current vaccines have proven to be invaluable tools for protecting public health and have saved countless lives.

First generation lipid nanoparticle mRNA vaccines including Comirnaty (Pfizer-BioNTech, previously BNT162b2) and Spikevax (Moderna, previously mRNA-1273) became available in the United States in December, 2020, and to this day remain the most utilized vaccines in many parts of the world.[481] These vaccines are both well established as providing temporary prevention of SARS-CoV-2 infection as well as longer-term protection from severe COVID-19 and death[482,483]. The primary challenges faced by vaccination-based protection at this stage in the pandemic are antibody waning and the emergence variants of concern (VOCs) with decreasing responsiveness to the original vaccine formulation[374,484]. Additional vaccine boosters given months after initial vaccination have been shown to provide partial protection against novel variants including Omicron[396,485]. However, the most protective immune responses are seen after a combination of vaccination and natural infection, also known as hybrid immunity[372,392,486,487].

Several key variables influence the protective efficacy of SARS-CoV-2 immunity. The first is the mechanisms by which immunity is elicited, which may include natural infection or vaccination with any of the different vaccine types[372,488]. The second is viral antigenic variation, which encompasses differences in the amino acid sequence and post-translational modification of viral antigens depending on which variant of SARS-CoV-2 the antigens were derived from[385,398]. The third is timing between repeat exposures, including the interval between vaccine doses and the much less studied interval between vaccination and natural infection[489–492]. Additionally, following the last exposure, immunity can wane, leading to decreased protection. However, the durability of responses from different exposure modes can vary greatly[362,372,493]. Finally, other variables exist which have important implications for immunity including age, sex, comorbidities, and certain therapeutic agents. Understanding the impact of these variables is key for risk-stratifying populations and guiding general vaccination strategies.

As the pandemic continues, separating these variables' individual contributions to immunity becomes increasingly complex, particularly as global efforts to track infections lose momentum. Further, as SARS-CoV-2 transitions to a globally endemic virus, hybrid immunity from combined vaccination and natural infection will be the dominant form of immunity, and while hybrid immunity is currently the subject of intense focus, very little work has been done thus far to determine the impact of exposure timing on its development.

Here, we report results of studies of 2 cohorts: the first is comprised of individuals recovered from COVID-19 and paired infection-naïve, vaccinated controls from whom serum samples were collected both before and after vaccination; the second cohort builds on our experience from the first cohort and includes vaccinated individuals with prior COVID-19, vaccinated individuals that then experienced breakthrough infection, and infection-naïve vaccinated controls. The second cohort includes individuals with a wide range of intervals (35-404 days) between PCR-confirmed COVID-19 and vaccination. We utilized enzyme-linked immunosorbent assays (ELISA) and live-virus neutralization assays with the original SARS-CoV-2 (WA1) and the variants of concern (Alpha, Beta, Gamma, Delta, Omicron BA.1, and Omicron BA.2) to discern how the interval between vaccination and infection affects the resulting level of humoral immunity. We find that the magnitude, potency, and breadth of the hybrid immune response against variants continue to improve for at least 400 days. These results suggest that the primary immune response to either vaccination or natural infection continues developing for over a year after first exposure, in the absence of additional exposures and that boosting with the vaccine or infection leads to a hybrid immunity with dramatically improved antibody quantity and quality as measured by their capacity to recognize and neutralize emergent SARS-CoV-2 variants.

Section 9.3: Results

9.3.1 A longitudinal cohort of vaccinees with previous COVID-19 displayed improved SARS-CoV-2 neutralization compared to vaccination alone.

Between December 2020 and March 2021, we recruited 10 individuals who experienced PCR-confirmed COVID-19 prior to vaccination and collected blood samples before and after a standard two-dose BNT162b2 vaccine regimen (Table 9.1) and 20 age- and sex-matched with no self-reported history of prior COVID-19 infection, verified by negative nucleocapsid ELISA, and collected blood samples before and after vaccination. We then measured and compared serum neutralizing titers in these two groups using a live virus focus reduction neutralization test (FRNT) (Figure 9.1A-B). Serum neutralizing titers increased in both groups pre- and post-vaccination and were significantly higher among those with prior infection compared with vaccination for all strains tested, including ancestral strain of SARS-CoV-2 (WA1) and the early VOCs Alpha, Beta, and Gamma (Figure 9.1C). These results suggested that hybrid immunity from the combination of vaccination and natural infection may result in meaningfully improved neutralizing serum antibody titers.

9.3.2 A cross-sectional cohort of hybrid immune individuals including both prior infection and vaccine breakthrough.

To more comprehensively study our initial findings that suggested infection followed by vaccination elicited higher levels of SARS-CoV-2 specific antibodies compared to vaccination alone, we next expanded on our cohort by recruiting additional vaccinated persons with or without hybrid immunity due to previous COVID-19 (Table 9.1). This larger hybrid immune group included 23 individuals with PCR-confirmed infections prior to vaccination and 23 with vaccine

Table 9.1: Demographics

		Pre/post vaccination (longitudinal)			Post vaccine (cross-sectional)				
		All	Vaccine only	Prior infection	All	Vaccine only	Hybrid immunity		
							All	Prior infection	Breakthrough infection
Cohort size	n	30	20	10	66	20	46	23	23
Age	Years median [range]	39.5 [23-63]	41.5 [25-63]	36.5 [23-61]	39.5 [23-73]	39.5 [23-63]	40 [23-73]	47 [23-73]	38 [24-63]
Sex	Male n (%)	10 (33)	6 (30)	4 (40)	18 (27)	3 (15)	15 (33)	10 (43)	5 (22)
	Female n (%)	20 (67)	14 (70)	6 (60)	48 (73)	17 (85)	31 (67)	13 (57)	18 (78)
disease severity	Asymptomatic n (%)	-	-	2 (20)	-	-	3 (7)	3 (13)	0 (0)
	Mild n (%)	-	-	7 (70)	-	-	39 (85)	19 (83)	20 (87)
	Moderate n (%)	-	-	1 (10)	-	-	3 (7)	1 (4)	2 (9)
between vaccine doses	Days median [range]	22 [20-32]	21 [21-32]	22 [20-25]	21 [17-45]	21 [21-25]	21 [17-45]	22 [18-45]	21 [17-32]
exposure interval*	Days median [range]	-	-	98 [40-303]	-	-	221 [35-404]	299 [40-404]	215 [35-238]
collection interval**	Days median [range]	17 [10-28]	16 [10-25]	18 [14-28]	23 [10-53]	19.5 [10-28]	25.5 [10-53]	25 [11-53]	27 [10-49]

breakthrough infections, as both vaccination/infection histories have been shown to provide similar levels of serological immunity[392]. To assure a more uniform comparison, sera were collected less than 60 days following vaccination or PCR-confirmed breakthrough infection. The participants with infection prior to vaccination had all contracted COVID-19 during the pre-VOC era and are thus believed to have been infected with ancestral SARS-CoV-2 variants, while breakthrough cohort participants were recruited after the emergence of the VOCs, but prior to the Omicron era (Figure 9.1D). Using a subset of subjects for whom appropriate samples were available, viral sequences were obtained from 17 of 23 breakthrough participants showing that the majority of infections were caused by the Alpha and Delta VOCs (Table 9.2).

Table 9.2: Variants of infections

	N	%
Prior infection	23	100
Not sequenced*	23	100
Breakthrough infection	23	100
Alpha	4	17
Beta	1	4
Gamma	2	9
Delta	10	43
Not sequenced**	6	26

Figure 9.1: Longitudinal cohort of previously infected vaccinees shows improved variant neutralization compared to vaccination alone

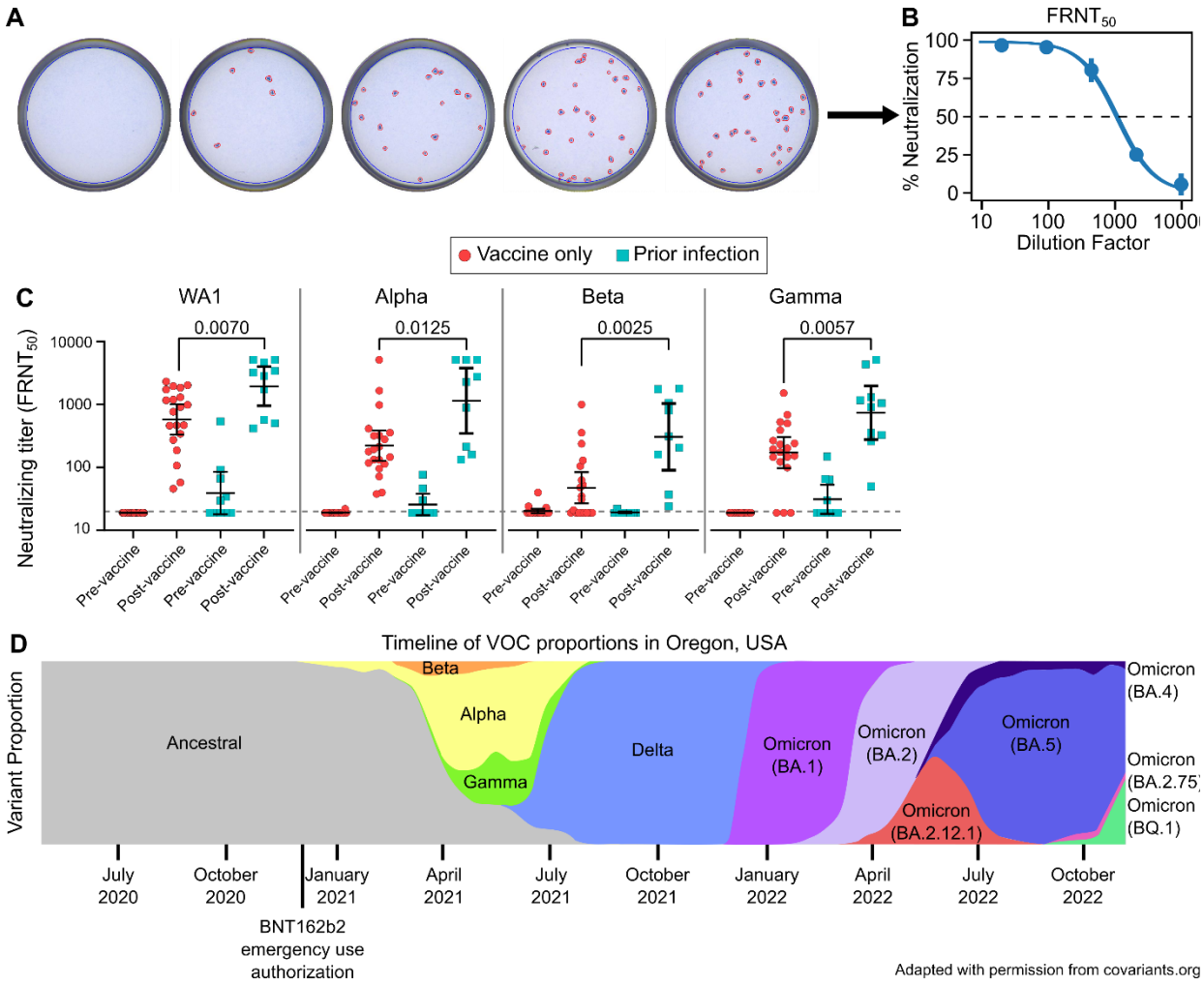

(**A**) Representative focus reduction neutralization test (FRNT) results showing wells infected with live SARS-CoV-2 with the addition of serially diluted serum which were stained and counted. (**B**) Representative focus reduction neutralization curve showing the average neutralization of duplicates as a percent of no serum controls and fit to a dose-response curve to find the 50% neutralizing titer ($FRNT_{50}$). (**C**) Live virus $FRNT_{50}$ measurements against original SARS-CoV-2 (WA1) and the Alpha, Beta, and Gamma variants before and after vaccination. (**D**) Timeline depicting the prevalence of impactful variants in the study location, Oregon, USA.[494] Vaccine-only participants are represented by red circles and hybrid immune participants by cyan squares. Error bars represent the geometric mean with 95% confidence intervals. P values in C show the result of Mann-Whitney U tests. All P values are two-tailed and 0.05 was considered significant. For panel C, n=20 for the vaccine only group and n=10 for the prior infection group.

9.3.3 Elevated antibody levels and neutralizing titers with hybrid immunity.

We next measured spike-specific antibody levels in our larger cohort with a series of ELISA experiments. Against purified RBD protein, total antigen-specific antibody levels were 3.6-fold greater with hybrid immunity compared to vaccine only (Figure 9.2A). Class-specific ELISAs showed that this was primarily driven by increases in IgG levels, which increased 3.7-fold (Figure 9.2B), while the less abundant IgA improved by 3.2-fold (Figure 9.2C), and IgM levels showed no significant difference between groups (Figure 9.2D). Total antibody levels against the full-length spike protein, which includes the entire S1 and S2 domains, were also improved with hybrid immunity by 3.1-fold (Figure 9.2E).

Similarly, neutralizing antibody titers against SARS-CoV-2 and every SARS-CoV-2 variant tested rose significantly in the hybrid immune group compared to vaccination alone (Figure

2F). Neutralizing titers increased by 8.4-fold against WA1, 12.5-fold against Alpha, 22.7-fold against Beta, 9.6-fold against Delta, 19.0-fold against Omicron BA.1, and 13.3-fold against Omicron BA.2. The largest fold-increases were seen against the most vaccine resistant variants, Beta and Omicron (BA.1 and BA.2). Further, it appears that these increases were not restricted to variants with which the cohort was experienced, as all samples were collected prior to the emergence of Omicron.

Figure 9.2: Cross-sectional cohort of individuals with hybrid immunity show improved antibody levels and variant neutralization

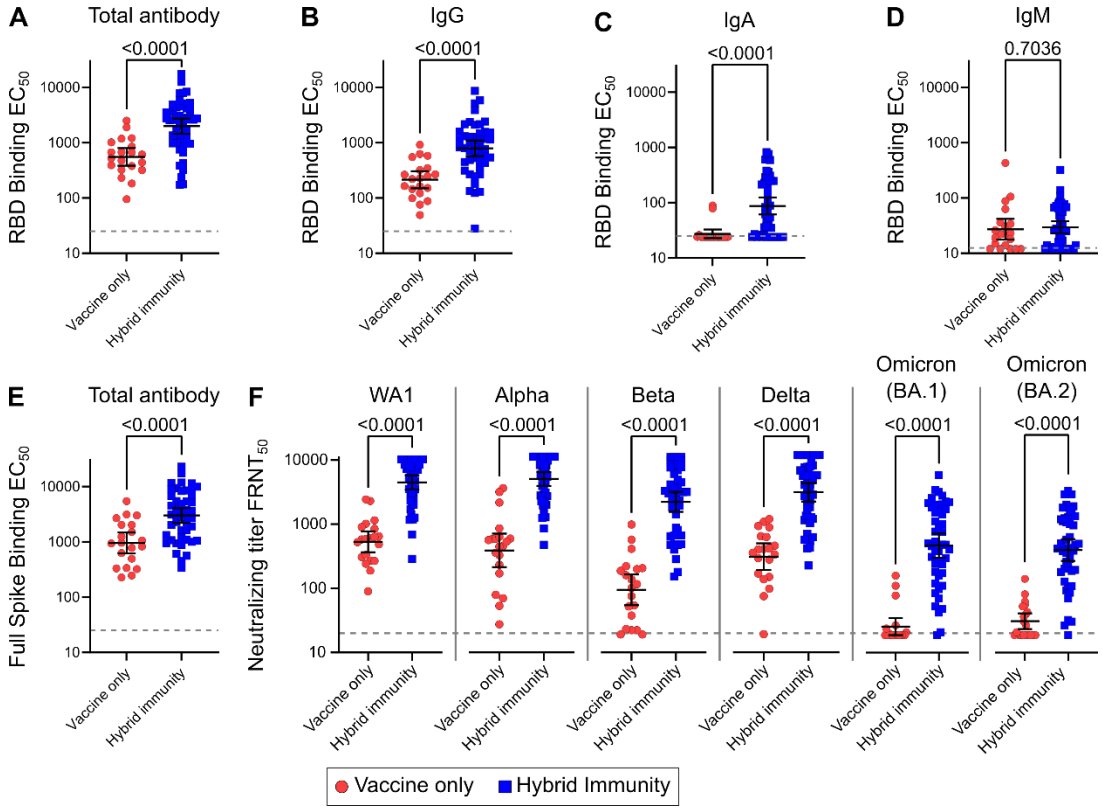

(**A–D**) Levels of SARS-CoV-2 spike receptor binding domain (RBD)-specific total (IgG/A/M) antibody (**A**), IgG (**B**), IgA (**C**), and IgM (**D**). (**E**) Levels of full-length spike-specific total antibody. (**F**) Live virus $FRNT_{50}$ measurements against original SARS-CoV-2 (WA1) and the Alpha, Beta, Delta, Omicron (BA.1), and Omicron (BA.2) variants. Vaccine only participants

are represented by red circles and hybrid immune participants by blue squares. Error bars represent the geometric mean with 95% confidence intervals. P values in **A-F** show the result of Mann-Whitney U tests. All P values are two-tailed and 0.05 was considered significant. For panels **A-F**, n=20 for the vaccine only group and n=46 for the hybrid immunity group.

9.3.4 Improved antibody quality among hybrid immune individuals.

To assess the breadth of the neutralizing antibody response, we then looked at the relative ability to neutralize variants. This was measured by dividing the neutralizing titer for each variant by the neutralizing titer for WA1. The hybrid immunity cohort showed considerably greater cross-reactivity against Alpha and Beta variants compared to the vaccine-only cohort, where an appreciable deficit in cross-neutralization against Alpha and Beta were seen (Figure 9.3A and 9.3B). In contrast, cross-reactivity against Delta was comparable in the two cohorts, where neutralization against Delta and WA1 were similar (Figure 9.3C). Cross-neutralization against Omicron BA.1 and BA.2 was substantially reduced in both cohorts, but less so in the hybrid immunity group, where high titers were associated with better cross-reactivity (Figure 9.3D and 9.3E, and summarized in Figure 9.3F and supplemental figure 9.1).

To assess the potency of the neutralizing antibody responses, we then calculated the neutralizing potency index (NPI) for the individuals in each cohort against each variant. The NPI is the neutralizing titer divided by the quantity of full-length spike specific total antibody levels as measured by ELISA. NPI scores indicate the efficiency with which antigen-specific antibodies neutralize virus on a per total antibody basis in which higher scores indicate that fewer antibodies are necessary to achieve a given neutralization titer. We found that the NPI of hybrid immune individuals increased significantly for all variants tested, with indexes of 2.7-fold (WA1), 4.0-fold (Alpha), 7.2-fold (Beta), 3.0-fold (Delta), 6.1-fold (Omicron BA.1), and 4.2-fold (Omicron BA.2),

indicating a significant improvement in the neutralizing efficiency of the antibodies produced by hybrid immunity compared to vaccination alone (Figure 9.3G).

Figure 9.3: Antibody quality and variant cross-neutralization are improved with hybrid immunity

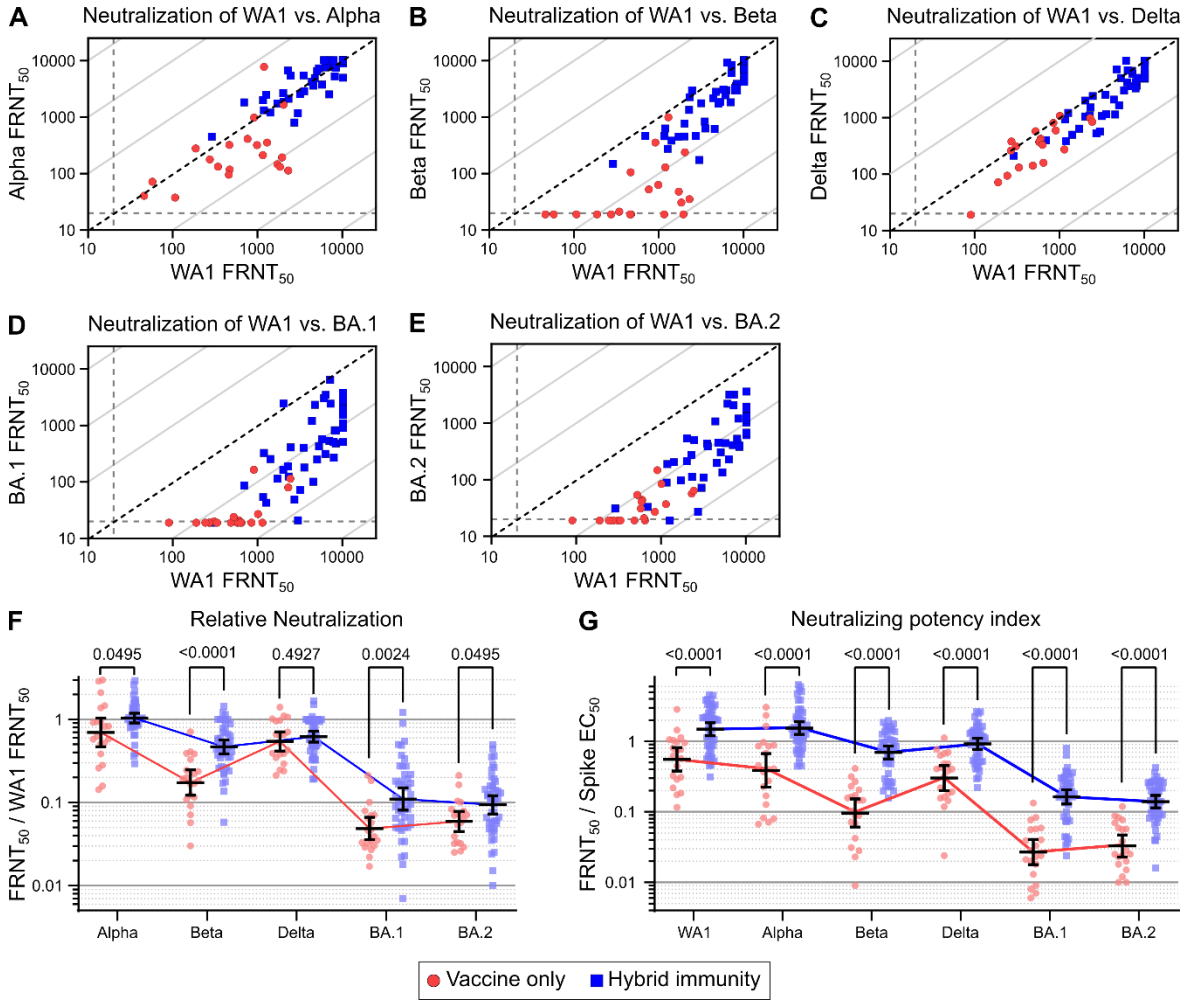

(**A-E**) Individual neutralizing $FRNT_{50}$ values against WA1 versus Alpha (**A**), Beta (**B**), Delta (**C**), Omicron (BA.1) (**D**), and Omicron (BA.2) (**E**). Diagonal broken line indicates equal neutralization of WA1 and variant in **A-E**. (**F**) Relative neutralization, calculated as the neutralizing titer against each of the variants divided by the neutralizing titer against WA1. (**G**) Neutralizing potency index indicates the neutralizing $FRNT_{50}$ against the indicated variant divided by full-length spike protein EC_{50} antibody levels. Vaccine-only participants are

represented by red circles and hybrid immune participants by blue squares. Error bars represent the geometric mean with 95% confidence intervals. P values in **F-G** show the result of Mann-Whitney U tests with the Holm-Šídák multiple comparison correction. All P values are two-tailed and 0.05 was considered significant. For panels **A-G**, n=20 for the vaccine only group and n=46 for the hybrid immunity group.

9.3.5 The interval between vaccination and natural infection dictates neutralizing titer levels.

The hybrid immune cohort included individuals who developed COVID-19 between 40 and 404 days post-vaccination, as well as individuals who were vaccinated between 35 and 283 days after testing positive for COVID-19. This range of hybrid exposure intervals allowed us to determine the impact of time intervals on the resulting neutralizing antibody response. We also characterized the correlation between antibody levels and neutralizing titers with our demographic data on age, exposure interval, sex, and the time form last exposure to sample collection. Only neutralizing antibody titers and antibody levels were significantly correlated with exposure interval. The strongest correlations were seen for full-length spike-specific antibody level, as well as neutralization of WA1, Alpha, Beta, Delta, Omicron BA.1 and Omicron BA.2 (Figure 9.4A-G).

The magnitude of increase seen over time was also different for each of the variants. Using linear regression, we found the neutralizing titer against WA1 increased 5.3-fold by day 400 (Figure 4). This increase was 4.8-fold for Alpha, 11.5-fold for Beta, 11.2-fold for Delta, 17.6-fold for Omicron BA.1, and 14.3-fold for Omicron BA.2. The largest increases were seen against the more contemporary variants, which also tend to be more vaccine-resistant (Figure 9.2F). To validate that these trends were not an artifact of linear regression, we also subdivided the cohort into 100-day exposure interval bins, which recapitulated the previous findings (Figure 9.4H).

Figure 9.4: Exposure interval determines strength of hybrid immunity

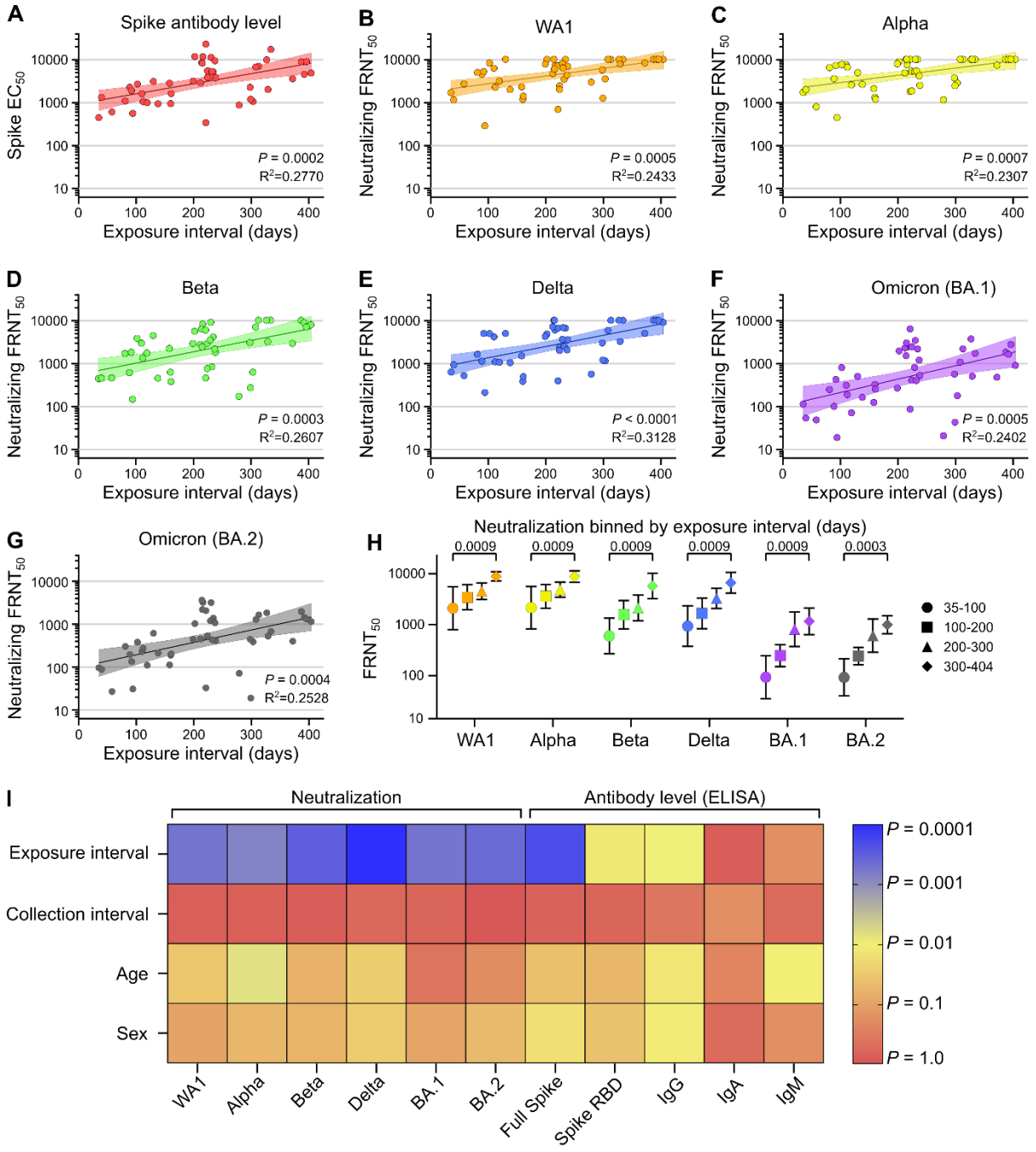

(**A-F**) Comparison of exposure interval, the time between first and last antigen exposure, with full-length spike EC_{50} antibody levels (**A**), and neutralization of WA1 (**B**), Alpha (**C**), Beta (**D**), Delta (**E**), Omicron (BA.1) (**F**), and Omicron (BA.2) (**G**). (**H**) Neutralization of variants binned

by exposure interval in days. (**I**) Heat map of correlation significance between explanatory and response variables. Individual values in **A-G** are shown as filled circles and the shaded area indicates the linear fit with 95% confidence interval. R^2 is indicated for each curve fit. P values in **A-G** show the result of an F-test using a zero slope null hypothesis, P values in **H** show the result of Mann-Whitney U tests with the Holm-Šídák multiple comparison correction, and colors in **I** represent the P values of pearson r correlation coefficients according to the scale bar. All P values are two-tailed and 0.05 was considered significant. For panels **A-G** and **I**, n=46. For panel **H**, n=7 for the 35-100 days group, n=10 for the 101-200 days group, n=18 for the 201-300 days group, and n=11 for the 301-404 days group.

Steady increases are seen each 100 days, resulting in a final increase of 4.2-fold against WA1, 4.1-fold against Alpha, 9.6-fold against Beta, 7.1-fold against Delta, 12.5-fold against Omicron BA.1, and 10.7-fold against Omicron BA.2 between the 35-100 and 300-404 day exposure interval groups. Both methods of analysis found that a large and significant improvement in neutralizing antibody titers occurs over an increased duration between the antigen exposures provided by vaccination and natural infection. Further, these correlations were maintained when measured separately for individuals with infection prior to vaccination and individuals with vaccine breakthrough infections (Supplemental figures 9.2 and 9.3). Observed separately, neutralizing titers from individuals from the breakthrough group appeared to increase faster than those in the prior infection group, but no statistically significant difference could be measured. RBD-specific total antibody and IgG levels correlated less strongly, while RBD-specific IgA and IgM did not correlate significantly with exposure interval (Supplemental figure 9.4).

We then assessed for interactions between exposure interval and other variables that could confound our analyses, including age, sex, or the time between final antigen exposure (either

vaccination or COVID-19 infection) and serum sample collection, all of which have been previously shown to affect antibody levels[369,482,495]. As expected, titers weakly correlated with age and sex, but did not approached the relative contribution of exposure interval (Figure 9.4I). Collection interval was not significantly correlated with any variable, likely due to our strict 60-day limit on collection interval for inclusion in the study.

Variant cross-neutralization improves with greater exposure intervals.

After observing the increases in variant cross-neutralization between hybrid immunity and vaccine only, we sought to determine whether there was an equivalent dependence on the exposure interval duration. Alpha is the least vaccine-resistant variant and did not improve relative to WA1 because it started at a ratio of 1 from the beginning (Figure 9.5A). For the more vaccine-resistant variants, which started well below 1, all saw increased variant cross-neutralization with increasing exposure interval (Figure 9.5B-E). This indicates that the neutralizing antibody response is becoming more broadly neutralizing over time, between exposures. No significant trends were seen with NPI over time (Supplemental figure 9.5). This indicates that while the variant cross-reactivity is increasing with longer exposure intervals, the proportion of antibodies which are capable of neutralization is maintained.

Figure 9.5: Exposure interval increases variant cross-neutralization by hybrid immune sera

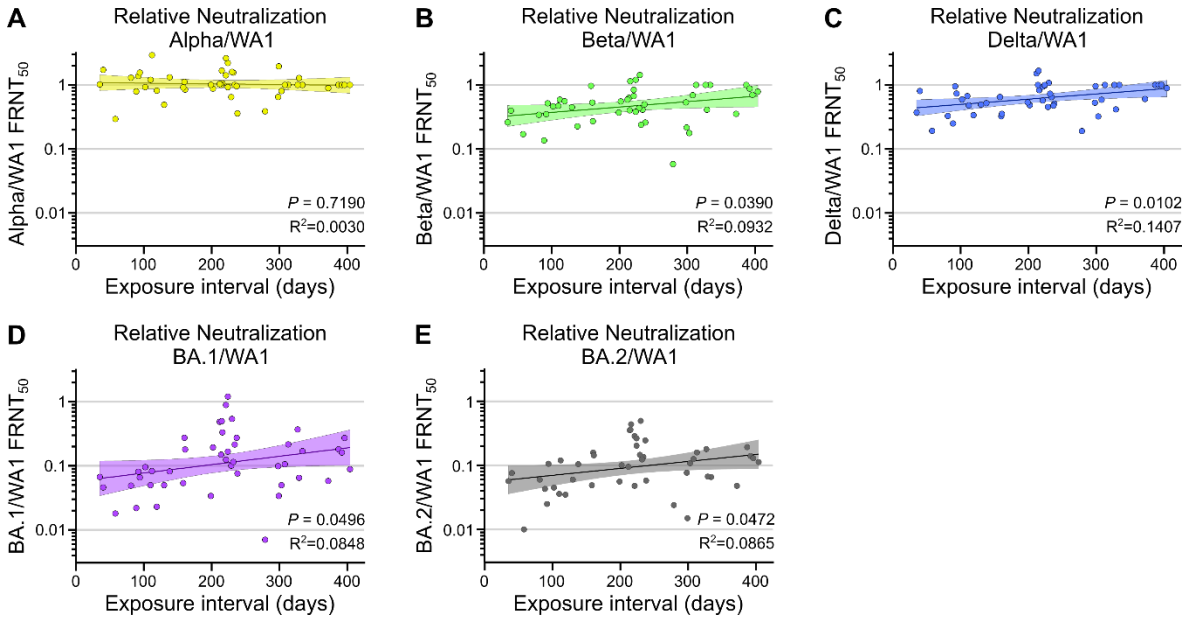

(**A-E**) Comparison of exposure interval, the time between first and last antigen exposure, with relative neutralization of Alpha (**A**), Beta (**B**), Delta (**C**), Omicron (BA.1) (**D**), and Omicron (BA.2) (**E**) over wildtype (WA1). Individual values are shown as filled circles and the shaded area indicates the linear fit with 95% confidence interval. R^2 is indicated for each curve fit. P values show the result of an F-test using a zero slope null hypothesis. All P values are two-tailed and 0.05 was considered significant. For panels **A-E**, n=46.

Section 9.4: Discussion

This study reports superior variant-neutralizing serum antibody titers with hybrid immunity from combined vaccination and natural infection compared to vaccination alone. It further shows that longer intervals, up to at least 400 days, between vaccination and infection result in the largest improvements in titers as well as better cross-neutralization of variants. The greatest increases were seen against BA.1 Omicron, which is noteworthy because the samples used in this study were

collected prior to BA.1 emergence. In fact, half of the study participants were infected in the pre-vaccine era, before the emergence of any VOCs.

In our cohort, infection alone provided poor neutralizing antibody responses, while two-dose mRNA vaccination provided robust responses against original SARS-CoV-2 and the early variants, but very poor neutralization of Omicron. Hybrid immunity has been shown previously to result in greater humoral responses than two-dose vaccination[372,392,486,487], and our study expands upon this by identifying the hybrid exposure interval (the time between infection and vaccination) as an important factor in determining the strength of the neutralizing response. This was also recently suggested in a study of breakthrough cases over intervals up to 100 days[491]. The finding that this effect extends to all hybrid immunity, including infection prior to vaccination is interesting because it suggests that there is nothing inherently different about the order of two different exposure modes (vaccination and infection) from the standpoint of neutralizing antibody development. Further, because our prior infection group was never exposed to variant spike protein, it suggests that many of the conserved epitopes that shape the memory response are present and recognizable on both the original strain of SARS-CoV-2 and every VOC including Omicron-BA.1. This hypothesis is consistent with previous work has shown that memory B cells generated by infection with original SARS-CoV-2 can recognize the variants[202], and that germinal center responses can continue for an extended period that improve cross-reactivity[204,496,497]. Further, a recent study found that recruitment of B cells to germinal centers is controlled by the balance of existing antibody titers and availability of antigen[498], suggesting that antibody waning may play a direct role in broadening the antibody response over time. However, an alternative explanation is that each of the two types of hybrid immunity increase via distinct mechanisms. For instance, breakthrough infections may be more severe after longer intervals due to antibody waning in the

interim, and more severe infections may lead to greater final titers. Conversely, for infection prior to vaccination, it is possible that high titers from shorter intervals result in poorer vaccine responses than at later timepoints. Neither of these alternative hypotheses explain the observation of improved variant cross-reactivity after longer intervals.

The results of this study demonstrate gradually improving memory responses to SARS-CoV-2 infection and vaccination, consistent with previous studies on the importance of an increased interval between the first two vaccine doses in achieving higher antibody levels[489,490,492,499]. While booster vaccination has been shown to improve vaccine efficacy, there are relatively few studies that have focused on the effects of different boosting intervals[500,501]. Currently, fourth doses are being deployed worldwide, and while early results are promising, it remains to be seen if continued boosting results in long-term benefits or simply a transitory bump in protective antibody levels[217,502]. One limitation of this study is that we did not include individuals who received 3 vaccine doses, and therefore we cannot directly distinguish between the immunological effects of natural infection per se and the effects of a third antigenic exposure.

Some studies have pointed to evidence of improved durability of hybrid immune responses[372,487,503,504], which may be greater than that provided by boosters[505], but further studies are needed to establish whether vaccines which can elicit the same level of response and durability provided by hybrid immunity; perhaps the best strategy for long-term protection will involve addition of alternative vaccine types that better mimic natural infection. While hybrid immunity currently appears to offer the strongest and possibly most durable protection, intentional infection with natural COVID-19 as a means to achieve immunity is not a reasonable public health approach given the risks of severe illness, long-term complications, and death that can result from real SARS-CoV-2 infection[506]. To the contrary, our results support increased access to vaccines.

Demonstration that longer infection-vaccination intervals improve antibody responses implies that even greatly delayed vaccination will yield sizeable benefits, particularly against emerging vaccine-resistant variants. Simultaneously, our results point to a future where inevitable vaccine breakthrough infections would be expected to help build a reservoir of population-level immunity that can help blunt future waves and reduce the opportunity for further viral evolution.

Section 9.5: Methods

9.5.1 Cohort

The longitudinal cohort participants were enrolled at Oregon Health & Science University (OHSU) at the time they were receiving their first dose of the BNT162b2 COVID-19 vaccine. A pre-vaccination blood sample was collected at this time. Participants received a second vaccine dose between 20 and 32 days following the first dose, then returned between 10 and 30 days later for follow up, at which time a post-vaccination blood sample was collected.

The cross-sectional cohort was comprised of health care workers who were enrolled at OHSU, and individuals were selected from a previously established cohort based on the following criteria[392]: Individuals who experienced COVID-19 prior to vaccination were included if serum samples were collected less than 60 days after their second vaccine dose. Vaccinated individuals who experienced vaccine breakthrough COVID-19 infections were included if serum samples were collected less than 60 days after the date of receiving a positive PCR-based COVID-19 test. Vaccinated individuals with no history of COVID-19 (vaccine only) were selected based on age, sex, days between vaccine doses, and days between final vaccine dose and sample collection in order to match the hybrid immune (combined prior infection and breakthrough) group as closely as possible.

For all participants, 4-6 mL whole blood samples were collected and then centrifuged at 1000xg for 10 minutes to isolate sera. Sera were aliquoted, heat inactivated at 65°C for 30 minutes, and frozen at -20°C until needed for laboratory tests.

9.5.2 Enzyme linked Immunosorbent Assays (ELISA)

ELISA experiments were performed as previously described[392]. Briefly, 96-well plates were coated overnight at 4°C with 1 μg/mL recombinant SARS-CoV-2 spike receptor binding domain (RBD) protein, or recombinant full-length SARS-CoV-2 spike protein. Plates were washed in phosphate buffered saline (PBS) with 0.05% Tween-20 (PBST) and blocked with PBST with 5% milk powder (dilution buffer) for one hour at room temperature (RT). Four-fold serum dilutions were prepared in dilution buffer starting at 1:50 for IgG/A/M, IgG, and IgA and 1:25 for IgM, then incubated at RT for an hour. Plates were then washed three times and incubated with secondary antibody in dilution buffer for another hour at RT. The secondary antibodies used were 1:10,000 α-IgG/A/M-HRP (Invitrogen, A18847), 1:3,000 α-IgA-HRP (Biolegend, 411002), 1:3,000 α-IgG-HRP (BD Biosciences, 555788), and 1:3,000 α-IgM-HRP (Bethyl Laboratories, A80-100P). Plates were washed three more times with PBST and developed with o-phenylenediamine (OPD) for 20 minutes then stopped with 1N HCl. Absorbance was measured at 492nm on a CLARIOstar plate reader and normalized by subtracting the average of negative control wells and dividing by the highest concentration from a positive control serum. The serum dilution that resulted in half-maximal binding was calculated by fitting normalized absorbance values to a dose-response curve as previously described[370], and inverse serum dilution values were reported as 50% effective concentrations (EC_{50}).

9.5.3 Viruses

SARS-CoV-2 clinical isolates were obtained from BEI Resources: Isolate USA-WA1/2020 [wildtype] (BEI Resources NR-52281); Isolate USA/CA_CDC_5574/2020 [Alpha - B.1.1.7] (BEI Resources NR-54011); Isolate hCoV-54 19/South Africa/KRISP-K005325/2020 [B.1.351] (BEI Resources NR-54009); Isolate hCoV-19/Japan/TY7-503/2021 [P.1] (BEI Resources NR-54982); and Isolate hCoV-19/USA/PHC658/2021 [B.1.617.2] (BEI Resources NR-55611). Isolates were propagated and titrated in Vero E6 cells as previously described[392]. Vero E6 cells were seeded in tissue culture flasks such that they were 70-90% confluent at the time of infection. In minimal volume of Opti-MEM plus 2% FBS, flasks were infected at an MOI of 0.05 for 1 hour at 37°C before adding additional DMEM plus 10% FBS, 1% penicillin-streptomycin, 1% nonessential amino acids (complete media) to manufacturer's recommended culture volume. Flasks were incubated until cytopathic effects were observed, 24-96 hours. Collected supernatants were centrifuged at 1,000×g for 10 minutes, aliquoted and frozen at -80°C. Titrations were performed by preparing 10-fold dilutions of frozen aliquots and incubating 30 µL for 1 hour on 96-well plates of sub-confluent Vero E6 cells before adding Opti-MEM plus 2% FBS, 1% methylcellulose (overlay media). Titration plates were incubated for 24 hours, or 48 hours for Omicron sublineages, then fixed with 4% formaldehyde for 1 hour. The formaldehyde was removed, and plates were blocked for 30 minutes at RT with PBS plus 0.1% saponin, 0.1% bovine serum albumin (perm buffer). The blocking buffer was then replaced with 1:5,000 anti-SARS-CoV-2 alpaca serum (Capralogics Inc.) in perm buffer and incubated overnight at 4°C. The plates were then washed three times for 5 minutes in PBST and incubated with 1:20,000 anti-alpaca-HRP (Novus, NB7242) for 2 hours at RT. Plates were then washed three more times with PBST for 5 minutes each, then developed with TrueBlue (SeraCare 5510-0030) for 30 minutes or until foci were strongly stained.

Wells were imaged with a CTL ImmunoSpot Analyzer. Focus counts were used to calculate the concentration of focus forming units (FFU) in the virus stock aliquots.

9.5.4 Focus Reduction Neutralization Test (FRNT)

Focus forming assays were performed as previously described[392]. Briefly, Vero E6 (ATCC CRL-1586) cells were plated at 20,000 cells/well 16-24 hours before starting the assay. Sera were diluted in Opti-MEM plus 2% FBS (dilution media). Virus stocks were diluted to 3,333 FFU/mL (determined by titration) and combined 1:1 with serum dilutions. Initial serum dilutions started at 1:10, which became 1:20 after the 1:1 dilution with virus, and 30 µL of serum/virus mixture was added to each well for 1 hour at 37°C. Dilution series were performed in duplicate with one no serum control well for each replicate. Overlay media was added to each well and plates were incubated for 24 hours, or 48 hours for Omicron sublinages. Plates were fixed with 4% formaldehyde for 1 hour and then stained similarly to titration plates as described above. Foci in well images were counted with Viridot (1.0) in R (3.6.3)[382]. Percent neutralization for each well was calculated relative to the average of all no serum control wells on each plate. The serum dilution that resulted in 50% neutralization was calculated by fitting percent neutralization values to a dose-response curve as previously described[370], and inverse serum dilution values were reported as 50% focus reduction neutralization test ($FRNT_{50}$) titers. For each sample, $FRNT_{50}$ values were first calculated separately for each duplicate and verified to be within 4-fold. Combined $FRNT_{50}$ values were calculated for all samples which passed this test, and samples which failed this test were excluded from further analysis.

9.5.5 Statistical Analysis

The limit of detection (LOD) of each assay was defined by the lowest dilution tested, values below the LOD were set to LOD – 1 for both ELISA and FRNT experiments. Graphing and

statistical tests were performed in GraphPad Prism. Pairwise comparisons were performed using the Mann-Whitney U test. The Holm-Šídák multiple comparison correction was used anywhere data are shown on a continuous X-axis. Simple linear regression was performed on log transformed EC_{50} and $FRNT_{50}$ values and significance was determined with an F test with a zero-slope null hypothesis. Correlations were calculated using Pearson's method. All P values are two-tailed and P=0.05 was the cutoff for significance.

9.5.6 Study Approval

This study was conducted in accordance with the Oregon Health & Science University Institutional Review Board (IRB # 00022511), and written informed consent was obtained from all participants.

Section 9.6: Supplemental Figures

Figure S9.1: Variant cross-neutralization by hybrid immune sera is improved compared to vaccination alone

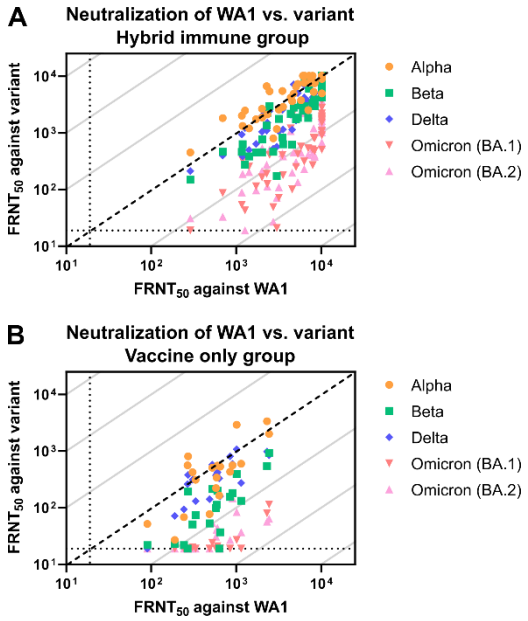

(**A**) Individual neutralizing $FRNT_{50}$ values for each of the variants against WA1 for the hybrid immune group (**A**), and two-dose vaccine only group (**B**). Diagonal broken line indicates equal neutralization of WA1 and variant. For panels **A-B**, n=20 for the vaccine only group and n=46 for the hybrid immunity group.

Figure S9.2: Infection prior to vaccination group neutralizing responses correlate with exposure interval

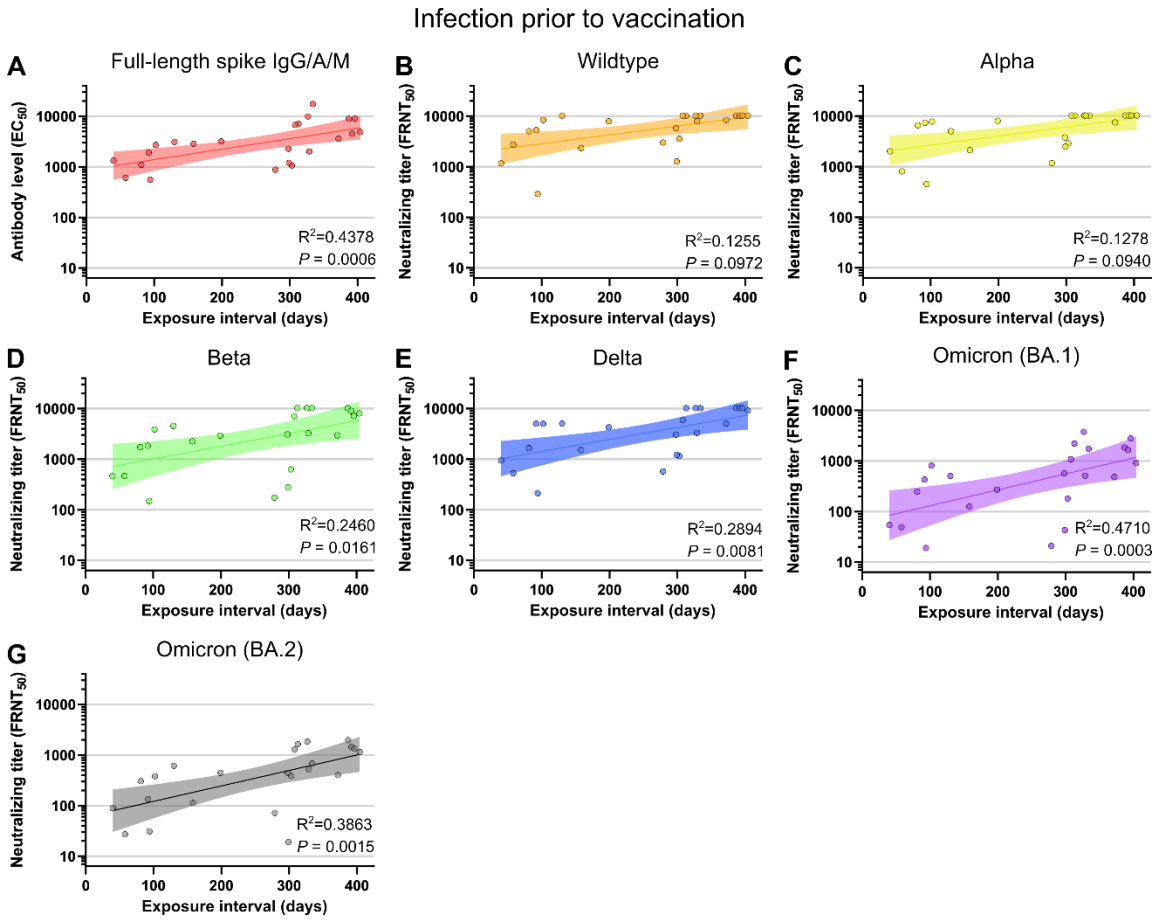

(**A-G**) Comparison of exposure interval, the time between first and last antigen exposure, among individuals with SARS-CoV-2 infection prior to vaccination. Correlations are shown for full-length spike EC_{50} antibody levels (**A**), and neutralization of WA1 (**B**), Alpha (**C**), Beta (**D**), Delta (**E**), Omicron (BA.1) (**F**), and Omicron (BA.2) (**G**). Individual values are shown as filled circles and the shaded area indicates the linear fit with 95% confidence interval. R^2 is indicated for each curve fit and P values show the result of an F-test using a zero slope null hypothesis. All P values are two-tailed and 0.05 was considered significant. For panels **A-G**, n=23.

Figure S9.3: Vaccine breakthrough group neutralizing responses correlate with exposure interval

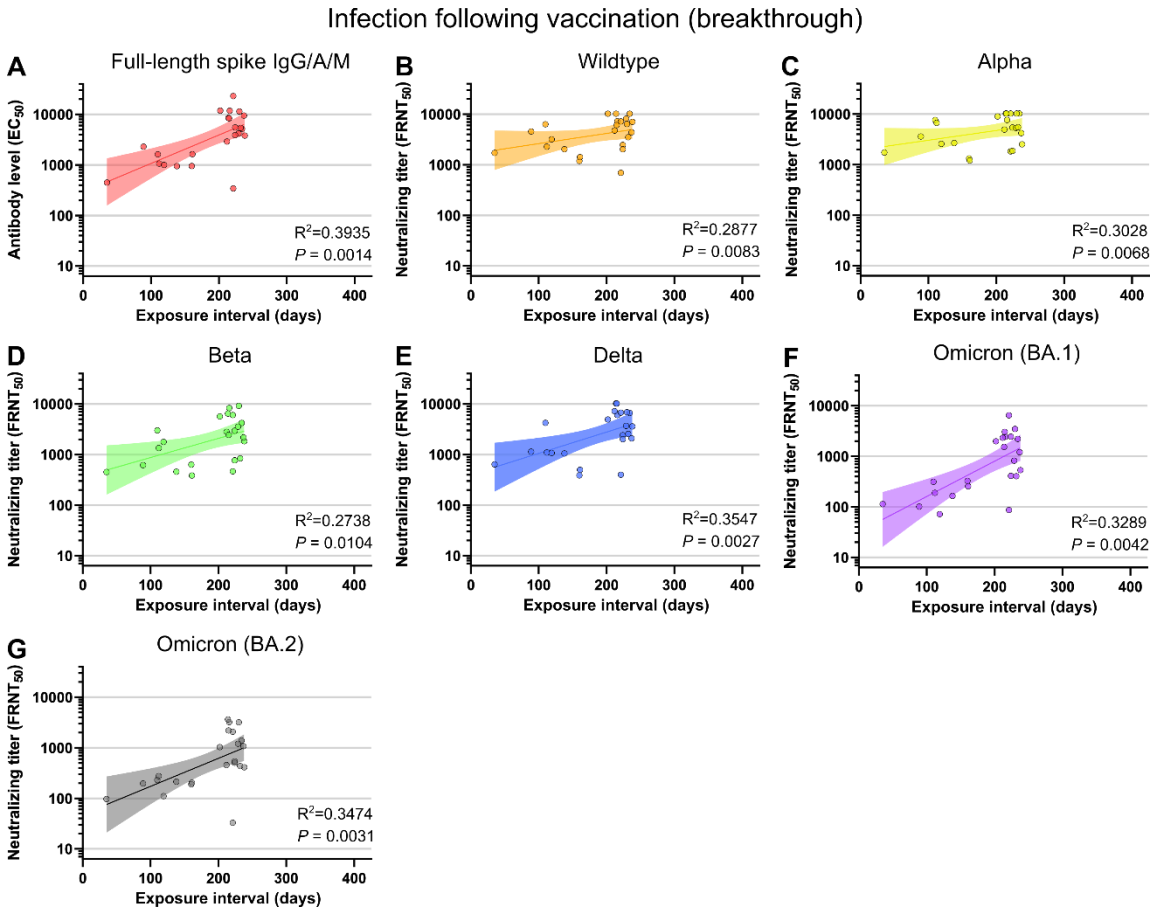

(**A-G**) Comparison of exposure interval, the time between first and last antigen exposure, among individuals with vaccine breakthrough infections. Correlations are shown for full-length spike EC_{50} antibody levels (**A**), and neutralization of WA1 (**B**), Alpha (**C**), Beta (**D**), Delta (**E**), Omicron (BA.1) (**F**), and Omicron (BA.2) (**G**). Individual values are shown as filled circles and the shaded area indicates the linear fit with 95% confidence interval. R^2 is indicated for each curve fit and P values show the result of an F-test using a zero slope null hypothesis. All P values are two-tailed and 0.05 was considered significant. For panels **A-G**, n=23.

Figure S9.4: Other antibody isotypes correlate less well with exposure interval

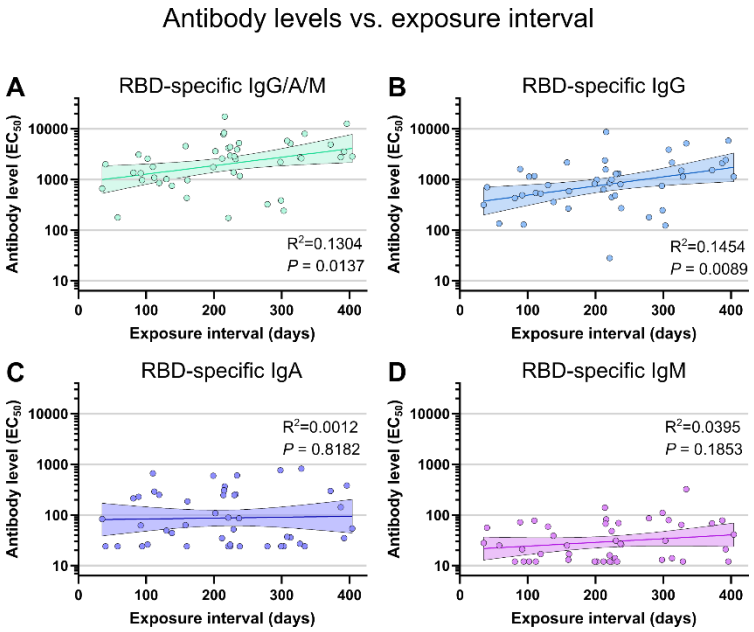

(**A-D**) Comparison of exposure interval, the time between first and last antigen exposure, with total (IgG/A/M) spike RBD (**A**), IgG (**B**), IgA (**C**), and IgM (**D**) EC_{50} antibody levels. Individual values are shown as filled circles and the shaded areas indicate the linear fit with 95% confidence interval. R^2 is indicated for each curve fit and P values show the result of an F-test using a zero slope null hypothesis. All P values are two-tailed and 0.05 was considered significant. For panels **A-D**, n=46.

Figure S9.5: Neutralizing potency index does not correlate with exposure interval

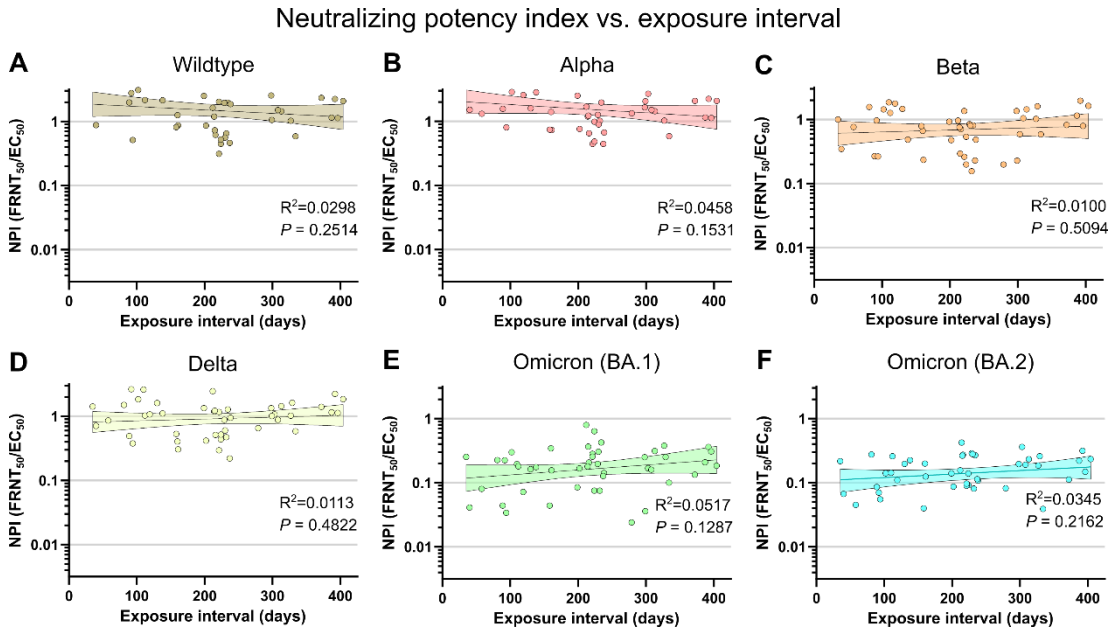

(**A-F**) Comparison of exposure interval, the time between first and last antigen exposure, with neutralization potency index ($FRNT_{50}$ / full-length spike EC_{50}) of wildtype (WA1) (**A**), Alpha (**B**), Beta (**C**), Delta (**D**), Omicron (BA.1) (**E**), and Omicron (BA.2) (**F**). Individual values are shown as filled circles and the shaded area indicates the linear fit with 95% confidence interval. R^2 is indicated for each curve fit. P values show the result of an F-test using a zero slope null hypothesis. All P values are two-tailed and 0.05 was considered significant. For panels **A-F**, n=46.

Section 9.7: Acknowledgements

9.7.1 Author Contributions

TAB, HCL, WBM, MEC, FGT conceptualization. TAB, HCL, SKM, ZLL, DXL methodology. TAB software. TAB, HCL, SKM, DS, WBM, FGT, MEC validation. TAB, DS, WBM formal analysis. TAB, HCL, SKM, DS investigation. WBM, MEC, FGT resources. TAB, HCL, DS data curation. TAB writing – original draft. TAB, HCL, SKM, DS, ZLL, DXL, WBM, MEC, FGT writing – review & editing. TAB, DS visualization. TAB, WBM, MEC, FGT supervision. TAB, WBM, MEC, FGT project administration. TAB, WBM, MEC, FGT funding acquisition.

9.7.2 Funding

This study was funded by a grant from the M. J. Murdock Charitable Trust (to MEC), an unrestricted grant from the OHSU Foundation (to MEC), the NIH training grant T32HL083808 (to TAB), NIH grant R011R01AI141549-01A1 (to FGT), OHSU Innovative IDEA grant 1018784 (to FGT), and NIH grant R01AI145835 (to WBM).

9.7.3 Acknowledgements

We thank the participants of this study for their contribution. We additionally thank the OHSU COVID-19 serology study team and the OHSU department of Occupational Health for recruiting participants and collecting samples, and the OHSU clinical laboratory under the direction of D. Hansel and X. Qin for SARS-CoV-2 testing and reporting.

Chapter 10: Thesis Summary

Section 10.1: Chapter Highlights

10.1.1 Chapter 1 highlights: SARS-CoV-2

1. SARS-CoV-2 is a novel coronavirus that enters cells via ACE2 using its S protein.
2. S-specific antibodies can neutralize the virus, preventing infection.
3. The vaccines can safely provide substantial immunity to SARS-CoV-2 infection.
4. Emergence of variants has reduced overall vaccine effectiveness.

10.1.2 Chapter 2 highlights: Cross-reactivity of SARS-CoV structural protein antibodies against SARS-CoV-2

1. SARS-CoV antibodies commonly cross-react with SARS-CoV-2 proteins.
2. Such cross-reactive antibodies can serve as valuable reagents for early work.
3. Neutralization of SARS-CoV-2 by antibodies that neutralized SARS-CoV is rare.

10.1.3 Chapter 3 highlights: Neutralization of SARS-CoV-2 variants by convalescent and BNT162b2 vaccinated serum

1. SARS-CoV-2 variants are partially resistant to neutralization by immune sera.
2. Neutralizing antibody titers are proportional to total RBD-reactive antibody levels.
3. Vaccine response appears to diminish among individuals over 50 years old.
4. Natural infection is an unreliable predictor of neutralizing antibody levels.
5. Antibody levels likely peak between 14-90 days following natural infection.

10.1.4 Chapter 4 highlights: Age-Dependent Neutralization of SARS-CoV-2 and P.1 Variant by Vaccine Immune Serum Samples

1. Age predicts antibody response to vaccination for at least ages 20 through 80.
2. This relationship is apparent for the original SARS-CoV-2 and the Gamma variant.

10.1.5 Chapter 5 highlights: Antibody Response and Variant Cross-Neutralization After SARS-CoV-2 Breakthrough Infection

1. Breakthrough infection results in significantly increased IgG and IgA levels.
2. Breakthrough infection significantly improves neutralization of variants (through Delta).
3. Delta breakthrough results in homotypic boosting that improves Delta-specific responses to a larger degree than non-Delta infections.

10.1.6 Chapter 6 highlights: Vaccination before or after SARS-CoV-2 infection leads to robust humoral response and antibodies that effectively neutralize variants

1. Hybrid immunity from both breakthrough infection and prior infection result in similarly increased antibody levels (IgG and IgA) against S and RBD.
2. Hybrid immunity also improves ADCP, a measure of antibody effector function.
3. Both types of hybrid immunity similarly increase neutralizing titers against the variants (through Delta).
4. Antibody quality, neutralizing potency, is improved with hybrid immunity.
5. The age-based reduction in vaccine response is eliminated with hybrid immunity.
6. For those with previous infection, a single vaccine dose was sufficient to induce a fully-fledged antibody response.

10.1.7 Chapter 7 highlights: Omicron neutralizing antibody response following booster vaccination compared with breakthrough infection

1. Third dose boosters increase antibody levels similarly to breakthrough infection.
2. Boosters also increased variant neutralization (through Omicron BA.2).
3. Neutralizing potency of antibodies improved similarly with booster and breakthrough infection.
4. Neutralization of variants improves weakly (BA.1) or insignificantly (Delta, BA.2) beyond that seen against original SARS-CoV-2.
5. The negative correlation between age and vaccine response is maintained after booster vaccination but not breakthrough infection.

10.1.8 Chapter 8 highlights: BNT162b2 induced neutralizing and non-neutralizing antibody functions against SARS-CoV-2 diminish with age

1. Neutralizing titer correlates with Fc receptor binding.
2. Neutralizing titer correlates with effector function (NK activation).
3. Vaccine-induced S-specific antibodies contain more sialic acid, fucose, and galactose.
4. Age correlates with Fc receptor binding and effector function.

10.1.9 Chapter 9 highlights: An extended interval between vaccination and infection enhances hybrid immunity against SARS-CoV-2 variants

1. Hybrid immunity leads to improved variant neutralizing antibody quantity and quality.
2. Longer exposure intervals, between infection and vaccination, lead to increased neutralizing antibody titers.
3. Longer intervals also lead to more broadly variant cross-neutralizing antibodies.

Section 10.2: Vaccine Effectiveness

Overall, the new mRNA vaccines have been a windfall for humanity. The COVID-19 pandemic is estimated to have killed almost 15 million people in 2020 and 2021[507], but the vaccines are estimated to have averted approximately 14 million deaths in 2021 alone[508]. While it is impossible to prove models of hypothetical situations, other groups have come up with similar estimates for the number of deaths caused by COVID-19 and the number of deaths prevented by vaccination[509]. While there is still room for improvement in vaccine efficacy and distribution, the success of these vaccines is undeniable. It is also important to remember that although protection from symptomatic infection has periodically faltered, excellent protection from severe disease and death have been largely maintained, even among vulnerable groups such as the elderly[270,510].

It is also important to remember that many areas of the world still lack full access to high quality vaccines. For instance, some areas in Africa and eastern Europe still report vaccination rates below 10%[481]. Vaccine access for these areas is urgently needed to save lives and to prevent outbreaks among communities that likely also have less access to the medical infrastructure necessary to treat severe disease. Luckily, we have found that even a single vaccine dose can dramatically improve disease outcomes[511]. We also published a study with collaborators in Ethiopia showing that among those who previously recovered from COVID-19, a single vaccine dose was sufficient to drive antibody levels similar to those provided by a full course of two vaccine doses[512], which agrees with what we noted in the supplement of Chapter 6.

The waning that has been observed appears to primarily affect the risk of symptomatic infection, but unfortunately the rate of continued spread is tied much more strongly to the rate of symptomatic infection than to that of severe disease. In fact, having less severe infections may cause some to take less care when they are ill, which may aid transmission. Regardless, COVID-

19 cases have shown few signs of disappearing, and as of January 2023, global weekly confirmed infections have not fallen below 2.5 million since they first passed that threshold in October of 2020[80]. The continued transmission of SARS-CoV-2 suggests that vaccination alone is insufficient to reduce community spread below this threshold, but as more individuals are vaccinated and have subsequent breakthrough infections, a greater proportion of people will gain strong hybrid immunity, which may eventually drive down case counts further.

Section 10.3: Hybrid Immunity

Hybrid immunity appears to involve several key features: elevated total S-specific antibody levels, including IgG and IgA; elevated neutralizing antibody titers that better recognize variants; improved antibody effector function, capable of driving antibody-dependent phagocytosis; elimination of the age-based reduction in vaccine response; and improved antibody quality, as shown by increased neutralization potency index. This is remarkable given the significant neutralizing antibody response provided by vaccination alone, and the fairly inconsistent immune response from infection alone. It is also very interesting to see the large improvement in the quality of the hybrid immune response after extended intervals, especially against the variants. The ongoing evolution of the immune response one year post-infection indicates that antigen is likely available for continued GC responses. Another possibility is that the survival of memory B cell clones are tied to their quality, and the observed improvement has more to do with removal of lower quality clones that are shorter lived. However, this does not explain why total S-specific antibody levels are increased following longer intervals, because one would expect there to be fewer total B cells if the primary mechanism for improvement was the removal of a large fraction of total clones.

It is also quite interesting, and encouraging, that variant cross-reactivity seems to improve over time, because the hybrid immune groups used in these studies were never exposed to any of the Omicron variants. This suggests a natural shift towards more cross-reactive epitopes and/or a tendency of antibodies to become more tolerant to mutations within their binding sites. A possible mechanism for this could be the diversification of high quality clones, which one might think would be dependent on the presence of antigen. Another possibility is that spike mutations that are naturally generated during an infection are somehow allowing the immune system to sample mutational space. This would suggest, but not strictly require, some level of persistence of SARS-CoV-2, which has some support in the literature[513–516]. It has also been suggested, albeit somewhat dubiously, that mRNA vaccines may be able to rarely integrate into the genome, resulting in a small number of cells continuing to produce spike protein for an extended time[517–519]. Conventional wisdom would suggest that any such cells would be unceremoniously eliminated by CD8 killer T cells or ADCC-based mechanisms, but it is notoriously difficult to disprove rare phenomena, and it would serve as a convenient low-level source of S protein for immune training that could help dull the impact of new variants.

Section 10.4: The Variants

The rate at which new impactful variants have emerged has been an unwelcome surprise. The exact rate of change has been somewhat variable, but on average, the dominant SARS-CoV-2 strain at any time has had just over 1 S mutation for each month of the pandemic. The rate of mutation is controlled by a large number of factors, but in order for a mutation to take hold, it must occur by random chance during viral replication inside a cell, which is limited by the number of people with active infections at any given time. It is further limited by the opportunity for spread, which is in turn dictated by the number of susceptible individuals that an infected person makes

contact with while infectious, making it even more important to provide worldwide access to high quality vaccines.

Still, some mutations have had greater impacts than others, several of which were predicted ahead of time[59]. The immune context in which new SARS-CoV-2 variants must replicate and the constantly changing milieu of competing variants both determine which mutations are favored at any one time, which adds another layer of complexity and makes predictions harder. Fortunately, the built-in complexity of our immune systems and the high quality antigen provided by the vaccines has led to immune responses that are largely unaffected by small changes in the composition of the S protein. The best way to combat the slow creep of antigenic drift may simply involve releasing updated vaccines every so often, as is currently done to combat seasonal influenza. As with influenza, work is being undertaken to develop pan-coronavirus vaccines that target more conserved epitopes in order to improve variant and species cross-neutralization[520].

Section 10.5 Future Directions

There are uncountably many questions still unanswered about the immune response to SARS-CoV-2, the vaccines, and the combination thereof. My collaborators and I have had the opportunity to study unique cohorts of vaccinated and/or infected individuals which, in the very near future, will be much more difficult to assemble. We studied neutralizing antibody responses in groups with known infection histories and simple vaccination histories, but future vaccine studies will have to account for a diversity of previous vaccination timings and previous infections with unknown variants. Ever-changing variant prevalence has already created difficulties for both clinical and research studies, which will only be further complicated by the increasing magnitude of possible orders of infections and variant-specific boosters.

More specific questions which I would like to see explored include the differences in antibody glycosylation and effector function in hybrid immunity, the durability of hybrid immunity compared with boosters, and whether hybrid immune responses correlate with severity of the infection. It would also be highly interesting to learn the true mechanisms behind my key findings, such as the observed improvement in variant cross-neutralization against variants that have not yet been encountered.

I also expect to see dramatic improvements in mRNA vaccine technology driven by careful research into the existing COVID-19 vaccines. The generation of a durable neutralizing response is an important target, but there is also much to learn about how to protect from severe disease and transmission with non-neutralizing antibodies and T cells. Both non-neutralizing antibodies and T cells are more generally cross-reactive and harder for pathogens to evade, and there is strong evidence that the current COVID-19 mRNA vaccines do successfully induce long-lived T cell immunity[521]. The generation of mucosal immunity should also be a priority of future work and may involve more targeted delivery methods or optimized adjuvants.

Section 10.6: Final Thoughts

The COVID-19 pandemic is among the most studied events in human history, with over 319,000 PubMed-indexed articles as of January 2023. In 2021 alone, there were 138,418 articles posted, representing just under 18% of all indexed articles for that year (774,026). I think it is fair to say that it would be impossible for any one person to fully appreciate the entire scope of COVID-19 literature, but it is my hope that this dissertation has helped distill some of the more salient details and findings about the COVID-19 vaccines and how their effectiveness and utilization have evolved over these first three years of the pandemic. I am proud of what my collaborators and I have accomplished in this short time, only some of which I was able to include in this dissertation,

and I am grateful to the study participants who each gave a literal piece of themselves so that we might learn enough to save more lives in the future.

References Cited

1. CDC. CDC Museum COVID-19 Timeline. *Centers for Disease Control and Prevention* https://www.cdc.gov/museum/timeline/covid19.html (2022).
2. Coronavirus: Timeline. *U.S. Department of Defense* https://www.defense.gov/Explore/Spotlight/Coronavirus-DOD-Response/Timeline/.
3. Cohen, J. Where did the pandemic start? Anywhere but here, argue papers by Chinese scientists echoing party line. http://www.science.org/content/article/pandemic-start-anywhere-but-here-argue-papers-chinese-scientists-echoing-party-line.
4. Worobey, M. *et al.* The Huanan Seafood Wholesale Market in Wuhan was the early epicenter of the COVID-19 pandemic. *Science* **377**, 951–959 (2022).
5. Worobey, M. Dissecting the early COVID-19 cases in Wuhan. *Science* **374**, 1202–1204 (2021).
6. Lu, R. *et al.* Genomic characterisation and epidemiology of 2019 novel coronavirus: implications for virus origins and receptor binding. *The Lancet* **395**, 565–574 (2020).
7. Bloom, J. D. *et al.* Investigate the origins of COVID-19. *Science* **372**, 694–694 (2021).
8. Vineis, P. & Salmaso, S. The Origin of Sars-CoV-2: Why It Matters. *Front Public Health* **9**, 719914 (2021).
9. Gorbalenya, A. E. *et al.* The species Severe acute respiratory syndrome-related coronavirus : classifying 2019-nCoV and naming it SARS-CoV-2. *Nature Microbiology* **5**, 536–544 (2020).
10. Zhou, Z., Qiu, Y. & Ge, X. The taxonomy, host range and pathogenicity of coronaviruses and other viruses in the Nidovirales order. *Animal Diseases* **1**, 5 (2021).

11. Coronaviridae - Positive Sense RNA Viruses - Positive Sense RNA Viruses (2011). *International Committee on Taxonomy of Viruses (ICTV)* https://talk.ictvonline.org/ictv-reports/ictv_9th_report/positive-sense-rna-viruses-2011/w/posrna_viruses/222/coronaviridae.
12. McIntosh, K., Dees, J. H., Becker, W. B., Kapikian, A. Z. & Chanock, R. M. Recovery in tracheal organ cultures of novel viruses from patients with respiratory disease. *Proc Natl Acad Sci U S A* **57**, 933–940 (1967).
13. Almeida, J. D. & Tyrrell, D. A. The morphology of three previously uncharacterized human respiratory viruses that grow in organ culture. *J Gen Virol* **1**, 175–178 (1967).
14. Schalk, A. F. & Hawn, M. C. An apparently new respiratory disease of baby chicks. *J. Am. Vet. Med. Assoc.* **78**, 413–422 (1931).
15. Peiris, J. S. M. *et al.* Coronavirus as a possible cause of severe acute respiratory syndrome. *Lancet* **361**, 1319–1325 (2003).
16. Drosten, C. *et al.* Identification of a novel coronavirus in patients with severe acute respiratory syndrome. *N Engl J Med* **348**, 1967–1976 (2003).
17. El-Sahly, H. M., Atmar, R. L., Glezen, W. P. & Greenberg, S. B. Spectrum of Clinical Illness in Hospitalized Patients with "Common Cold" Virus Infections. *Clinical Infectious Diseases* **31**, 96–100 (2000).
18. Llanes, A. *et al.* Betacoronavirus Genomes: How Genomic Information has been Used to Deal with Past Outbreaks and the COVID-19 Pandemic. *Int J Mol Sci* **21**, 4546 (2020).
19. Khailany, R. A., Safdar, M. & Ozaslan, M. Genomic characterization of a novel SARS-CoV-2. *Gene Reports* **19**, 100682 (2020).

20. Gordon, D. E. *et al.* A SARS-CoV-2 protein interaction map reveals targets for drug repurposing. *Nature* 1–13 (2020) doi:10.1038/s41586-020-2286-9.

21. Redondo, N., Zaldívar-López, S., Garrido, J. J. & Montoya, M. SARS-CoV-2 Accessory Proteins in Viral Pathogenesis: Knowns and Unknowns. *Frontiers in Immunology* **12**, (2021).

22. Wrapp, D. *et al.* Cryo-EM structure of the 2019-nCoV spike in the prefusion conformation. *Science* **367**, 1260–1263 (2020).

23. Díaz-Salinas, M. A. *et al.* Conformational dynamics and allosteric modulation of the SARS-CoV-2 spike. *eLife* **11**, e75433 (2022).

24. Neuman, B. W. *et al.* A structural analysis of M protein in coronavirus assembly and morphology. *Journal of Structural Biology* **174**, 11–22 (2011).

25. Schoeman, D. & Fielding, B. C. Coronavirus envelope protein: current knowledge. *Virology Journal* **16**, 69 (2019).

26. Mandala, V. S. *et al.* Structure and drug binding of the SARS-CoV-2 envelope protein transmembrane domain in lipid bilayers. *Nat Struct Mol Biol* **27**, 1202–1208 (2020).

27. Zhang, Z. *et al.* Structure of SARS-CoV-2 membrane protein essential for virus assembly. *Nat Commun* **13**, 4399 (2022).

28. McBride, R., Van Zyl, M. & Fielding, B. C. The Coronavirus Nucleocapsid Is a Multifunctional Protein. *Viruses* **6**, 2991–3018 (2014).

29. Hoffmann, M. *et al.* SARS-CoV-2 Cell Entry Depends on ACE2 and TMPRSS2 and Is Blocked by a Clinically Proven Protease Inhibitor. *Cell* (2020) doi:10.1016/j.cell.2020.02.052.

30. V'kovski, P., Kratzel, A., Steiner, S., Stalder, H. & Thiel, V. Coronavirus biology and replication: implications for SARS-CoV-2. *Nat Rev Microbiol* **19**, 155–170 (2021).

31. Jackson, C. B., Farzan, M., Chen, B. & Choe, H. Mechanisms of SARS-CoV-2 entry into cells. *Nat Rev Mol Cell Biol* **23**, 3–20 (2022).

32. Bayati, A., Kumar, R., Francis, V. & McPherson, P. S. SARS-CoV-2 infects cells after viral entry via clathrin-mediated endocytosis. *J Biol Chem* **296**, 100306 (2021).

33. Klein, S. *et al.* SARS-CoV-2 structure and replication characterized by in situ cryo-electron tomography. *Nat Commun* **11**, 5885 (2020).

34. Roingeard, P. *et al.* The double-membrane vesicle (DMV): a virus-induced organelle dedicated to the replication of SARS-CoV-2 and other positive-sense single-stranded RNA viruses. *Cell Mol Life Sci* **79**, 425 (2022).

35. Moeller, N. H. *et al.* Structure and dynamics of SARS-CoV-2 proofreading exoribonuclease ExoN. *Proc. Natl. Acad. Sci. U.S.A.* **119**, e2106379119 (2022).

36. Shannon, A. *et al.* Rapid incorporation of Favipiravir by the fast and permissive viral RNA polymerase complex results in SARS-CoV-2 lethal mutagenesis. *Nat Commun* **11**, 4682 (2020).

37. Abavisani, M. *et al.* Mutations in SARS-CoV-2 structural proteins: a global analysis. *Virology Journal* **19**, 220 (2022).

38. Sanjuán, R., Nebot, M. R., Chirico, N., Mansky, L. M. & Belshaw, R. Viral Mutation Rates. *Journal of Virology* **84**, 9733–9748 (2010).

39. Elbe, S. & Buckland-Merrett, G. Data, disease and diplomacy: GISAID's innovative contribution to global health. *Global Challenges* **1**, 33–46 (2017).

40. Rambaut, A. *et al.* A dynamic nomenclature proposal for SARS-CoV-2 lineages to assist genomic epidemiology. *Nat Microbiol* **5**, 1403–1407 (2020).

41. Hadfield, J. *et al.* Nextstrain: real-time tracking of pathogen evolution. *Bioinformatics* **34**, 4121–4123 (2018).

42. Tracking SARS-CoV-2 variants. https://www.who.int/activities/tracking-SARS-CoV-2-variants.

43. Updated Nextstrain SARS-CoV-2 clade naming strategy. https://nextstrain.org//blog/2021-01-06-updated-SARS-CoV-2-clade-naming.

44. Starr, T. N. *et al.* Shifting mutational constraints in the SARS-CoV-2 receptor-binding domain during viral evolution. *Science* eabo7896 doi:10.1126/science.abo7896.

45. Giovanetti, M. *et al.* Evolution patterns of SARS-CoV-2: Snapshot on its genome variants. *Biochem Biophys Res Commun* **538**, 88–91 (2021).

46. Plante, J. A. *et al.* The variant gambit: COVID-19's next move. *Cell Host & Microbe* **29**, 508–515 (2021).

47. Khaledian, E. *et al.* Sequence determinants of human-cell entry identified in ACE2-independent bat sarbecoviruses: A combined laboratory and computational network science approach. *EBioMedicine* **79**, 103990 (2022).

48. Díez-Fuertes, F. *et al.* A Founder Effect Led Early SARS-CoV-2 Transmission in Spain. *J Virol* **95**, e01583-20 (2021).

49. Zhou, B. *et al.* SARS-CoV-2 spike D614G change enhances replication and transmission. *Nature* **592**, 122–127 (2021).

50. Collier, D. A. *et al.* Sensitivity of SARS-CoV-2 B.1.1.7 to mRNA vaccine-elicited antibodies. *Nature* 1–10 (2021) doi:10.1038/s41586-021-03412-7.

51. Dejnirattisai, W. *et al.* SARS-CoV-2 Omicron-B.1.1.529 leads to widespread escape from neutralizing antibody responses. *Cell* (2022) doi:10.1016/j.cell.2021.12.046.

52. Dejnirattisai, W. *et al.* Antibody evasion by the P.1 strain of SARS-CoV-2. *Cell* **0**, (2021).

53. Wang, Q. *et al.* Antibody evasion by SARS-CoV-2 Omicron subvariants BA.2.12.1, BA.4, & BA.5. *Nature* 1–3 (2022) doi:10.1038/s41586-022-05053-w.

54. Boehm, E. *et al.* Novel SARS-CoV-2 variants: the pandemics within the pandemic. *Clinical Microbiology and Infection* **27**, 1109–1117 (2021).

55. Levine-Tiefenbrun, M. *et al.* Viral loads of Delta-variant SARS-CoV-2 breakthrough infections after vaccination and booster with BNT162b2. *Nat Med* 1–3 (2021) doi:10.1038/s41591-021-01575-4.

56. Meng, B. *et al.* Altered TMPRSS2 usage by SARS-CoV-2 Omicron impacts infectivity and fusogenicity. *Nature* **603**, 706–714 (2022).

57. Plante, J. A. *et al.* Spike mutation D614G alters SARS-CoV-2 fitness. *Nature* **592**, 116–121 (2021).

58. Korber, B. *et al.* Tracking Changes in SARS-CoV-2 Spike: Evidence that D614G Increases Infectivity of the COVID-19 Virus. *Cell* **182**, 812-827.e19 (2020).

59. Starr, T. N. *et al.* Deep Mutational Scanning of SARS-CoV-2 Receptor Binding Domain Reveals Constraints on Folding and ACE2 Binding. *Cell* **182**, 1295-1310.e20 (2020).

60. Wang, Z. *et al.* mRNA vaccine-elicited antibodies to SARS-CoV-2 and circulating variants. *Nature* **592**, 616–622 (2021).

61. Greaney, A. J. *et al.* Complete Mapping of Mutations to the SARS-CoV-2 Spike Receptor-Binding Domain that Escape Antibody Recognition. *Cell Host Microbe* **29**, 44-57.e9 (2021).

62. Liu, Z. *et al.* Identification of SARS-CoV-2 spike mutations that attenuate monoclonal and serum antibody neutralization. *Cell Host & Microbe* **29**, 477-488.e4 (2021).

63. Pondé, R. A. A. Physicochemical effect of the N501Y, E484K/Q, K417N/T, L452R and T478K mutations on the SARS-CoV-2 spike protein RBD and its influence on agent fitness and on attributes developed by emerging variants of concern. *Virology* **572**, 44–54 (2022).

64. Zahradník, J. *et al.* SARS-CoV-2 variant prediction and antiviral drug design are enabled by RBD in vitro evolution. *Nat Microbiol* **6**, 1188–1198 (2021).

65. Greaney, A. J. *et al.* Mapping mutations to the SARS-CoV-2 RBD that escape binding by different classes of antibodies. *Nat Commun* **12**, 4196 (2021).

66. Huang, W. *et al.* Evaluation of SARS-CoV-2 transmission in COVID-19 isolation wards: On-site sampling and numerical analysis. *J Hazard Mater* **436**, 129152 (2022).

67. Zhang, Y. *et al.* A review on COVID-19 transmission, epidemiological features, prevention and vaccination. *Med Rev (Berl)* **2**, 23–49.

68. Cheng, P. *et al.* Predominant airborne transmission and insignificant fomite transmission of SARS-CoV-2 in a two-bus COVID-19 outbreak originating from the same pre-symptomatic index case. *Journal of Hazardous Materials* **425**, 128051 (2022).

69. Davis, G., Li, K., Thankam, F. G., Wilson, D. R. & Agrawal, D. K. Ocular transmissibility of COVID-19: possibilities and perspectives. *Mol Cell Biochem* **477**, 849–864 (2022).

70. Goldman, E. Exaggerated risk of transmission of COVID-19 by fomites. *Lancet Infect Dis* **20**, 892–893 (2020).

71. Lewis, D. COVID-19 rarely spreads through surfaces. So why are we still deep cleaning? *Nature* **590**, 26–28 (2021).

72. Morawska, L. & Milton, D. K. It Is Time to Address Airborne Transmission of Coronavirus Disease 2019 (COVID-19). *Clinical Infectious Diseases* **71**, 2311–2313 (2020).

73. Harbourt, D. E. *et al.* Modeling the stability of severe acute respiratory syndrome coronavirus 2 (SARS-CoV-2) on skin, currency, and clothing. *PLoS Negl Trop Dis* **14**, e0008831 (2020).

74. CDC. Healthcare Workers. *Centers for Disease Control and Prevention* https://www.cdc.gov/coronavirus/2019-ncov/hcp/infection-control-recommendations.html (2020).

75. Bazant, M. Z. & Bush, J. W. M. A guideline to limit indoor airborne transmission of COVID-19. *Proceedings of the National Academy of Sciences* **118**, e2018995118 (2021).

76. Delamater, P. L., Street, E. J., Leslie, T. F., Yang, Y. T. & Jacobsen, K. H. Complexity of the Basic Reproduction Number (R0). *Emerg Infect Dis* **25**, 1–4 (2019).

77. Dietz, K. The estimation of the basic reproduction number for infectious diseases. *Stat Methods Med Res* **2**, 23–41 (1993).

78. Guerra, F. M. *et al.* The basic reproduction number (R0) of measles: a systematic review. *The Lancet Infectious Diseases* **17**, e420–e428 (2017).

79. Kucharski, A. J. & Althaus, C. L. The role of superspreading in Middle East respiratory syndrome coronavirus (MERS-CoV) transmission. *Eurosurveillance* **20**, 21167 (2015).

80. Dong, E., Du, H. & Gardner, L. An interactive web-based dashboard to track COVID-19 in real time. *The Lancet Infectious Diseases* **20**, 533–534 (2020).

81. Havers, F. P. *et al.* Seroprevalence of Antibodies to SARS-CoV-2 in 10 Sites in the United States, March 23-May 12, 2020. *JAMA Internal Medicine* **180**, 1576–1586 (2020).

82. Qasmieh, S. A. *et al.* The prevalence of SARS-CoV-2 infection and other public health outcomes during the BA.2/BA.2.12.1 surge, New York City, April-May 2022. 2022.05.25.22275603 Preprint at https://doi.org/10.1101/2022.05.25.22275603 (2022).

83. Reese, H. *et al.* Estimated Incidence of Coronavirus Disease 2019 (COVID-19) Illness and Hospitalization—United States, February–September 2020. *Clinical Infectious Diseases* **72**, e1010–e1017 (2021).

84. Lau, H. *et al.* Evaluating the massive underreporting and undertesting of COVID-19 cases in multiple global epicenters. *Pulmonol* **27**, 110–115 (2021).

85. Moriarty, L. F. Public Health Responses to COVID-19 Outbreaks on Cruise Ships — Worldwide, February–March 2020. *MMWR Morb Mortal Wkly Rep* **69**, (2020).

86. IHME | COVID-19 Projections. *Institute for Health Metrics and Evaluation* https://covid19.healthdata.org/.

87. The pandemic's true death toll. *The Economist* https://www.economist.com/graphic-detail/coronavirus-excess-deaths-estimates.

88. Excess Deaths Associated with COVID-19. https://www.cdc.gov/nchs/nvss/vsrr/covid19/excess_deaths.htm (2022).

89. Killingley, B. *et al.* Safety, tolerability and viral kinetics during SARS-CoV-2 human challenge in young adults. *Nat Med* 1–11 (2022) doi:10.1038/s41591-022-01780-9.

90. Singanayagam, A. *et al.* Community transmission and viral load kinetics of the SARS-CoV-2 delta (B.1.617.2) variant in vaccinated and unvaccinated individuals in the UK: a prospective, longitudinal, cohort study. *Lancet Infect Dis* S1473-3099(21)00648–4 (2021) doi:10.1016/S1473-3099(21)00648-4.

91. Lakdawala, S. S. & Menachery, V. D. Catch Me if You Can: Superspreading of COVID-19. *Trends Microbiol* **29**, 919–929 (2021).

92. Edwards, D. A. *et al.* Exhaled aerosol increases with COVID-19 infection, age, and obesity. *Proceedings of the National Academy of Sciences* **118**, e2021830118 (2021).

93. Tsang, T. K. *et al.* The effect of variation of individual infectiousness on SARS-CoV-2 transmission in households. *eLife* **12**, e82611.

94. Ziegler, C. G. K. *et al.* SARS-CoV-2 Receptor ACE2 Is an Interferon-Stimulated Gene in Human Airway Epithelial Cells and Is Detected in Specific Cell Subsets across Tissues. *Cell* **181**, 1016-1035.e19 (2020).

95. Lamers, M. M. & Haagmans, B. L. SARS-CoV-2 pathogenesis. *Nat Rev Microbiol* **20**, 270–284 (2022).

96. Liu, J. *et al.* SARS-CoV-2 cell tropism and multiorgan infection. *Cell Discov* **7**, 1–4 (2021).

97. Delorey, T. M. *et al.* COVID-19 tissue atlases reveal SARS-CoV-2 pathology and cellular targets. *Nature* **595**, 107–113 (2021).

98. Samavati, L. & Uhal, B. D. ACE2, Much More Than Just a Receptor for SARS-COV-2. *Frontiers in Cellular and Infection Microbiology* **10**, (2020).

99. Ghimire, S. *et al.* Diarrhea Is Associated with Increased Severity of Disease in COVID-19: Systemic Review and Metaanalysis. *SN Compr Clin Med* **3**, 28–35 (2021).

100. Osuchowski, M. F. *et al.* The COVID-19 puzzle: deciphering pathophysiology and phenotypes of a new disease entity. *The Lancet Respiratory Medicine* **9**, 622–642 (2021).

101. Barbaro, R. P. *et al.* Extracorporeal membrane oxygenation for COVID-19: evolving outcomes from the international Extracorporeal Life Support Organization Registry. *The Lancet* **398**, 1230–1238 (2021).

102. Clinical Spectrum. *COVID-19 Treatment Guidelines* https://www.covid19treatmentguidelines.nih.gov/overview/clinical-spectrum/.

103. Dessie, Z. G. & Zewotir, T. Mortality-related risk factors of COVID-19: a systematic review and meta-analysis of 42 studies and 423,117 patients. *BMC Infect Dis* **21**, 855 (2021).

104. CDC. Cases, Data, and Surveillance. *Centers for Disease Control and Prevention* https://www.cdc.gov/coronavirus/2019-ncov/covid-data/investigations-discovery/hospitalization-death-by-age.html (2020).

105. Griffin, J. B. *et al.* SARS-CoV-2 Infections and Hospitalizations Among Persons Aged ≥16 Years, by Vaccination Status - Los Angeles County, California, May 1-July 25, 2021. *MMWR Morb Mortal Wkly Rep* **70**, 1170–1176 (2021).

106. Wang, C. *et al.* Differences in incidence and fatality of COVID-19 by SARS-CoV-2 Omicron variant versus Delta variant in relation to vaccine coverage: A world-wide review. *J Med Virol* 10.1002/jmv.28118 (2022) doi:10.1002/jmv.28118.

107. Abu-Raddad, L. J. *et al.* Severity, Criticality, and Fatality of the Severe Acute Respiratory Syndrome Coronavirus 2 (SARS-CoV-2) Beta Variant. *Clinical Infectious Diseases* **75**, e1188–e1191 (2022).

108. Yek, C., Warner, S., Mancera, A. & Kadri, S. S. Misclassification bias in estimating clinical severity of SARS-CoV-2 variants. *The Lancet* **400**, 809 (2022).

109. Merad, M., Blish, C. A., Sallusto, F. & Iwasaki, A. The immunology and immunopathology of COVID-19. *Science* **375**, 1122–1127 (2022).

110. Asakura, H. & Ogawa, H. COVID-19-associated coagulopathy and disseminated intravascular coagulation. *Int J Hematol* **113**, 45–57 (2021).

111. Castanares-Zapatero, D. *et al.* Pathophysiology and mechanism of long COVID: a comprehensive review. *Ann Med* **54**, 1473–1487.

112. Killerby, M. E. *et al.* Human coronavirus circulation in the United States 2014–2017. *Journal of Clinical Virology* **101**, 52–56 (2018).

113. Moss, P. The T cell immune response against SARS-CoV-2. *Nat Immunol* **23**, 186–193 (2022).

114. Notarbartolo, S. *et al.* Integrated longitudinal immunophenotypic, transcriptional and repertoire analyses delineate immune responses in COVID-19 patients. *Sci Immunol* **6**, eabg5021 (2021).

115. Wherry, E. J. & Barouch, D. H. T cell immunity to COVID-19 vaccines. *Science* **377**, 821–822 (2022).

116. Bange, E. M. *et al.* CD8+ T cells contribute to survival in patients with COVID-19 and hematologic cancer. *Nat Med* **27**, 1280–1289 (2021).

117. Tarke, A. *et al.* Comprehensive analysis of T cell immunodominance and immunoprevalence of SARS-CoV-2 epitopes in COVID-19 cases. *Cell Rep Med* **2**, 100204 (2021).

118. Swain, S. L., McKinstry, K. K. & Strutt, T. M. Expanding roles for CD4+ T cells in immunity to viruses. *Nat Rev Immunol* **12**, 136–148 (2012).

119. Chen, J. S. *et al.* High-affinity, neutralizing antibodies to SARS-CoV-2 can be made without T follicular helper cells. *Science Immunology* **7**, eabl5652 (2021).

120. Zhao, J. *et al.* Antibody Responses to SARS-CoV-2 in Patients With Novel Coronavirus Disease 2019. *Clinical Infectious Diseases* **71**, 2027–2034 (2020).

121. Carrillo, J. *et al.* Humoral immune responses and neutralizing antibodies against SARS-CoV-2; implications in pathogenesis and protective immunity. *Biochemical and Biophysical Research Communications* **538**, 187–191 (2021).

122. Dias, S., Xu, W., Graves, S. & Kee, B. Current Opinions in Genetics and Development: Transcriptional Regulation of Lymphocyte Development. *Curr Opin Genet Dev* **18**, 441–448 (2008).

123. Garcia-Beltran, W. F. *et al.* COVID-19-neutralizing antibodies predict disease severity and survival. *Cell* **184**, 476-488.e11 (2021).

124. Dispinseri, S. *et al.* Neutralizing antibody responses to SARS-CoV-2 in symptomatic COVID-19 is persistent and critical for survival. *Nature Communications* **12**, 2670 (2021).

125. Khoury, D. S. *et al.* Neutralizing antibody levels are highly predictive of immune protection from symptomatic SARS-CoV-2 infection. *Nature Medicine* 1–7 (2021) doi:10.1038/s41591-021-01377-8.

126. Pantaleo, G. & Koup, R. A. Correlates of immune protection in HIV-1 infection: what we know, what we don't know, what we should know. *Nat Med* **10**, 806–810 (2004).

127. Arvin, A. M. IMMUNE RESPONSES TO VARICELLA-ZOSTER VIRUS* *Studies discribed in this article were supported by Public Health Service Grants AI 20459, AI 22280, and AI 18499 from the National Institute of Allerge and Infectious Disease, by Merck Research Laboratories, and by the National Cancer Institute (CA 49605). *Infectious Disease Clinics of North America* **10**, 529–570 (1996).

128. Carter, J. J. & Galloway, D. A. Humoral immune response to human papillomavirus infection. *Clinics in Dermatology* **15**, 229–236 (1997).

129. Bertoletti, A. & Ferrari, C. Kinetics of the immune response during HBV and HCV infection. *Hepatology* **38**, 4–13 (2003).

130. Griffin, D. E. Immune responses during measles virus infection. *Curr Top Microbiol Immunol* **191**, 117–134 (1995).

131. Seet, B. T. *et al.* Poxviruses and immune evasion. *Annu Rev Immunol* **21**, 377–423 (2003).

132. Huang, Q., Han, X. & Yan, J. Structure-based neutralizing mechanisms for SARS-CoV-2 antibodies. *Emerging Microbes & Infections* **11**, 2412–2422 (2022).

133. Taylor, P. C. *et al.* Neutralizing monoclonal antibodies for treatment of COVID-19. *Nature Reviews Immunology* 1–12 (2021) doi:10.1038/s41577-021-00542-x.

134. Suryadevara, N. *et al.* Neutralizing and protective human monoclonal antibodies recognizing the N-terminal domain of the SARS-CoV-2 spike protein. *Cell* **184**, 2316-2331.e15 (2021).

135. Zohar, T. & Alter, G. Dissecting antibody-mediated protection against SARS-CoV-2. *Nat Rev Immunol* 1–3 (2020) doi:10.1038/s41577-020-0359-5.

136. Forthal, D. N. Functions of Antibodies. *Microbiol Spectr* **2**, 1–17 (2014).

137. Siewert, L. K. *et al.* Identification of the Bartonella autotransporter CFA as a protective antigen and hypervariable target of neutralizing antibodies in mice. *Proceedings of the National Academy of Sciences* **119**, e2202059119 (2022).

138. Abdelnoor, A. M., Harvie, N. R. & Johnson, A. G. Neutralization of bacteria- and endotoxin-induced hypotension by lipoprotein-free human serum. *Infection and Immunity* **38**, 157–161 (1982).

139. Lu, L. L., Suscovich, T. J., Fortune, S. M. & Alter, G. Beyond binding: antibody effector functions in infectious diseases. *Nat Rev Immunol* **18**, 46–61 (2018).

140. Weiskopf, K. & Weissman, I. L. Macrophages are critical effectors of antibody therapies for cancer. *MAbs* **7**, 303–310 (2015).

141. Phelps, M. & Balazs, A. B. Contribution to HIV Prevention and Treatment by Antibody-Mediated Effector Function and Advances in Broadly Neutralizing Antibody Delivery by Vectored Immunoprophylaxis. *Front Immunol* **12**, 734304 (2021).

142. Tyler, D. S., Lyerly, H. K. & Weinhold, K. J. Minireview Anti-HIV-1 ADCC. *AIDS Research and Human Retroviruses* **5**, 557–563 (1989).

143. Dans, A. L., Dans, L. F., Lansang, M. A. D., Silvestre, M. A. A. & Guyatt, G. H. Controversy and debate on dengue vaccine series-paper 1: review of a licensed dengue vaccine: inappropriate subgroup analyses and selective reporting may cause harm in mass vaccination programs. *J Clin Epidemiol* **95**, 137–139 (2018).

144. Jennewein, M. F. & Alter, G. The Immunoregulatory Roles of Antibody Glycosylation. *Trends in Immunology* **38**, 358–372 (2017).

145. Brezski, R. J. & Georgiou, G. Immunoglobulin isotype knowledge and application to Fc engineering. *Current Opinion in Immunology* **40**, 62–69 (2016).

146. Chiu, M. L., Goulet, D. R., Teplyakov, A. & Gilliland, G. L. Antibody Structure and Function: The Basis for Engineering Therapeutics. *Antibodies* **8**, 55 (2019).

147. Lobner, E., Traxlmayr, M. W., Obinger, C. & Hasenhindl, C. Engineered IgG1-Fc--one fragment to bind them all. *Immunol Rev* **270**, 113–131 (2016).

148. Shi, L., Liu, T., Gross, M. L. & Huang, Y. Recognition of Human IgG1 by Fcγ Receptors: Structural Insights from Hydrogen-Deuterium Exchange and Fast Photochemical Oxidation of Proteins Coupled with Mass Spectrometry. *Biochemistry* **58**, 1074–1080 (2019).

149. Yu, J., Song, Y. & Tian, W. How to select IgG subclasses in developing anti-tumor therapeutic antibodies. *J Hematol Oncol* **13**, 45 (2020).

150. Damelang, T., Rogerson, S. J., Kent, S. J. & Chung, A. W. Role of IgG3 in Infectious Diseases. *Trends in Immunology* **40**, 197–211 (2019).

151. Steffen, U. *et al.* IgA subclasses have different effector functions associated with distinct glycosylation profiles. *Nat Commun* **11**, 120 (2020).

152. Russell, M. W., Moldoveanu, Z., Ogra, P. L. & Mestecky, J. Mucosal Immunity in COVID-19: A Neglected but Critical Aspect of SARS-CoV-2 Infection. *Front Immunol* **11**, 611337 (2020).

153. Chavda, V. P., Vora, L. K., Pandya, A. K. & Patravale, V. B. Intranasal vaccines for SARS-CoV-2: From challenges to potential in COVID-19 management. *Drug Discov Today* **26**, 2619–2636 (2021).

154. Quinti, I., Mortari, E. P., Fernandez Salinas, A., Milito, C. & Carsetti, R. IgA Antibodies and IgA Deficiency in SARS-CoV-2 Infection. *Front Cell Infect Microbiol* **11**, 655896 (2021).

155. LeBien, T. W. & Tedder, T. F. B lymphocytes: how they develop and function. *Blood* **112**, 1570–1580 (2008).

156. Moh, E. S. X., Lin, C.-H., Thaysen-Andersen, M. & Packer, N. H. Site-Specific N-Glycosylation of Recombinant Pentameric and Hexameric Human IgM. *J. Am. Soc. Mass Spectrom.* **27**, 1143–1155 (2016).

157. Sharp, T. H. *et al.* Insights into IgM-mediated complement activation based on in situ structures of IgM-C1-C4b. *Proceedings of the National Academy of Sciences* **116**, 11900–11905 (2019).

158. Keyt, B. A., Baliga, R., Sinclair, A. M., Carroll, S. F. & Peterson, M. S. Structure, Function, and Therapeutic Use of IgM Antibodies. *Antibodies (Basel)* **9**, 53 (2020).

159. Zeitlin, L. *et al.* Enhanced potency of a fucose-free monoclonal antibody being developed as an Ebola virus immunoprotectant. *Proceedings of the National Academy of Sciences* **108**, 20690–20694 (2011).

160. Umaña, P., Jean-Mairet, J., Moudry, R., Amstutz, H. & Bailey, J. E. Engineered glycoforms of an antineuroblastoma IgG1 with optimized antibody-dependent cellular cytotoxic activity. *Nat Biotechnol* **17**, 176–180 (1999).

161. Shields, R. L. *et al.* Lack of fucose on human IgG1 N-linked oligosaccharide improves binding to human Fcgamma RIII and antibody-dependent cellular toxicity. *J Biol Chem* **277**, 26733–26740 (2002).

162. Kaneko, Y., Nimmerjahn, F. & Ravetch, J. V. Anti-Inflammatory Activity of Immunoglobulin G Resulting from Fc Sialylation. *Science* **313**, 670–673 (2006).

163. Washburn, N. *et al.* Controlled tetra-Fc sialylation of IVIg results in a drug candidate with consistent enhanced anti-inflammatory activity. *Proceedings of the National Academy of Sciences* **112**, E1297–E1306 (2015).

164. Thomann, M., Reckermann, K., Reusch, D., Prasser, J. & Tejada, M. L. Fc-galactosylation modulates antibody-dependent cellular cytotoxicity of therapeutic antibodies. *Molecular Immunology* **73**, 69–75 (2016).

165. Karsten, C. M. *et al.* Anti-inflammatory activity of IgG1 mediated by Fc galactosylation and association of FcγRIIB and dectin-1. *Nat Med* **18**, 1401–1406 (2012).

166. Nishima, W., Miyashita, N., Yamaguchi, Y., Sugita, Y. & Re, S. Effect of Bisecting GlcNAc and Core Fucosylation on Conformational Properties of Biantennary Complex-Type N-Glycans in Solution. *J. Phys. Chem. B* **116**, 8504–8512 (2012).

167. González-Morelo, K. J., Vega-Sagardía, M. & Garrido, D. Molecular Insights Into O-Linked Glycan Utilization by Gut Microbes. *Frontiers in Microbiology* **11**, (2020).

168. Barratt, J., Smith, A. C. & Feehally, J. The pathogenic role of IgA1 O-linked glycosylation in the pathogenesis of IgA nephropathy (Review Article). *Nephrology* **12**, 275–284 (2007).

169. Ohyama, Y. *et al.* Analysis of O-glycoforms of the IgA1 hinge region by sequential deglycosylation. *Sci Rep* **10**, 671 (2020).

170. Klarić, L. *et al.* Glycosylation of immunoglobulin G is regulated by a large network of genes pleiotropic with inflammatory diseases. *Science Advances* **6**, eaax0301 (2020).

171. Sun, Y., Huang, T., Hammarström, L. & Zhao, Y. The Immunoglobulins: New Insights, Implications, and Applications. *Annu Rev Anim Biosci* **8**, 145–169 (2020).

172. Ribatti, D., Crivellato, E. & Vacca, A. The contribution of Bruce Glick to the definition of the role played by the bursa of Fabricius in the development of the B cell lineage. *Clin Exp Immunol* **145**, 1–4 (2006).

173. Zhao, Y. *et al.* Identification of IgF, a hinge-region-containing Ig class, and IgD in Xenopus tropicalis. *Proceedings of the National Academy of Sciences* **103**, 12087–12092 (2006).

174. Khalid, Z. *et al.* IgNAR antibody: Structural features, diversity and applications. *Fish & Shellfish Immunology* **121**, 467–477 (2022).

175. Greenberg, A. S. *et al.* A new antigen receptor gene family that undergoes rearrangement and extensive somatic diversification in sharks. *Nature* **374**, 168–73 (1995).

176. Chi, X., Li, Y. & Qiu, X. V(D)J recombination, somatic hypermutation and class switch recombination of immunoglobulins: mechanism and regulation. *Immunology* **160**, 233–247 (2020).

177. Schatz, D. G., Oettinger, M. A. & Baltimore, D. The V(D)J recombination activating gene, RAG-1. *Cell* **59**, 1035–1048 (1989).

178. Mikocziova, I., Greiff, V. & Sollid, L. M. Immunoglobulin germline gene variation and its impact on human disease. *Genes Immun* **22**, 205–217 (2021).

179. Winkler, T. H. & Mårtensson, I.-L. The Role of the Pre-B Cell Receptor in B Cell Development, Repertoire Selection, and Tolerance. *Frontiers in Immunology* **9**, (2018).

180. Alberts, B. *et al.* The Generation of Antibody Diversity. *Molecular Biology of the Cell. 4th edition* (2002).

181. Briney, B., Inderbitzin, A., Joyce, C. & Burton, D. R. Commonality despite exceptional diversity in the baseline human antibody repertoire. *Nature* **566**, 393–397 (2019).

182. Cambier, J. C., Gauld, S. B., Merrell, K. T. & Vilen, B. J. B-cell anergy: from transgenic models to naturally occurring anergic B cells? *Nat Rev Immunol* **7**, 633–643 (2007).

183. Halperin, B. A. *et al.* Kinetics of the antibody response to tetanus-diphtheria-acellular pertussis vaccine in women of childbearing age and postpartum women. *Clin Infect Dis* **53**, 885–892 (2011).

184. Kardava, L. *et al.* Early human B cell signatures of the primary antibody response to mRNA vaccination. *Proc Natl Acad Sci U S A* **119**, e2204607119 (2022).

185. Ibarrondo, F. J. *et al.* Primary, Recall, and Decay Kinetics of SARS-CoV-2 Vaccine Antibody Responses. *ACS Nano* **15**, 11180–11191 (2021).

186. Welliver, R. C. *et al.* The antibody response to primary and secondary infection with respiratory syncytial virus: kinetics of class-specific responses. *J Pediatr* **96**, 808–813 (1980).

187. Kawai, R. *et al.* Evaluation of canine T-cell dependent antibody response to the primary and secondary immunization with keyhole limpet hemocyanin. *J Toxicol Sci* **38**, 571–579 (2013).

188. Sande, C. *et al.* Kinetics of the Neutralizing Antibody Response to Respiratory Syncytial Virus Infections in a Birth Cohort. *J Med Virol* **85**, 2020–2025 (2013).

189. Jaffe, D. B. *et al.* Functional antibodies exhibit light chain coherence. *Nature* **611**, 352–357 (2022).

190. Morbach, H., Eichhorn, E. M., Liese, J. G. & Girschick, H. J. Reference values for B cell subpopulations from infancy to adulthood. *Clin Exp Immunol* **162**, 271–279 (2010).

191. Coutinho, A. & Möller, G. Thymus-independent B-cell induction and paralysis. *Adv Immunol* **21**, 113–236 (1975).

192. Zhou, Y. *et al.* Transitional B cells involved in autoimmunity and their impact on neuroimmunological diseases. *Journal of Translational Medicine* **18**, 131 (2020).

193. MacLennan, I. C. M. *et al.* Extrafollicular antibody responses. *Immunological Reviews* **194**, 8–18 (2003).

194. Jacob, J., Kelsoe, G., Rajewsky, K. & Weiss, U. Intraclonal generation of antibody mutants in germinal centres. *Nature* **354**, 389–392 (1991).

195. Mesin, L., Ersching, J. & Victora, G. D. GERMINAL CENTER B CELL DYNAMICS. *Immunity* **45**, 471–482 (2016).

196. Akkaya, M., Kwak, K. & Pierce, S. K. B cell memory: building two walls of protection against pathogens. *Nat Rev Immunol* **20**, 229–238 (2020).

197. Xu, Z., Zan, H., Pone, E. J., Mai, T. & Casali, P. Immunoglobulin class-switch DNA recombination: induction, targeting and beyond. *Nat Rev Immunol* **12**, 517–531 (2012).

198. Ruggiero, A. *et al.* SARS-CoV-2 vaccination elicits unconventional IgM specific responses in naïve and previously COVID-19-infected individuals. *eBioMedicine* **77**, (2022).

199. Legros, V. *et al.* A longitudinal study of SARS-CoV-2-infected patients reveals a high correlation between neutralizing antibodies and COVID-19 severity. *Cell Mol Immunol* **18**, 318–327 (2021).

200. Garcia, L. *et al.* Kinetics of the SARS-CoV-2 Antibody Avidity Response Following Infection and Vaccination. *Viruses* **14**, 1491 (2022).

201. Wei, J. *et al.* Anti-spike antibody response to natural SARS-CoV-2 infection in the general population. *Nat Commun* **12**, 6250 (2021).

202. Lyski, Z. L. *et al.* Severe Acute Respiratory Syndrome Coronavirus 2 (SARS-CoV-2)–Specific Memory B Cells From Individuals With Diverse Disease Severities Recognize SARS-CoV-2 Variants of Concern. *J Infect Dis* **225**, 947–956 (2021).

203. Turner, J. S. *et al.* SARS-CoV-2 infection induces long-lived bone marrow plasma cells in humans. *Nature* **595**, 421–425 (2021).

204. Turner, J. S. *et al.* SARS-CoV-2 mRNA vaccines induce persistent human germinal centre responses. *Nature* **596**, 109–113 (2021).

205. Gray, D. A role for antigen in the maintenance of immunological memory. *Nat Rev Immunol* **2**, 60–65 (2002).

206. Carrasco, Y. R. & Batista, F. D. B cell recognition of membrane-bound antigen: an exquisite way of sensing ligands. *Curr Opin Immunol* **18**, 286–291 (2006).

207. Wienands, J. & Engels, N. The Memory Function of the B Cell Antigen Receptor. in *B Cell Receptor Signaling* (eds. Kurosaki, T. & Wienands, J.) 107–121 (Springer International Publishing, 2016). doi:10.1007/82_2015_480.

208. Holmes, E. Novel 2019 coronavirus genome. *Virological* https://virological.org/t/novel-2019-coronavirus-genome/319 (2020).

209. Dinnes, J. *et al.* Rapid, point-of-care antigen and molecular-based tests for diagnosis of SARS-CoV-2 infection. *Cochrane Database Syst Rev* **2020**, CD013705 (2020).

210. CDC. EUA Authorized Serology Test Performance. *FDA* (2022).

211. Oliver, S. E. The Advisory Committee on Immunization Practices' Interim Recommendation for Use of Pfizer-BioNTech COVID-19 Vaccine — United States, December 2020. *MMWR Morb Mortal Wkly Rep* **69**, (2020).

212. Oliver, S. E. The Advisory Committee on Immunization Practices' Interim Recommendation for Use of Moderna COVID-19 Vaccine — United States, December 2020. *MMWR Morb Mortal Wkly Rep* **69**, (2021).

213. Feikin, D. R. *et al.* Duration of effectiveness of vaccines against SARS-CoV-2 infection and COVID-19 disease: results of a systematic review and meta-regression. *Lancet* **399**, 924–944 (2022).

214. Falsey, A. R. *et al.* Phase 3 Safety and Efficacy of AZD1222 (ChAdOx1 nCoV-19) Covid-19 Vaccine. *N Engl J Med* NEJMoa2105290 (2021) doi:10.1056/NEJMoa2105290.

215. Bergman, P. *et al.* Safety and efficacy of the mRNA BNT162b2 vaccine against SARS-CoV-2 in five groups of immunocompromised patients and healthy controls in a prospective open-label clinical trial. *EBioMedicine* **74**, 103705 (2021).

216. Mahallawi, W. H. & Mumena, W. A. Reactogenicity and Immunogenicity of the Pfizer and AstraZeneca COVID-19 Vaccines. *Frontiers in Immunology* **12**, (2021).

217. Regev-Yochay, G. *et al.* Efficacy of a Fourth Dose of Covid-19 mRNA Vaccine against Omicron. *N Engl J Med* **386**, 1377–1380 (2022).

218. Supasa, P. *et al.* Reduced neutralization of SARS-CoV-2 B.1.1.7 variant by convalescent and vaccine sera. *Cell* **0**, (2021).

219. Saadat, S. *et al.* Binding and Neutralization Antibody Titers After a Single Vaccine Dose in Health Care Workers Previously Infected With SARS-CoV-2. *JAMA* (2021) doi:10.1001/jama.2021.3341.

220. Dulbecco, R. Production of Plaques in Monolayer Tissue Cultures by Single Particles of an Animal Virus. *Proc Natl Acad Sci U S A* **38**, 747–752 (1952).

221. Mendoza, E. J., Manguiat, K., Wood, H. & Drebot, M. Two Detailed Plaque Assay Protocols for the Quantification of Infectious SARS-CoV-2. *Curr Protoc Microbiol* **57**, cpmc105 (2020).

222. Case, J. B., Bailey, A. L., Kim, A. S., Chen, R. E. & Diamond, M. S. Growth, detection, quantification, and inactivation of SARS-CoV-2. *Virology* **548**, 39–48 (2020).

223. Masci, A. L. *et al.* Integration of Fluorescence Detection and Image-Based Automated Counting Increases Speed, Sensitivity, and Robustness of Plaque Assays. *Molecular Therapy - Methods & Clinical Development* **14**, 270–274 (2019).

224. Hofmann, N., Grossegesse, M., Neumann, M., Schaade, L. & Nitsche, A. Evaluation of a commercial ELISA as alternative to plaque reduction neutralization test to detect neutralizing antibodies against SARS-CoV-2. *Sci Rep* **12**, 3549 (2022).

225. Murray, M. J. *et al.* Validation of a commercially available indirect assay for SARS-CoV-2 neutralising antibodies using a pseudotyped virus assay. *Journal of Infection* **82**, 170–177 (2021).

226. Crawford, K. H. D. *et al.* Protocol and Reagents for Pseudotyping Lentiviral Particles with SARS-CoV-2 Spike Protein for Neutralization Assays. *Viruses* **12**, 513 (2020).

227. Muik, A. *et al.* Neutralization of SARS-CoV-2 lineage B.1.1.7 pseudovirus by BNT162b2 vaccine–elicited human sera. *Science* (2021) doi:10.1126/science.abg6105.

228. Gilbert, P. B. *et al.* Immune correlates analysis of the mRNA-1273 COVID-19 vaccine efficacy clinical trial. *Science* **375**, 43–50.

229. Folegatti, P. M. *et al.* Safety and immunogenicity of the ChAdOx1 nCoV-19 vaccine against SARS-CoV-2: a preliminary report of a phase 1/2, single-blind, randomised controlled trial. *Lancet* **396**, 467–478 (2020).

230. Syed, A. M. *et al.* Rapid assessment of SARS-CoV-2–evolved variants using virus-like particles. *Science* **374**, 1626–1632 (2021).

231. Vial, C. *et al.* Comparison of VSV Pseudovirus and Focus Reduction Neutralization Assays for Measurement of Anti-Andes orthohantavirus Neutralizing Antibodies in Patient Samples. *Frontiers in Cellular and Infection Microbiology* **10**, (2020).

232. Tolah, A. M. K. *et al.* Evaluation of a Pseudovirus Neutralization Assay for SARS-CoV-2 and Correlation with Live Virus-Based Micro Neutralization Assay. *Diagnostics (Basel)* **11**, 994 (2021).

233. Poon, M. M. L. *et al.* SARS-CoV-2 infection generates tissue-localized immunological memory in humans. *Science Immunology* (2021) doi:10.1126/sciimmunol.abl9105.

234. Kotagiri, P. *et al.* B cell receptor repertoire kinetics after SARS-CoV-2 infection and vaccination. *Cell Reports* **38**, 110393 (2022).

235. Tong, P. *et al.* Memory B cell repertoire for recognition of evolving SARS-CoV-2 spike. *Cell* **184**, 4969-4980.e15 (2021).

236. Galson, J. D. *et al.* Deep Sequencing of B Cell Receptor Repertoires From COVID-19 Patients Reveals Strong Convergent Immune Signatures. *Frontiers in Immunology* **11**, (2020).

237. Setliff, I. *et al.* High-Throughput Mapping of B Cell Receptor Sequences to Antigen Specificity. *Cell* **179**, 1636-1646.e15 (2019).

238. Ehling, R. A. *et al.* SARS-CoV-2 reactive and neutralizing antibodies discovered by single-cell sequencing of plasma cells and mammalian display. *Cell Reports* **38**, (2022).

239. Muñoz-Fontela, C. *et al.* Animal models for COVID-19. *Nature* **586**, 509–515 (2020).

240. Chu, H., Chan, J. F.-W. & Yuen, K.-Y. Animal models in SARS-CoV-2 research. *Nat Methods* **19**, 392–394 (2022).

241. Kim, J., Koo, B.-K. & Knoblich, J. A. Human organoids: model systems for human biology and medicine. *Nat Rev Mol Cell Biol* **21**, 571–584 (2020).

242. Baptista, L. S., Porrini, C., Kronemberger, G. S., Kelly, D. J. & Perrault, C. M. 3D organ-on-a-chip: The convergence of microphysiological systems and organoids. *Frontiers in Cell and Developmental Biology* **10**, (2022).

243. Rapeport, G. *et al.* SARS-CoV-2 Human Challenge Studies — Establishing the Model during an Evolving Pandemic. *New England Journal of Medicine* **385**, 961–964 (2021).

244. Singh, J. & Aballay, A. Neuro-immune circuits in C. elegans. *Curr Opin Neurobiol* **62**, 34–40 (2020).

245. Perdue, P. C. *China Marches West: The Qing Conquest of Central Eurasia*. (Harvard University Press, 2005).

246. Plotkin, S. A. Vaccines: past, present and future. *Nat Med* **11**, S5–S11 (2005).

247. Yutu, J. A., Jing, M. & Guang, X. H. Outbreaks of smallpox due to variolation in China, 1962-1965. *Am J Epidemiol* **128**, 39–45 (1988).

248. White, P. J. & Shackelford, P. G. Edward Jenner, MD, and the Scourge That Was. *American Journal of Diseases of Children* **137**, 864–869 (1983).

249. Molteni, C., Forni, D., Cagliani, R., Clerici, M. & Sironi, M. Genetic ancestry and population structure of vaccinia virus. *npj Vaccines* **7**, 1–9 (2022).

250. Pasteur, L. *La vaccination charbonneuse*. (G. Baillière, 1883).

251. Kolmer, J. A. Vaccination Against Acute Anterior Poliomyelitis. *Am J Public Health Nations Health* **26**, 126–135 (1936).

252. Salk, J. E. *et al.* Formaldehyde Treatment and Safety Testing of Experimental Poliomyelitis Vaccines. *Am J Public Health Nations Health* **44**, 563–570 (1954).

253. Plotkin, S. A. Vaccines: the Fourth Century. *Clin Vaccine Immunol* **16**, 1709–1719 (2009).

254. McAleer, W. J. *et al.* Human hepatitis B vaccine from recombinant yeast. *Nature* **307**, 178–180 (1984).

255. Firdaus, F. Z., Skwarczynski, M. & Toth, I. Developments in Vaccine AdjuvantsAdjuvants. in *Vaccine Design: Methods and Protocols, Volume 3. Resources for Vaccine Development* (ed. Thomas, S.) 145–178 (Springer US, 2022). doi:10.1007/978-1-0716-1892-9_8.

256. Rose, R. C., Bonnez, W., Reichman, R. C. & Garcea, R. L. Expression of Human Papillomavirus Type 11 Li Protein in Insect Cells: In Vivo and In Vitro Assembly of Viruslike Particles. *J. VIROL.*

257. Vaccine Types | NIH: National Institute of Allergy and Infectious Diseases. https://www.niaid.nih.gov/research/vaccine-types.

258. Houser, K. V. *et al.* Safety and immunogenicity of a ferritin nanoparticle H2 influenza vaccine in healthy adults: a phase 1 trial. *Nat Med* **28**, 383–391 (2022).

259. Nooraei, S. *et al.* Virus-like particles: preparation, immunogenicity and their roles as nanovaccines and drug nanocarriers. *Journal of Nanobiotechnology* **19**, 59 (2021).

260. de Vries, R. D. & Rimmelzwaan, G. F. Viral vector-based influenza vaccines. *Hum Vaccin Immunother* **12**, 2881–2901 (2016).

261. FDA. FDA Takes Key Action in Fight Against COVID-19 By Issuing Emergency Use Authorization for First COVID-19 Vaccine. *FDA* https://www.fda.gov/news-events/press-announcements/fda-takes-key-action-fight-against-covid-19-issuing-emergency-use-authorization-first-covid-19 (2020).

262. Polack, F. P. *et al.* Safety and Efficacy of the BNT162b2 mRNA Covid-19 Vaccine. *N Engl J Med* **383**, 2603–2615 (2020).

263. Baden, L. R. *et al.* Efficacy and Safety of the mRNA-1273 SARS-CoV-2 Vaccine. *N Engl J Med* (2020) doi:10.1056/NEJMoa2035389.

264. Center for Biologics Evaluation and Research. Novavax COVID-19 Vaccine, Adjuvanted. *FDA* (2022).

265. Dunkle, L. M. *et al.* Efficacy and Safety of NVX-CoV2373 in Adults in the United States and Mexico. *New England Journal of Medicine* **386**, 531–543 (2022).

266. Sadoff, J. *et al.* Safety and Efficacy of Single-Dose Ad26.COV2.S Vaccine against Covid-19. *New England Journal of Medicine* (2021) doi:10.1056/NEJMoa2101544.

267. FDA. Coronavirus (COVID-19) Update: FDA Authorizes Moderna, Pfizer-BioNTech Bivalent COVID-19 Vaccines for Use as a Booster Dose. *FDA* https://www.fda.gov/news-events/press-announcements/coronavirus-covid-19-update-fda-authorizes-moderna-pfizer-biontech-bivalent-covid-19-vaccines-use (2022).

268. New Covid boosters, which target BA.5, haven't yet been tested in people. How well will they work? *NBC News* https://www.nbcnews.com/health/health-news/fda-authorize-new-covid-boosters-data-tests-people-rcna45387.

269. Chalkias, S. *et al.* A Bivalent Omicron-Containing Booster Vaccine against Covid-19. *N Engl J Med* (2022) doi:10.1056/NEJMoa2208343.

270. Tenforde, M. W. Early Estimates of Bivalent mRNA Vaccine Effectiveness in Preventing COVID-19–Associated Emergency Department or Urgent Care Encounters and Hospitalizations Among Immunocompetent Adults — VISION Network, Nine States, September–November 2022. *MMWR Morb Mortal Wkly Rep* **71**, (2022).

271. Sanofi-Aventis. Press Release: Sanofi and GSK's next-generation COVID-19 booster vaccine VidPrevtyn® Beta approved by the European Commission. *GlobeNewswire News Room* https://www.globenewswire.com/news-release/2022/11/10/2553486/0/en/Press-Release-Sanofi-and-GSK-s-next-generation-COVID-19-booster-vaccine-VidPrevtyn-Beta-approved-by-the-European-Commission.html (2022).

272. Al Kaabi, N. *et al.* Effect of 2 Inactivated SARS-CoV-2 Vaccines on Symptomatic COVID-19 Infection in Adults: A Randomized Clinical Trial. *JAMA* **326**, 35–45 (2021).

273. Logunov, D. Y. *et al.* Safety and efficacy of an rAd26 and rAd5 vector-based heterologous prime-boost COVID-19 vaccine: an interim analysis of a randomised controlled phase 3 trial in Russia. *The Lancet* **397**, 671–681 (2021).

274. Tanriover, M. D. *et al.* Efficacy and safety of an inactivated whole-virion SARS-CoV-2 vaccine (CoronaVac): interim results of a double-blind, randomised, placebo-controlled, phase 3 trial in Turkey. *Lancet* **398**, 213–222 (2021).

275. Ella, R. *et al.* Efficacy, safety, and lot-to-lot immunogenicity of an inactivated SARS-CoV-2 vaccine (BBV152): interim results of a randomised, double-blind, controlled, phase 3 trial. *The Lancet* **398**, 2173–2184 (2021).

276. Lazarus, R. *et al.* Immunogenicity and safety of an inactivated whole-virus COVID-19 vaccine (VLA2001) compared with the adenoviral vector vaccine ChAdOx1-S in adults in

the UK (COV-COMPARE): interim analysis of a randomised, controlled, phase 3, immunobridging trial. *The Lancet Infectious Diseases* **22**, 1716–1727 (2022).

277. Halperin, S. A. *et al.* Final efficacy analysis, interim safety analysis, and immunogenicity of a single dose of recombinant novel coronavirus vaccine (adenovirus type 5 vector) in adults 18 years and older: an international, multicentre, randomised, double-blinded, placebo-controlled phase 3 trial. *The Lancet* **399**, 237–248 (2022).
278. Matveeva, O. & Ershov, A. Retrospective Cohort Study of the Effectiveness of the Sputnik V and EpiVacCorona Vaccines against the SARS-CoV-2 Delta Variant in Moscow (June–July 2021). *Vaccines* **10**, 984 (2022).
279. Hager, K. J. *et al.* Efficacy and Safety of a Recombinant Plant-Based Adjuvanted Covid-19 Vaccine. *New England Journal of Medicine* **386**, 2084–2096 (2022).
280. Pallesen, J. *et al.* Immunogenicity and structures of a rationally designed prefusion MERS-CoV spike antigen. *Proceedings of the National Academy of Sciences* **114**, E7348–E7357 (2017).
281. Pardi, N. *et al.* Zika virus protection by a single low-dose nucleoside-modified mRNA vaccination. *Nature* **543**, 248–251 (2017).
282. Vogel, A. B. *et al.* BNT162b vaccines protect rhesus macaques from SARS-CoV-2. *Nature* **592**, 283–289 (2021).
283. Xia, X. Detailed Dissection and Critical Evaluation of the Pfizer/BioNTech and Moderna mRNA Vaccines. *Vaccines (Basel)* **9**, 734 (2021).
284. Sahin, U. *et al.* BNT162b2 vaccine induces neutralizing antibodies and poly-specific T cells in humans. *Nature* **595**, 572–577 (2021).

285. Ramanathan, A., Robb, G. B. & Chan, S.-H. mRNA capping: biological functions and applications. *Nucleic Acids Res* **44**, 7511–7526 (2016).

286. Orlandini von Niessen, A. G. *et al.* Improving mRNA-Based Therapeutic Gene Delivery by Expression-Augmenting 3′ UTRs Identified by Cellular Library Screening. *Mol Ther* **27**, 824–836 (2019).

287. Schoenmaker, L. *et al.* mRNA-lipid nanoparticle COVID-19 vaccines: Structure and stability. *International Journal of Pharmaceutics* **601**, 120586 (2021).

288. Reichmuth, A. M., Oberli, M. A., Jaklenec, A., Langer, R. & Blankschtein, D. mRNA vaccine delivery using lipid nanoparticles. *Therapeutic Delivery* **7**, 319–334 (2016).

289. Evers, M. J. W. *et al.* State-of-the-Art Design and Rapid-Mixing Production Techniques of Lipid Nanoparticles for Nucleic Acid Delivery. *Small Methods* **2**, 1700375 (2018).

290. Trougakos, I. P. *et al.* Adverse effects of COVID-19 mRNA vaccines: the spike hypothesis. *Trends in Molecular Medicine* **28**, 542–554 (2022).

291. Heinz, F. X. & Stiasny, K. Distinguishing features of current COVID-19 vaccines: knowns and unknowns of antigen presentation and modes of action. *npj Vaccines* **6**, 1–13 (2021).

292. Pardi, N., Hogan, M. J., Porter, F. W. & Weissman, D. mRNA vaccines — a new era in vaccinology. *Nat Rev Drug Discov* **17**, 261–279 (2018).

293. Yang, E. *et al.* Decay Rates of Human mRNAs: Correlation With Functional Characteristics and Sequence Attributes. *Genome Res* **13**, 1863–1872 (2003).

294. Park, J. W., Lagniton, P. N. P., Liu, Y. & Xu, R.-H. mRNA vaccines for COVID-19: what, why and how. *Int J Biol Sci* **17**, 1446–1460 (2021).

295. Tam, H. H. *et al.* Sustained antigen availability during germinal center initiation enhances antibody responses to vaccination. *Proc Natl Acad Sci U S A* **113**, E6639–E6648 (2016).

296. Teijaro, J. R. & Farber, D. L. COVID-19 vaccines: modes of immune activation and future challenges. *Nat Rev Immunol* **21**, 195–197 (2021).

297. Taub, D. D. *et al.* Immunity from Smallpox Vaccine Persists for Decades. *Am J Med* **121**, 1058–1064 (2008).

298. Pegu, A. *et al.* Durability of mRNA-1273 vaccine–induced antibodies against SARS-CoV-2 variants. *Science* **373**, 1372–1377 (2021).

299. Gao, F. *et al.* Robust T cell responses to Pfizer/BioNTech vaccine compared to infection and evidence of attenuated peripheral CD8+ T cell responses due to COVID-19. *Immunity* (2023) doi:10.1016/j.immuni.2023.03.005.

300. Yonker, L. M. *et al.* Circulating Spike Protein Detected in Post–COVID-19 mRNA Vaccine Myocarditis. *Circulation* **0**,.

301. Zhu, N. *et al.* A Novel Coronavirus from Patients with Pneumonia in China, 2019. *New England Journal of Medicine* **382**, 727–733 (2020).

302. Forni, D., Cagliani, R., Clerici, M. & Sironi, M. Molecular Evolution of Human Coronavirus Genomes. *Trends Microbiol* **25**, 35–48 (2017).

303. Severance, E. G. *et al.* Development of a Nucleocapsid-Based Human Coronavirus Immunoassay and Estimates of Individuals Exposed to Coronavirus in a U.S. Metropolitan Population. *Clin Vaccine Immunol* **15**, 1805–1810 (2008).

304. Li, F. Structure, Function, and Evolution of Coronavirus Spike Proteins. *Annu Rev Virol* **3**, 237–261 (2016).

305. Zhou, P. *et al.* A pneumonia outbreak associated with a new coronavirus of probable bat origin. *Nature* **579**, 270–273 (2020).

306. Ahmed, S. F., Quadeer, A. A. & McKay, M. R. Preliminary Identification of Potential Vaccine Targets for the COVID-19 Coronavirus (SARS-CoV-2) Based on SARS-CoV Immunological Studies. *Viruses* **12**, 254 (2020).

307. Lv, H. *et al.* Cross-reactive Antibody Response between SARS-CoV-2 and SARS-CoV Infections. *Cell Reports* **31**, (2020).

308. Tian, X. *et al.* Potent binding of 2019 novel coronavirus spike protein by a SARS coronavirus-specific human monoclonal antibody. *Emerg Microbes Infect* **9**, 382–385 (2020).

309. Wrapp, D. *et al.* Structural Basis for Potent Neutralization of Betacoronaviruses by Single-Domain Camelid Antibodies. *Cell* **181**, 1004-1015.e15 (2020).

310. Yuan, M. *et al.* A highly conserved cryptic epitope in the receptor binding domains of SARS-CoV-2 and SARS-CoV. *Science* **368**, 630–633 (2020).

311. Martin, J. E. *et al.* A SARS DNA vaccine induces neutralizing antibody and cellular immune responses in healthy adults in a Phase I clinical trial. *Vaccine* **26**, 6338–6343 (2008).

312. Yu, J. *et al.* DNA vaccine protection against SARS-CoV-2 in rhesus macaques. *Science* (2020) doi:10.1126/science.abc6284.

313. Sullivan, H. C. & Roback, J. D. Convalescent Plasma: Therapeutic Hope or Hopeless Strategy in the SARS-CoV-2 Pandemic. *Transfus Med Rev* (2020) doi:10.1016/j.tmrv.2020.04.001.

314. Zhang, L. *et al.* Anti-SARS-CoV-2 virus antibody levels in convalescent plasma of six donors who have recovered from COVID-19. *Aging (Albany NY)* **12**, 6536–6542 (2020).

315. Guo, X. *et al.* Long-Term Persistence of IgG Antibodies in SARS-CoV Infected Healthcare Workers. *medRxiv* 2020.02.12.20021386 (2020) doi:10.1101/2020.02.12.20021386.

316. Yasui, F. *et al.* Phagocytic cells contribute to the antibody-mediated elimination of pulmonary-infected SARS coronavirus. *Virology* **454–455**, 157–168 (2014).

317. Tripp, R. A. *et al.* Monoclonal antibodies to SARS-associated coronavirus (SARS-CoV): Identification of neutralizing and antibodies reactive to S, N, M and E viral proteins. *Journal of Virological Methods* **128**, 21–28 (2005).

318. ter Meulen, J. *et al.* Human Monoclonal Antibody Combination against SARS Coronavirus: Synergy and Coverage of Escape Mutants. *PLoS Med* **3**, (2006).

319. Walls, A. C. *et al.* Structure, Function, and Antigenicity of the SARS-CoV-2 Spike Glycoprotein. *Cell* **181**, 281-292.e6 (2020).

320. Pauthner, M. G. & Hangartner, L. Broadly Neutralizing Antibodies to Highly Antigenically Variable Viruses as Templates for Vaccine Design. in *Vaccination Strategies Against Highly Variable Pathogens* (eds. Hangartner, L. & Burton, D. R.) 31–87 (Springer International Publishing, 2020). doi:10.1007/82_2020_221.

321. Sicca, F., Neppelenbroek, S. & Huckriede, A. Effector mechanisms of influenza-specific antibodies: neutralization and beyond. *Expert Review of Vaccines* **17**, 785–795 (2018).

322. Duan, K. *et al.* Effectiveness of convalescent plasma therapy in severe COVID-19 patients. *Proc Natl Acad Sci U S A* **117**, 9490–9496 (2020).

323. Shrock, E. *et al.* Viral epitope profiling of COVID-19 patients reveals cross-reactivity and correlates of severity. *Science* (2020) doi:10.1126/science.abd4250.

324. Long, Q.-X. *et al.* Antibody responses to SARS-CoV-2 in patients with COVID-19. *Nature Medicine* **26**, 845–848 (2020).

325. Wu, F. *et al.* A new coronavirus associated with human respiratory disease in China. *Nature* **579**, 265–269 (2020).

326. Jacobs, J. J. L. Neutralizing antibodies mediate virus-immune pathology of COVID-19. *Medical Hypotheses* **143**, 109884 (2020).

327. Chi, X. *et al.* A neutralizing human antibody binds to the N-terminal domain of the Spike protein of SARS-CoV-2. *Science* (2020) doi:10.1126/science.abc6952.

328. Stadlbauer, D. *et al.* SARS-CoV-2 Seroconversion in Humans: A Detailed Protocol for a Serological Assay, Antigen Production, and Test Setup. *Current Protocols in Microbiology* **57**, e100 (2020).

329. Noh, J. & Danuser, G. Estimation of the fraction of COVID-19 infected people in U.S. states and countries worldwide. *PLOS ONE* **16**, e0246772 (2021).

330. Liu, Y. *et al.* Neutralizing Activity of BNT162b2-Elicited Serum. *New England Journal of Medicine* (2021) doi:10.1056/NEJMc2102017.

331. Sabino, E. C. *et al.* Resurgence of COVID-19 in Manaus, Brazil, despite high seroprevalence. *The Lancet* **397**, 452–455 (2021).

332. Tegally, H. *et al.* Detection of a SARS-CoV-2 variant of concern in South Africa. *Nature* 1–6 (2021) doi:10.1038/s41586-021-03402-9.

333. Walensky, R. P., Walke, H. T. & Fauci, A. S. SARS-CoV-2 Variants of Concern in the United States-Challenges and Opportunities. *JAMA* **325**, 1037–1038 (2021).

334. Lan, J. *et al.* Structure of the SARS-CoV-2 spike receptor-binding domain bound to the ACE2 receptor. *Nature* **581**, 215–220 (2020).

335. Robbiani, D. F. *et al.* Convergent Antibody Responses to SARS-CoV-2 in Convalescent Individuals. *Nature* **584**, 437–442 (2020).

336. Gobeil, S. M.-C. *et al.* D614G Mutation Alters SARS-CoV-2 Spike Conformation and Enhances Protease Cleavage at the S1/S2 Junction. *Cell Reports* **34**, 108630 (2021).

337. Tian, F. *et al.* Mutation N501Y in RBD of Spike Protein Strengthens the Interaction between COVID-19 and its Receptor ACE2. *bioRxiv* 2021.02.14.431117 (2021) doi:10.1101/2021.02.14.431117.

338. Weisblum, Y. *et al.* Escape from neutralizing antibodies by SARS-CoV-2 spike protein variants. *Elife* **9**, e61312 (2020).

339. Garcia-Beltran, W. F. *et al.* Circulating SARS-CoV-2 variants escape neutralization by vaccine-induced humoral immunity. *medRxiv* 2021.02.14.21251704 (2021) doi:10.1101/2021.02.14.21251704.

340. Mahase, E. Covid-19: Novavax vaccine efficacy is 86% against UK variant and 60% against South African variant. *BMJ* **372**, n296 (2021).

341. Xie, X. *et al.* Neutralization of SARS-CoV-2 spike 69/70 deletion, E484K and N501Y variants by BNT162b2 vaccine-elicited sera. *Nature Medicine* **27**, 620–621 (2021).

342. Forni, G. & Mantovani, A. COVID-19 vaccines: where we stand and challenges ahead. *Cell Death & Differentiation* **28**, 626–639 (2021).

343. Planas, D. *et al.* Sensitivity of infectious SARS-CoV-2 B.1.1.7 and B.1.351 variants to neutralizing antibodies. *Nature Medicine* 1–8 (2021) doi:10.1038/s41591-021-01318-5.

344. Doria-Rose, N. *et al.* Antibody Persistence through 6 Months after the Second Dose of mRNA-1273 Vaccine for Covid-19. *New England Journal of Medicine* **0**, null (2021).

345. Lyski, Z. L. *et al.* SARS-CoV-2 specific memory B-cells from individuals with diverse disease severities recognize SARS-CoV-2 variants of concern. *medRxiv* 2021.05.28.21258025 (2021) doi:10.1101/2021.05.28.21258025.

346. Wang, Z. *et al.* Naturally enhanced neutralizing breadth against SARS-CoV-2 one year after infection. *Nature* 1–10 (2021) doi:10.1038/s41586-021-03696-9.

347. Barnes, C. O. *et al.* SARS-CoV-2 neutralizing antibody structures inform therapeutic strategies. *Nature* **588**, 682–687 (2020).

348. Bates, T. A. *et al.* Cross-reactivity of SARS-CoV structural protein antibodies against SARS-CoV-2. *Cell Reports* 108737 (2021) doi:10.1016/j.celrep.2021.108737.

349. Zuo, J. *et al.* Robust SARS-CoV-2-specific T cell immunity is maintained at 6 months following primary infection. *Nature Immunology* 1–7 (2021) doi:10.1038/s41590-021-00902-8.

350. Rosenthal, N., Cao, Z., Gundrum, J., Sianis, J. & Safo, S. Risk Factors Associated With In-Hospital Mortality in a US National Sample of Patients With COVID-19. *JAMA Netw Open* **3**, (2020).

351. Kustin, T. *et al.* Evidence for increased breakthrough rates of SARS-CoV-2 variants of concern in BNT162b2 mRNA vaccinated individuals. *medRxiv* 2021.04.06.21254882 (2021) doi:10.1101/2021.04.06.21254882.

352. Holshue, M. L. *et al.* First Case of 2019 Novel Coronavirus in the United States. *N Engl J Med* **382**, 929–936 (2020).

353. Freed, N. E., Vlková, M., Faisal, M. B. & Silander, O. K. Rapid and inexpensive whole-genome sequencing of SARS-CoV-2 using 1200 bp tiled amplicons and Oxford Nanopore Rapid Barcoding. *Biol Methods Protoc* **5**, (2020).

354. Adey, A. *et al.* Rapid, low-input, low-bias construction of shotgun fragment libraries by high-density in vitro transposition. *Genome Biol* **11**, R119 (2010).

355. Vitak, S. A. *et al.* Sequencing thousands of single-cell genomes with combinatorial indexing. *Nat Methods* **14**, 302–308 (2017).

356. Wilm, A. *et al.* LoFreq: a sequence-quality aware, ultra-sensitive variant caller for uncovering cell-population heterogeneity from high-throughput sequencing datasets. *Nucleic Acids Res* **40**, 11189–11201 (2012).

357. Ye, K., Schulz, M. H., Long, Q., Apweiler, R. & Ning, Z. Pindel: a pattern growth approach to detect break points of large deletions and medium sized insertions from paired-end short reads. *Bioinformatics* **25**, 2865–2871 (2009).

358. Kontopantelis, E., Mamas, M. A., Deanfield, J., Asaria, M. & Doran, T. Excess mortality in England and Wales during the first wave of the COVID-19 pandemic. *J Epidemiol Community Health* **75**, 213–223 (2021).

359. Haas, E. J. *et al.* Impact and effectiveness of mRNA BNT162b2 vaccine against SARS-CoV-2 infections and COVID-19 cases, hospitalisations, and deaths following a nationwide vaccination campaign in Israel: an observational study using national surveillance data. *The Lancet* **397**, 1819–1829 (2021).

360. COVID-19 Vaccine Breakthrough Infections Reported to CDC — United States, January 1–April 30, 2021. *MMWR Morb Mortal Wkly Rep* **70**, (2021).

361. Bates, T. A. *et al.* Neutralization of SARS-CoV-2 variants by convalescent and vaccinated serum. *medRxiv* 2021.04.04.21254881 (2021) doi:10.1101/2021.04.04.21254881.

362. Levin, E. G. *et al.* Waning Immune Humoral Response to BNT162b2 Covid-19 Vaccine over 6 Months. *N Engl J Med* **385**, e84 (2021).

363. Chen, R. E. *et al.* Resistance of SARS-CoV-2 variants to neutralization by monoclonal and serum-derived polyclonal antibodies. *Nature Medicine* 1–10 (2021) doi:10.1038/s41591-021-01294-w.

364. Lopez Bernal, J. *et al.* Effectiveness of Covid-19 Vaccines against the B.1.617.2 (Delta) Variant. *New England Journal of Medicine* **385**, 585–594 (2021).

365. Bergwerk, M. *et al.* Covid-19 Breakthrough Infections in Vaccinated Health Care Workers. *N Engl J Med* NEJMoa2109072 (2021) doi:10.1056/NEJMoa2109072.

366. Chau, N. V. V. *et al.* An observational study of breakthrough SARS-CoV-2 Delta variant infections among vaccinated healthcare workers in Vietnam. *EClinicalMedicine* **41**, 101143 (2021).

367. Falsey, A. R. *et al.* SARS-CoV-2 Neutralization with BNT162b2 Vaccine Dose 3. *New England Journal of Medicine* **385**, 1627–1629 (2021).

368. Fan, G., Qin, X., Streblow, D. N., Hoyos, C. M. & Hansel, D. E. Comparison of SARS-CoV-2 PCR-Based Detection Using Saliva or Nasopharyngeal Swab Specimens in Asymptomatic Populations. *Microbiol Spectr* **9**, e0006221 (2021).

369. Bates, T. A. *et al.* Age-Dependent Neutralization of SARS-CoV-2 and P.1 Variant by Vaccine Immune Serum Samples. *JAMA* **326**, 868–869 (2021).

370. Bates, T. A. *et al.* Neutralization of SARS-CoV-2 variants by convalescent and BNT162b2 vaccinated serum. *Nat Commun* **12**, 5135 (2021).

371. Thomas, S. J. *et al.* Safety and Efficacy of the BNT162b2 mRNA Covid-19 Vaccine through 6 Months. *New England Journal of Medicine* (2021) doi:10.1056/NEJMoa2110345.

372. Goldberg, Y. *et al.* Protection and Waning of Natural and Hybrid Immunity to SARS-CoV-2. *N Engl J Med* **386**, 2201–2212 (2022).

373. Nanduri, S. *et al.* Effectiveness of Pfizer-BioNTech and Moderna Vaccines in Preventing SARS-CoV-2 Infection Among Nursing Home Residents Before and During Widespread

Circulation of the SARS-CoV-2 B.1.617.2 (Delta) Variant — National Healthcare Safety Network, March 1–August 1, 2021. *MMWR Morb Mortal Wkly Rep* **70**, 1163–1166 (2021).

374. Tartof, S. Y. *et al.* Effectiveness of mRNA BNT162b2 COVID-19 vaccine up to 6 months in a large integrated health system in the USA: a retrospective cohort study. *Lancet* **398**, 1407–1416 (2021).
375. Cavanaugh, A. M. Reduced Risk of Reinfection with SARS-CoV-2 After COVID-19 Vaccination — Kentucky, May–June 2021. *MMWR Morb Mortal Wkly Rep* **70**, (2021).
376. Butt, A. A., Yan, P., Shaikh, O. S. & Mayr, F. B. Outcomes among patients with breakthrough SARS-CoV-2 infection after vaccination in a high-risk national population. *EClinicalMedicine* **40**, (2021).
377. Yang, H. S. *et al.* Association of Age With SARS-CoV-2 Antibody Response. *JAMA Network Open* **4**, e214302 (2021).
378. Wang, Z. *et al.* Naturally enhanced neutralizing breadth against SARS-CoV-2 one year after infection. *Nature* **595**, 426–431 (2021).
379. Rydyznski Moderbacher, C. *et al.* Antigen-Specific Adaptive Immunity to SARS-CoV-2 in Acute COVID-19 and Associations with Age and Disease Severity. *Cell* **183**, 996-1012.e19 (2020).
380. Keeton, R. *et al.* Prior infection with SARS-CoV-2 boosts and broadens Ad26.COV2.S immunogenicity in a variant-dependent manner. *Cell Host Microbe* **29**, 1611-1619.e5 (2021).
381. Leier, H. C. *et al.* Previously infected vaccinees broadly neutralize SARS-CoV-2 variants. *medRxiv* 2021.04.25.21256049 (2021) doi:10.1101/2021.04.25.21256049.

382. Katzelnick, L. C. *et al.* Viridot: An automated virus plaque (immunofocus) counter for the measurement of serological neutralizing responses with application to dengue virus. *PLOS Neglected Tropical Diseases* **12**, e0006862 (2018).

383. Ackerman, M. E. *et al.* A robust, high-throughput assay to determine the phagocytic activity of clinical antibody samples. *Journal of Immunological Methods* **366**, 8–19 (2011).

384. Schmidt, F. *et al.* Plasma Neutralization of the SARS-CoV-2 Omicron Variant. *New England Journal of Medicine* **0**, null (2021).

385. Rössler, A., Riepler, L., Bante, D., von Laer, D. & Kimpel, J. SARS-CoV-2 Omicron Variant Neutralization in Serum from Vaccinated and Convalescent Persons. *New England Journal of Medicine* **386**, 698–700 (2022).

386. Hachmann, N. P. *et al.* Neutralization Escape by SARS-CoV-2 Omicron Subvariants BA.2.12.1, BA.4, and BA.5. *New England Journal of Medicine* (2022) doi:10.1056/NEJMc2206576.

387. Park, Y.-J. *et al.* Antibody-mediated broad sarbecovirus neutralization through ACE2 molecular mimicry. *Science* (2022) doi:10.1126/science.abm8143.

388. Cameroni, E. *et al.* Broadly neutralizing antibodies overcome SARS-CoV-2 Omicron antigenic shift. *Nature* 1–9 (2021) doi:10.1038/s41586-021-04386-2.

389. VanBlargan, L. A. *et al. A potently neutralizing anti-SARS-CoV-2 antibody inhibits variants of concern by binding a highly conserved epitope*. 2021.04.26.441501 https://www.biorxiv.org/content/10.1101/2021.04.26.441501v1 (2021) doi:10.1101/2021.04.26.441501.

390. Cavazzoni, P. Coronavirus (COVID-19) Update: FDA Limits Use of Certain Monoclonal Antibodies to Treat COVID-19 Due to the Omicron Variant. *FDA*

https://www.fda.gov/news-events/press-announcements/coronavirus-covid-19-update-fda-limits-use-certain-monoclonal-antibodies-treat-covid-19-due-omicron (2022).

391. Cele, S. *et al.* Omicron extensively but incompletely escapes Pfizer BNT162b2 neutralization. *Nature* 1–5 (2021) doi:10.1038/s41586-021-04387-1.

392. Bates, T. A. *et al.* Vaccination before or after SARS-CoV-2 infection leads to robust humoral response and antibodies that effectively neutralize variants. *Science Immunology* **7**, eabn8014 (2022).

393. Antonelli, M. *et al.* Risk factors and disease profile of post-vaccination SARS-CoV-2 infection in UK users of the COVID Symptom Study app: a prospective, community-based, nested, case-control study. *The Lancet Infectious Diseases* **22**, 43–55 (2022).

394. Atmar, R. L. *et al.* Homologous and Heterologous Covid-19 Booster Vaccinations. *New England Journal of Medicine* **0**, null (2022).

395. Muik, A. *et al.* Neutralization of SARS-CoV-2 Omicron by BNT162b2 mRNA vaccine–elicited human sera. *Science* (2022).

396. Garcia-Beltran, W. F. *et al.* mRNA-based COVID-19 vaccine boosters induce neutralizing immunity against SARS-CoV-2 Omicron variant. *Cell* **185**, 457-466.e4 (2022).

397. Shrotri, M. *et al.* Spike-antibody waning after second dose of BNT162b2 or ChAdOx1. *The Lancet* **0**, (2021).

398. Bates, T. A. *et al.* Antibody Response and Variant Cross-Neutralization After SARS-CoV-2 Breakthrough Infection. *JAMA* **327**, 179–181 (2022).

399. Johnson, A. G. COVID-19 Incidence and Death Rates Among Unvaccinated and Fully Vaccinated Adults with and Without Booster Doses During Periods of Delta and Omicron

Variant Emergence — 25 U.S. Jurisdictions, April 4–December 25, 2021. *MMWR Morb Mortal Wkly Rep* **71**, (2022).

400. Pfizer and BioNTech Announce Omicron-Adapted COVID-19 Vaccine Candidates Demonstrate High Immune Response Against Omicron | Pfizer. https://www.pfizer.com/news/press-release/press-release-detail/pfizer-and-biontech-announce-omicron-adapted-covid-19.
401. Chalkias, S. *et al. Safety, Immunogenicity and Antibody Persistence of a Bivalent Beta-Containing Booster Vaccine*. https://www.researchsquare.com/article/rs-1555201/v1 (2022) doi:10.21203/rs.3.rs-1555201/v1.
402. Rubin, R. COVID-19 Boosters This Fall to Include Omicron Antigen, but Questions Remain About Its Value. *JAMA* **328**, 412–414 (2022).
403. Patalon, T. *et al.* Waning effectiveness of the third dose of the BNT162b2 mRNA COVID-19 vaccine. *Nat Commun* **13**, 3203 (2022).
404. Liu, J. *et al.* BNT162b2-elicited neutralization of B.1.617 and other SARS-CoV-2 variants. *Nature* 1–3 (2021) doi:10.1038/s41586-021-03693-y.
405. Planas, D. *et al.* Considerable escape of SARS-CoV-2 Omicron to antibody neutralization. *Nature* **602**, 671–675 (2022).
406. Noori, M. *et al.* Potency of BNT162b2 and mRNA-1273 vaccine-induced neutralizing antibodies against severe acute respiratory syndrome-CoV-2 variants of concern: A systematic review of in vitro studies. *Reviews in Medical Virology* **32**, e2277 (2022).
407. Altarawneh, H. N. *et al.* Effects of Previous Infection and Vaccination on Symptomatic Omicron Infections. *N Engl J Med* **387**, 21–34 (2022).

408. Collie, S., Champion, J., Moultrie, H., Bekker, L.-G. & Gray, G. Effectiveness of BNT162b2 Vaccine against Omicron Variant in South Africa. *N Engl J Med* **386**, 494–496 (2022).

409. Nasreen, S. *et al.* Effectiveness of COVID-19 vaccines against symptomatic SARS-CoV-2 infection and severe outcomes with variants of concern in Ontario. *Nat Microbiol* **7**, 379–385 (2022).

410. Tang, P. *et al.* BNT162b2 and mRNA-1273 COVID-19 vaccine effectiveness against the SARS-CoV-2 Delta variant in Qatar. *Nat Med* 1–8 (2021) doi:10.1038/s41591-021-01583-4.

411. Lucas, C. *et al.* Delayed production of neutralizing antibodies correlates with fatal COVID-19. *Nat Med* **27**, 1178–1186 (2021).

412. Savage, H. R. *et al.* Prevalence of neutralising antibodies against SARS-CoV-2 in acute infection and convalescence: A systematic review and meta-analysis. *PLoS Negl Trop Dis* **15**, e0009551 (2021).

413. Bégin, P. *et al.* Convalescent plasma for hospitalized patients with COVID-19: an open-label, randomized controlled trial. *Nat Med* 1–13 (2021) doi:10.1038/s41591-021-01488-2.

414. RECOVERY Collaborative Group. Convalescent plasma in patients admitted to hospital with COVID-19 (RECOVERY): a randomised controlled, open-label, platform trial. *Lancet* **397**, 2049–2059 (2021).

415. Writing Committee for the REMAP-CAP Investigators *et al.* Effect of Convalescent Plasma on Organ Support-Free Days in Critically Ill Patients With COVID-19: A Randomized Clinical Trial. *JAMA* **326**, 1690–1702 (2021).

416. Pincetic, A. *et al.* Type I and type II Fc receptors regulate innate and adaptive immunity. *Nat Immunol* **15**, 707–716 (2014).

417. Schäfer, A. *et al.* Antibody potency, effector function, and combinations in protection and therapy for SARS-CoV-2 infection in vivoIn vivo efficacy of anti–SARS-CoV-2 antibodies. *Journal of Experimental Medicine* **218**, e20201993 (2020).

418. Ullah, I. *et al.* Live imaging of SARS-CoV-2 infection in mice reveals that neutralizing antibodies require Fc function for optimal efficacy. *Immunity* **54**, 2143-2158.e15 (2021).

419. Yamin, R. *et al.* Fc-engineered antibody therapeutics with improved anti-SARS-CoV-2 efficacy. *Nature* **599**, 465–470 (2021).

420. Winkler, E. S. *et al.* Human neutralizing antibodies against SARS-CoV-2 require intact Fc effector functions for optimal therapeutic protection. *Cell* **184**, 1804-1820.e16 (2021).

421. Farkash, I. *et al.* Anti-SARS-CoV-2 antibodies elicited by COVID-19 mRNA vaccine exhibit a unique glycosylation pattern. *Cell Rep* **37**, 110114 (2021).

422. Petrović, T. *et al.* Composition of the immunoglobulin G glycome associates with the severity of COVID-19. *Glycobiology* **31**, 372–377 (2021).

423. Vicente, M. M. *et al.* Altered IgG glycosylation at COVID-19 diagnosis predicts disease severity. *Eur J Immunol* **52**, 946–957 (2022).

424. Chakraborty, S. *et al.* Proinflammatory IgG Fc structures in patients with severe COVID-19. *Nat Immunol* **22**, 67–73 (2021).

425. Chakraborty, S. *et al.* Early non-neutralizing, afucosylated antibody responses are associated with COVID-19 severity. *Science Translational Medicine* **14**, eabm7853 (2022).

426. Larsen, M. D. *et al.* Afucosylated IgG characterizes enveloped viral responses and correlates with COVID-19 severity. *Science* **371**, eabc8378 (2021).

427. Hoepel, W. *et al.* High titers and low fucosylation of early human anti-SARS-CoV-2 IgG promote inflammation by alveolar macrophages. *Sci Transl Med* **13**, eabf8654 (2021).

428. Junqueira, C. *et al.* FcγR-mediated SARS-CoV-2 infection of monocytes activates inflammation. *Nature* **606**, 576–584 (2022).

429. Lofano, G. *et al.* Antigen-specific antibody Fc glycosylation enhances humoral immunity via the recruitment of complement. *Sci Immunol* **3**, eaat7796 (2018).

430. Peschke, B., Keller, C. W., Weber, P., Quast, I. & Lünemann, J. D. Fc-Galactosylation of Human Immunoglobulin Gamma Isotypes Improves C1q Binding and Enhances Complement-Dependent Cytotoxicity. *Front Immunol* **8**, 646 (2017).

431. Quast, I. *et al.* Sialylation of IgG Fc domain impairs complement-dependent cytotoxicity. *J Clin Invest* **125**, 4160–4170 (2015).

432. van Osch, T. L. J. *et al.* Fc Galactosylation Promotes Hexamerization of Human IgG1, Leading to Enhanced Classical Complement Activation. *J Immunol* **207**, 1545–1554 (2021).

433. Adeniji, O. S. *et al.* COVID-19 Severity Is Associated with Differential Antibody Fc-Mediated Innate Immune Functions. *mBio* **12**, e00281-21 (2021).

434. Bartsch, Y. C. *et al.* Humoral signatures of protective and pathological SARS-CoV-2 infection in children. *Nat Med* **27**, 454–462 (2021).

435. Herman, J. D. *et al.* Functional convalescent plasma antibodies and pre-infusion titers shape the early severe COVID-19 immune response. *Nat Commun* **12**, 6853 (2021).

436. Selva, K. J. *et al.* Systems serology detects functionally distinct coronavirus antibody features in children and elderly. *Nat Commun* **12**, 2037 (2021).

437. Klingler, J. *et al.* Detection of Antibody Responses Against SARS-CoV-2 in Plasma and Saliva From Vaccinated and Infected Individuals. *Front Immunol* **12**, 759688 (2021).

438. Lustig, Y. *et al.* BNT162b2 COVID-19 vaccine and correlates of humoral immune responses and dynamics: a prospective, single-centre, longitudinal cohort study in health-care workers. *Lancet Respir Med* **9**, 999–1009 (2021).

439. Alter, G. *et al.* Immunogenicity of Ad26.COV2.S vaccine against SARS-CoV-2 variants in humans. *Nature* 1–5 (2021) doi:10.1038/s41586-021-03681-2.

440. Gorman, M. J. *et al.* Fab and Fc contribute to maximal protection against SARS-CoV-2 following NVX-CoV2373 subunit vaccine with Matrix-M vaccination. *Cell Rep Med* **2**, 100405 (2021).

441. Kaplonek, P. *et al.* mRNA-1273 and BNT162b2 COVID-19 vaccines elicit antibodies with differences in Fc-mediated effector functions. *Sci Transl Med* **14**, eabm2311 (2022).

442. Brewer, R. C. *et al.* BNT162b2 vaccine induces divergent B cell responses to SARS-CoV-2 S1 and S2. *Nat Immunol* **23**, 33–39 (2022).

443. Collier, D. A. *et al.* Age-related immune response heterogeneity to SARS-CoV-2 vaccine BNT162b2. *Nature* **596**, 417–422 (2021).

444. Evans, J. P. *et al.* Neutralization of SARS-CoV-2 Omicron sub-lineages BA.1, BA.1.1, and BA.2. *Cell Host Microbe* (2022) doi:10.1016/j.chom.2022.04.014.

445. Kurhade, C. *et al.* Neutralization of Omicron BA.1, BA.2, and BA.3 SARS-CoV-2 by 3 doses of BNT162b2 vaccine. *Nat Commun* **13**, 3602 (2022).

446. Scully, E. P., Haverfield, J., Ursin, R. L., Tannenbaum, C. & Klein, S. L. Considering how biological sex impacts immune responses and COVID-19 outcomes. *Nat Rev Immunol* **20**, 442–447 (2020).

447. Kawasuji, H. *et al.* Age-Dependent Reduction in Neutralization against Alpha and Beta Variants of BNT162b2 SARS-CoV-2 Vaccine-Induced Immunity. *Microbiology Spectrum* **9**, e00561-21 (2021).

448. Nimmerjahn, F. & Ravetch, J. V. Divergent immunoglobulin g subclass activity through selective Fc receptor binding. *Science* **310**, 1510–1512 (2005).

449. Alter, G., Ottenhoff, T. H. M. & Joosten, S. A. Antibody glycosylation in inflammation, disease and vaccination. *Semin Immunol* **39**, 102–110 (2018).

450. Chung, A. W. *et al.* Dissecting Polyclonal Vaccine-Induced Humoral Immunity against HIV Using Systems Serology. *Cell* **163**, 988–998 (2015).

451. Arnold, J. N., Wormald, M. R., Sim, R. B., Rudd, P. M. & Dwek, R. A. The impact of glycosylation on the biological function and structure of human immunoglobulins. *Annu Rev Immunol* **25**, 21–50 (2007).

452. CDC COVID-19 Response Team. Severe Outcomes Among Patients with Coronavirus Disease 2019 (COVID-19) - United States, February 12-March 16, 2020. *MMWR Morb Mortal Wkly Rep* **69**, 343–346 (2020).

453. Andrews, N. *et al.* Duration of Protection against Mild and Severe Disease by Covid-19 Vaccines. *N Engl J Med* **386**, 340–350 (2022).

454. Beaudoin-Bussières, G. *et al.* A Fc-enhanced NTD-binding non-neutralizing antibody delays virus spread and synergizes with a nAb to protect mice from lethal SARS-CoV-2 infection. *Cell Reports* **38**, (2022).

455. Dufloo, J. *et al.* Asymptomatic and symptomatic SARS-CoV-2 infections elicit polyfunctional antibodies. *Cell Rep Med* **2**, 100275 (2021).

456. van de Bovenkamp, F. S., Hafkenscheid, L., Rispens, T. & Rombouts, Y. The Emerging Importance of IgG Fab Glycosylation in Immunity. *J Immunol* **196**, 1435–1441 (2016).

457. He, W. *et al.* Epitope specificity plays a critical role in regulating antibody-dependent cell-mediated cytotoxicity against influenza A virus. *Proc Natl Acad Sci U S A* **113**, 11931–11936 (2016).

458. Yamaguchi, Y. *et al.* The Fab portion of immunoglobulin G has sites in the CL domain that interact with Fc gamma receptor IIIa. *MAbs* **14**, 2038531 (2022).

459. Jeffery-Smith, A. *et al.* SARS-CoV-2-specific memory B cells can persist in the elderly who have lost detectable neutralizing antibodies. *J Clin Invest* **132**, e152042 (2022).

460. Coler, R. N. *et al.* The TLR-4 agonist adjuvant, GLA-SE, improves magnitude and quality of immune responses elicited by the ID93 tuberculosis vaccine: first-in-human trial. *NPJ Vaccines* **3**, 34 (2018).

461. Fuentes-Villalobos, F. *et al.* Sustained Antibody-Dependent NK Cell Functions in Mild COVID-19 Outpatients During Convalescence. *Front Immunol* **13**, 796481 (2022).

462. Lee, W. S. *et al.* Decay of Fc-dependent antibody functions after mild to moderate COVID-19. *CR Med* **2**, (2021).

463. Tso, F. Y. *et al.* Presence of antibody-dependent cellular cytotoxicity (ADCC) against SARS-CoV-2 in COVID-19 plasma. *PLoS One* **16**, e0247640 (2021).

464. Mlcochova, P. *et al.* SARS-CoV-2 B.1.617.2 Delta variant replication and immune evasion. *Nature* 1–8 (2021) doi:10.1038/s41586-021-03944-y.

465. Wang, P. *et al.* Antibody resistance of SARS-CoV-2 variants B.1.351 and B.1.1.7. *Nature* 1–6 (2021) doi:10.1038/s41586-021-03398-2.

466. Keeton, R. *et al.* T cell responses to SARS-CoV-2 spike cross-recognize Omicron. *Nature* **603**, 488–492 (2022).

467. CDC. COVID Data Tracker. *Centers for Disease Control and Prevention* https://covid.cdc.gov/covid-data-tracker (2020).

468. Richardson, S. I. *et al.* SARS-CoV-2 Beta and Delta variants trigger Fc effector function with increased cross-reactivity. *CR Med* **3**, (2022).

469. Bartsch, Y. C. *et al.* IgG Fc sialylation is regulated during the germinal center reaction following immunization with different adjuvants. *J Allergy Clin Immunol* **146**, 652-666.e11 (2020).

470. Boudreau, C. M. *et al.* Selective induction of antibody effector functional responses using MF59-adjuvanted vaccination. *J Clin Invest* **130**, 662–672 (2020).

471. Mahan, A. E. *et al.* Antigen-Specific Antibody Glycosylation Is Regulated via Vaccination. *PLOS Pathogens* **12**, e1005456 (2016).

472. Oefner, C. M. *et al.* Tolerance induction with T cell-dependent protein antigens induces regulatory sialylated IgGs. *J Allergy Clin Immunol* **129**, 1647-1655.e13 (2012).

473. Brown, E. P. *et al.* Multiplexed Fc array for evaluation of antigen-specific antibody effector profiles. *J Immunol Methods* **443**, 33–44 (2017).

474. Mahan, A. E. *et al.* A method for high-throughput, sensitive analysis of IgG Fc and Fab glycosylation by capillary electrophoresis. *J Immunol Methods* **417**, 34–44 (2015).

475. Váradi, C., Lew, C. & Guttman, A. Rapid magnetic bead based sample preparation for automated and high throughput N-glycan analysis of therapeutic antibodies. *Anal Chem* **86**, 5682–5687 (2014).

476. Lu, L. L. *et al.* A Functional Role for Antibodies in Tuberculosis. *Cell* **167**, 433-443 e14 (2016).

477. Darrah, P. A. *et al.* Multifunctional TH1 cells define a correlate of vaccine-mediated protection against Leishmania major. *Nat Med* **13**, 843–850 (2007).

478. Fischinger, S. *et al.* A high-throughput, bead-based, antigen-specific assay to assess the ability of antibodies to induce complement activation. *Journal of Immunological Methods* **473**, 112630 (2019).

479. Gunn, B. M. *et al.* Survivors of Ebola Virus Disease Develop Polyfunctional Antibody Responses. *J Infect Dis* **221**, 156–161 (2020).

480. Barber, R. M. *et al.* Estimating global, regional, and national daily and cumulative infections with SARS-CoV-2 through Nov 14, 2021: a statistical analysis. *The Lancet* **399**, 2351–2380 (2022).

481. Ritchie, H. *et al.* Coronavirus Pandemic (COVID-19). *Our World in Data* (2020).

482. Cohn, B. A., Cirillo, P. M., Murphy, C. C., Krigbaum, N. Y. & Wallace, A. W. SARS-CoV-2 vaccine protection and deaths among US veterans during 2021. *Science* **375**, 331–336 (2022).

483. Rosenberg, E. S. New COVID-19 Cases and Hospitalizations Among Adults, by Vaccination Status — New York, May 3–July 25, 2021. *MMWR Morb Mortal Wkly Rep* **70**, 1306–1311 (2021).

484. Goldberg, Y. *et al.* Waning Immunity after the BNT162b2 Vaccine in Israel. *N Engl J Med* **385**, e85 (2021).

485. Choi, A. *et al.* Safety and immunogenicity of SARS-CoV-2 variant mRNA vaccine boosters in healthy adults: an interim analysis. *Nat Med* 1–7 (2021) doi:10.1038/s41591-021-01527-y.

486. Wratil, P. R. *et al.* Three exposures to the spike protein of SARS-CoV-2 by either infection or vaccination elicit superior neutralizing immunity to all variants of concern. *Nat Med* **28**, 496–503 (2022).

487. Pilz, S., Theiler-Schwetz, V., Trummer, C., Krause, R. & Ioannidis, J. P. A. SARS-CoV-2 reinfections: Overview of efficacy and duration of natural and hybrid immunity. *Environ Res* **209**, 112911 (2022).

488. Cromer, D. *et al.* Neutralising antibody titres as predictors of protection against SARS-CoV-2 variants and the impact of boosting: a meta-analysis. *The Lancet Microbe* **3**, e52–e61 (2022).

489. Payne, R. P. *et al.* Immunogenicity of standard and extended dosing intervals of BNT162b2 mRNA vaccine. *Cell* **184**, 5699-5714.e11 (2021).

490. Hall, V. G. *et al.* Delayed-interval BNT162b2 mRNA COVID-19 vaccination enhances humoral immunity and induces robust T cell responses. *Nat Immunol* 1–6 (2022) doi:10.1038/s41590-021-01126-6.

491. Miyamoto, S. *et al.* Vaccination-infection interval determines cross-neutralization potency to SARS-CoV-2 Omicron after breakthrough infection by other variants. *Med* **3**, 249-261.e4 (2022).

492. Sanchez, S., Palacio, N., Dangi, T., Ciucci, T. & Penaloza-MacMaster, P. Fractionating a COVID-19 Ad5-vectored vaccine improves virus-specific immunity. *Science Immunology* **6**, eabi8635 (2021).

493. Ferdinands, J. M. Waning 2-Dose and 3-Dose Effectiveness of mRNA Vaccines Against COVID-19–Associated Emergency Department and Urgent Care Encounters and Hospitalizations Among Adults During Periods of Delta and Omicron Variant Predominance — VISION Network, 10 States, August 2021–January 2022. *MMWR Morb Mortal Wkly Rep* **71**, 255–263 (2022).

494. Hodcroft, E. B. CoVariants: SARS-CoV-2 Mutations and Variants of Interest. https://covariants.org/ (2021).

495. Anastassopoulou, C. *et al.* Age and sex associations of SARS-CoV-2 antibody responses post BNT162b2 vaccination in healthcare workers: A mixed effects model across two vaccination periods. *PLOS ONE* **17**, e0266958 (2022).

496. Sakharkar, M. *et al.* Prolonged evolution of the human B cell response to SARS-CoV-2 infection. *Science Immunology* **6**, eabg6916 (2021).

497. Kim, W. *et al.* Germinal centre-driven maturation of B cell response to mRNA vaccination. *Nature* 1–8 (2022) doi:10.1038/s41586-022-04527-1.

498. Tas, J. M. J. *et al.* Antibodies from primary humoral responses modulate the recruitment of naive B cells during secondary responses. *Immunity* **55**, 1856-1871.e6 (2022).

499. Grunau, B. *et al.* Immunogenicity of Extended mRNA SARS-CoV-2 Vaccine Dosing Intervals. *JAMA* **327**, 279–281 (2022).

500. Zhao, X. *et al.* Effects of a Prolonged Booster Interval on Neutralization of Omicron Variant. *N Engl J Med* **386**, 894–896 (2022).

501. Andrews, N. *et al.* Effectiveness of COVID-19 booster vaccines against COVID-19-related symptoms, hospitalization and death in England. *Nat Med* **28**, 831–837 (2022).

502. Magen, O. *et al.* Fourth Dose of BNT162b2 mRNA Covid-19 Vaccine in a Nationwide Setting. *New England Journal of Medicine* **386**, 1603–1614 (2022).

503. Epsi, N. J. *et al.* Understanding "Hybrid Immunity": Comparison and Predictors of Humoral Immune Responses to Severe Acute Respiratory Syndrome Coronavirus 2 Infection (SARS-CoV-2) and Coronavirus Disease 2019 (COVID-19) Vaccines. *Clin Infect Dis* ciac392 (2022) doi:10.1093/cid/ciac392.

504. Nordström, P., Ballin, M. & Nordström, A. Risk of SARS-CoV-2 reinfection and COVID-19 hospitalisation in individuals with natural and hybrid immunity: a retrospective, total population cohort study in Sweden. *The Lancet Infectious Diseases* **22**, 781–790 (2022).

505. Vanshylla, K. *et al.* Durability of omicron-neutralising serum activity after mRNA booster immunisation in older adults. *The Lancet Infectious Diseases* **22**, 445–446 (2022).

506. Al-Aly, Z., Bowe, B. & Xie, Y. Long COVID after breakthrough SARS-CoV-2 infection. *Nat Med* 1–7 (2022) doi:10.1038/s41591-022-01840-0.

507. Msemburi, W. *et al.* The WHO estimates of excess mortality associated with the COVID-19 pandemic. *Nature* **613**, 130–137 (2023).

508. Watson, O. J. *et al.* Global impact of the first year of COVID-19 vaccination: a mathematical modelling study. *The Lancet Infectious Diseases* **22**, 1293–1302 (2022).

509. Sah, P. *et al.* Estimating the impact of vaccination on reducing COVID-19 burden in the United States: December 2020 to March 2022. *JOGH* https://jogh.org/2022/jogh-12-03062/ (2022).

510. McConeghy, K. W. Effectiveness of a Second COVID-19 Vaccine Booster Dose Against Infection, Hospitalization, or Death Among Nursing Home Residents — 19 States, March 29–July 25, 2022. *MMWR Morb Mortal Wkly Rep* **71**, (2022).

511. Kaura, A. *et al.* Comparing the longer-term effectiveness of a single dose of the Pfizer-BioNTech and Oxford-AstraZeneca COVID-19 vaccines across the age spectrum. *eClinicalMedicine* **46**, (2022).

512. Gelanew, T. *et al.* A single dose ChAdOx1 nCoV-19 vaccine elicits high antibody responses in individuals with prior SARS-CoV-2 infection comparable to that of double dose vaccinated SARS-CoV-2 infection naïve individuals. *Res Sq* rs.3.rs-1250175 (2022) doi:10.21203/rs.3.rs-1250175/v1.

513. Stein, S. R. *et al.* SARS-CoV-2 infection and persistence in the human body and brain at autopsy. *Nature* **612**, 758–763 (2022).

514. Roe, K. SARS-CoV-2 and Toxoplasma gondii shared symptoms suggest muscle cells and neurons are their chronic infection reservoirs. *Hum Cell* **36**, 483–485 (2023).

515. Truong, T. T. *et al.* Increased viral variants in children and young adults with impaired humoral immunity and persistent SARS-CoV-2 infection: A consecutive case series. *EBioMedicine* **67**, 103355 (2021).

516. Jacobs, J. J. L. Persistent SARS-2 infections contribute to long COVID-19. *Med Hypotheses* **149**, 110538 (2021).

517. Aldén, M. *et al.* Intracellular Reverse Transcription of Pfizer BioNTech COVID-19 mRNA Vaccine BNT162b2 In Vitro in Human Liver Cell Line. *Curr Issues Mol Biol* **44**, 1115–1126 (2022).

518. Domazet-Lošo, T. mRNA Vaccines: Why Is the Biology of Retroposition Ignored? *Genes (Basel)* **13**, 719 (2022).

519. Lowe, D. Integration Into the Human Genome? https://www.science.org/content/blog-post/integration-human-genome.

520. Dolgin, E. Pan-coronavirus vaccine pipeline takes form. *Nature Reviews Drug Discovery* **21**, 324–326 (2022).

521. Goel, R. R. *et al.* mRNA vaccines induce durable immune memory to SARS-CoV-2 and variants of concern. *Science* **0**, eabm0829.